frontiers | Research Topics

Women in plant physiology 2022

Edited by
Alessandra Boccaccini and Lydia Pui Ying Lam

Published in
Frontiers in Plant Science

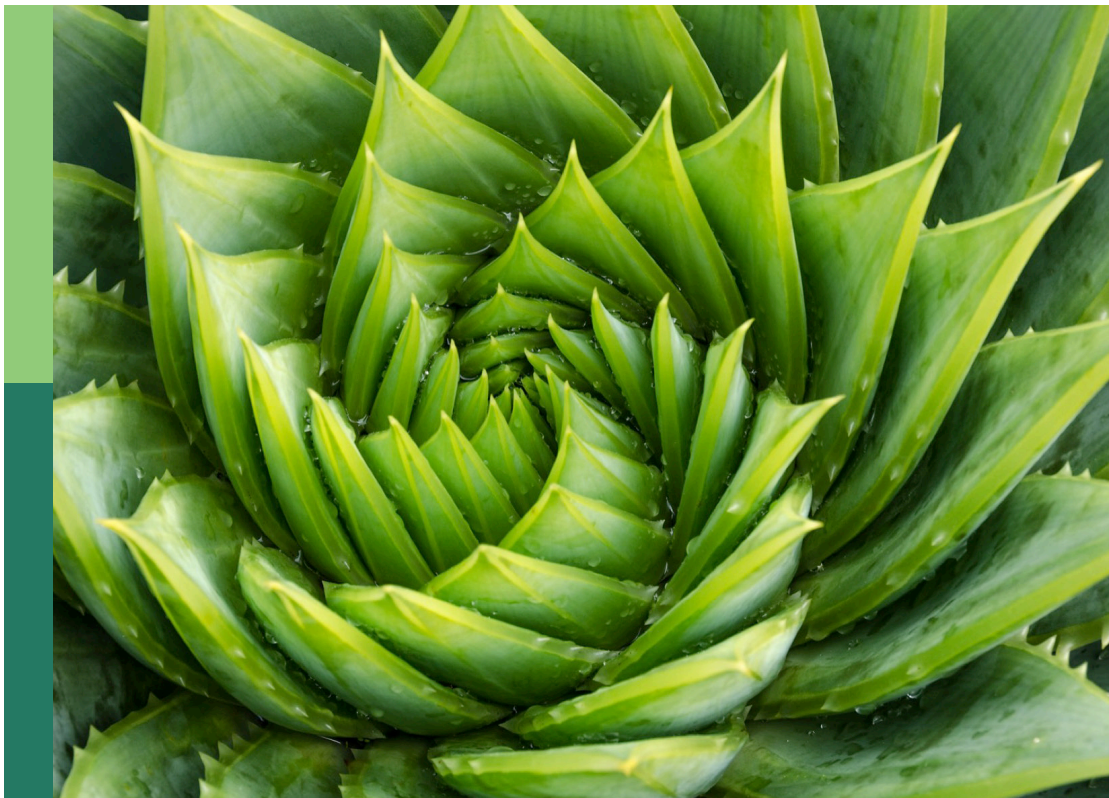

ISSN 1664-8714
ISBN 978-2-8325-2676-7
DOI 10.3389/978-2-8325-2676-7

About Frontiers

Frontiers is more than just an open access publisher of scholarly articles: it is a pioneering approach to the world of academia, radically improving the way scholarly research is managed. The grand vision of Frontiers is a world where all people have an equal opportunity to seek, share and generate knowledge. Frontiers provides immediate and permanent online open access to all its publications, but this alone is not enough to realize our grand goals.

Frontiers journal series

The Frontiers journal series is a multi-tier and interdisciplinary set of open-access, online journals, promising a paradigm shift from the current review, selection and dissemination processes in academic publishing. All Frontiers journals are driven by researchers for researchers; therefore, they constitute a service to the scholarly community. At the same time, the *Frontiers journal series* operates on a revolutionary invention, the tiered publishing system, initially addressing specific communities of scholars, and gradually climbing up to broader public understanding, thus serving the interests of the lay society, too.

Dedication to quality

Each Frontiers article is a landmark of the highest quality, thanks to genuinely collaborative interactions between authors and review editors, who include some of the world's best academicians. Research must be certified by peers before entering a stream of knowledge that may eventually reach the public - and shape society; therefore, Frontiers only applies the most rigorous and unbiased reviews. Frontiers revolutionizes research publishing by freely delivering the most outstanding research, evaluated with no bias from both the academic and social point of view. By applying the most advanced information technologies, Frontiers is catapulting scholarly publishing into a new generation.

What are Frontiers Research Topics?

Frontiers Research Topics are very popular trademarks of the *Frontiers journals series*: they are collections of at least ten articles, all centered on a particular subject. With their unique mix of varied contributions from Original Research to Review Articles, Frontiers Research Topics unify the most influential researchers, the latest key findings and historical advances in a hot research area.

Find out more on how to host your own Frontiers Research Topic or contribute to one as an author by contacting the Frontiers editorial office: frontiersin.org/about/contact

Women in plant physiology: 2022

Topic editors
Alessandra Boccaccini — Università di Tor Vergata, Italy
Lydia Pui Ying Lam — Akita University, Japan

Citation
Boccaccini, A., Lam, L. P. Y., eds. (2023). *Women in plant physiology: 2022*. Lausanne: Frontiers Media SA. doi: 10.3389/978-2-8325-2676-7

Table of contents

frontiers | Frontiers in Plant Science

TYPE Editorial
PUBLISHED 26 May 2023
DOI 10.3389/fpls.2023.1203958

OPEN ACCESS

EDITED AND REVIEWED BY
Anna N. Stepanova,
North Carolina State University,
United States

*CORRESPONDENCE
Alessandra Boccaccini
alessandra.boccaccini@outlook.it
Lydia Pui Ying Lam
lam@gipc.akita-u.ac.jp

†PRESENT ADDRESS
Alessandra Boccaccini,
IRCCS-Fondazione Bietti, Rome, Italy

RECEIVED 11 April 2023
ACCEPTED 02 May 2023
PUBLISHED 26 May 2023

CITATION
Boccaccini A and Lam LPY (2023) Editorial: Women in plant physiology: 2022.
Front. Plant Sci. 14:1203958.
doi: 10.3389/fpls.2023.1203958

Editorial: Women in plant physiology: 2022

Alessandra Boccaccini[1*†] and Lydia Pui Ying Lam[2*]

[1]Center for TeleInfrastructure (CTIF), University of Rome Tor Vergata, Rome, Italy, [2]Graduate School of Engineering Science, Akita University, Akita, Japan

KEYWORDS

plant physiology, environment, photosynthesis, abiotic stress, biotic stress, biotechnology

Editorial on the Research Topic
Women in plant physiology: 2022

Plants are essential for life on earth, not only because they produce oxygen *via* photosynthesis, but also because our everyday life highly depends on them. They provide us with clothes, food, and shelter. Ancient and modern medicine use plant metabolites as drugs for disease treatment. Moreover, plants can be engineered to produce vaccines, antibodies, and pharmaceutical proteins. Plants have a positive impact on the ecosystem, cleaning the environment by filtering toxic contaminates from the air, soil, and water. All these aspects demonstrate the importance of studying plants because only a deep understanding of how plants work can ensure smart exploitation of them and the development of new solutions for pressing problems. Hence, this Research Topic wanted to embrace all aspects of plant physiology, giving a voice to less-represented scientists in this field. According to UNESCO, women represent only 30% of the world's researchers. Hence, by promoting their works through this dedicated Research Topic on Women in Plant Physiology, Frontiers wanted to support women's careers, reducing the gender gap.

Half of the papers in this collection focused on studying plant-environment interactions (Figure 1). Since plants are sessile organisms that cannot flee or change their habitats depending on the seasons and nutrient availability, they have evolved mechanisms to cope with the ever-changing environment by adapting their growth and development to it. Among the external stimuli, light is one of the most important because it is required in photosynthesis to provide energy. Dukic et al. used *Arabidopsis thaliana* to dissect the molecular mechanism that regulates photosynthesis in the presence of limiting light. The authors found that phosphorylation of the light-harvesting complex II, happening in low light, depends on the Cl^- channel ClCe that regulates H^+ flux and ATP synthase activities. Moreover, phenotypic analyses of the *clc* mutant demonstrates the importance of this channel in controlling the acclimation of plants under low light. In addition, Mahati and Padmasree studied photosynthesis, focusing on the effect of brassinolide on the crosstalk between mitochondria and chloroplasts to regulate the Calvin-Benson cycle.

Light is not only a source of energy, but also provides information about the environment. The number of hours of light during the day is used by plants to

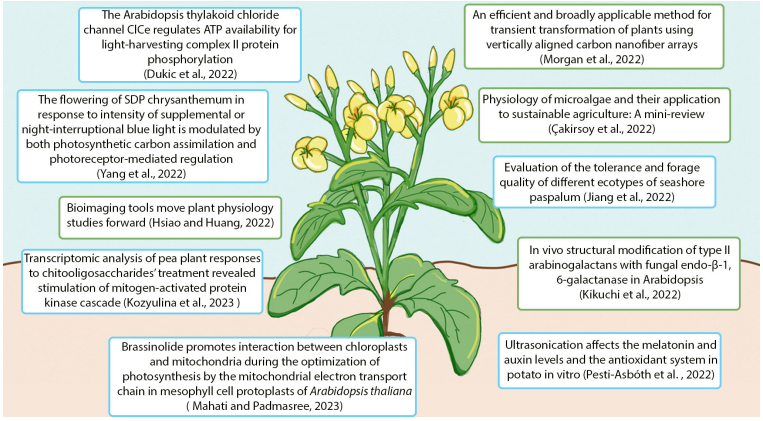

FIGURE 1
Summary of the contents of the Research Topic "Women in Plant Physiology." Blue boxes represent articles focused on plant-environment interactions, while green boxes indicate articles that discussed biotechnology and applied science.

determine the season, which is critical to decide when to flower (Freytes et al., 2021). The flowering time is particularly important in commercial plant species. For this reason, Yang et al. studied how supplementing with blue light during the day or an interrupting blue light pulse during the night affects the flowering of the Gaya Glory cultivar of *Chrysanthemum morifolium*.Even if plants are great at responding to environmental changes, some of these changes are considered stresses that negatively affect plant fitness. However, some species have evolved to grow in habitats that are hostile to other species. This is the case for *Seashore paspalum*, which can grow in the presence of a high concentration of salt, as presented by Jiang et al. These authors analyzed the salt tolerance and forage quality of 16 different ecotypes of *Seashore paspalum*, suggesting that the ecotype with the best salt-resistant phenotype and high nutritional quality could be exploited in agriculture and animal husbandry. Finding salt-resistant genotypes is particularly important for modern agriculture, which is endangered by soil salinization aggravated by climate change and anthropogenic activities (Mukhopadhyay et al., 2021).

Ultrasound is an abiotic stress that impacts plant growth and development. Pesti-Asbóth et al. discovered that ultrasonication reduces the growth and chlorophyll content of potato, activates antioxidant pathway, increases auxins production, and decreases melatonin accumulation. Their data provide new insights into how plants cope with ultrasound stress.

In addition to abiotic stresses, plants are also often attacked by herbivores and pathogens such as fungi, viruses, and bacteria. The mechanisms used to respond to pathogen attack are known as plant immunity, and can be elicited by natural compounds such as chitooligosaccharides. The article by Kozyulina et al. describes the transcriptional response to chitooligosaccharides of the pea plant, identifying several cellular pathways affected by this treatment and demonstrating the importance of studying plant elicitors in crops.

The other half of this collection focused on applied science and biotechnology (Figure 1). For sustainable agricultural development, microalgae have emerged as a renewable alternative to chemical fertilizers. Microalgae could efficiently take up nutrients from wastewater, and their biomass could be used as fertilizers. Çakirsoy et al. described and highlighted the potential of using microalgae for nutrient recycling, their physiological properties that enable rapid growth and efficient nutrient uptake, the properties and advantages of microalga-based fertilizers, as well as challenges in their actual applications.

Arabinogalactan-proteins (AGPs) are plant extracellular glycoproteins that are decorated by type II arabinogalactans (Ma and Johnson, 2023). To study the functions of the long β-1,6-galactohexaose (β-1,6-Gal6) side chains of AGPs, Kikuchi et al. generated transgenic arabidopsis with reduced long β-1,6-galactan side chains by expressing a dexamethasone inducible fungal endo-β-1,6-galactanase, Tv6GAL, that could degrade these long side chains. After dexamethasone treatment, these plants showed retarded growth, higher extensibility, lower breaking load, and reduced cellulose content, suggesting the role of long β-1,6-galactan side chains in cellulose production and/or deposition, which could influence cell growth.

Finally, tools for studying plant physiology have been developed or summarized. Transient gene expression in plants is widely employed to study gene functions. Morgan et al. developed an efficient transient transformation method that could be applied to different plant species (Arabidopsis, poplar, lettuce, *Nicotiana benthamiana*, and tomato) and organs by using vertically aligned carbon nanofiber arrays. This method holds potential for application in species that are recalcitrant to being transformed by *Agrobacterium*. Bioimagining tools are also widely used in the study of plant physiology. Their applications span from tracking morphogenesis to visualizing macromolecular dynamics. Hsiao and

Huang summarized the key contributions of female scientists to the development of bioimaging techniques, which have moved plant physiology study forward. In addition, this opinion article also describes the history of these female scientists, aiming to encourage and inspire the next generation of female researchers to grow their interest in studying plant physiology and cell biology.

Hence, this Research Topic addresses a variety of questions in the plant physiology field and highlights the necessity of constant crosstalk between basic and applied research to move forward the knowledge in this field.

Author contributions

All authors listed have made a substantial, direct, and intellectual contribution to the work and approved it for publication.

Conflict of interest

The authors declare that the research was conducted in the absence of any commercial or financial relationships that could be construed as a potential conflict of interest.

Publisher's note

References

Freytes, S. N., Canelo, M., and Cerdán, P. D. (2021). Regulation of flowering time: when and where? *Curr. Opin. Plant Biol.* 63, 102049. doi: 10.1016/j.pbi.2021.102049

Ma, Y., and Johnson, K. (2023). Arabinogalactan proteins – multifunctional glycoproteins of the plant cell wall. *Cell Surface* 9, 100102. doi: 10.1016/j.tcsw.2023.100102

Mukhopadhyay, R., Sarkar, B., Jat, H. S., Sharma, P. C., and Bolan, N. S. (2021). Soil salinity under climate change: challenges for sustainable agriculture and food security. *J. Environ. Manage.* 280, 111736. doi: 10.1016/j.jenvman.2020.111736

frontiers | Frontiers in Plant Science

TYPE Original Research
PUBLISHED 16 September 2022
DOI 10.3389/fpls.2022.981143

OPEN ACCESS

EDITED BY
Alessandra Boccaccini,
Università di Tor Vergata,
Italy

REVIEWED BY
Vasiliki Zacharaki,
Swedish University of Agricultural Sciences, Sweden
Jing Sun,
Yangzhou University, China

*CORRESPONDENCE
Byoung Ryong Jeong
brjeong@gnu.ac.kr

SPECIALTY SECTION
This article was submitted to Plant Physiology, a section of the journal Frontiers in Plant Science

RECEIVED 29 June 2022
ACCEPTED 02 September 2022
PUBLISHED 16 September 2022

CITATION
Yang J, Song J and Jeong BR (2022) The flowering of SDP chrysanthemum in response to intensity of supplemental or night-interruptional blue light is modulated by both photosynthetic carbon assimilation and photoreceptor-mediated regulation.
Front. Plant Sci. 13:981143.
doi: 10.3389/fpls.2022.981143

The flowering of SDP chrysanthemum in response to intensity of supplemental or night-interruptional blue light is modulated by both photosynthetic carbon assimilation and photoreceptor-mediated regulation

Jingli Yang[1], Jinnan Song[1] and Byoung Ryong Jeong[1,2,3]*

[1]Department of Horticulture, Division of Applied Life Science (BK21 Four Program), Graduate School of Gyeongsang National University, Jinju, South Korea, [2]Institute of Agriculture and Life Science, Gyeongsang National University, Jinju, South Korea, [3]Research Institute of Life Science, Gyeongsang National University, Jinju, South Korea

The photoreceptor-mediated photoperiodic sensitivity determines the obligate short-day flowering in chrysanthemum (*Chrysanthemum morifolium* Ramat.) when the night length is longer than a critical minimum, otherwise, flowering is effectively inhibited. The reversal of this inhibition by subsequent exposure to a short period of supplemental (S) or night-interruptional (NI) blue (B) light (S-B; NI-B) indicates the involvement of B light-received photoreceptors in the flowering response. Flowering is mainly powered by sugars produced through photosynthetic carbon assimilation. Thus, the light intensity can be involved in flowering regulation by affecting photosynthesis. Here, it is elucidated that the intensity of S-B or NI-B in photoperiodic flowering regulation of chrysanthemums by applying 4-h of S-B or NI-B with either 0, 10, 20, 30, or 40 $\mu mol \cdot m^{-2} \cdot s^{-1}$ photosynthetic photon flux density (PPFD) in a 10-h short-day (SD10) [SD10 + 4B or + NI-4B (0, 10, 20, 30, or 40)] or 13-h long-day (LD13) condition [LD13 + 4B or + NI-4B (0, 10, 20, 30, or 40)] provided by 300 $\pm$ 5 $\mu mol \cdot m^{-2} \cdot s^{-1}$ PPFD white (W) LEDs. After 60 days of photoperiodic light treatments other than the LD13 and LD13 + NI-4B (40), flowering with varying degrees was observed, although the SD10 gave the earliest flowering. And the LD13 + 4B (30) produced the greatest number of flowers. The flowering pattern in response to the intensity of S-B or NI-B was consistent as it was gradually promoted from 10 to 30 $\mu mol\ m^{-2}\ s^{-1}$ PPFD and inhibited by 40B regardless of the photoperiod. In SD conditions, the same intensity of S-B and NI-B did not significantly affect flowering, while differential flowering inhibition was observed with any intensity of NI-B in LDs. Furthermore, the 30 $\mu mol \cdot m^{-2} \cdot s^{-1}$ PPFD of S-B or NI-B up-regulated the expression of floral meristem identity or florigen genes, as well as the chlorophyll content, photosynthetic efficiency,

and carbohydrate accumulation. The 40B also promoted these physiological traits but led to the unbalanced expression of florigen or anti-florigen genes. Overall, the photoperiodic flowering in response to the intensity of S-B or NI-B of the SDP chrysanthemum suggests the co-regulation of photosynthetic carbon assimilation and differential photoreceptor-mediated control.

KEYWORDS

photoperiodic response, light intensity, supplemental blue light, night-interruptional blue light, photosynthetic efficiency, carbohydrate accumulation, photoreceptors, florigen or anti-florigen genes

Introduction

The change from the vegetative to the regenerative stage is perhaps the main formative stage in the life cycle of plants. The timing of blooming during the year, which is a significant versatile attribute that unequivocally impacts reproductive fitness, is impacted by both endogenous and ecological variables. Changes in photoperiod (day length) are among the most significant and solid signals for plants to reproduce in favorable seasons. In 1920, Garner and Allard showed that some plant species bloomed depending on the changes in day length and depicted this peculiarity as "photoperiodism" (Garner and Allard, 1920). Plants are grouped by their photoperiodic reactions as short-day plants (SDPs), in which blooming happens when the night duration is longer than a critical minimum; long-day plants (LDPs), in which blossoming happens when the day duration turns out to be longer than some crucial length; and day-neutral plants (DNPs). According to the photoperiodic reactions, there are obligate (qualitative) and facultative (quantitative) types within the SDPs and LDPs. The particular photoperiod is absolute for obligate-type plants to make responses. Chrysanthemum is a kind of obligate SDP. *Chrysanthemum morifolium* is one of 30 flowering species in the *Chrysanthemum* genus of the *Asteraceae* family (Jeong et al., 2012). The flower bud will be induced when the night length ≈ 12 h or more, while the specific minor differences in the photoperiod sensitivity of flower formation are species- or cultivar-depending (McMahon and Kelly, 1999; Higuchi et al., 2013).

Light is well known to functionally regulate flowering in several plant species. So how do plants sense and transmit light signals to induce flowering? It soon became clear that leaves perceive the day-length signals (Knott, 1934). Multiple photoreceptors are mainly located in plant leaves to sense the environmental light signals and seasonal changes in photoperiod, which they take as signals to flower. Different photoreceptors control plant growth and development differently, thus this is the case for the photoperiodic-perception process (Davis, 2002). Both cryptochromes and phytochromes abundance relies on light, which shows the importance of the photoreceptors regarding determining day length (Somers et al., 1998). Additionally, photoreceptors are also sensitive to light quality. Phytochrome B (PHYB) promotes early flowering in *Arabidopsis* in response to low-red/far-red (R/FR) along with PHYD and E (Franklin et al., 2003), however, this response of PHYB in shade avoidance is distinct from photoperiodism, which is inhibitory (Mockler et al., 2003). Furthermore, cryptochromes mediate plant responses to B light and UV-A. Two members of the cryptochromes (CRY1 and 2) are present in *Arabidopsis* and led to early flowers, indicating that cryptochromes play a role to promote flowering (Mockler et al., 1999). Some researchers believed that light does not separately regulate the photoperiod sensitivity in plants, it should be accomplished by combining endogenous circadian rhythms (Biinning, 1936; Pittendrigh and Minis, 1964). Later confirmed that light directly modulated the activity of clock-controlled genes (CCGs), and controlled the circadian phase of the CCGs by resetting the circadian clock (Yanovsky and Kay, 2003; Kobayashi and Weigel, 2007). Overall, these photoreceptors influence flowering by detecting the specific light quality and directing light input to the circadian clock, as well as by altering the protein stability of CONSTANS (CO), a key activator of FLOWERING LOCUS T (FT) (Somers et al., 1998; Valverde et al., 2004).

After plants receive the light signals, a transmissible factor, florigen, is synthesized in leaves, which is the vector of received photoperiodic signals. And the flowering improvement "florigen" was proposed by Chailakhyan in 1936, through a chrysanthemum experiment (Chailakhyan, 1936). Currently, many studies have reported that FT and its orthologs are synthesized in several species' leaves, which act as florigens (Kobayashi and Weigel, 2007; Zeevaart, 2008; Turnbull, 2011; Mcgarry and Ayre, 2012). In *Arabidopsis*, FT moves into the shoot apical meristem (SAM) through the phloem and in there structures a transcriptional complex with FD, an essential leucine zipper (bZIP) record factor; subsequently activates the *FRUITFULL* (*FUL*) and

APETALA 1 (*AP1*), the transcription of floral regulator genes, leading to flowering (Abe et al., 2005; Wigge et al., 2005). *FT* encodes a phosphatidylethanolamine–binding protein-like (PEBP-like) small protein, that is florigen. The PEBP family has developed both the activators and repressors of blooming. There are five more members of the *FT* gene family in *Arabidopsis*: *TERMINAL FLOWER 1* (*TFL1*), *MOTHER OF FT AND TFL1* (*MFT*), *BROTHER OF FT AND TFL1* (*BFT*), *TWIN SISTER OF FT* (*TSF*), and *Arabidopsis thaliana CENTRORADIALIS homolog* (*ATC*). Based on numerous studies of the FT family: FT and TSF work as floral activators (Kobayashi et al., 1999; Kardailsky et al., 1999; Yamaguchi et al., 2005) while TFL1, ATC, and BFT act as floral repressors (Bradley et al., 1997; Mimida et al., 2001; Yoo et al., 2010), moreover, MFT is related to seed germination (Xi et al., 2010). Additionally, the expression of ATC and TFL1 are observed in vasculature tissue and shoot apex, respectively, even though they are known as non-cell-autonomous (Conti and Bradley, 2007; Huang et al., 2012). Floral repressors also known as an antiflorigenic stimulus are synthesized in leaves too (Thomas and Vince-Prue, 1996), which has clearly confirmed by the classical physiological experiments of the flowering inhibition experiment with grafted leaves in tobacco cultivars under non-floral-inductive light-duration environments (Lang et al., 1977). And the anti-floral factors were also observed in chrysanthemum leaves under flowering unfavorable day-length conditions (Tanaka, 1967). These studies strongly support the idea that the balanced signals of florigens and anti-florigens synthesized in leaves might be involved in differential photoreceptor-mediated regulation in photoperiodic flowering in plants.

Light intensity-related photosynthetic efficiency and carbon assimilation also affect plant flowering, which is associated with altered carbon and nitrogen metabolism (Eckardt et al., 1997; Walters et al., 2004). Low light generally delays the first flowering period of plants, prolongs the flowering period, and decreases the flowering index, which has been studied mostly in tomatoes and some flowering plants (Fc, 1997). The reduced accumulation of nutrients in tomato plants under low light and the poor ability of reproductive growth to compete for photosynthetic products lead to delayed floral bud differentiation, increased flowering nodes, reduced bud quality, and flower number (Kinet, 1977). Additionally, the effect of light intensity on the flowering time of plants under strong light varies widely, and it is generally believed that increasing light intensity has a negative effect on flowering. Since light intensity is related to the photosynthesis and assimilation efficiency of plants, and the photoreceptors of plants are chlorophyll and other photosynthetic pigments, it is possible that the regulation of flowering time is related to changes in photosynthetic and carbon assimilation efficiency. One study found that the delayed flowering in *phya* mutants under low irradiation but not high irradiation, suggesting that the function of *PHYA* might be indirectly mediated through photosynthesis in *Arabidopsis*, however, it still needs further study (Bagnall and King, 2001). Moreover, the flowering of parthenogenic short-day plants was studied at different light intensities (42, 45, 92, and 119 $\mu mol \cdot m^{-2} \cdot s^{-1}$ PPFD), and it was found that the plants flowered earliest at low irradiance (42 $\mu mol \cdot m^{-2} \cdot s^{-1}$ PPFD) (Jalal-Ud-Din et al., 2013). Hence, light intensity involves flowering regulation by affecting photoperiodic carbon assimilation which might be mediated indirectly by *PHYA* at the same time.

Since the technical skills are widely used in chrysanthemum cultivation, the photoperiodic limitation in its flowering time is lifted by blackouts or artificial colorful lighting, day-length extension, or night break (NB) to fulfill the need for marketable flowers consistently. Light supplementation might appear as valuable light in a foundation of regular light, or extra light that expands the day length (Zheng et al., 2018). NB interrupts the continued dark duration with lighting, thus making modulated LD environments (Yamada et al., 2008; Park et al., 2015). Higuchi et al. (2012) revealed the effect of B light on photoperiodic regulation of flowering in chrysanthemums, which found that for plants grown under SD conditions with white (W) light, NB treatment with monochromatic red (R) light was effective in inhibiting flowering, while the monochromatic B light or far red (FR) light was less effective in inhibiting flowering. And the 4-h low level of B light supplied either at the supplementary or NI in SD conditions all flowered and did no significant differences when compared with the normal SD environment (Park and Jeong, 2020). Especially in LD conditions, the non-flowered plants were flowered after being treated with 4-h low-intensity of S-B or NI-B, just deferred flower bud formation (Park and Jeong, 2019; Park and Jeong, 2020). However, the extension of the natural sunlight during the first 11 h of the photoperiod with either R or B sole light, inhibited flowering in *Chrysanthemum morifolium* (SharathKumar et al., 2021). Thus, there is the cultivar specific- or other subtle details- depending (such as intensity, photoperiod, supplementary, or NB) on the flowering response to the B light.

Here, we determined the photoperiodic response of SDP *Chrysanthemum morifolium* to various intensities of S-B or NI-B by setting the experiment with the pot plants of the 'Gaya Glory' cultivar under 18 different photoperiodic light treatments. Our results demonstrated that the photoperiodic flowering of chrysanthemums by the co-regulation of sugar accumulation produced by photosynthetic carbon assimilation and the expression of florigen and anti-florigen genes mediated by differential photoreceptors.

Materials and methods

Plant materials and growth conditions

The pot experiment was conducted in a closed-type plant factory (770.0 cm long × 250.0 cm wide × 269.5 cm high, Green

Industry Co. Ltd., Changwon, Korea) at Gyeongsang National University, Jinju, Korea, in early September of 2021. The ornamental species chrysanthemum (*Chrysanthemum morifolium* Ramat.) 'Gaya Glory', a qualitative SDP, was selected as experimental material in this study. The rooted cuttings with 8 ± 1 leaves per plant were obtained from the Flowers Breeding Research Institute, Gyeongnam Agricultural Research & Extension Services, Changwon, Gyeongnam, Korea and separately transplanted into 10 cm plastic pots with commercial medium (BVB Medium, Bas Van Buuren Substrates, EN-12580, De Lier, The Netherlands), one plant per pot. After planting, plants were moved to this closed–type plant factory and acclimated to 23/18°C (light/dark), 70 ± 10% RH, and 270 ± 5 μmol·m^{-2}·s^{-1} PPFD supplied with F48T12-CW-VHO fluorescent lamps (Philips Co., Ltd., Eindhoven, The Netherlands). CO_2 was provided by a compressed gas tank to timely supplement plant photosynthesis and maintained a concentration of 350 ± 50 parts per million (PPM) through an electrolyte CO_2 sensor (Model No. GMT220 Carbocap, Vaisala) monitored online. The air circulation system here was installed with the fans evenly and the conditioned air could blow horizontally into the developing rooms through multiple regularly distributed apertures. After one week of acclimatization (the 16-h LD), the plants were subjected to photoperiodic light treatments. And the daily irrigation with the multipurpose nutrient solution (macro-elements: Ca^{2+}, Mg^{2+}, K^+, NH_4^+, NO_3^-, SO_4^{2-}, and $H_2PO_4^-$; microelements: B, Cu, Fe, Mn, Mo, and Zn; pH = 6.5) (Yang et al., 2022) was from 8:30 ~ 9:30 a.m. Additionally, the three-replication randomized complete block design with eight plants per replication, a total of 24 plants in each treatment, and randomly located among replications to minimize the influences of light positioning in an opaque compartment.

Light treatments

The 'Gaya Glory' cultivar of *Chrysanthemum morifolium* shows an obligate photoperiodic flowering response in which flowering occurs under a ≥ 13-h dark period and is inhibited under a< 12-h dark period. Thus, based on our previous tests, the short-day 10 h (SD10) and long-day 13 h (LD13) photoperiods were used in this study, which can effectively initiate or inhibit flower formation, respectively (Park and Jeong, 2020). The light duration was started every day at 8:00 a.m. Plants were grown with daily light at an intensity of 300 ± 5 μmol·m^{-2}·s^{-1} PPFD provided by white (W) MEF50120 LEDs (More Electronics Co. Ltd., Changwon, Korea) with a wide spectrum ranging from 400 to 720 nm and a distinct peak at 435 nm in blue (Figure 1A). The 4-h blue (B) (450 nm) LED light with either 0, 10, 20, 30, or 40 μmol·m^{-2}·s^{-1} PPFD of intensities was used to (1) supplement the W light at the end of the SD10 (SD10 + 4B) and LD13 (LD13 + 4B) or (2) provide night-interruption (NI) in the SD10 (SD10 + NI-4B) and LD13 (LD13 + NI-4B) (Figures 1A, B). The control or constructed by exposing the plants to SD10 (positive control) or LD13 (negative control) conditions, without any B light. The "SD10 or LD13 + 4B (10, 20, 30, or 40)" and "SD10 or LD13 + NI-4B (10, 20, 30, or 40)" were set as experimental groups for the photoperiodic light treatments. Moreover, the experimental layout in the plant factory was shown in Figure 1C. Light distribution was recorded at 1 nm wavelength intervals using a spectroradiometer (USB 2000 Fiber Optic Spectrometer, Ocean Optics Inc., Dunedin, FL, USA; detects wavelength between 200 to 1000 nm) and uniformity was verified by measuring the light intensity at three points of each light treatment at the canopy level through a quantum radiation probe (FLA 623 PS, ALMEMO, Holzkirchen, Germany).

Measurements of growth parameters

For *Chrysanthemum morifolium*, the period between the start of the SD period and flowering under optimal conditions (reaction time) can vary between 6~11 weeks (Thakur and Grewal, 2019). Based on Park and Jeong (2020), 41-days of photoperiodic B light treatment duration was enough for observing the changes in chrysanthemum photoperiodic flowering. Experimenting repeatedly, we extended the experimental duration to 60 days to ensure the complete response of chrysanthemums in each light treatment. Thus, the plant growth parameters, such as plant height, stem diameter, number of branches, leaves, and flowers per plant, and days to the first visible flower buds were collected after 60 days of light treatments. The days to visible flower buds in each treatment were determined by counting the number of days from light treatment to the date when the first flower bud appeared. The number of flowers per plant contained both blooming flowers and visible flower buds at the harvest stage. The stem diameter was measured according to the middle parts of the main stem. And the leaves with a length > 1 cm were counted to determine the total number of leaves per plant. For the biomass measurement, after careful cleaning, divided samples of shoots and roots were oven-dried (the drying oven, Venticell-222, MMM Medcenter Einrichtungen GmbH., Munich, Germany) at 85°C for five ~ seven days until a constant mass was reached to determine dry weight. Additionally, the harvested samples were kept in liquid nitrogen immediately and then stocked in the −80°C refrigerator for subsequent physiological investigations.

Microscopic observation of stomata

After 60 days of light treatment, the stomatal traits were observed directly through fixed and discolored leaf samples due to the easiness observation of stomata in chrysanthemum leaves. At

10.3389/fpls.2022.981143

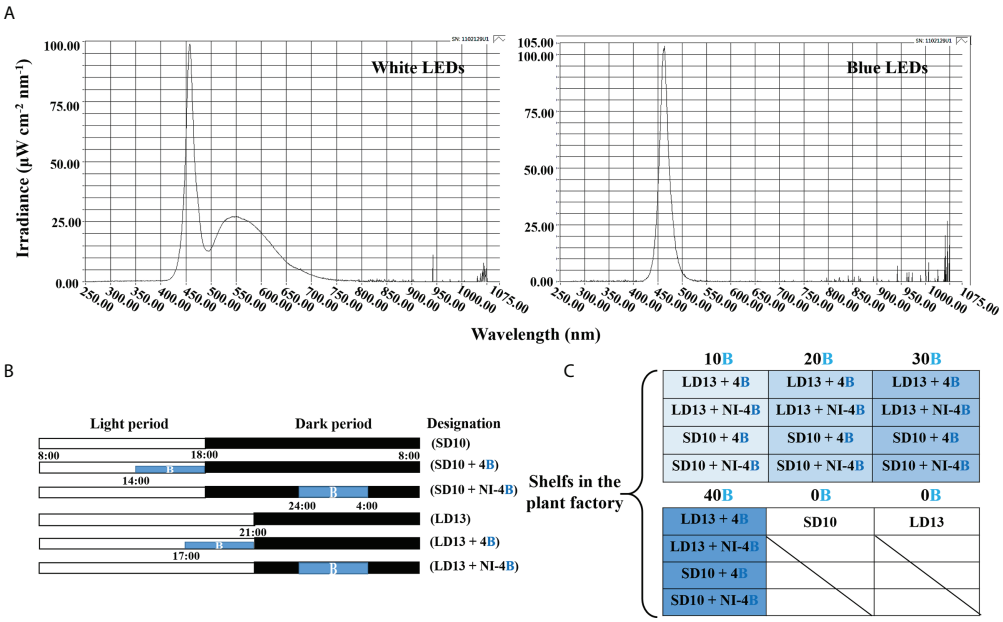

FIGURE 1
The light spectral distribution of experimental light treatments **(A)**: the daily white light (~400-720 nm, and peaked at 435 nm) provided by white LEDs and blue light (peaked at 450 nm) from blue LEDs used as the supplemental or night-interruptional light. The experimental light schemes employed in this study **(B)**: the light period started and the dark period ended at everyday 8:00 a.m.; plants in the control groups were with a 10-h short-day (SD10, positive control) or 13-h long-day (LD13, negative control) condition, without any blue light; the 4-h blue light with either 10, 20, 30, or 40 μmol·m^{-2}·s^{-1} PPFD of intensities was used to (1) supplement the white light at the end of the SD10 (SD10 + 4B) and LD13 (LD13 + 4B) or (2) provide night-interruption (NI) in the SD10 (SD10 + NI-4B) and LD13 (LD13 + NI-4B). B, blue light. The experimental layout in the plant factory **(C)**: for each treatment, three replications (eight plants/replication) were located alone in an opaque compartment; the 0B, 10B, 20B, 30B, and 40B refer to the blue light with intensities of either 0, 10, 20, 30, or 40 μmol·m^{-2}·s^{-1} PPFD.

9:00 a.m., an hour after the daily photoperiodic treatments began, the greatest stomatal opening was usually observed due to the highest photoperiodic rates. The top fourth leaves in the main stem counting from the apex (the fully expanded mature leaves) were selected from the individual plant as a biological replicate, and for each experiment, two technical and six biological replicates were performed. The excised leaf circular segments (diameter = 1 cm) were fixed at 4°C for 24 ~ 48 h in the formalin-acetic acid-alcohol (FAA) solution including 50% (*v*/*v*) ethanol, 45% (*v*/*v*) paraformaldehyde, and 5% (*v*/*v*) glacial acetic acid; secondly, dehydration in a graded series of ethanol solutions (95, 75, 50, 25, and 10% (*v*/*v*) ethanol), 15 min in each solution, three times totally; thirdly, decolorization in a mixed solution containing 45% (*v*/*v*) ethanol, 45% (*v*/*v*) acetone, and 10% (*v*/*v*) distilled water at 4°C for 24~48 h incubation; finally, mounted the treated sample slices on glass slides and leaf abaxial side was observed with an optical microscope (ECLIPSE Ci-L, Nikon Corporation, Tokyo, Japan) (stomatal density, magnification 20×; length and width of stomatal pores, magnification 40×), and analyzed with ImageJ (ImageJ 1.48v, NIH, USA). Additionally, the stomatal density was measured according to Sack and Buckley's description (Sack and Buckley, 2016), while the length and width of stomatal pores were defined by Chen et al. (2012).

Chlorophyll content

Leaf chlorophyll (Chl) content was determined according to Lichtenthaler and Buschmann (2001). After 60 days of light treatment and at 9:00 a.m., the 0.2 g of fresh leaf samples were collected from the top fourth mature leaves in the main stem counting from the apex and ground using liquid nitrogen and extracted in 2 mL 80% (*v*/*v*) acetone overnight at 4°C until the leaf samples were discolored completely. A UV spectrophotometer (Libra S22, Biochrom Ltd., Cambridge, UK) was used for colorimetry at $A_{663\ nm}$ and $A_{646\ nm}$. The pigment contents were calculated from the following equations: chlorophyll a (Chl a) = 12.25 × A_{663} − 2.79 × A_{646}; chlorophyll b (Chl b) = 21.50 × A_{646} − 5.10 × A_{663}. For each experiment, two technical and six biological replicates were performed.

Measurement of photosynthesis and chlorophyll fluorescence

The net photosynthetic rate (P_n), transpiration rate (T_r), stomatal conductance (G_s), and intercellular CO_2 concentration (C_i) of the top fourth fully expended mature leaves in each plant

were measured by the leaf porometer (SC-1, Decagon Device Inc., Pullman, WA, USA) at the harvest time. Four positions on each leaf were measured and the average result was used. From 9:00 to 11:00 a.m., these parameters were measured in the closed-type plant factory to keep the same steady conditions.

The leaf chlorophyll fluorescence measurements were conducted using a photosystem (Fluor Pen FP 100, Photon Systems Instruments, PSI, Drásov, Czech Republic). Same as above, the top fourth fully expended mature leaves in each plant were selected for these measurements. Leaves were dark-adapted with a leaf clip for 30 min, then a 0.6 s saturating light pulse (3450 μmol·m^{-2}·s^{-1} PPFD) was given to obtain the maximal fluorescence (*F*m) and minimal fluorescence (*F*0). Then, the leaf was light-adapted with 5 min continuous actinic light (300 μmol·m^{-2}·s^{-1} PPFD, similar to the growing condition) with saturating pulses every 25 s, after that, the maximum light-adapted fluorescence (*F*m′) and steady-state fluorescence (*F*s) were recorded. The maximal PSII quantum yield (*Fv*/*F*m) was calculated as *Fv*/*F*m = (*F*m − *F*0)/*F*m (Genty et al., 1989). The actinic light was turned off and a far-red pulse was applied to obtain minimal fluorescence after the PSI excitation (*F*0′). The photochemical efficiency of PSII (*Fv*′/*F*m′) was calculated as *Fv*′/*F*m′ = (*F*m′ − *F*s)/*F*m′. Moreover, the photochemical quenching coefficient (*qP*) was calculated as *qP* = (*F*m′ − *F*s)/(*F*m′ − *F*0′) (Roháček, 2002). For each experiment of photosynthesis or chlorophyll fluorescence, two technical and six biological replicates were performed.

Accumulation of carbohydrates and soluble proteins

Weighed −80°C stocked leaf samples of 0.3 g, which were harvested at 10:00 p.m. after 60 days of light treatment, and measured the contents of starch and soluble sugar based on the anthrone colorimetric method (Loewus, 1952; Yemm and Willis, 1954). For total soluble protein extraction, stocked leaf samples were collected and immediately immersed in liquid nitrogen, then ground into a fine powder over an ice bath. 0.1 g of the powder was homogenized in 50 mM PBS (1 mM EDTA, 1 mM polyvinylpyrrolidone, and 0.05% (*v*/*v*) triton-X, pH 7.0). The resulting mixture was then centrifuged (13,000 rpm, 4 ° C, 20 min) to obtain the supernatant that would be used afterward for the total protein estimation and enzyme activity assay. The total protein estimations were conducted by Bradford (1976). In addition, the contents of soluble sugars, starch, and soluble proteins were measured with a UV spectrophotometer (Libra S22, Biochrom Ltd., Cambridge, UK) at $A_{630\ nm}$, $A_{485\ nm}$, and $A_{590\ nm}$, respectively. For each experiment, two technical and six biological replicates were performed.

Enzyme activities

The total protein solution obtained from the previous step was used to analyze the enzymatic activities and measured through a UV spectrophotometer (Libra S22, Biochrom Ltd., Cambridge, UK). For each enzymatic measurement, two technical and six biological replicates were performed. The sucrose synthase (SS) and sucrose phosphate synthase (SPS) were determined in a 1-mL reaction mixture containing a 500 μL enzyme extract at 34°C for 1 h. A 300 μL 30% (*v*/*v*) KOH was added to this mixture and was then placed in a water bath at 100° C for 10 min, after which it was gradually cooled to room temperature. The mixture was subjected to incubation at 40°C for 20 min after a 200 μL 0.15% (*v*/*v*) anthrone–sulfuric acid solution was applied and the enhancement of $A_{620\ nm}$ was monitored. The phosphoenolpyruvate carboxykinase (PEPC) was assayed in a 1 mL reaction mixture consisting of 50 mM Tris-HCl (pH 8.0), 5 mM $MnCl_2$, 2 mM DTT, 10 mM $NaHCO_3$, 0.2 mM NADH, 5 unit NAD-MDH, and a 160 μL enzyme extract. The reaction was initiated by adding 2.5 mM phosphoenolpyruvate (PEP). The phosphoenolpyruvate phosphatase (PEPP) was determined in a 1.5 mL reaction mixture containing 100 mM imidazole-HCl (pH 7.5), 50 mM KCl, 10 mM $MgCl_2$, 0.05% (*w*/*v*) BSA, 2 mM DTT, 150 μM NADH, 1 unit LDH, 2 mM ADP, and a 150 μL enzyme extract. The reaction was initiated with 2 mM PEP, and the increase in the $A_{412\ nm}$ was monitored. The Ribulose 1,5-diphosphate carboxylase/oxygenase (RuBisCO) total activity was measured by injecting 100 μL of the supernatant into 400 μL of an assay mixture consisting of 50 mM Tris-HCl (pH 8.0), 5 mM DTT, 10 mM $MgCl_2$, 0.1 mM EDTA, and 20 mM $NaH_{14}CO_3$ (2.0 GBq mmol^{-1}) at 30°C. After a 5-min activation period, the reaction was initiated *via* the addition of RuBP to 0.5 mmol L^{-1} and was terminated after 30 s with 100 μL of 6 mol L^{-1} HCl. Moreover, the activities of soluble starch synthase (SSS), adenosine diphosphate glucose pyro-phosphorylase (ADPGPPase) and uridine diphosphate glucose pyro-phosphorylase (UDGPPase) were measured according to the protocol described by Doehlert et al. (1988) and Liang et al. (1994). The above description of enzymatic activities was conducted in accordance with the directions provided by Yang et al. (2012) and Feng et al. (2019).

Real-time quantitative PCR verification

Total RNA was extracted using an RNeasy Plant Mini Kit (Takara Bio Inc., Tokyo, Japan), and treated with RNase-free DNase (Takara Bio Inc., Tokyo, Japan) according to the manufacturer's instructions. A PrimeScript ® Reverse Transcriptase (Takara Bio Inc., Tokyo, Japan) was used to

synthesize cDNA from 1 μg of total RNA, in accordance with the manufacturer's instructions. The cDNA was diluted 10-fold, and 5 μL was used in 15-μL quantitative RT-PCR (qRT-PCR) reactions with SYBR Premix Ex Taq™ II (Takara Bio Inc., Tokyo, Japan), performed in a Roche Light Cycler 96 real-time fluorescence quantitative PCR instrument (Roche, Basel, Switzerland). The $2^{-\Delta\Delta Ct}$ method (Livak and Schmittgen, 2001) was used to determine the relative expression levels of each gene. The chrysanthemum homologues of *Arabidopsis* were written as "*Cm* + *gene*" in our study. Data were averagely normalized against the expression of *CmACTIN* and *CmEF1α* (elongation factor 1α) reference genes (Gu et al., 2011; Higuchi et al., 2012). The primer sequences and PCR conditions used in the analyses were listed in Table 1. For each experiment, two technical and six biological replicates were performed.

Statistical analysis

In our study, all plants were randomly sampled. The data were processed, plotted, and statistically analyzed in Excel 2016 and DPS software package (DPS for Windows, 2009). Significant differences among the treatments were assessed by an analysis of variance (ANOVA), followed by Duncan's multiple range test at a probability (p) ≤ 0.05 with a statistical program (SAS, Statistical Analysis System, V. 9.1, Cary, NC, USA). The differences between each treatment were tested by Student's t-test (p) ≤ 0.05. Fisher's least significant difference test was used for the *F*-test between treatments. Moreover, the experimental assays used to obtain all results were repeated six times and were presented as the mean ± standard error.

Results

Flowering and growth parameters

In our study, the supplemental B (S-B) or night-interruptional B (NI-B) light with various intensities significantly affected the photoperiodic flowering and morphology of chrysanthemums in photoperiodic treatments. Firstly, the most interesting part is the flowering of chrysanthemums under different intensities of S-B or NI-B, after 60 days of exposure to the photoperiodic light treatments. At the harvested stage, except for LD13 (the negative control) and LD13 + NI-4B (40), these SDPs under various treatments all flowered to varying degrees (Figure 2A) but later than those grown under SD10 condition, especially the SD10 + 4B (40) or + NI-4B (40), LD13 + 4B (40), and LD13 + NI-4B (10, 20, or 30) treatments markedly delayed the date to the first visible flower buds (Figure 2C). Regardless of the photoperiodic conditions, the flowering pattern in response to the intensity of S-B or NI-B was presented consistently: gradually promoted from 10 to 30 μmol m^{-2} s^{-1} PPFD while inhibited by 40B in different degrees (Figure 2A). No matter the B light as the supplementary or NI in the SD conditions, it did no significant difference in the total flower number per plant with the same light intensity. While in LD conditions, when compared with the NI-B, the S-B with any intensity obviously increased the total number of blooming flowers and flower buds, especially the LD13 + 4B (30) led to the most flower number, however, the LD13 + NI-4B (10, 20, or 30) notably decreased flowers, until LD13 + NI-4B (40) completely inhibited flowering in chrysanthemums (Figure 2D).

TABLE 1 The primers and PCR conditions used to quantify the gene expression levels.

Name	AccessionNumber	Forward Primer(5' to 3')	Reverse Primer(5' to 3')
CmACTIN	AB205087	GATGACGCAGATCATGTTCG	AGCATGTGGAAGTGCATACC
CmEF1α	AB548817	CTTGTTGCTTGATGACTGTGG	CTTGTTGCTTGATGACTGTGG
CmTFL1	AB839767	CCATCATCAAGGCACAATTTCA	TTTCCCTTTGGCAGTTGAAGAA
CDM111	AY173054	GGTCTCAAGAATATTCGCAC	TCATTAGTCATCCCATCAGC
CmAFL1	AB451218	CAAGCTCAACCATCAATAGTC	TGCAGCACATGAACGAGTAG
CmFL	AB451217	CATTGATGCCATATTTAACTC	ACACGGATCATTCATTGTATA
CmFTL1	AB679270	AATCGTGTGCTATGAGAGCC	GCTTGTAACGTCCTCTTCATGC
CmFTL2	AB679271	ATGTGTTATTCCGGCAATTGGGTCG	AAATATGCATTTGTAACGTCATGTG
CmFTL3	AB679272	GGGAAAGTGGATTTGGTGGACG	GTCTTACAATTTGGTACTGTCG
CmAFT	AB839766	CAAGCAAAAAGCAAGGCAATCA	CAACCGGTAACCCCAAGTCATT
CmPHYA	AB733629	TGGAAGCAGTATGGATGCAA	TCGCAGGTATTGCACATCTC
CmPHYB	AB733630	TCCAAGAGGGTCATTTGGAG	ACCTGGCTAACCACAGCATC
CmCRY1	NM-116961	CGTAAGGGATCACCGAGTAAAG	CTTTTAGGTGGGAGTTGTGGAG
PCR Conditions		PCR was performed with an initial denaturing step at 95°C for 5 min, followed by 40 cycles at 95°C for 5 s, 60°C for 20 s, 72°C for 30 s, and 72°C for 10 min to final extension. Fluorescence was quantified after the incubation at 72°C.	

Secondly, we also investigated how the morphology of chrysanthemums in response to the intensity of S-B or NI-B in photoperiodic light treatments. As shown in Figures 2B, E, the plants grown in LD conditions are usually higher than those in SD environments, especially the LD13 caused the highest plants during all treatments. In LDs, applied various intensities of S-B or NI-B non-differently and slightly shortened the shoot height than LD13. However, there were no significant differences in shoot height among all plants which were grown under SD conditions. Moreover, our results showed that the B light benefitted in improving the stem diameter, especially in the LD conditions, the thickest stems were observed in 30 or 40B, regardless of the S-B or NI-B (Figure 2F). Additionally, the LD conditions appeared to be more favorable to the formation of leaves and branches than SDs, and the non-flowered treatments of LD13 and LD13 + NI-4B (40) resulted in the most branches and leaves among all treatments. Moreover, no matter the B light as the supplementary or NI in photoperiodic treatments, similar changing patterns in the number of leaves and branches were observed under different blue light intensities: more flowers and fewer branches or leaves (Figures 2G, H), which was shown a kind of competitive relationship between flower induction with leaf or branch formation.

Stomata characteristics

Figure 3 shows the effects of S-B or NI-B intensity on the stomatal traits of chrysanthemums in photoperiodic treatments, and a notable interaction was observed for the different stomatal parameters. SD10 + NI-4B (30 or 40), LD13 + 4B or + NI-4B (30 or 40) significantly increased the stomatal density, followed by SD10 + 4B (30 or 40), however, it did not differently respond to the 0, 10, or 20 μmol m^{-2} s^{-1} PPFD of S-B or NI-B in both LDs and SDs (Figures 3A, C). Moreover, the stomatal aperture parameters were also influenced by different light treatments but mainly responded to the B light intensity. SD10 and LD13 led to the minimum stomatal aperture width and length, and then the second smallest aperture width was observed in SD10 + 4B (10 or 20), other treatments all obviously promoted stomatal opening, especially the 30 and 40B which were caused the greatest stomatal aperture width. There were no significant

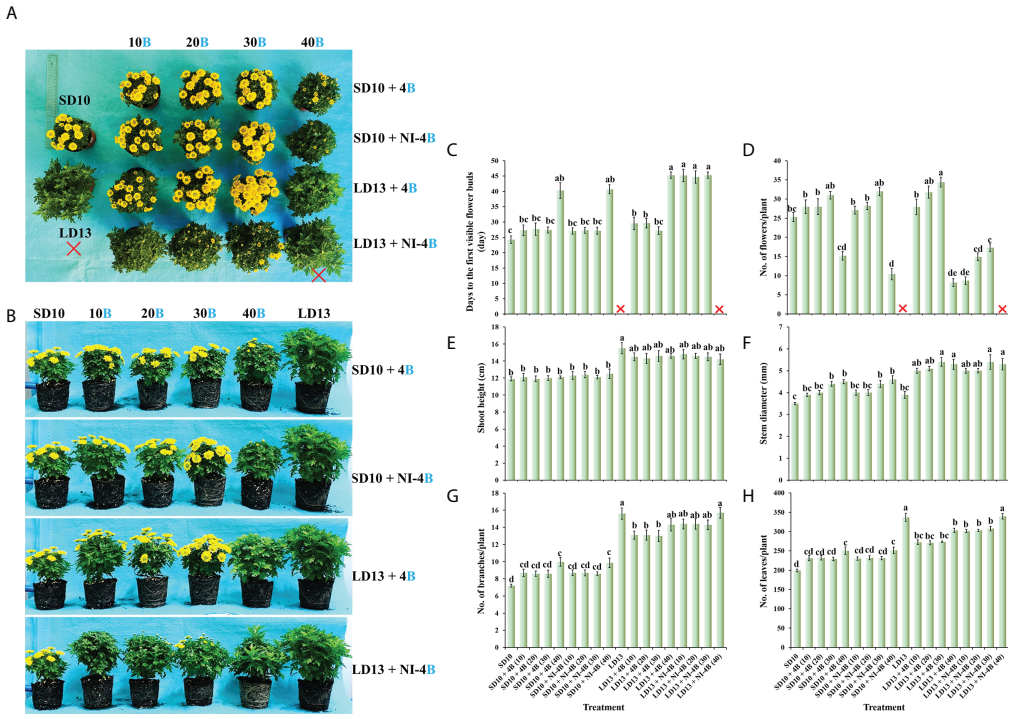

FIGURE 2
The flowering and morphology of chrysanthemum 'Gaya Glory' under different intensities of supplemental or night-interruptional blue light, after 60 days of exposure to the photoperiodic light treatments: the top view **(A)**, side view **(B)**, the days to the first visible flower buds **(C)**, the number of flowers per plant **(D)**, shoot height **(E)**, stem diameter **(F)**, the number of branches per plant **(G)**, and the number of leaves per plant **(H)**. The red cross, the non-flowered treatment. Vertical bars indicate the means ± standard error (n = 6). Different lowercase letters indicate significant separation within treatments by Duncan's multiple range test at $p \leq 0.05$. See Figure 1 for details of photoperiodic light treatments with blue light.

10.3389/fpls.2022.981143

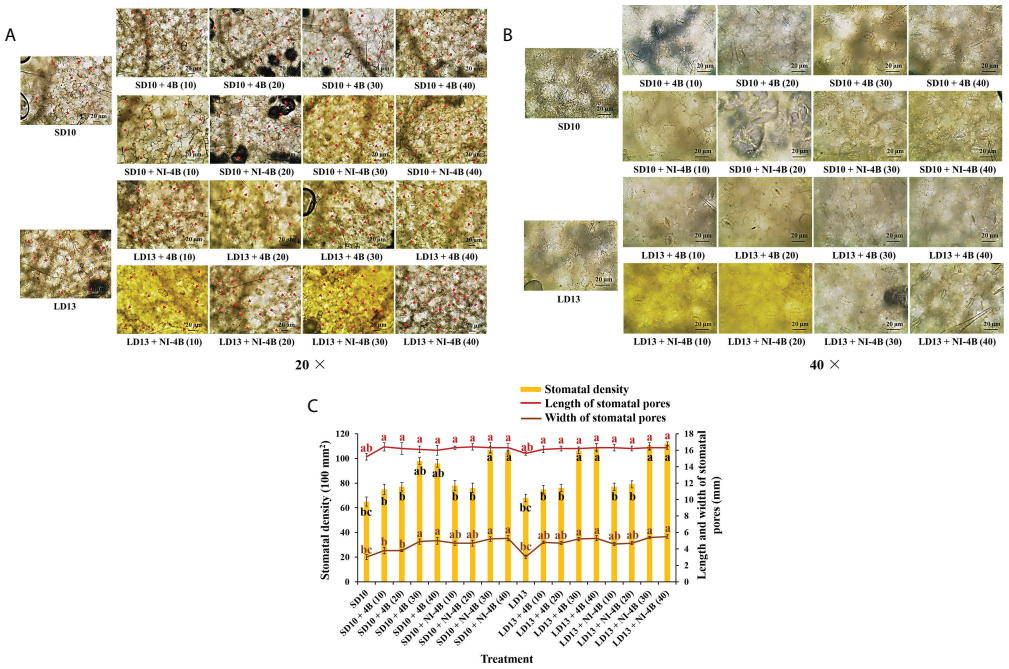

FIGURE 3
The stomatal traits of chrysanthemum 'Gaya Glory' under different intensities of supplemental or night-interruptional blue light, after 60 days of exposure to the photoperiodic light treatments: the micrographs of stomatal density (magnification 20×) **(A)** and specific state of stomatal pores (magnification 40×) **(B)**; the analysis chart **(C)** of stomatal density and pores. The red arrows indicate the locations of stomata in Figure **(A)** Bars indicate 20 μm in Figures A and **(B)** Vertical bars indicate the means ± standard error (n = 6). Different lowercase letters indicate significant separation within treatments by Duncan's multiple range test at $p \leq 0.05$. See Figure 1 for details of photoperiodic light treatments with blue light.

effects of S-B or NI-B intensity and photoperiods on stomatal aperture length (Figures 3B, C).

Chlorophyll content

Different intensities of S-B or NI-B in photoperiodic treatments significantly affected the leaf Chl content and the value of Chl a/b. From our results in Figure 4A, LD conditions promoted more Chl accumulation than SDs. Chl a was more sensitive than Chl b in response to the S-B or NI-B intensity, and the 30 and 40B usually caused the most Chl a, followed by 10 and 20B, while 0 μmol m^{-2} s^{-1} PPFD of B light resulted in the minimum content of Chl a. The content of Chl b was comparatively stable under photoperiodic treatments and showed non-difference within 10, 20, 30, and 40B but always higher than 0B, though this promotion was slightly obvious in LD conditions. Thus, the changing pattern of Chl a + b was the same as Chl a. Similar to the changing trend of Chl a content, the Chl a/b ratios also increased by 30 and 40B, and then were 10 and 20B, however, the overall change tends to be more moderate and with little difference (Figure 4B).

Photosynthetic index and chlorophyll fluorescence

In photoperiodic treatments, the various intensities of S-B or NI-B signally affected the photoperiodic indexes, such as *Pn*, *Tr*, *Gs*, and *Ci* (Table 2). The 30 and 40B interacted with the NI in LDs significantly increased the *Pn*, followed by LD13 + 4B (30 or 40), and LD13 + 4B or + NI-4B (10 or 20) did no difference in *Pn* promotion, but always better than 0B. The changing pattern of *Pn* in SDs was shown that SD10 + 4B and + NI-4B (30 or 40) ≥ SD10 + 4B and + NI-4B (10 or 20) > SD10. And this promotion on *Pn* was more obvious in LD conditions. Moreover, other photosynthetic indexes (*Tr*, *Gs*, and *Ci*) were highly related to the stomatal state and mainly responded to the B light intensity. Consistent with the changing patterns of stomatal density and aperture width (Figure 3C), the 30 and 40B of supplementary or NI always induced the greatest values of *Tr*, *Gs*, and *Ci*, and then were 10 and 20B, 0B always resulted in the lowest values of those, regardless of the photoperiods.

Furthermore, the intensity of S-B or NI-B in photoperiodic treatments also influenced chlorophyll fluorescence parameters in chrysanthemums (Table 2). A similar trend of *Fv*/*Fm*, *Fv*'/

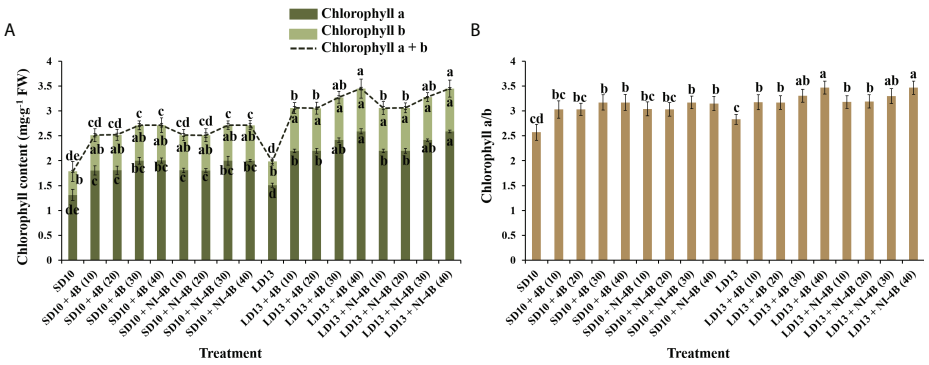

FIGURE 4
The effects on the chlorophyll content of chrysanthemum 'Gaya Glory' under different intensities of supplemental or night-interruptional blue light, after 60 days of exposure to the photoperiodic light treatments: the contents of chlorophyll a, b, and a + b **(A)** and chlorophyll a/b **(B)**. Vertical bars indicate the means ± standard error (n = 6). Different lowercase letters indicate significant separation within treatments by Duncan's multiple range test at $p \leq 0.05$. See Figure 1 for details of photoperiodic light treatments with blue light.

*F*m', and *qP* was observed, from highest to lowest: LD13 + NI-4B (30 or 40) = LD13 + 4B (30 or 40) = SD10 + NI-4B (30 or 40) = SD10 + 4B (30 or 40) ≥ LD13 + NI-4B (10 or 20) = LD13 + 4B (10 or 20) ≥ SD10 + NI-4B (10 or 20) = SD10 + 4B (10 or 20) > LD13 ≥ SD10. Our results showed that applying 30 or 40 μmol m^{-2} s^{-1} PPFD of B light, especially in LD conditions significantly improved the light energy conversion efficiency of the PSII reaction center and enhanced the actual light energy capture efficiency. Eventually, LD13 + 4B or + NI-4B (30 or 40) led to the greater *P*n among all treatments.

Plant dry mass, accumulation of carbohydrates and soluble proteins

The plant dry mass, accumulation of carbohydrates and soluble proteins differently responded to the intensity of S-B or NI-B in photoperiodic treatments (Figure 5). The chrysanthemums under LD conditions generally represented the obvious higher plant dry mass and contents of starch and soluble proteins than SDs, while the changing pattern of soluble sugar content in response to the photoperiods was not significant. Furthermore, the intensity of S-B or NI-B in photoperiodic treatments differently increased the accumulation of organic nutrients, 40B and 30B performed the best, followed by 20B and 10B, and always better than 0B, regardless of the photoperiods.

Enzyme activities

We further investigated the activities of carbohydrate synthesis and photosynthesis-related enzymes in chrysanthemums to explore the response to various intensities of S-B or NI-B in photoperiodic treatments (Figure 6). In general, regardless of the photoperiods, S-B, or NI-B, the sucrose synthesis-related enzymes (sucrose synthase (SS), sucrose phosphate synthase (SPS), phosphoenolpyruvate carboxykinase (PEPC), and phosphoenolpyruvate phosphatase (PEPP)) and starch synthesis-related enzymes (soluble starch synthase (SSS), adenosine diphosphate glucose pyro-phosphorylase (ADPGPPase), and uridine diphosphate glucose pyro-phosphorylase (UDGPPase)) were mainly responded to the intensity, still, the 30B and 40B were the best-performing intensities while the promotion in enzymatic activity of 10B and 20B were slightly weak (Figures 6A-D). A similar response of total activities (both activated and non-activated) of Ribulose 1,5-diphosphate carboxylase/oxygenase (RuBisCO) to B light intensity was performed as above, while the promotion of 30B and 40B was more obvious in LD conditions (Figure 6E).

Expression level of photoreceptors and flowering-related genes

To study the tissue-specific expression patterns of flowering-related genes in *C. morifolium*, the chrysanthemum homologues of *Arabidopsis*: the anti-florigenic *TFL1/CEN*-like gene (*CmTFL1*) (Higuchi et al., 2013), and three well-characterized floral meristem identity genes *APETALA1* (*CDM111*), *FRUITFULL* (*CmAFL1*), and *LEAFY* (*CmFL*) (Shchennikova et al., 2004; Li et al., 2009) were selected and analyzed by qRT-PCR in leaves and shoot apexes, respectively (Figure 7A). After 60 days of exposure to the photoperiodic light treatments, at the harvest stage, these floral forming-related genes were all highly expressed in shoot apices, in contrast, the extremely lower or barely detectable expression was observed in leaves. The expression of the anti-florigenic gene *CmTFL1* was generally higher in LD conditions than in SDs. And highly expressed in

TABLE 2 The photosynthetic and chlorophyll fluorescence characteristics of chrysanthemum 'Gaya Glory' under different intensities of supplemental or night-interruptional blue light, after 60 days of exposure to the photoperiodic light treatments.

Photoperiod (I)	Blue light treatment (II)	Blue light intensity (III)	*Pn*[1] (μmol CO_2 $m^{-2}·s^{-1}$)	*Tr*[2] (mmol H_2O $m^{-2}·s^{-1}$)	*Gs*[3] (mol H_2O $m^{-2}·s^{-1}$)	*Ci*[4] (μmol CO_2 mol^{-1})	*Fv*/*Fm*[5]	*Fv*′/*Fm*′[6]	*qP*[7]
SD10	None	0	12.98 ± 0.12e[8]	1.49 ± 0.02c	0.38 ± 0.012c	323.23 ± 2.12b	0.77 ± 0.011bc	0.41 ± 0.008c	0.39 ± 0.002cd
	+ 4B	10	16.54 ± 0.34d	1.79 ± 0.04b	0.58 ± 0.010b	412.17 ± 3.14ab	0.83 ± 0.017ab	0.56 ± 0.003ab	0.51 ± 0.003b
		20	16.72 ± 0.27d	1.80 ± 0.03b	0.60 ± 0.013b	413.03 ± 1.56ab	0.83 ± 0.009ab	0.55 ± 0.007ab	0.53 ± 0.004b
		30	18.43 ± 0.36cd	2.09 ± 0.01ab	0.79 ± 0.009a	472.14 ± 3.79a	0.87 ± 0.013a	0.59 ± 0.010a	0.55 ± 0.004ab
		40	18.67 ± 0.41cd	2.10 ± 0.03ab	0.81 ± 0.014a	469.99 ± 4.23a	0.88 ± 0.017a	0.58 ± 0.009a	0.56 ± 0.011ab
	+ NI-4B	10	16.31 ± 0.23d	1.80 ± 0.04b	0.60 ± 0.010b	411.16 ± 2.31ab	0.83 ± 0.010ab	0.56 ± 0.014ab	0.52 ± 0.010b
		20	16.27 ± 0.20d	1.78 ± 0.02b	0.61 ± 0.009b	413.01 ± 2.47ab	0.84 ± 0.024ab	0.56 ± 0.011ab	0.52 ± 0.009b
		30	18.79 ± 0.34cd	2.11 ± 0.01ab	0.80 ± 0.007a	473.56 ± 3.01a	0.87 ± 0.012a	0.59 ± 0.008a	0.56 ± 0.005ab
		40	18.83 ± 0.47cd	2.10 ± 0.02ab	0.80 ± 0.014a	479.72 ± 5.23a	0.88 ± 0.015a	0.59 ± 0.005a	0.56 ± 0.010ab
LD13	None	0	19.98 ± 0.56c	1.50 ± 0.01c	0.40 ± 0.011c	367.38 ± 4.38b	0.80 ± 0.014b	0.50 ± 0.004b	0.43 ± 0.004c
	+ 4B	10	21.76 ± 0.60b	1.81 ± 0.03b	0.63 ± 0.007b	411.11 ± 3.79ab	0.84 ± 0.011ab	0.57 ± 0.011ab	0.55 ± 0.007ab
		20	21.51 ± 0.34b	1.80 ± 0.02b	0.63 ± 0.012b	412.09 ± 1.20ab	0.85 ± 0.012ab	0.56 ± 0.009ab	0.55 ± 0.003ab
		30	23.98 ± 0.62ab	2.26 ± 0.04a	0.82 ± 0.010a	473.17 ± 2.00a	0.87 ± 0.013a	0.60 ± 0.003a	0.57 ± 0.006a
		40	24.03 ± 0.11ab	2.27 ± 0.03a	0.81 ± 0.011a	475.03 ± 4.12a	0.87 ± 0.011a	0.59 ± 0.005a	0.58 ± 0.005a
	+ NI-4B	10	21.53 ± 0.24b	1.80 ± 0.01b	0.64 ± 0.008b	410.02 ± 4.07ab	0.85 ± 0.015ab	0.56 ± 0.003ab	0.55 ± 0.007ab
		20	21.64 ± 0.31b	1.79 ± 0.01b	0.65 ± 0.005b	410.17 ± 3.17ab	0.84 ± 0.007ab	0.55 ± 0.004ab	0.56 ± 0.009ab
		30	24.99 ± 0.29a	2.30 ± 0.02a	0.82 ± 0.012a	478.23 ± 4.23a	0.88 ± 0.009a	0.60 ± 0.007a	0.60 ± 0.006a
		40	25.01 ± 0.17a	2.29 ± 0.03a	0.83 ± 0.007a	479.07 ± 5.37a	0.88 ± 0.005a	0.61 ± 0.001a	0.59 ± 0.011a
F-test	I		***	NS	NS	NS	*	**	**
	II		***	***	***	**	**	**	***
	III		**	***	***	**	**	**	**
	I × II		***	**	**	**	**	**	**
	I × III		***	**	**	*	*	*	**
	II × III		***	***	***	***	**	**	**
	I × II × III		***	***	***	***	***	**	***

[1.] Net photosynthetic rate (*Pn*). [2.] Transpiration rate (*Tr*). [3.] Stomatal conductance (*Gs*). [4.] Intercellular CO_2 concentration (*Ci*). [5.] The maximal PSII quantum yield (*Fv*/*Fm*). [6.] The photochemical efficiency of PSII (*Fv*′/*Fm*′). [7.] The photochemical quenching coefficient (*qP*). [8.] Mean separation within columns by Duncan's multiple range test at $p \leq 0.05$ and the values are average ± standard error (n = 6). NS, *, **, and *** mean non-significant or significant at $p \leq 0.05$, 0.01, or 0.001, respectively. See Figure 1 for details of photoperiodic light treatments with blue light.

treatments with significantly inhibited flowering or no flowering, especially in LD13 and LD13 + NI-4B (40) treatments. The general rule of this anti-florigenic gene was: inversely proportional to flowering capacity. The tissue-specific expression patterns of three floral meristem identity genes *CDM111*, *CmAFL1*, and *CmFL* were roughly the opposite of *CmTFL1*, highly expressed in SD10 + 4B, SD10 + NI-4B, and LD13 + 4B treatments, and gradually promoted from 10 to 30

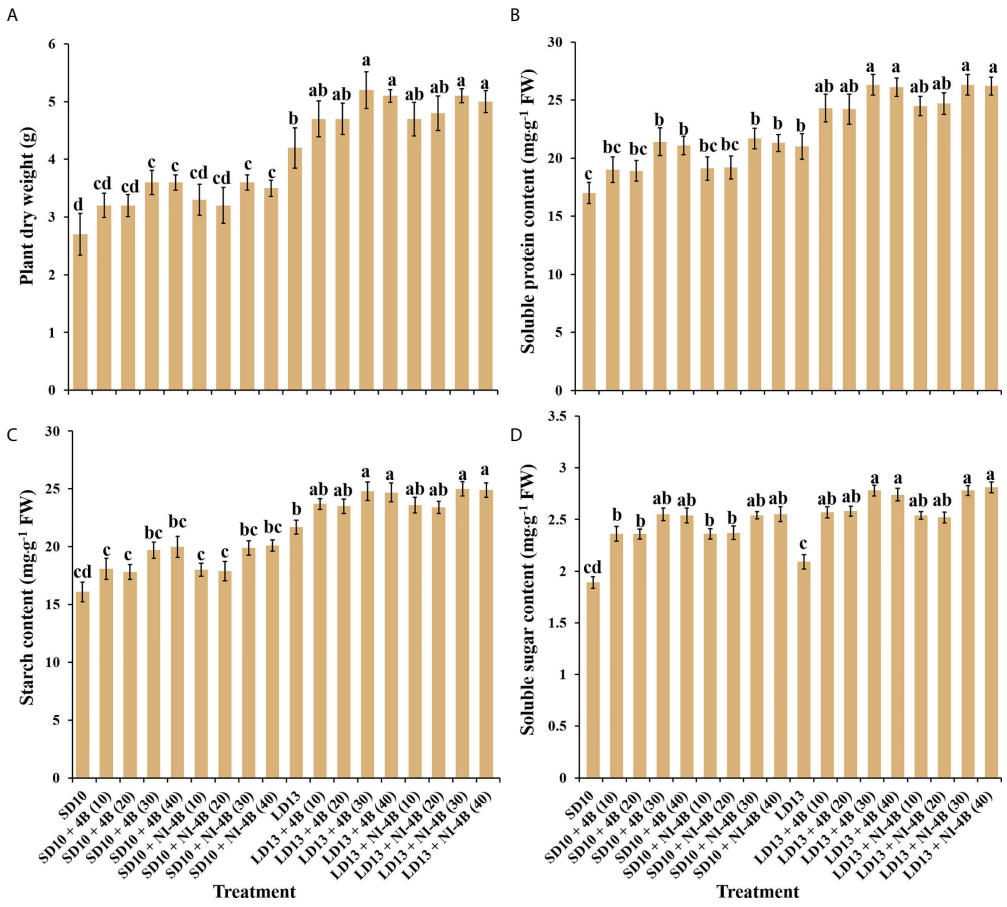

FIGURE 5
The effects on the plant dry weight **(A)**, soluble protein **(B)**, starch **(C)**, and soluble sugar **(D)** contents of chrysanthemum 'Gaya Glory' under different intensities of supplemental or night-interruptional blue light, after 60 days of exposure to the photoperiodic light treatments. Vertical bars indicate the means ± standard error (n = 6). Different lowercase letters indicate significant separation within treatments by Duncan's multiple range test at $p \leq 0.05$. See Figure 1 for details of photoperiodic light treatments with blue light.

μmol m^{-2} s^{-1} PPFD and inhibited by 40B. Moreover, they were generally lower in LD13 + NI-4B and barely expressed in non-flowered LD13 and LD13 + NI-4B (40) treatments. The general rule of these floral meristem identity genes was: proportional to flowering capacity. Overall, these expression levels were correlated with the extent of flower induction in our study (Figure 2A).

The expression pattern of photoreceptor or flowering-related homologues of *Arabidopsis* in *Chrysanthemum morifolium* leaves after 60 days of photoperiodic light treatments were also investigated (Figure 7B). The *FT*-like genes (*CmFTL1*, *CmFTL2*, and *CmFTL3*) (Higuchi et al., 2012; Sun et al., 2017), anti-florigenic FT/TFL1 family *TFL1/CEN/BFT*-like gene (*CmAFT*) (Zhao et al., 2022), and three photoreceptor genes [*Phytochrome A* (*CmPHYA*), *Phytochrome B* (*CmPHYB*), and *Cryptochrome 1* (*CmCRY1*)] (Higuchi et al., 2012; Park et al., 2015) were selected. Their expression patterns can be broadly classified into three types: (1) one florigen gene *CmFTL3* and two photoreceptor genes—*CmPHYA* and *CmCRY1* in *Chrysanthemum morifolium* highly expressed in SD10 + 4B, SD10 + NI-4B, and LD13 + 4B treatments and gradually promoted from 10B to 30B and inhibited by 40B. Moreover, they were generally lower in LD13 + NI-4B and barely expressed in non-flowered LD13 and LD13 + NI-4B (40) treatments; (2) the anti-florigenic gene *CmAFT* and a photoreceptor gene *CmPHYB* were expressed like the expression pattern of *CmTFL1* in Figure 7A, generally higher in LD conditions and highly expressed in treatments with significantly inhibited flowering or no flowering, especially in LD13 and LD13 + NI-4B (40) treatments; (3) The *CmFTL1* and *CmFTL2* were highly expressed in the leaves under flower inductive conditions (LD13 + 4B (10, 20, 30, or 40) and LD13 + NI-4B (10, 20, or 30)), but relatively lower in SD conditions and really poor in non-flowered

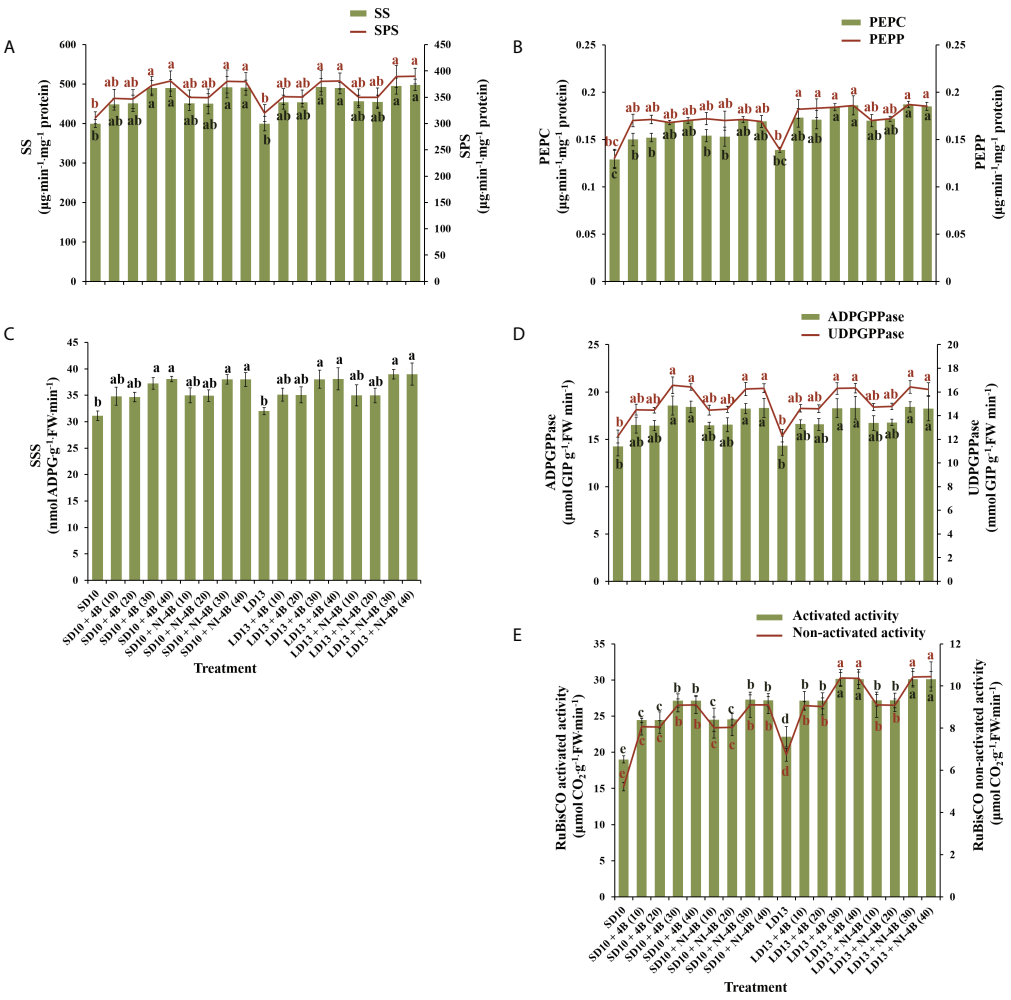

FIGURE 6
The effects on the enzymatic activities of chrysanthemum 'Gaya Glory' under different intensities of supplemental or night-interruptional blue light, after 60 days of exposure to the photoperiodic light treatments. Sucrose synthesis enzymes: **(A)** sucrose synthase (SS) and sucrose phosphate synthase (SPS), **(B)** phosphoenolpyruvate carboxykinase (PEPC) and phosphoenolpyruvate phosphatase (PEPP). Starch synthesis enzymes: **(C)** soluble starch synthase (SSS), **(D)** adenosine diphosphate glucose pyro-phosphorylase (ADPGPPase) and uridine diphosphate glucose pyro-phosphorylase (UDGPPase). And photosynthesis-related enzyme: **(E)** the activated or non-activated activity of Ribulose 1,5-diphosphate carboxylase/oxygenase (RuBisCO). Vertical bars indicate the means ± standard error (n = 6). Different lowercase letters indicate significant separation within treatments by Duncan's multiple range test at $p \leq 0.05$. See Figure 1 for details of photoperiodic light treatments with blue light.

LD13 and LD13 + NI-4B (40) treatments. The constitutive expression of *CmFTL1* and *CmFTL2* in *Chrysanthemum morifolium* leaves revealed weak florigenic activity. *CmFTL1* and *CmFTL2* might function as an LD florigen similar to *RICE FLOWERING LOCUS T1* (*RFT1*) as suggested in rice, a facultative SDP (Komiya et al., 2009).

Because the photoreceptors and flowering-related genes in chrysanthemum have a clear diurnal rhythm and they fluctuate a lot depending on the light or dark conditions. Thus we also studied the temporal expression patterns of *CmFTL1*, *CmFTL2*, *CmFTL3*, *CmAFT*, *CmPHYA*, *CmPHYB*, and *CmCRY1* in leaves of *Chrysanthemum morifolium* (Figure 8). After 7 days of exposure to the photoperiodic light treatments, the top leaves were harvested at 0, 4, 8, 12, 16, 20, and 24h after lights-on (from 8:00 a.m.), respectively. Based on the pattern of curve changes within 24 hours, we roughly divided these seven genes into three groups: (1) one florigen gene *CmFTL3* and two photoreceptor genes—*CmPHYA* and *CmCRY1*; (2) the anti-florigenic gene *CmAFT* and a photoreceptor gene *CmPHYB*; (3) the LD florigen-*RFT1* like genes *CmFTL1* and *CmFTL2*.

Firstly, the expression patterns of *CmFTL3*, *CmPHYA*, and *CmCRY1* expressed similarly *and* showed clear diurnal rhythms,

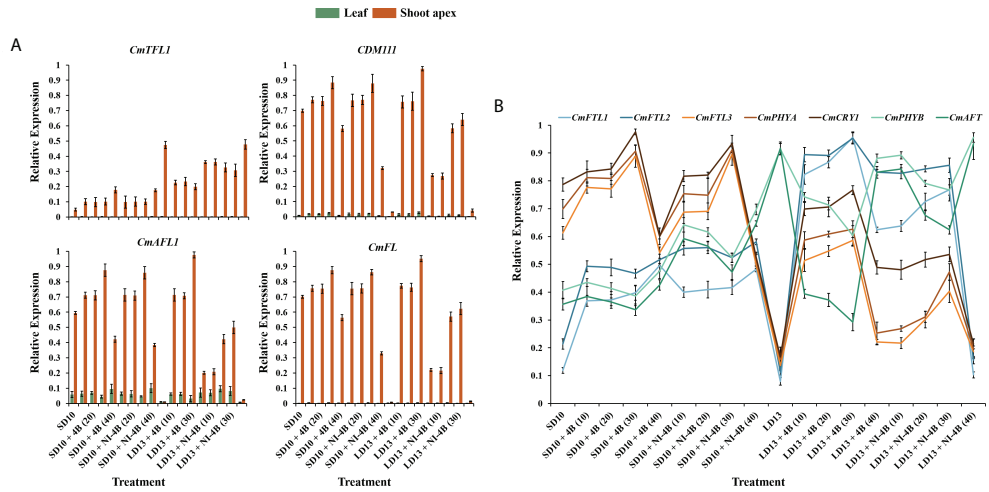

FIGURE 7
Expression patterns of flowering-related genes in chrysanthemum 'Gaya Glory' under different intensities of supplemental or night-interruptional blue light, after 60 days of exposure to the photoperiodic light treatments: **(A)** the tissue-specific expression patterns of flowering-related genes in leaves and shoot apexes and **(B)** the expression levels of flowering or photoreceptor-related genes in leaves. The top leaves (the fourth true leaves from the shoot apex) and shoot apexes were harvested at ZT4 (4 h after lights-on, from 8:00 a.m.) for RNA extraction and RT-PCR. Data were averagely normalized against the expression of *CmACTIN and CmEF1α*. The maximum value in each experiment was set to "1". Vertical bars indicate the means ± standard error of six biological replicates (n = 6), using RNA from separate plants. See Figure 1 for details of photoperiodic light treatments with blue light.

which dropped to a low point at the beginning of the lights-on periods (4 h or 8 h after lights-on in SD and LD conditions), and peaked at the beginning of the NI-B (16 h after lights-on in LDs) or at the end of the NI-B (20 h after lights-on in SDs). Moreover, the expression of those three genes was highest under SD conditions, lowest under LD13 and LD13 + NI-4B conditions, and intermediate under LD13 + 4B conditions. Secondly, the expression patterns of *CmAFT* and *CmPHYB* peaked at the beginning of the S-B (4 h or 8 h after lights-on in SD or LD conditions, respectively) and dropped to a low point at the beginning of the NI-B (16 h after lights-on in SDs) or at the end of the NI-B (20 h after lights-on in LDs). Both *CmAFT* and *CmPHYB* were highly expressed in LD conditions. The expression of *CmAFT* was scattered between treatments, and the highest expression levels were observed in non-flowered treatments LD13 and LD13 + NI-4B (40). Thirdly, the expression patterns of *CmFTL1* and *CmFTL2* were similar, the expression was higher under the flower-inducted treatments in LD conditions, lower under non-flowered LD13 and LD13 + NI-4B conditions, and intermediate under SD conditions. And they peaked at the beginning of the NI-B (16 h after lights-on in LDs) or at the end of the NI-B (20 h after lights-on in SDs). Furthermore, the expression of both *CmFTL3* and *CmAFT* was regulated by the light-signalling-mediated gene *CmPHYB*, up-regulated *CmAFT*, and down-regulated *CmFTL3*, which also strengthened our confidence in photoperiodic flowering regulated by photoreceptor-mediated control.

Discussion

The growth and physiology of chrysanthemum plant in response to intensity of supplemental or night-interruptional blue light in photoperiodic treatments

Light affects plant growth and development by lighting duration (photoperiod), intensity, and quality (Kami et al., 2010). Within the appropriate range of lighting intensity, the higher daily light integral (DLI) plants receive, the stronger they grow and produce a higher yield. Thus, for greater vegetative growth it is usually better to provide the optimal light intensities over a longer photoperiod (Pearcy, 2000). In SD periods, the non-produced night time is longer than the light duration, and plants tend to spare accumulated sugars by limiting their growth (Gent, 2018). In our current study, compared to SD environments, all LD conditions generally improved plant height (Figure 2E), stem diameter (Figure 2F), total chlorophyll content (Figure 4A), plant dry weight (Figure 5A), soluble protein content (Figure 5B), and starch content (Figure 5C). The photoperiod is not only involved in energy provision but also in the regulation of branch or leaf formation. SDPs only grow nutritionally and do not flower in LD conditions (Garner, 1933). Consistent with our results that the LDs caused more branches and leaves in SDP chrysanthemum (Figures 2G,

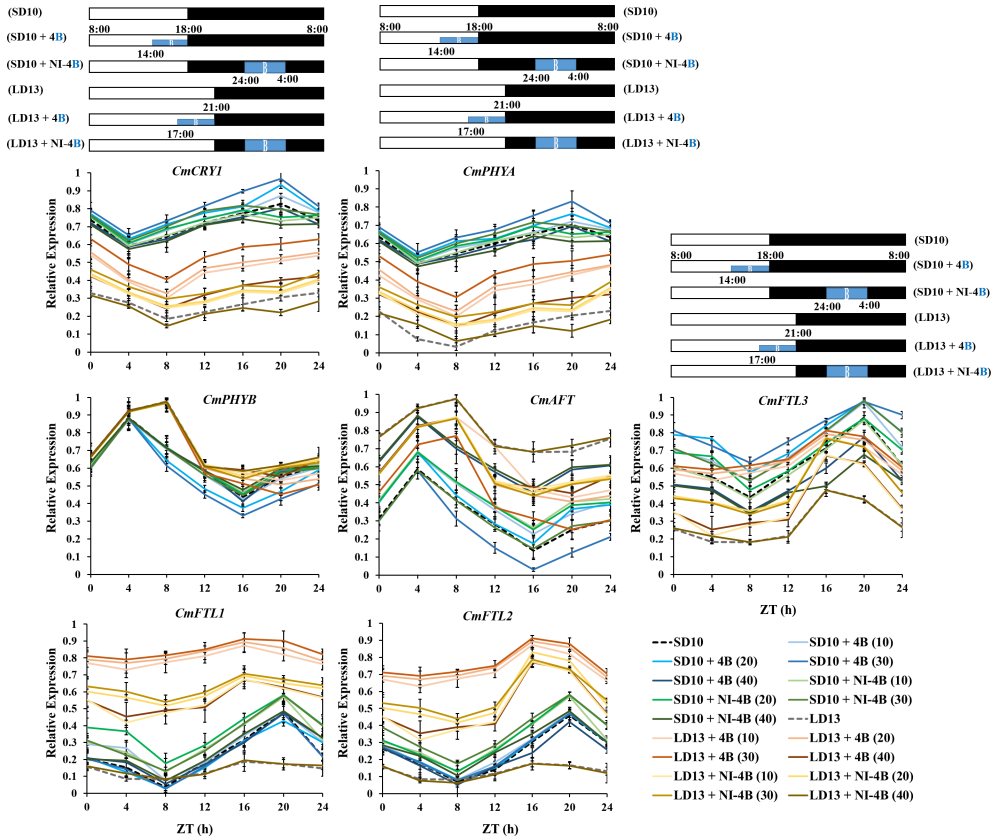

FIGURE 8
The temporal expression patterns of flowering-related genes in leaves of chrysanthemum 'Gaya Glory' under different intensities of supplemental or night-interruptional blue light, after 7 days of exposure to the photoperiodic light treatments. For RNA extraction and RT-PCR, the top leaves (the fourth true leaves from the shoot apex) were harvested at 0, 4, 8, 12, 16, 20, and 24h after lights-on (from 8:00 a.m.), respectively (ZT 0, 4, 8, 12, 16, 20, and 24). The horizontal white and black bars represent the period of day and night, respectively; the blue bars represent the periods with different intensities of supplemental or night-interruptional blue light. Data were averagely normalized against the expression of *CmACTIN and CmEF1α*. The maximum value in each experiment was set to "1". Vertical bars indicate the means ± standard error of six biological replicates (n = 6), using RNA from separate plants. See Figure 1 for details of photoperiodic light treatments with blue light.

H). Moreover, a higher net photosynthetic rate (*P*n) was observed in LD conditions (Table 2), which was due to the continued respiration during the day and night.

Furthermore, the B light effect in plants involves various aspects, such as photoreceptors, signal transduction, pigment biosynthesis, carbon metabolism, nitrogen metabolism, chloroplast development, morphogenesis, and stomatal movement et al. The shortest plants, thickest stems, the best protein content, carbohydrate content, and dry matter quality are usually observed under B light than in other conditions (Xu et al., 2015). In general, B light is required for chlorophyll synthesis, chloroplast formation, high chlorophyll a/b ratio, and high photosynthetic rates in higher plants (Thomas, 1981). B light promotes the *de novo* synthesis of the core protein D1 (QB) protein of the PSII reaction center complex (Richter and Wessel, 1985), thereby promoting photosynthesis. Stomatal conductance, transcript levels of key photosynthetic genes, total soluble sugars and sucrose, and starch content are higher in plants grown under B light than those grown under white light (Wang et al., 2009). Moreover, B light not only activates many enzymes in the carbohydrate synthesis, photosynthetic carbon assimilation and photorespiration, and chlorophyll synthesis pathways, but also induces the synthesis of Rubisco (Hundrieser and Richter, 1982; Roscher and Zetsche, 1986), uridine diphosphate glucose (UDPG) pyrophosphorylase, and PEPC (Kamiya and Miyachi, 1975) to enhance Rubisco and nicotinamide adenine dinucleotide phosphate (NADP)-dependent phosphoglycerate dehydrogenase (Conradt and Ruyters, 1980). Supported by those positive effects of B light in plant growth and development, S-B and NI-B applied in photoperiodic light treatment differently improved those morphological and physiological traits which are mentioned above, and generally, the 30 and 40 μmol m^{-2} s^{-1} PPFD of S-B or NI-B were more

effective in improving chrysanthemum growth and development regardless of the photoperiod. However, the intensity of S-B or NI-B during photoperiodic treatments did non-significant effects on some growth or physiological indexes, such as the shoot height (Figure 2E), stomatal aperture length (Figure 3C), and chlorophyll b content (Figure 4A), which might due to reason of the B light accounting for the proportion of the main white light is too weak. Overall, various intensities of S-B or NI-B applied in photoperiodic light treatments effectively promote the chrysanthemum growth and physiology, while the B light does not work completely alone and interacted with the photoperiod to co-regulate the plant development.

The flowering and branching of chrysanthemum plant in response to the *CmTFL1* under various intensities of supplemental or night-interruptional blue light in photoperiodic treatments

According to Gao et al. (2019), the secondary branching in *Arabidopsis* and the axillary buds in *Chrysanthemum* were all improved by the *CmTFL1* gene, which indicated that the high expression level of *CmTFL1* in stem promoted the development of lateral meristems. Similar phenomena were seen in other species with homologous *TFL1* genes. In *Lolium perenne* L., the *LpTFL1* gene not only recovered the *tfl1* mutant's phenotype but also produced a high number of secondary branches and leaves with better vegetative development (Jensen et al., 2001). Moreover, the *AtTFL1* in *Arabidopsis*, the *PsTFL1* in *Prunus serotine*, and the *LjCEN1* gene in *Lotus japonicas* all increased the number of branches and leaves (Ratcliffe et al., 1998; Guo et al., 2006; Wang and Pijut, 2013). Therefore, the *TFL1* gene shows a conserved function in regulating branching and leafing. Additionally, the constitutive expression of *CsTFL1* was extremely delayed in the flower formation in SD conditions of *Chrysanthemum seticuspe*. Further verified the function of *CmTFL1* with five transgenic lines, and showed that *CmTFL1* functionally affected flower development in *Chrysanthemum morifolium* (Higuchi et al., 2013; Higuchi and Hisamatsu, 2015). Similarly, transgenic *JcTFL1b*-RNAi *Jatropha* consistently presented a relatively early flowering (Li et al., 2017). In our current study, no matter the S-B or NI-B, similar changing patterns in the number of leaves and branches were observed under different blue light intensities: more branches or leaves and fewer flowers (Figures 2G, H). And the expression of *CmTFL1* was generally higher in LD conditions, and highly expressed in treatments with an obvious more number of branches and leaves, especially in LD13 and LD13 + NI-4B (40) treatments (Figure 7A). Overall, the *CmTFL1* gene positively regulates branching and leafing but inhibits flowering, which makes the plant bushier. Therefore, *CmTFL1* can as a candidate gene for regulating both the production and quality of plants.

Chrysanthemum flowering in response to photoreceptor-mediated florigenic and anti-florigenic genes under various intensities of supplemental or night-interruptional blue light in photoperiodic treatments

It is commonly established that inductive photoperiods induce leaves to synthesize a floral stimulus ("florigen"). It has been postulated, nevertheless, that an anti-florigenic signal generated in leaves may control photoperiodic floral induction; the correct day duration would then result in the elimination of an anti-florigen. (Lang and Melchers, 1943; Thomas and Vince-Prue, 1996). AFT, an anti-florigenic FT/TFL1 family protein, was discovered in *Chrysanthemum seticuspe*, and it was convincingly demonstrated that CsAFT protein operates as a systemic floral inhibitor—an anti-florigenic signal generated in leaves under non-inductive circumstances. And the investigation of photoperiodic responses of *CsAFT*-RNAi plants supports the need for the anti-florigenic signal (CsAFT) to sustain the vegetative state (Higuchi et al., 2013). Thus, it is most important for active flowering through the photoperiodic regulation in florigen synthesis, and the *CmPHYB*-mediated anti-florigen *CmAFT* gene also has a predominant role in the obligatory photoperiodic flowering response in chrysanthemum, enabling for strict vegetative maintenance under non-inductive photoperiods (Figures 2A, 7B, and 8). Chrysanthemum is an obligate SDP that remains vegetative in the absence of inductive LD conditions, such as LD13 and LD13 + NI-4B (40) treatments in our study (Figure 2A). Nevertheless, rice (*Oryza sativa*), a facultative SDP, may blossom even in non-inductive LD circumstances. Two florigen genes (*Hd3a* and *RFT1*) of rice are activated depending on the length of the day, and the RFT1 protein is proposed as the LD florigen (Komiya et al., 2009). In the chrysanthemum, *CmFTL1* might similar to *RFT1* in rice and function as an LD florigen gene. It can be assumed that residual *CmFTL3* and increased *CmFTL1* under photoperiod-unfavorable conditions (Figure 7B) eventually make the flowering with various degrees in LD13 + 4B (10, 20, 30, or 40) and LD13 + NI-4B (10, 20, or 30) (Figure 2A). Therefore, the photoperiodic flowering in chrysanthemum should be co-regulated by both florigen and anti-florigen, and the balanced synthesis of both of them determines the flowering response to photoperiodic light treatments.

Flowering-related gene expression investigations in shoot apexes and leaves have improved our understanding of how to control chrysanthemum flowering. Currently, *CsFTL1*, *CsFTL2*, and *CsFTL3* were identified-three chrysanthemum orthologues

of *FT* in *Chrysanthemum seticuspe*, and the expression of *CsFTL3* was observed as a key regulator in chrysanthemum photoperiodic flowering (Oda et al., 2012). In the flower-inductive SD conditions, *CsFTFL3* up-regulated the floral-identity genes to promote flowering events occurring in the SAM (Oda et al., 2012). Moreover, overexpressed *CsFTL3* induced SDP chrysanthemum flowering in LD environments, indicating that *CsFTL3* has the potential to induce chrysanthemum flowering under photoperiod-unfavorable conditions. In the present study, after 60 days of photoperiodic treatments, *CmFTL3* with two photoreceptor genes—*CmPHYA* and *CmCRY1* in *Chrysanthemum morifolium* were highly expressed in SD10 + 4B, SD10 + NI-4B, and LD13 + 4B treatments and gradually promoted from 10B to 30B and inhibited by 40B. Moreover, they were generally lower in LD13 + NI-4B and barely expressed in non-flowered LD13 and LD13 + NI-4B (40) treatments (Figure 7B). Moreover, during the temporal expression patterns of flowering-related genes in chrysanthemum leaves, the expression of *CmFTL3* was down-regulated by the light-signalling-mediated gene *CmPHYB* (Figure 8). All of our results indicate the chrysanthemum photoperiodic flowering is correlated with the photoreceptor-mediated control.

Chrysanthemum flowering in response to co-regulation of photoperiod- and sucrose-mediated regulation under various intensities of supplemental or night-interruptional blue light in photoperiodic treatments

Sugar signaling is crucial for a variety of developmental activities, such as controlling the induction of flowers (Yu et al., 2013; Moghaddam and Ende, 2013; Yang et al., 2013). The most typical sugar produced by plants is sucrose, which is a more transportable substance due to its more stable molecule than either of its monosaccharide components, glucose or fructose. When a leaf of a photosensitive plant is exposed to a single inductive photoperiod, the amount of leaf sucrose increases quickly (Houssa et al., 1991). In *Arabidopsis*, feeding the aerial portion of dark-grown plants sucrose encourages flowering (Ohto et al., 2001). Sucrose produced by photosynthetic activity in *Arabidopsis* plants growing in LD causes *miR156* (Yu et al., 2013; Yang et al., 2013) to be down-regulated, which leads to the accumulation of the SQUAMOSA PROMOTER BINDING PROTEIN-LIKE gene (*SPL*) transcript and increases the expression of *FT* (Wahl et al., 2013). A photoperiod-based transcriptional regulation of florigen cannot fully explain the blooming response of chrysanthemum because the transition from vegetative to reproductive development is closely regulated (Higuchi et al., 2013). In SDP *Chrysanthemum morifolium*, gibberellin and photoperiod pathways cooperate to induce blooming in 'Floral Yuuka' plants growing in short days. Additionally, plants treated with sucrose growing under either an SD or an SD+NB regime continued to accumulate *CmFTL2* transcript (Sun et al., 2017), indicating that in 'Floral Yuuka', both photoperiod and sucrose affect *CmFTLs* transcription. Sugar signaling is more significant under LD circumstances (Ren et al., 2016). These findings imply that in 'Floral Yuuka' plants grown on short days, sucrose signaling may not play a significant role in floral induction. In our results, *CmFTL2* were highly expressed in the leaves under flower inductive conditions (LD13 + 4B (10, 20, 30, or 40) and LD13 + NI-4B (10, 20, or 30)) followed by all SD conditions, but really poor in non-flowered LD13 and LD13 + NI-4B (40) treatments. Moreover, LD13 + 4B (10, 20, or 30) also resulted the higher expression of florigen genes (like *CDM111*, *CmAFL1*, and *CmFL*) (Figure 7B). And, the carbohydrate was also significantly higher in these treatments (Figures 5C, D). Furthermore, the temporal expression pattern of *CmFTL2* was similar to *CmPHYA* and *CmCRY1*, but in contrast to *CmPHYB* (Figure 8). The florigen complex is most likely affected by *CmFTL2* rather than the anti-florigen complex. It is still unknown how *CmFTL2* functions in the regulatory network as well as the specifics of the cross-talk between photoperiod and endogenous sucrose levels during floral induction. The photoperiod- and sucrose-mediated regulation of blooming time in chrysanthemums may be significantly influenced by the sugar-induced *CmFTL2* pathway.

Conclusions

In a conclusion, the S-B or NI-B interacts with the intensity and photoperiod differently affecting the morphology and physiology of the chrysanthemum plant. Generally, 30 μmol m^{-2} s^{-1} PPFD S-B (in both SD and LD conditions) and NI-B (in SD conditions) were more effective in promoting growth, flowering, and the expression of florigen genes. However, 40B leads to the unbalanced expression of florigen or anti-florigen genes, resulting in flowering inhibition, although it also can obviously improve morphological and physiological traits. Our current findings suggest the photoperiodic flowering of SDP chrysanthemum by the co-regulation of carbohydrate accumulation produced by photosynthetic carbon assimilation and the expression of florigen and anti-florigen genes mediated by differential photoreceptors in response to the intensity of S-B or NI-B. Moreover, *CmTFL1* affects chrysanthemum morphologies by promoting branching and leafing but inhibiting flowering. And the photoperiod- and sucrose-mediated regulation of flowering time in chrysanthemums may be significantly influenced by the sugar-induced *CmFTL2*

pathway. Furthermore, the SDP chrysanthemum under LD13 + 4B (10, 20, 30, or 40) and LD13 + NI-4B (10, 20, or 30) conditions might be regulated by the LD florigen-like gene *CmFTL1* and sugar-induced *CmFTL2* eventually make the flowering. Further studies, the molecular mechanisms involved in these photoreceptor-mediated photoperiodic regulatory systems need to be explored in depth.

Data availability statement

The original contributions presented in the study are included in the article/supplementary materials. Further inquiries can be directed to the corresponding author.

Author contributions

JY and BRJ conceived and designed the study. JY and JS performed the experiments. JY analyzed the data and drafted the manuscript. JY and BJ edited and finalized the manuscript. All authors read and approved the submitted version.

Funding

This research received no external funding. Jingli Yang and Jinnan Song were supported by the BK21 Four Program, Ministry of Education, Republic of Korea.

Conflict of interest

The authors declare that the research was conducted in the absence of any commercial or financial relationships that could be construed as a potential conflict of interest.

Publisher's note

All claims expressed in this article are solely those of the authors and do not necessarily represent those of their affiliated organizations, or those of the publisher, the editors and the reviewers. Any product that may be evaluated in this article, or claim that may be made by its manufacturer, is not guaranteed or endorsed by the publisher.

References

Abe, M., Kobayashi, Y., Yamamoto, S., Daimon, Y., Yamaguchi, A., Ikeda, Y., et al. (2005). FD, a bZIP protein mediating signals from the floral pathway integrator FT at the shoot apex. *Science* 309, 1052–1056. doi: 10.1126/science.1115983

Bagnall, D. J., and King, R. W. (2001). Phytochrome, photosynthesis and flowering of *Arabidopsis thaliana*: photophysiological studies using mutants and transgenic lines. *Funct. Plant Biol.* 28, 401–408. doi: 10.1071/PP99123

Biinning, E. (1936). Die endogene tagesrhythmik als grundlage der photoperiodischen reaktion. *Ber. Dtsch. Bot. Ges.* 54, 590–607.

Bradford, M. M. (1976). A rapid and sensitive method for the quantitation of microgram quantities of protein utilizing the principle of protein-dye binding. *Anal. Biochem.* 72 (1-2), 248–254. doi: 10.1016/0003-2697(76)90527-3

Bradley, D., Ratcliffe, O., Vincent, C., Carpenter, R., and Coen, E. (1997). Inflorescence commitment and architecture in *Arabidopsis*. *Sci.* 275, 80–83. doi: 10.1126/science.275.5296.80

Chailakhyan, M. K. (1936). "About the mechanism of the photoperiodic response", In: *Dokl Akad Nauk SSSR)*, 85–89.

Chen, Z. H., Hills, A., Bätz, U., Amtmann, A., Lew, V. L., and Blatt, M. R. (2012). Systems dynamic modeling of the stomatal guard cell predicts emergent behaviors in transport, signaling, and volume control. *Plant Physiol.* 159 (3), 1235–1251. doi: 10.1104/pp.112.197350

Conradt, W., and Ruyters, G. (1980). "Blue light-effects on enzymes of the carbohydrate metabolism in chlorella 2. glyceraldehyde 3-phosphate dehydrogenase (NADP-dependent)," in *The blue light syndrome* (Berlin, Heidelberg: Springer), 368–371.

Conti, L., and Bradley, D. (2007). TERMINAL FLOWER1 is a mobile signal controlling *Arabidopsis* architecture. *Plant Cell* 19, 767–778. doi: 10.1105/tpc.106.049767

Davis, S. J. (2002). Photoperiodism: the coincidental perception of the season. *Curr. Biol.* 12 (24), R841–R843. doi: 10.1016/S0960-9822(02)01348-9

Doehlert, D. C., Kuo, T. M., and Felker, F. C. (1988). Enzymes of sucrose and hexose metabolism in developing kernels of two inbreds of maize. *Plant Physiol.* 86 (4), 1013–1019. doi: 10.1104/pp.86.4.1013

Eckardt, N. A., Snyder, G. W., Portis, A. R. Jr., and Ogren, W. L. (1997). Growth and photosynthesis under high and low irradiance of *Arabidopsis thaliana* antisense mutants with reduced ribulose-1, 5-bisphosphate carboxylase/oxygenase activase content. *Plant Physiol.* 113, 575–586. doi: 10.1104/pp.113.2.575

Fc, L. (1997). The effects of low light level in tomato seedling stage on flowering and fruit growth. *Tianjin. Agr. Sci.* 3, 11–13.

Feng, L., Raza, M. A., Li, Z., Chen, Y., Khalid, M. H. B., Du, J., et al. (2019). The influence of light intensity and leaf movement on photosynthesis characteristics and carbon balance of soybean. *Front. Plant Sci.* 9, 1952. doi: 10.3389/fpls.2018.01952

Franklin, K. A., Praekelt, U., Stoddart, W. M., Billingham, O. E., Halliday, K. J., and Whitelam, G. C. (2003). Phytochromes b, d, and e act redundantly to control multiple physiological responses in *Arabidopsis*. *Plant Physiol.* 131 (3), 1340–1346. doi: 10.1104/pp.102.015487

Gao, Y., Gao, Y., Wu, Z., Bu, X., Fan, M., and Zhang, Q. (2019). Characterization of *TEMINAL FLOWER1* homologs *CmTFL1c* gene from *Chrysanthemum morifolium*. *Plant Mol. Biol.* 99 (6), 587–601. doi: 10.1007/s11103-019-00838-6

Garner, W. W. (1933). Comparative responses of long-day and short-day plants to relative length of day and night. *Plant Physiol.* 8 (3), 347. doi: 10.1104/pp.8.3.347

Garner, W. W., and Allard, H. A. (1920). Effect of the relative length of day and night and other factors of the environment on growth and reproduction in plants. *Mon. Weather. Rev.* 48 (7), 415–415. doi: 10.1175/1520-0493(1920)48<415b:EOTRLO>2.0.CO;2

Gent, M. P. (2018). Dynamic carbohydrate supply and demand model of vegetative growth: response to temperature, light, carbon dioxide, and day length. *Agronomy* 8, 21. doi: 10.3390/agronomy8020021

Genty, B., Briantais, J. M., and Baker, N. R. (1989). The relationship between the quantum yield of photosynthetic electron transport and quenching of chlorophyll fluorescence. *BBA-Gen. Subj.* 990 (1), 87–92. doi: 10.1016/S0304-4165(89)80016-9

Gu, C., Chen, S., Liu, Z., Shan, H., Luo, H., Guan, Z., et al. (2011). Reference gene selection for quantitative real-time PCR in chrysanthemum subjected to biotic and abiotic stress. *Mol. Biotechnol.* 49 (2), 192–197. doi: 10.1007/s12033-011-9394-6

Guo, X., Zhao, Z., Chen, J., Hu, X., and Luo, D. (2006). A putative *CENTRORADIALIS/TERMINAL FLOWER 1*-like gene, *Ljcen1*, plays a role in phase transition in *Lotus japonicus*. *J. Plant Physiol.* 163 (4), 436–444. doi: 10.1016/j.jplph.2005.04.037

Higuchi, Y., and Hisamatsu, T. (2015). CsTFL1, a constitutive local repressor of flowering, modulates floral initiation by antagonising florigen complex activity in chrysanthemum. *Plant Sci.* 237, 1–7. doi: 10.1016/j.plantsci.2015.04.011

Higuchi, Y., Narumi, T., Oda, A., Nakano, Y., Sumitomo, K., Fukai, S., et al. (2013). The gated induction system of a systemic floral inhibitor, antiflorigen, determines obligate short-day flowering in chrysanthemums. *P. Natl. Acad. Sci. U.S.A.* 110 (42), 17137–17142. doi: 10.1073/pnas.1307617110

Higuchi, Y., Sumitomo, K., Oda, A., Shimizu, H., and Hisamatsu, T. (2012). Day light quality affects the night-break response in the short-day plant chrysanthemum, suggesting differential phytochrome-mediated regulation of flowering. *J. Plant Physiol.* 169 (18), 1789–1796. doi: 10.1016/j.jplph.2012.07.003

Houssa, P., Bernier, G., and Kinet, J. (1991). Qualitative and quantitative analysis of carbohydrates in leaf exudate of the short-day plant, *Xanthium strumarium* l. during floral transition. *J. Plant Physiol.* 138, 24–28. doi: 10.1016/S0176-1617(11)80724-8

Huang, N. C., Jane, W. N., Chen, J., and Yu, T. S. (2012). *Arabidopsis thaliana CENTRORADIALIS homologue* (*ATC*) acts systemically to inhibit floral initiation in *Arabidopsis*. *Plant J.* 72, 175–184. doi: 10.1111/j.1365-313X.2012.05076.x

Hundrieser, J., and Richter, G. (1982). Blue light-induced synthesis of ribulosebisphosphate carboxylase in cultured plant cells. *Plant Cell Rep.* 1 (3), 115–118. doi: 10.1007/BF00272367

Jalal-Ud-Din, B., Munir, M., and Abid, M. (2013). Flowering response of facultative short day ornamental annuals to artificial light intensities. *Pak. J. Bot.* 45, 999–1004.

Jensen, C. S., Salchert, K., and Nielsen, K. K. (2001). A *TERMINAL FLOWER1*-like gene from perennial ryegrass involved in floral transition and axillary meristem identity. *Plant Physiol.* 125 (3), 1517–1528. doi: 10.1104/pp.125.3.1517

Jeong, S. W., Park, S., Jin, J. S., Seo, O. N., Kim, G. S., Kim, Y. H., et al. (2012). Influences of four different light-emitting diode lights on flowering and polyphenol variations in the leaves of chrysanthemum (*Chrysanthemum morifolium*). *J. Agric. Food Chem.* 60 (39), 9793–9800. doi: 10.1021/jf302272x

Kami, C., Lorrain, S., Hornitschek, P., and Fankhauser, C. (2010). Light-regulated plant growth and development. *Curr. Top. Dev. Biol.* 91, 29–66. doi: 10.1016/S0070-2153(10)91002-8

Kamiya, A., and Miyachi, S. (1975). Blue light-induced formation of phosphoenolpyruvate carboxylase in colorless *Chlorella* mutant cells. *Plant Cell Physiol.* 16 (4), 729–736. doi: 10.1093/oxfordjournals.pcp.a075193

Kardailsky, I., Shukla, V. K., Ahn, J. H., Dagenais, N., Christensen, S. K., Nguyen, J. T., et al. (1999). Activation tagging of the floral inducer *FT*. *Science* 286, 1962–1965. doi: 10.1126/science.286.5446.1962

Kinet, J. (1977). Effect of light conditions on the development of the inflorescence in tomato. *Sci. Hortic.* 6, 15–26. doi: 10.1016/0304-4238(77)90074-7

Knott, J. E. (1934). Effect of a localized photoperiod on spinach, in. *Proc. Amer. Soc. Hortic. Sci.* 31, 152–154.

Kobayashi, Y., Kaya, H., Goto, K., Iwabuchi, M., and Araki, T. (1999). A pair of related genes with antagonistic roles in mediating flowering signals. *Science* 286, 1960–1962. doi: 10.1126/science.286.5446.1960

Kobayashi, Y., and Weigel, D. (2007). Move on up, it's time for change–mobile signals controlling photoperiod-dependent flowering. *Genes Dev.* 21 (19), 2371–2384. doi: 10.1101/gad.1589007

Komiya, R., Yokoi, S., and Shimamoto, K. (2009). A gene network for long-day flowering activates *RFT1* encoding a mobile flowering signal in rice. *Development* 136 (20), 3443–3450. doi: 10.1242/dev.040170

Lang, A., Chailakhyan, M. K., and Frolova, I. (1977). Promotion and inhibition of flower formation in a day neutral plant in grafts with a short-day plant and a long-day plant. *P. Natl. Acad. Sci. U.S.A.* 74, 2412–2416. doi: 10.1073/pnas.74.6.2412

Lang, A., and Melchers, G. (1943). Die photoperiodische reaktion von *Hyoscyamus niger*. *Planta* 33 (5. H), 653–702. doi: 10.1007/BF01916588

Liang, J. S., Cao, X., Xu, S., Zhu, Q., and Song, P. (1994). Studies on the relationship between the grain sink strength and its starch accumulation in rice (O. *sativa*). *Acta Agron. Sin.* 20, 685–691.

Lichtenthaler, H. K., and Buschmann, C. (2001). Chlorophylls and carotenoids: Measurement and characterization by UV-VIS spectroscopy. *Curr. Protoc. Food Anal. Chem.* 1 (1), F4.3.1–F4.3.8. doi: 10.1002/0471142913.faf0403s01

Li, C., Fu, Q., Niu, L., Luo, L., Chen, J., and Xu, Z. F. (2017). Three *TFL1* homologues regulate floral initiation in the biofuel plant *Jatropha curcas*. *Sci. Rep.* 7 (1), 1–9. doi: 10.1038/srep43090

Li, T., Niki, T., Nishijima, T., Douzono, M., Koshioka, M., and Hisamatsu, T. (2009). Roles of *CmFL*, *CmAFL1*, and *CmSOC1* in the transition from vegetative to reproductive growth in *Chrysanthemum morifolium* ramat. *J. Hortic. Sci. Biotech.* 84 (4), 447–453. doi: 10.1080/14620316.2009.11512547

Livak, K. J., and Schmittgen, T. D. (2001). Analysis of relative gene expression data using real-time quantitative PCR and the $2^{-\Delta\Delta CT}$ method. *Methods* 25 (4), 402–408. doi: 10.1006/meth.2001.1262

Loewus, F. A. (1952). Improvement in anthrone method for determination of carbohydrates. *Anal. Chem.* 24 (1), 219–219. doi: 10.1021/ac60061a050

Mcgarry, R. C., and Ayre, B. G. (2012). Manipulating plant architecture with members of the CETS gene family. *Plant Sci.* 188, 71–81. doi: 10.1016/j.plantsci.2012.03.002

McMahon, M., and Kelly, J. (1999). $CuSO_4$ filters influence flowering of chrysanthemum cv. spears. *Sci. Hortic.* 79 (3-4), 207–215. doi: 10.1016/S0304-4238(98)00208-8

Mimida, N., Goto, K., Kobayashi, Y., Araki, T., Ahn, J. H., Weigel, D., et al. (2001). Functional divergence of the *TFL1*-like gene family in *Arabidopsis* revealed by characterization of a novel homologue. *Genes Cells* 6, 327–336. doi: 10.1046/j.1365-2443.2001.00425.x

Mockler, T. C., Guo, H., Yang, H., Duong, H., and Lin, C. (1999). Antagonistic actions of *Arabidopsis* cryptochromes and phytochrome b in the regulation of floral induction. *Development* 126 (10), 2073–2082. doi: 10.1242/dev.126.10.2073

Mockler, T., Yang, H., Yu, X., Parikh, D., Cheng, Y. C., Dolan, S., et al. (2003). Regulation of photoperiodic flowering by *Arabidopsis* photoreceptors. *P. Natl. Acad. Sci. U.S.A.* 100 (4), 2140–2145. doi: 10.1073/pnas.0437826100

Moghaddam, M. R. B., and Ende, W. V. D. (2013). Sugars, the clock and transition to flowering. *Front. Plant Sci.* 4, 22. doi: 10.3389/fpls.2013.00022

Oda, A., Narumi, T., Li, T., Kando, T., Higuchi, Y., Sumitomo, K., et al. (2012). *CsFTL3*, a chrysanthemum *FLOWERING LOCUS T-like* gene, is a key regulator of photoperiodic flowering in chrysanthemums. *J. Exp. Bot.* 63 (3), 1461–1477. doi: 10.1093/jxb/err387

Ohto, M.-A., Onai, K., Furukawa, Y., Aoki, E., Araki, T., and Nakamura, K. (2001). Effects of sugar on vegetative development and floral transition in *Arabidopsis*. *Plant Physiol.* 127, 252–261. doi: 10.1104/pp.127.1.252

Park, Y. G., and Jeong, B. R. (2019). Night interruption light quality changes morphogenesis, flowering, and gene expression in *Dendranthema grandiflorum*. *Hortic. Environ. Biotechnol.* 60 (2), 167–173. doi: 10.1007/s13580-018-0114-z

Park, Y. G., and Jeong, B. R. (2020). How supplementary or night-interrupting low-intensity blue light affects the flower induction in chrysanthemum, a qualitative short-day plant. *Plants* 9 (12), 1694. doi: 10.3390/plants9121694

Park, Y. G., Muneer, S., and Jeong, B. R. (2015). Morphogenesis, flowering, and gene expression of *Dendranthema grandiflorum* in response to shift in light quality of night interruption. *Int. J. Mol. Sci.* 16 (7), 16497–16513. doi: 10.3390/ijms160716497

Pearcy, R. W. (2000). "Radiation and light measurements," in *Plant physiological ecology* (Dordrecht: Springer), 97–116.

Pittendrigh, C. S., and Minis, D. H. (1964). The entrainment of circadian oscillations by light and their role as photoperiodic clocks. *Am. Nat.* 98 (902), 261–294. doi: 10.1086/282327

Ratcliffe, O. J., Amaya, I., Vincent, C. A., Rothstein, S., Carpenter, R., Coen, E. S., et al. (1998). A common mechanism controls the life cycle and architecture of plants. *Development* 125 (9), 1609–1615. doi: 10.1242/dev.125.9.1609

Ren, L., Liu, T., Cheng, Y., Sun, J., Gao, J., Dong, B., et al. (2016). Transcriptomic analysis of differentially expressed genes in the floral transition of the summer flowering chrysanthemum. *BMC Genomics* 17, 1–15. doi: 10.1186/s12864-016-3024-4

Richter, G., and Wessel, K. (1985). Red light inhibits blue light-induced chloroplast development in cultured plant cells at the mRNA level. *Plant Mol. Biol.* 5 (3), 175–182. doi: 10.1007/BF00015681

Roháček, K. (2002). Chlorophyll fluorescence parameters: the definitions, photosynthetic meaning, and mutual relationships. *Photosynthetica* 40 (1), 13–29. doi: 10.1023/A:1020125719386

Roscher, E., and Zetsche, K. (1986). The effects of light quality and intensity on the synthesis of ribulose-1, 5-bisphosphate carboxylase and its mRNAs in the green alga *Chlorogonium elongatum*. *Planta* 167 (4), 582–586. doi: 10.1007/BF00391236

Sack, L., and Buckley, T. N. (2016). The developmental basis of stomatal density and flux. *Plant Physiol.* 171 (4), 2358–2363. doi: 10.1104/pp.16.00476

SharathKumar, M., Heuvelink, E., Marcelis, L. F., and Van Ieperen, W. (2021). Floral induction in the short-day plant chrysanthemum under blue and red extended long-days. *Front. Plant Sci.* 11, 610041. doi: 10.3389/fpls.2020.610041

Shchennikova, A. V., Shulga, O. A., Immink, R., Skryabin, K. G., and Angenent, G. C. (2004). Identification and characterization of four chrysanthemum MADS-box genes, belonging to the *APETALA1*/*FRUITFULL* and *SEPALLATA3* subfamilies. *Plant Physiol.* 134 (4), 1632–1641. doi: 10.1104/pp.103.036665

Somers, D. E., Devlin, P. F., and Kay, S. A. (1998). Phytochromes and cryptochromes in the entrainment of the *Arabidopsis* circadian clock. *Science* 282 (5393), 1488–1490. doi: 10.1126/science.282.5393.1488

Sun, J., Wang, H., Ren, L., Chen, S., Chen, F., and Jiang, J. (2017). *CmFTL2* is involved in the photoperiod-and sucrose-mediated control of flowering time in chrysanthemum. *Hortic. Res.* 4, 17001. doi: 10.1038/hortres.2017.1

Tanaka, T. (1967). Studies on the regulation of chrysanthemum flowering with special reference to plant regulators i. the inhibiting action of non-induced leaves on floral stimulus. *J. Jpn. Soc Hortic. Sci.* 36, 339–347. doi: 10.2503/jjshs.36.339

Thakur, T., and Grewal, H. (2019). Growth regulation and off-season flowering through night breaks in *Chrysanthemum morifolium* ramat cv. *Anmol. Bangl. J. Bot.* 48 (2), 373–378. doi: 10.3329/bjb.v48i2.47684

Thomas, B. (1981). Specific effects of blue light on plant growth and development. *Plants Daylight. Spectr.*, 443–459.

Thomas, B., and Vince-Prue, D. (1996). *Photoperiodism in plants* (San Diego, California, USA: Elsevier).

Turnbull, C. (2011). Long-distance regulation of flowering time. *J. Exp. Bot.* 62, 4399–4413. doi: 10.1093/jxb/err191

Valverde, F., Mouradov, A., Soppe, W., Ravenscroft, D., Samach, A., and Coupland, G. (2004). Photoreceptor regulation of CONSTANS protein in photoperiodic flowering. *Science* 303 (5660), 1003–1006. doi: 10.1126/science.1091761

Wahl, V., Ponnu, J., Schlereth, A., Arrivault, S., Langenecker, T., Franke, A., et al. (2013). Regulation of flowering by trehalose-6-phosphate signaling in *Arabidopsis thaliana*. *Science* 339, 704–707. doi: 10.1126/science.1230406

Walters, R. G., Ibrahim, D. G., Horton, P., and Kruger, N. J. (2004). A mutant of *Arabidopsis* lacking the triose-phosphate/phosphate translocator reveals metabolic regulation of starch breakdown in the light. *Plant Physiol.* 135, 891–906. doi: 10.1104/pp.104.040469

Wang, H., Gu, M., Cui, J., Shi, K., Zhou, Y., and Yu, J. (2009). Effects of light quality on CO_2 assimilation, chlorophyll-fluorescence quenching, expression of Calvin cycle genes and carbohydrate accumulation in *Cucumis sativus*. *J. Photoch. Photobio. B.* 96 (1), 30–37. doi: 10.1016/j.jphotobiol.2009.03.010

Wang, Y., and Pijut, P. M. (2013). Isolation and characterization of a *TERMINAL FLOWER 1* homolog from *Prunus serotina* ehrh. *Tree Physiol.* 33 (8), 855–865. doi: 10.1093/treephys/tpt051

Wigge, P. A., Kim, M. C., Jaeger, K. E., Busch, W., Schmid, M., Lohmann, J. U., et al. (2005). Integration of spatial and temporal information during floral induction in *Arabidopsis*. *Science* 309, 1056–1059. doi: 10.1126/science.1114358

Xi, W., Liu, C., Hou, X., and Yu, H. (2010). *MOTHER OF FT AND TFL1* regulates seed germination through a negative feedback loop modulating ABA signaling in *Arabidopsis*. *Plant Cell* 22, 1733–1748. doi: 10.1105/tpc.109.073072

Xu, D., Gao, W., and Ruan, J. (2015). Effects of light quality on plant growth and development. *Plant Physiol. J.* 51 (8), 1217–1234.

Yamada, A., Tanigawa, T., Suyama, T., Matsuno, T., and Kunitake, T. (2008). Night break treatment using different light sources promotes or delays growth and flowering of *Eustoma grandiflorum* (Raf.) shinn. *J. Jpn. Soc Hortic. Sci.* 77 (1), 69–74. doi: 10.2503/jjshs1.77.69

Yamaguchi, A., Kobayashi, Y., Goto, K., Abe, M., and Araki, T. (2005). *TWIN SISTER OF FT* (*TSF*) acts as a floral pathway integrator redundantly with *FT*. *Plant Cell Physiol.* 46, 1175–1189. doi: 10.1093/pcp/pci151

Yang, L. T., Chen, L. S., Peng, H. Y., Guo, P., Wang, P., and Ma, C. L. (2012). Organic acid metabolism in *Citrus grandis* leaves and roots is differently affected by nitric oxide and aluminum interactions. *Sci. Hortic.* 133, 40–46. doi: 10.1016/j.scienta.2011.10.011

Yang, J., Song, J., and Jeong, B. R. (2022). Low-intensity blue light supplemented during photoperiod in controlled environment induces flowering and antioxidant production in kalanchoe. *Antioxidants* 11 (5), 811. doi: 10.3390/antiox11050811

Yang, L., Xu, M., Koo, Y., He, J., and Poethig, R. S. (2013). Sugar promotes vegetative phase change in *Arabidopsis thaliana* by repressing the expression of *MIR156A* and *MIR156C*. *elife* 2. doi: 10.7554/eLife.00260.017

Yanovsky, M. J., and Kay, S. A. (2003). Living by the calendar: how plants know when to flower. *Nat. Rev. Mol. Cell Bio.* 4 (4), 265–276. doi: 10.1038/nrm1077

Yemm, E., and Willis, A. (1954). The estimation of carbohydrates in plant extracts by anthrone. *Biochem. J.* 57 (3), 508. doi: 10.1042/bj0570508

Yoo, S. J., Chung, K. S., Jung, S. H., Yoo, S. Y., Lee, J. S., and Ahn, J. H. (2010). *BROTHER OF FT AND TFL1* (*BFT*) has *TFL1*-like activity and functions redundantly with *TFL1* in inflorescence meristem development in *Arabidopsis*. *Plant J.* 63, 241–253. doi: 10.1111/j.1365-313X.2010.04234.x

Yu, S., Cao, L., Zhou, C. M., Zhang, T. Q., Lian, H., Sun, Y., et al. (2013). Sugar is an endogenous cue for juvenile-to-adult phase transition in plants. *elife* 2, e00269. doi: 10.7554/eLife.00269

Zeevaart, J. A. (2008). Leaf-produced floral signals. *Curr. Opin. Plant Biol.* 11, 541–547. doi: 10.1016/j.pbi.2008.06.009

Zhao, K., Li, S., Jia, D., Xing, X., Wang, H., Song, A., et al. (2022). Characterization of the MADS-box gene *CmFL3* in chrysanthemum. *Agronomy* 12 (7), 1716. doi: 10.3390/agronomy12071716

Zheng, Q., Weng, Q., Huang, L., Wang, K., Deng, J., Jiang, R., et al. (2018). A new source of multi-spectral high spatial resolution night-time light imagery–JL1-3B. *Remote Sens. Environ.* 215, 300–312. doi: 10.1016/j.rse.2018.06.016

frontiers | Frontiers in Plant Science

TYPE Opinion
PUBLISHED 20 September 2022
DOI 10.3389/fpls.2022.976627

OPEN ACCESS

EDITED BY
Pui Ying Lam,
Akita University, Japan

REVIEWED BY
Tomomichi Fujita,
Hokkaido University, Japan
Jinbo Shen,
Zhejiang Agriculture and Forestry University, China

*CORRESPONDENCE
An-Shan Hsiao
anshanhsiao@gmail.com

SPECIALTY SECTION
This article was submitted to Plant Physiology, a section of the journal Frontiers in Plant Science

RECEIVED 23 June 2022
ACCEPTED 05 September 2022
PUBLISHED 20 September 2022

CITATION
Hsiao A-S and Huang J-Y (2022) Bioimaging tools move plant physiology studies forward. *Front. Plant Sci.* 13:976627. doi: 10.3389/fpls.2022.976627

Bioimaging tools move plant physiology studies forward

An-Shan Hsiao [1]* and Ji-Ying Huang [2]

[1]Biosciences, College of Life and Environmental Sciences, University of Exeter, Exeter, United Kingdom, [2]Cell Biology Core Lab, Institute of Plant and Microbial Biology, Academia Sinica, Taipei, Taiwan

KEYWORDS

Cell Biology, plant physiology, Microscopy, biosensor, microfluid, chemicals

Introduction

Cell biology investigation is important for plant physiology research in terms of dissecting biological processes from plants/organs to macromolecular scales in various spatial and temporal manners and integrating these processes into plant developmental programs and stress responses. Bioimaging tools can be simply divided into two categories: "hard" microscopy and "soft" biosensors/probes. New imaging techniques for microscopy improvement have increased the speed and depth of acquisition, sensitivity, and spatial resolution (Grossmann et al., 2018; Clark et al., 2020). The development of improved fluorescent proteins, genetically encoded biosensors/reporters and pharmaceutical treatments have helped in measuring the spatiotemporal dynamics of cell physiological parameters (Uslu and Grossmann, 2016; Rodriguez-Furlan et al., 2017; Colin et al., 2022). Readers are invited to visit the excellent review papers on microscopy techniques and probe development (Uslu and Grossmann, 2016; Grossmann et al., 2018; Clark et al., 2020; Colin et al., 2022). Because of the importance of bioimaging tools for advancing study of mechanisms in plant physiology research, here we discuss combinatory microscopy improvement and biosensor innovation, describing their application from morphogenesis to macromolecule dynamics. We discuss the microdevice innovation in tip growth study and the latest chemical cell biology application, which provide reversible and conditional approaches to dissect the intracellular dynamics overcoming the problems of redundancy and lethality in plant physiology study (Figure 1A). For the Research Topic "Women in Plant Physiology", this article emphasizes the intelligence and innovation of female scientists in the recent progress of bioimaging techniques. By highlighting their contributions and efforts to move the field forward, we aim to encourage the younger generation of female scientists interested in the study of cell biology and plant physiology.

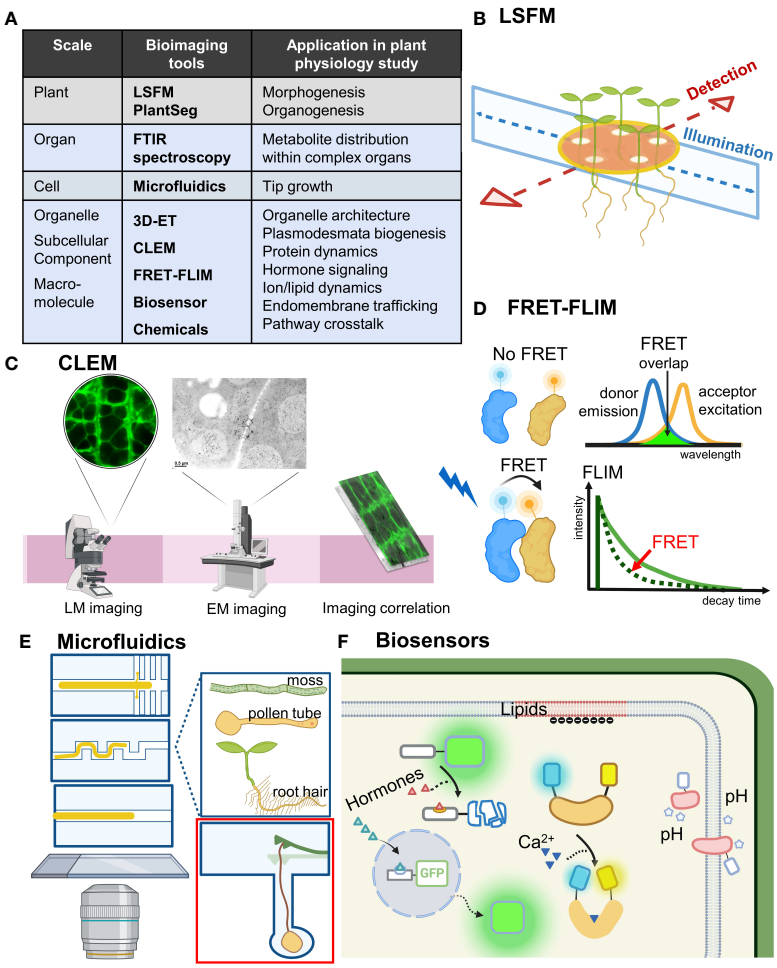

FIGURE 1
Bioimaging tools move plant physiology studies forward. **(A)** Bioimaging tools ranged from an organism scale to a subcellular scale. Their application in plant physiology research is shown. Bioimaging tools mentioned in the text are in bold. **(B)** LSFM achieves optical sectioning by selective illumination on one single plane with a sheet of laser light while simultaneously detecting emitted fluorescence orthogonal to the illumination plane. Incorporating MAGIC, LSFM can allow for high-throughput time-course imaging of multiple samples under near-physiological conditions. **(C)** Combining the advantages of electron and light microscopy-based imaging, CLEM enables precise molecular localization and provides structure–function analysis. **(D)** By measuring the lifetime of the FRET donor fluorescence, FRET-FLIM can detect location-specific protein–protein interaction *in vivo*. **(E)** Microfluid techniques can be flexibly designed and adjusted and are especially useful for observing tip growth cells such as root hairs, pollen tubes and moss. Red inset shows a microfluidic lab-on-a-chip device for quantifying the invasive growth force of pollen tubes developed by Ghanbari et al. **(F)** Biosensors for detecting hormones, Ca^{2+}, pH and lipids allow for real-time studies of cell physiology and signaling events with high spatial and temporal resolution. LSFM, light sheet fluorescence microscopy; FTIR, Fourier-transform infrared; 3D-ET, three-dimensional electron tomography; CLEM, correlative light and electron microscopy; FRET-FLIM, Förster resonance energy transfer-fluorescence lifetime imaging microscopy; MAGIC, Multi-sample Arabidopsis Growth and Imaging Chamber.

Combinatory microscopy improvement: From morphogenesis to protein dynamics

Light sheet fluorescence microscopy (LSFM) has been advanced to achieve long-term live imaging by significantly reducing phototoxicity with fast acquisition of 3D data over time. The upright sample position in most LSFM setups is well suited for studying the fundamental aspects of plant organogenesis (Berthet and Maizel, 2016). However, certain challenges remain, such as the ability to image only one specimen at a time and the stress response generated by the imaging capillary system. Rosangela Sozzani and her team developed a Multi-sample Arabidopsis Growth and Imaging Chamber (MAGIC) that provides near-physiological imaging conditions and allows for high-throughput time-course imaging experiments with the ZEISS Lightsheet Z.1 microscope, with a semi-automatic image processing pipeline for data analysis (de Luis Balaguer et al., 2016; Figure 1B). Their innovation scales up

the existing commercial platforms with up to 48-h imaging capacity and efficient multiplexing of up to 12 seedlings, which can be used for imaging developmental processes such as root growth, cell division events as well as light-controlled experiments.

Microscopy improvement such as LSFM allows for capturing the anatomy and development of plants in terabytes of high-resolution volumetric images. However, accurate segmentation of individual cells in volumetric images of growing organs is needed. Anna Kreshuk and her colleagues released PlantSeg, an open-source software for 2D and 3D segmentation of cells with cell contour staining (Wolny et al., 2020). Recent research combining PlantSeg and ClearSee-based staining methods revealed a cellular growth pattern during Arabidopsis ovule development (Vijayan et al., 2021). Hence, PlantSeg can be used with modern clearing methods to study various developmental events of diverse plant organs and even animal tissues.

Time-course live imaging experiments are critical for understanding dynamic cellular processes. When cells undergoing cell division grow in length, studying them requires manual adjustment of the observation field over time. Thus, Marie-Cécile Caillaud and her colleagues developed a protocol for automatic time-lapse imaging of multiple growing root tips for several hours, which allows for easy temporal observation of cytokinesis and other cellular processes (Doumane et al., 2017).

Ljudmilla Borisjuk and her team established an imaging platform based on Fourier-transform infrared spectroscopy for analysing cereal crops (Gündel et al., 2018). This platform allows for the quantitative visualization of sucrose in individual vascular bundles or complex organs with high sensitivity and resolution. It can resolve the spatial distribution of metabolites and carbon allocation as well as storage in the context of crop improvement (Gündel et al., 2018).

Understanding 3D architectures of organelles during various developmental stages in different cell types is important for analyzing their functions in plant physiology research. Electron tomography (ET) approaches can retrieve 3D structural information from a series of 2D projections of a biological specimen at different angles to provide 3D structural evidence (Ercius et al., 2015; Otegui and Pennington, 2019). Marisa Otegui and her colleagues established ET approaches to analyze vesicular trafficking and *de novo* assembly of plant cell walls (Otegui and Pennington, 2019; Otegui, 2020). Their recent findings show that endosomal intralumenal vesicles are formed by a concatenation process in Arabidopsis root and tapetal cells (Buono et al., 2017; Goodman et al., 2021). This process contrasts with the current model established in the mammalian system in which endosomal intralumenal vesicles are free and formed individually (Murk et al., 2003). Therefore, the establishment of bioimaging tools in plants is critical to investigate the novel mechanism in plant cells, which are distinct from mammalian cells.

Combining electron microscopy and light microscopy, correlative light and electron microscopy (CLEM) can be used to visualize the ultrastructure for studying intracellular function (Begemann and Galic, 2016; Figure 1C). Lysiane Brocard and her colleagues developed a CLEM approach to study the graft interface of Arabidopsis grafting hypocotyls (Chambaud et al., 2022). With in-resin fluorescence CLEM combined with electron tomography, this method can provide the fine 3D ultrastructural details with up to the resolution of the bilayer of the plasma membrane (Chambaud et al., 2022). Classical CLEM usually results in low-resolution correlations because it is limited to the resolution of the light microscope, but this method can detect fluorescence signals and more accurately determine the ultrastructure position within electron tomograms.

Förster resonance energy transfer (FRET) is a well-established technique to study molecular interactions by monitoring non-radiative energy transfer from an excited fluorescent donor to a non-excited different fluorescent acceptor (Förster, 1948; Lakowicz, 2006; Müller et al., 2013). Fluorescence lifetime imaging microscopy (FLIM) can deliver information about the spatial distribution of a fluorescent molecule with its biochemical status or nano-environment (Brismar and Ulfhake, 1997; van Munster and Gadella, 2005). Determining the lifetime of the FRET donor fluorophore by FLIM, FRET-FLIM has been widely used to detect and visualize protein interactions spatially (Fäßler and Pimpl, 2017; Weidtkamp-Peters and Stahl, 2017; Figure 1D). Ikram Blilou and her team optimized FRET-FLIM technology in living Arabidopsis roots to show the physical proximity between the C2H2-type transcription factor JACKDAW, the mobile protein and cell fate regulator SHORTROOT, and its target SCARECROW compartments (Long et al., 2017). This optimized FRET-FLIM technology provides visualization of cell-specific protein–protein interactions, which is useful for observing cell type-specific complexes in many biological processes such as gene expression, signaling, cell size regulation, and growth.

Fluorescence correlation spectroscopy (FCS) is a powerful technique to measure fluorescence fluctuations for exploring the dynamic behaviours of proteins and the organization of membranes within living cells (Bacia et al., 2006; Li et al., 2016). Scanning FCS extends the application of FCS to receptor–ligand interactions by repeatedly scanning the detection volume through a vertical membrane perpendicularly (Ries et al., 2009). Rosangela Sozzani and her team used scanning FCS to track the mobility and interactions of the transcription factors SHORTROOT and its downstream target SCARECROW, which control root patterning and cell fate specification in plants (Clark et al., 2016). By combining scanning FCS and pair correlation functions, the team dissected the directionality of transcription-factor movement in various cell types quantitatively with a high spatiotemporal resolution. With its high fluorescence sensitivity, this FCS approach is more useful for resolving the dynamics and

interactions of fast diffusing macromolecules rather than immobile molecular interactions such as stable transcription factor binding events.

As FCS is used for *in vivo* imaging of transcription factor movement and interactions (Clark et al., 2016), single-particle tracking (SPT) is a valuable analytical method for unravelling the dynamics of membrane proteins in regulating signal transduction with super-spatiotemporal resolution (Cui et al., 2018; Wang et al., 2018). Xiaojun Li and her colleagues developed a SPT method for studying the distribution and dynamics of the plant membrane protein aquaporin (Li et al., 2011; Cui et al., 2021). This method can be used to study specific membrane protein motions during abiotic and biotic stress responses by directly "observing" how particles diffuse in living cells in front of our eyes (Cui et al., 2018). This "seeing is believing" technique has great potential in investigating cell signalling and membrane rafts.

Microfluid system for observing tip growth

Versatile microdevices have been used for live imaging of plants (Froelich et al., 2011; Kirchhelle and Moore, 2017; Clark et al., 2020). Microfluidic systems allow for live imaging of biological samples growing in defined channels with the stream of fluid continuously renewing the growth medium (Figure 1E). They facilitate quantitative and dynamic measurements and precisely control the microenvironment (Whitesides, 2006; Meier et al., 2010; Grossmann et al., 2011; Parashar and Pandey, 2011; Grossmann et al., 2018). Tip growth involves an expandable cell wall and localized exocytosis at the tip of a cell. Pollen tubes and root hairs are well-studied tip growth cells because of their important functions in plant breeding and nutrient uptake (de Ruijter and Malhó, 2000; Heath and Geitmann, 2000). Anja Geitmann and her team developed a multi-layer soft lithography process in a microfluidic lab-on-a-chip device featuring a microscopic cantilever to quantify the invasive growth force (Ghanbari et al., 2018; Figure 1E red inset). This platform can harbour growing pollen tubes while measuring instant growth force during the mechanical interactions, for a promising application for mechanobiological studies in growing cells (Ghanbari et al., 2018). The team of Anja Geitmann further improved lithography-based microfluidics as a low-cost alternative; this is a silicone-based spacer system with flexible design, which can be cleaned and reused repeatedly and allows for live cell imaging at high resolution of pollen tubes growing *in vitro* (Bertrand-Rakusová et al., 2020). Their innovation can provide a fundamental platform for studying the growth behavior and mechanosensing of pollen tubes.

With their fast apical growth, root hairs are easily visualized and accessible to variety of experimental manipulations and physiological tests, thus providing numerous advantages for basic studies of development, cell biology and physiology (Grierson et al., 2014). Marie-Edith Chabouté is interested in studying plant nuclear mechanics by using Arabidopsis root hairs as a model system. Her team invented a powerful coverslip-based microfluidic device to observe Arabidopsis root hair development with high-resolution confocal imaging as well as real-time monitoring of nuclear movement and shape changes (Singh et al., 2021). Nuclear movement is an important controlling point during development and signalling events, so their research provides a unique tool for studying the roles of nucleus dynamics in various biological processes.

The moss *Physcomitrium patens* has emerged as a good model to study tip growth in plants owing to its benefits of excellent rapid genetics and cytology (Rounds and Bezanilla, 2013; Bibeau et al., 2021). As a pioneer in moss research, Magdalena Bezanilla and her team described a continuous-culture method within microfluidic chambers for long-term imaging of development in the moss (Bascom et al., 2016). This method overcame the current long-term imaging challenges and allowed for continuous imaging over a long developmental time for weeks. These devices provide an opportunity to pursue the molecular basis of developmental events such as protonemal tissue differentiation, bud formation, and phyllid expansion at cellular and subcellular resolutions with available high-throughput pharmacological treatments.

Biosensors for hormone signaling, dynamics of Ca^{2+}, pH and lipids

Fluorescent protein-based genetically encoded biosensors are increasingly being used to visualize and analyse ion fluxes, signaling components, and metabolites for real-time studies of cellular processes with high spatial and temporal resolution (Gjetting et al., 2013; Hilleary et al., 2018; Walia et al., 2018; Walia et al., 2021; Waadt et al., 2021). Biosensors detecting hormone distribution and signaling have benefited physiology studies of plant development (Balcerowicz et al., 2021; Isoda et al., 2021; Figure 1F). Carolyn Rasmussen and her team modified a sensitive and dynamically responsive auxin signaling reporter based on the DII domain of Arabidopsis INDOLE-3-ACETIC ACID 28 for use in maize (Mir et al., 2017). This DII-based reporter responded to both exogenous indole-3-acetic acid and endogenous auxin, particularly transient areas of low auxin accumulation/perception, thus highlighting its utility in studying mechanisms of auxin signaling during maize development (Mir et al., 2017).

The group of Maya Bar recently reported the improved version of the cytokinin sensor two-component signaling sensor (TCS), TCSv2, with increased sensitivity and expression pattern, which is an ideal TCS version to study cytokinin response in a

host plant such as tomato and tissues such as leaves and flowers (Steiner et al., 2020). Their recent research used TCSv2 to understand the balance between cytokinin and gibberellin during tomato leaf development (Israeli et al., 2021), highlighting its utility in studying organ development and shape determination as well as the relationship between cytokinin and other hormones.

Jennifer Nemhauser and her team introduced a novel set of synthetic and modular hormone-activated Cas9-based repressors (HACRs) in Arabidopsis that respond to three hormones: auxin, gibberellins and jasmonates (Khakhar et al., 2018). In the gibberellin HACRs, this approach revealed an endosperm-specific gibberellin distribution corresponding to *AtGA3ox4* expression in early seed development. Because the HACR approach is modular, other gibberellin-targeted proteins can be investigated or other pathways dependent on regulated protein degradation quantified; thus it is useful for studying hormone signalling events. A further agricultural engineering application is to use HACR technology to reprogram development by changing the hormone signalling network.

As a second messenger, Ca^{2+}-mediated signaling participates in the regulation of plant cell physiology and cellular responses to the environment (Dodd et al., 2010). Melanie Krebs and Karin Schumacher established a standard protocol for combining the use of locally targeted genetically encoded calcium indicators and confocal laser scanning microscopy to measure cytosolic and nuclear Ca^{2+} dynamics in Arabidopsis roots (Krebs and Schumacher, 2013). The researchers improved the sensitivity and signal resolution of Ca^{2+} indicators from FRET-based R-GECO1 to ratiometric R-GECO1-mTurquoise (Keinath et al., 2015; Waadt et al., 2017). These Ca^{2+} indicators are useful for studying cytosolic Ca^{2+} oscillations in various cell types during fungal infection and hormonal responses related to abscisic acid and auxin, for example.

The study of pH in cellular physiology is important for understanding ionic balance, membrane regulation of ion channels and transporters as well as root growth (Moreau et al., 2021). Nadine Paris and her team generated membrane-anchored ratiometric pH sensors that allow for non-invasive pH measurement on both sides of the plasma membrane of living Arabidopsis roots (Martinière et al., 2018). By using this powerful tool, the researchers found that the cell wall plays a role in proton homeostasis in mature roots (Martinière et al., 2018). For acidic pH measurement, they further generated pH sensors with range from pH 3 to 8, called Acidins, which are useful to directly report physiological conditions related to cell elongation (Moreau et al., 2022).

Various lipid biosensors have been designed for studying lipid dynamics and membrane functions (Platre and Jaillais, 2016; Hammond et al., 2022). Marie-Cécile Caillaud and her colleagues generated a series of membrane-surface charge markers and lipid sensors to address the unique electrostatic signature of the plasma membrane, controlled by phosphatidylinositol-4-phosphate (PI4P) (Simon et al., 2016). Their recent research used a synthetic inducible system, inducible depletion of PI(4,5)P2 in plants (iDePP), to confirm that PI(4,5)P2 is critical for various aspects of plant development, including root growth, root-hair elongation and organ initiation (Doumane et al., 2021).

By using a bio-ortholog of choline, Kathrin Schrick and her team developed a click-chemistry–based method for imaging choline phospholipids in various cell types and tissues from Arabidopsis (Paper et al., 2018). Their method provides a direct way to metabolically tag and visualize specific lipid molecules in plant cells. Although click-chemistry in metabolic labelling is common in mammalian lipid research (Ancajas et al., 2020), this innovation represents a major progress in plant lipid research, which was at the stage of isotopic labeling for a long time (Allen et al., 2015). More research regarding lipid metabolism, trafficking and localization in plant cells with this approach is foreseeable.

Chemicals for probing intracellular processes

Besides click-chemistry in biosensor application, chemicals can be used to target specific proteins to affect their functions during signal transduction or in critical pathways (Li et al., 2012; Rodriguez-Furlan et al., 2017). Therefore, they are useful to dissect molecular mechanisms regarding hormone signaling, development, cell wall biogenesis, and plant immunity as well as to investigate dynamic intracellular processes such as protein subcellular localization, secretion and trafficking (Hicks and Raikhel, 2012; Dejonghe and Russinova, 2017). Traditional chemicals with known action mechanism such as brefeldin A can be used for investigating intracellular processes influenced by plant hormones (Peyroche et al., 1999). The quantitative microscopic analysis established by Eugenia Russinova's laboratory involves exocytosis and recycling, plasma membrane receptor dynamics and their roles in brassinosteroid signaling (Luo et al., 2015; Luo and Russinova, 2017). The team's recent research revealed that the human and plant endomembrane system showed different responses to the chemical effector endosidin9 (Dejonghe et al., 2019). This selective inhibition effect of small molecules is useful to dissect the different roles within protein families and distinct species. Such different responses to chemicals between human and plant endomembrane systems highlighted the importance to look at them not from the perspective of animal physiology but instead to establish a plant-based chemical toolbox for physiological study (Norambuena and Tejos, 2017).

More than a decade ago, Natasha V. Raikhel foresaw the merits of using chemicals to perturb the essential physiological processes in plants to overcome the problems of redundancy and lethality. Her team has been working on the discovery and use of

chemical tools to establish a chemical toolbox for plant physiological study (Hicks and Raikhel, 2012; Li et al., 2012; Hicks and Raikhel, 2014). Their research has revealed various valuable chemical probes such as Sortin1 for dissecting the regulation among flavonoid transport, vacuolar integrity and trafficking (Rosado et al., 2011) and endosidin17 for understanding the checkpoint for membrane fusion with the vacuole (Rodriguez-Furlan et al., 2019). Her foresight in using chemical tools for visualizing and manipulating cellular processes has led to interesting discoveries and prompted a new research area of chemical genetics for studying the functions of essential plant proteins.

Always moving forward

Compared to her research, the life story of Natasha V. Raikhel is even more encouraging (Raikhel, 2017). She was born in Germany and moved to Russia, where she grew up as a budding pianist and later changed her career goal from music to biology. Although it was a difficult realization that she was not destined to become a professional pianist, her pragmatism and hard work drove her to catch up in biology and chemistry at university, where she used classical cell biology for studying ciliates. The ciliate work was boring and descriptive and the fact that she could not ask deeper biological questions led to decisions that would lay the foundation for other scientists. During the difficult time, she always faced unfairness, shortages and limitations in both research and life, and the last straw was a horrific plane crash in 1978, which led to her decision to immigrate to the United States. There, she was reborn as a plant biologist studying lectin, cell wall and vesicular trafficking as well as the aforementioned chemical genomics tools for plant physiology research. In 1998, she was diagnosed with breast cancer, but just like other difficulties she met, she overcame the disease. She continued to work in the laboratory during the chemotherapy treatments, and after her recovery, she became the first and (so far) only female editor in chief of the journal *Plant Physiology* during 2000-2005, where she made a difference by highlight the latest technology-driven insights in plant biology. She retired from her university career in 2016, but she maintained her work in promoting women in science and music all around the world. The story of Natasha V. Raikhel represents how a female scientist overcame difficulties and pushed the field forward, just like other examples of female scientists have led to significant progress in plant physiology research. Changes and challenges always happen in life and research, if you don't know where to go, any road will lead you there. Just keep going and moving forward!

Author contributions

A-SH developed the concept and wrote the manuscript. A-SH and J-YH produced the data in Figure 1. J-YH prepared Figure 1. The authors contributed to the article and approved the submitted version.

Funding

A-SH was supported by a BBSRC research grant (BBSRC BB/T005424/1) led by Prof. Nicholas Smirnoff.

Acknowledgments

Confocal and immunogold TEM images were prepared in the Cell Biology Core Lab, Institute of Plant and Microbial Biology, Academia Sinica. Figure 1 was created with BioRender.com. The research data supporting this publication are provided within this paper. The authors thank both reviewers for their constructive suggestion to improve this manuscript.

Conflict of interest

The authors declare that the research was conducted in the absence of any commercial or financial relationships that could be construed as a potential conflict of interest.

Publisher's note

References

Allen, D. K., Bates, P. D., and Tjellström, H. (2015). Tracking the metabolic pulse of plant lipid production with isotopic labeling and flux analyses: Past, present and future. *Prog. Lipid Res.* 58, 97–120. doi: 10.1016/j.plipres.2015.02.002

Ancajas, C. F., Ricks, T. J., and Best, M. D. (2020). Metabolic labeling of glycerophospholipids *via* clickable analogs derivatized at the lipid headgroup. *Chem. Phys. Lipids* 232, 104971. doi: 10.1016/j.chemphyslip.2020.104971

Bacia, K., Kim, S. A., and Schwille, P. (2006). Fluorescence cross-correlation spectroscopy in living cells. *Nat. Methods* 3, 83–89. doi: 10.1038/nmeth822

Balcerowicz, M., Shetty, K. N., and Jones, A. M. (2021). Fluorescent biosensors illuminating plant hormone research. *Plant Physiol.* 187, 590–602. doi: 10.1093/plphys/kiab278

Bascom, C. S., Wu., S.-Z., Nelson, K., Oakey, J., and Bezanilla, M. (2016). Long-term growth of moss in microfluidi devices enables subcellular studies in development. *Plant Physiol.* 172, 28–37. doi: 10.1104/pp.16.00879

Begemann, I., and Galic, M. (2016). Correlative light electron microscopy: connecting synaptic structure and function. *Front. Synaptic Neurosci.* 8. doi: 10.3389/fnsyn.2016.00028

Berthet, B., and Maizel, A. (2016). Light sheet microscopy and live imaging of plants. *J. Microsc.* 263, 158–164. doi: 10.1111/jmi.12393

Bertrand-Rakusová, H., Chebli, Y., and Geitmann, A. (2020). Silicone chambers for pollen tube imaging in microstructured *in vitro* environments. *Methods Mol. Biol.* 2160, 211–221. doi: 10.1007/978-1-0716-0672-8_15

Bibeau, J. P., Galotto, G., Wu, M., Tüzel, E., and Vidali, L. (2021). Quantitative cell biology of tip growth in moss. *Plant Mol. Biol.* 107, 227–244. doi: 10.1007/s11103-021-01147-7

Brismar, H., and Ulfhake, B. (1997). Fluorescence lifetime measurements in confocal microscopy of neurons labeled with multiple fluorophores. *Nat. Biotechnol.* 15, 373–377. doi: 10.1038/nbt0497-373

Buono, R. A., Leier, A., Paez-Valencia, J., Pennington, J., Goodman, K., Miller, N., et al. (2017). ESCRT-mediated vesicle concatenation in plant endosomes. *J. Cell Biol.* 216, 2167–2177. doi: 10.1083/jcb.201612040

Chambaud, C., Cookson, S. J., Ollat, N., Bayer, E., and Brocard, L. (2022). A correlative light electron microscopy approach reveals plasmodesmata ultrastructure at the graft interface. *Plant Physiol.* 188, 44–55. doi: 10.1093/plphys/kiab485

Clark, N. M., Hinde, E., Winter, C. M., Fisher, A. P., Crosti, G., Blilou, I., et al. (2016). Tracking transcription factor mobility and interaction in arabidopsis roots with fluorescence correlation spectroscopy. *eLife* 5, e14770. doi: 10.7554/eLife.14770

Clark, N. M., Van den Broeck, L., Guichard, M., Stager, A., Tanner, H. G., Blilou, I., et al. (2020). Novel imaging modalities shedding light on plant biology: Start small and grow big. *Annu. Rev. Plant Biol.* 71, 789–816. doi: 10.1146/annurev-arplant-050718-100038

Colin, L., Martin-Arevalillo, R., Bovio, S., Bauer, A., Vernoux, T., Caillaud, M. C., et al. (2022). Imaging the living plant cell: From probes to quantification. *Plant Cell* 34, 247–272. doi: 10.1093/plcell/koab237

Cui, Y., Yu, M., Yao, X., Xing, J., Lin, J., and Li, X. (2018). Single-particle tracking for the quantification of membrane protein dynamics in living plant cells. *Mol. Plant* 11, 1315–1327. doi: 10.1016/j.molp.2018.09.008

Cui, Y., Zhao, Y., Lu, Y., Su, X., Chen, Y., Shen, Y., et al. (2021). *In vivo* single-particle tracking of the aquaporin AtPIP2;1 in stomata reveals cell type-specific dynamics. *Plant Physiol.* 185, 1666–1681. doi: 10.1093/plphys/kiab007

Dejonghe, W., and Russinova, E. (2017). Plant chemical genetics: from phenotype-based screens to synthetic biology. *Plant Physiol.* 174, 5–20. doi: 10.1104/pp.16.01805

Dejonghe, W., Sharma, I., Denoo, B., De Munck, S., Lu, Q., Mishev, K., et al. (2019). Disruption of endocytosis through chemical inhibition of clathrin heavy chain function. *Nat. Chem. Biol.* 15, 641–649. doi: 10.1038/s41589-019-0262-1

de Luis Balaguer, M. A., Ramos-Pezzotti, M., Rahhal, M. B., Melvin, C. E., Johannes, E., Hornet, T. J., et al. (2016). Multi-sample arabidopsis growth and imaging chamber (MAGIC) for long term imaging in the ZEISS light sheet Z.1. *Dev. Biol.* 419, 19–25. doi: 10.1016/j.ydbio.2016.05.029

de Ruijter, N. C., and Malhó, R. (2000). Plant fungal tip growth: where do we go from here? *Trends Plant Sci.* 5, 453–454. doi: 10.1016/s1360-1385(00)01768-4

Dodd, A. N., Kudla, J., and Sanders, D. (2010). The language of calcium signaling. *Annu. Rev. Plant Biol.* 61, 593–620. doi: 10.1146/annurev-arplant-070109-104628

Doumane, M., Lebecq, A., Colin, L., Fangain, A., Stevens, F. D., Bareille, J., et al. (2021). Inducible depletion of PI(4,5)P2 by the synthetic iDePP system in arabidopsis. *Nat. Plants* 7, 587–597. doi: 10.1038/s41477-021-00907-z

Doumane, M., Lionnet, C., Bayle, V., Jaillais, Y., and Caillaud, M. C. (2017). Automated tracking of root for confocal time-lapse imaging of cellular processes. *Bio Protoc.* 7, e2245. doi: 10.21769/BioProtoc.2245

Ercius, P., Alaidi, O., Rames, M. J., and Ren, G. (2015). Electron tomography: a three-dimensional analytic tool for hard and soft materials research. *Adv. Mat.* 27, 5638–5663. doi: 10.1002/adma.201501015

Fäßler, F., and Pimpl, P. (2017). *In vivo* interaction studies by measuring förster resonance energy transfer through fluorescence lifetime imaging microscopy (FRET/FLIM). *Methods Mol. Biol.* 1662, 159–170. doi: 10.1007/978-1-4939-7262-3_14

Förster, T. (1948). Intermolecular energy migration and fluorescence. *Ann. Phys.* 2, 55–75. doi: 10.1002/andp.19484370105

Froelich, D. R., Mullendore, D. L., Jensen, K. H., Ross-Elliott, T. J., Anstead, J. A., Thompson, G. A., et al. (2011). Phloem ultrastructure and pressure flow: Sieve-Element-Occlusion-Related agglomerations do not affect translocation. *Plant Cell* 23, 4428–4445. doi: 10.1105/tpc.111.093179

Ghanbari, M., Packirisamy, M., and Geitmann, A. (2018). Measuring the growth force of invasive plant cells using flexure integrated Lab-on-a-Chip (FiLoC). *Technology* 6, 101–109. doi: 10.1142/S2339547818500061

Gjetting, S. K., Schulz, A., and Fuglsang, A. T. (2013). Perspectives for using genetically encoded fluorescent biosensors in plants. *Front. Plant Sci.* 4. doi: 10.3389/fpls.2013.00234

Goodman, K., Paez-Valencia, J., Pennington, J., Sonntag, A., Ding, X., Lee, H. N., et al. (2021). ESCRT components ISTL1 and LIP5 are required for tapetal function and pollen viability. *Plant Cell* 33, 2850–2868. doi: 10.1093/plcell/koab132

Grierson, C., Nielsen, E., Ketelaarc, T., and Schiefelbein, J. (2014). Root hairs. *Arabidopsis Book Am. Soc. Plant Biologists* 12, e0172. doi: 10.1199/tab.0172

Grossmann, G., Guo, W.-J., Ehrhardt, D. W., Frommer, W. B., Sit, R. V., Quake, S. R., et al. (2011). The RootChip: An integrated microfluidic chip for plant science. *Plant Cell* 23, 4234–4240. doi: 10.1105/tpc.111.092577

Grossmann, G., Krebs, M., Maizel, A., Stahl, Y., Vermeer, J. E. M., and Ott, T. (2018). Green light for quantitative live-cell imaging in plants. *J. Cell Sci.* 131, jcs209270. doi: 10.1242/jcs.209270

Gündel, A., Rolletschek, H., Wagner, S., Muszynska, A., and Borisjuk, L. (2018). Micro imaging displays the sucrose landscape within and along its allocation pathways. *Plant Physiol.* 178, 1448–1460. doi: 10.1104/pp.18.00947

Hammond, G. R. V., Ricci, M. M. C., Weckerly, C. C., and Wills, R. C. (2022). An update on genetically encoded lipid biosensors. *Mol. Biol. Cell* 33, 5. doi: 10.1091/mbc.E21-07-0363

Heath, I. B., and Geitmann, A. (2000). Cell biology of plant and fungal tip growth-getting to the point. *Plant Cell* 12, 1513–1517. doi: 10.1105/tpc.12.9.1513

Hicks, G. R., and Raikhel, N. V. (2012). Small molecules present large opportunities in plant biology. *Annu. Rev. Plant Biol.* 63, 261–282. doi: 10.1146/annurev-arplant-042811-105456

Hicks, G. R., and Raikhel, N. V. (2014). Plant chemical biology: are we meeting the promise? *Front. Plant Sci.* 5. doi: 10.3389/fpls.2014.00455

Hilleary, R., Choi, W. G., Kim, S. H., Lim, S. D., and Gilroy, S. (2018). Sense and sensibility: the use of fluorescent protein-based genetically encoded biosensors in plants. *Curr. Opin. Plant Biol.* 46, 32–38. doi: 10.1016/j.pbi.2018.07.004

Isoda, R., Yoshinari, A., Ishikawa, Y., Sadoine, M., Simon, R., Frommer, W. B., et al. (2021). Sensors for the quantification, localization and analysis of the dynamics of plant hormones. *Plant J.* 105, 542–557. doi: 10.1111/tpj.15096

Israeli, A., Burko, Y., Shleizer-Burko, S., Zelnik, I. D., Sela, N., Hajirezaei, M. R., et al. (2021). Coordinating the morphogenesis-differentiation balance by tweaking the cytokinin-gibberellin equilibrium. *PloS Genet.* 17, e1009537. doi: 10.1371/journal.pgen.1009537

Keinath, N. F., Waadt, R., Brugman, R., Schroeder, J. I., Grossmann, G., Schumacher, K., et al. (2015). Live cell imaging with RGECO1sheds light on flg22- and chitin-induced transient [Ca2+]cyt patterns in arabidopsis. *Mol. Plant* 8, 1188–1200. doi: 10.1016/j.molp.2015.05.006

Khakhar, A., Leydon, A. R., Lemmex, A. C., Klavins, E., and Nemhauser, J. L. (2018). Synthetic hormone-responsive transcription factors can monitor and re-program plant development. *eLife* 7, e34702. doi: 10.7554/eLife.34702

Kirchhelle, C., and Moore, I. (2017). A simple chamber for long-term confocal imaging of root and hypocotyl development. *J. Vis. Exp.* 123, e55331. doi: 10.3791/55331

Krebs, M., and Schumacher, K. (2013). Live cell imaging of cytoplasmic and nuclear Ca2+ dynamics in arabidopsis roots. *Cold Spring Harb. Protoc.* 2013, 776–780. doi: 10.1101/pdb.prot073031

Lakowicz, J. R. (2006). *Principles of fluorescent spectroscopy. 3rd Edn* (New York, NY: Springer). doi: 10.1007/978-0-387-46312-4

Li, R., Raikhel, N. V., and Hicks, G. R. (2012). "Chemical effectors of plant endocytosis and endomembrane trafficking," in *Endocytosis in plants*. Ed. J. Samaj (Berlin: Springer-Verlag), 37–61. doi: 10.1007/978-3-642-32463-5_2

Li, X., Wang, X., Yang, Y., Li, R., He, Q., Fang, X., et al. (2011). Single-molecule analysis of PIP2;1 dynamics and partitioning reveals multiple modes of arabidopsis plasma membrane aquaporin regulation. *Plant Cell* 23, 3780–3797. doi: 10.1105/tpc.111.091454

Li, X., Xing, J., Qiu, Z., He, Q., and Lin, J. (2016). Quantification of membrane protein dynamics and interactions in plant cells by fluorescence correlation spectroscopy. *Mol. Plant* 9, 1229–1239. doi: 10.1016/j.molp.2016.06.017

Long, Y., Stahl, Y., Weidtkamp-Peters, S., Postma, M., Zhou, W., Goedhart, J., et al. (2017). *In vivo* FRET-FLIM reveals cell-type-specific protein interactions in arabidopsis roots. *Nature* 548, 97–102. doi: 10.1038/nature23317

Luo, Y., and Russinova, E. (2017). Quantitative microscopic analysis of plasma membrane receptor dynamics in living plant cells. *Methods Mol. Biol.* 1564, 121–132. doi: 10.1007/978-1-4939-6813-8_10

Luo, Y., Scholl, S., Doering, A., Zhang, Y., Irani, N. G., Rubbo, S. D., et al. (2015). V-ATPase activity in the TGN/EE is required for exocytosis and recycling in arabidopsis. *Nat. Plants* 1, 15094. doi: 10.1038/nplants.2015.94

Martinière, A., Gibrat, R., Sentenac, H., Dumont, X., Gaillard, I., and Paris, N. (2018). Uncovering pH at both sides of the root plasma membrane interface using noninvasive imaging. *Proc. Natl. Acad. Sci. U.S.A.* 115, 6488–6493. doi: 10.1073/pnas.1721769115

Meier, M., Lucchetta, E. M., and Ismagilov, R. F. (2010). Chemical stimulation of the arabidopsis thaliana root using multi-laminar flow on a microfluidic chip. *Lab. Chip.* 10, 2147–2153. doi: 10.1039/c004629a

Mir, R., Aranda, L. Z., Biaocchi, T., Luo, A., Sylvester, A. W., and Rasmussen, C. G. (2017). A DII domain-based auxin reporter uncovers low auxin signaling during telophase and early G1. *Plant Physiol.* 173, 863–871. doi: 10.1104/pp.16.01454

Moreau, H., Gaillard, I., and Paris, N. (2022). Genetically encoded fluorescent sensors adapted to acidic pH highlight subdomains within the plant cell apoplast. *J. Exp. Bot.* 23, erac210. doi: 10.1093/jxb/erac210

Moreau, H., Zimmermann, S. D., Gaillard, I., and Paris, N. (2021). pH biosensing in the plant apoplast-a focus on root cell elongation. *Plant Physiol.* 187, 504–514. doi: 10.1093/plphys/kiab313

Müller, S. M., Galliardt, H., Schneider, J., Barisas, B. G., and Seidel, T. (2013). Quantification of förster resonance energy transfer by monitoring sensitized emission in living plant cells. *Front. Plant Sci.* 4. doi: 10.3389/fpls.2013.00413

Murk, J. L. A. N., Humbel, B. M., Ziese, U., Griffith, J. M., Posthuma, G., Slot, J. W., et al. (2003). Endosomal compartmentalization in three dimensions: implications for membrane fusion. *Proc. Natl. Acad. Sci. U.S.A.* 100, 13332–13337. doi: 10.1073/pnas.2232379100

Norambuena, L., and Tejos, R. (2017). Chemical genetic dissection of membrane trafficking. *Annu. Rev. Plant Biol.* 68, 197–224. doi: 10.1146/annurev-arplant-042916-041107

Otegui, M. S. (2020). Electron tomography and immunogold labeling as tools to analyze *de novo* assembly of plant cell walls. *Methods Mol. Biol.* 2149, 365–382. doi: 10.1007/978-1-0716-0621-6_21

Otegui, M. S., and Pennington, J. G. (2019). Electron tomography in plant cell biology. *Microscopy (Oxf)* 68, 69–79. doi: 10.1093/jmicro/dfy133

Paper, J. M., Mukherjee, T., and Schrick, K. (2018). Bioorthogonal click chemistry for fluorescence imaging of choline phospholipids in plants. *Plant Methods* 14, 31. doi: 10.1186/s13007-018-0299-2

Parashar, A., and Pandey, S. (2011). Plant-in-chip: Microfluidic system for studying root growth and pathogenic interactions in arabidopsis. *Appl. Phys. Lett.* 98, 263703. doi: 10.1063/1.3604788

Peyroche, A., Antonny, B., Robineau, S., Acker, J., Cherfils, J., and Jackson, C. L. (1999). Brefeldin a acts to stabilize an abortive ARF-GDP-Sec7 domain protein complex: involvement of specific residues of the Sec7 domain. *Mol. Cell* 3, 275–285. doi: 10.1016/s1097-2765(00)80455-4

Platre, M. P., and Jaillais, Y. (2016). Guidelines for the use of protein domains in acidic phospholipid imaging. *Methods Mol. Biol.* 1376, 175–194. doi: 10.1007/978-1-4939-3170-5_15

Raikhel, N. V. (2017). Firmly planted, always moving. *Annu. Rev. Plant Biol.* 68, 1–27. doi: 10.1146/annurev-arplant-042916-040829

Ries, J., Yu, S. R., Burkhardt, M., Brand, M., and Schwille, P. (2009). Modular scanning FCS quantifies receptor-ligand interactions in living multicellular organisms. *Nat. Methods* 6, 643–645. doi: 10.1038/nmeth.1355

Rodriguez-Furlan, C., Domozych, D., Qian, W., Enquist, P. A., Li, X., Zhang, C., et al. (2019). Interaction between VPS35 and RABG3f is necessary as a checkpoint to control fusion of late compartments with the vacuole. *Proc. Natl. Acad. Sci. U.S.A.* 116, 21291–21301. doi: 10.1073/pnas.1905321116

Rodriguez-Furlan, C., Raikhel, N. V., and Hicks, G. R. (2017). Merging roads: Chemical tools and cell biology to study unconventional protein secretion. *J. Exp. Bot.* 69, 39–46. doi: 10.1093/jxb/erx261

Rosado, A., Hicks, G. R., Norambuena, L., Rogachev, I., Meir, S., Pourcel, L., et al. (2011). Sortin1-hypersensitive mutants link vacuolar-trafficking defects and flavonoid metabolism in arabidopsis vegetative tissues. *Chem. Biol.* 18, 187–197. doi: 10.1016/j.chembiol.2010.11.015

Rounds, C. M., and Bezanilla, M. (2013). Growth mechanisms in tip-growing plant cells. *Annu. Rev. Plant Biol.* 64, 243–265. doi: 10.1146/annurev-arplant-050312-120150

Simon, M. L., Platre, M. P., Marquès-Bueno, M. M., Armengot, L., Stanislas, T., Bayle, V., et al. (2016). A PtdIns(4)P-driven electrostatic field controls cell membrane identity and signalling in plants. *Nat. Plants* 2, 16089. doi: 10.1038/nplants.2016.89

Singh, G., Pereira, D., Baudrey, S., Hoffmann, E., Ryckelynck, M., Asnacios, A., et al. (2021). Real-time tracking of root hair nucleus morphodynamics using a microfluidic approach. *Plant J.* 108, 303–313. doi: 10.1111/tpj.15511

Steiner, E., Israeli, A., Gupta, R., Shwartz, I., Nir, I., Leibman-Markus, M., et al. (2020). Characterization of the cytokinin sensor TCSv2 in arabidopsis and tomato. *Plant Methods* 16, 152. doi: 10.1186/s13007-020-00694-2

Uslu, V. V., and Grossmann, G. (2016). The biosensor toolbox for plant developmental biology. *Curr. Opin. Plant Biol.* 29, 138–147. doi: 10.1016/j.pbi.2015.12.001

van Munster, E. B., and Gadella, T. W. (2005). Fluorescence lifetime imaging microscopy (FLIM). *Adv. Biochem. Eng. Biotechnol.* 95, 143–175. doi: 10.1007/b102213

Vijayan, A., Tofanelli, R., Strauss, S., Cerrone, L., Wolny, A., Strohmeier, J., et al. (2021). A digital 3D reference atlas reveals cellular growth patterns shaping the arabidopsis ovule. *Elife* 10, e63262. doi: 10.7554/eLife.63262

Waadt, R., Krebs, M., Kudla, J., and Schumacher, K. (2017). Multiparameter imaging of calcium and abscisic acid and high-resolution quantitative calcium measurements using r-GECO1-mTurquoise in arabidopsis. *N. Phytol.* 216, 303–320. doi: 10.1111/nph.14706

Waadt, R., Kudla, J., and Kollist, H. (2021). Multiparameter *in vivo* imaging in plants using genetically encoded fluorescent indicator multiplexing. *Plant Physiol.* 187, 537–549. doi: 10.1093/plphys/kiab399

Walia, A., Waadt, R., and Jones, A. M. (2018). Genetically encoded biosensors in plants: pathways to discovery. *Annu. Rev. Plant Biol.* 69, 497–524. doi: 10.1146/annurev-arplant-042817-040104

Wang, L., Xue, Y., Xing, J., Song, K., and Lin, J. (2018). Exploring the spatiotemporal organization of membrane proteins in living plant cells. *Annu. Rev. Plant Biol.* 69, 525–551. doi: 10.1146/annurev-arplant-042817-040233

Weidtkamp-Peters, S., and Stahl, Y. (2017). The use of FRET/FLIM to study proteins interacting with plant receptor kinases. *Methods Mol. Biol.* 1621, 163–175. doi: 10.1007/978-1-4939-7063-6_16

Whitesides, G. M. (2006). The origins and the future of microfluidics. *Nature* 442, 368–373. doi: 10.1038/nature05058

Wolny, A., Cerrone, L., Vijayan, A., Tofanelli, R., Barro, A. V., Louveaux, M., et al. (2020). Accurate and versatile 3D segmentation of plant tissues at cellular resolution. *eLife* 9, e57613. doi: 10.7554/eLife.57613

frontiers | Frontiers in Plant Science

TYPE Original Research
PUBLISHED 29 September 2022
DOI 10.3389/fpls.2022.979141

OPEN ACCESS

EDITED BY
Jennifer Brophy,
Stanford University, United States

REVIEWED BY
Zhenfeng Yang,
Zhejiang Wanli University, China
Chandana Haldar,
Banaras Hindu University, India

*CORRESPONDENCE
Judit Dobránszki
dobranszki@freemail.hu

†These authors have contributed equally to this work and share last authorship

SPECIALTY SECTION
This article was submitted to Plant Physiology, a section of the journal Frontiers in Plant Science

RECEIVED 27 June 2022
ACCEPTED 13 September 2022
PUBLISHED 29 September 2022

CITATION
Pesti-Asbóth G, Molnár-Bíróné P, Forgács I, Remenyik J and Dobránszki J (2022) Ultrasonication affects the melatonin and auxin levels and the antioxidant system in potato *in vitro*.
Front. Plant Sci. 13:979141.
doi: 10.3389/fpls.2022.979141

Ultrasonication affects the melatonin and auxin levels and the antioxidant system in potato *in vitro*

Georgina Pesti-Asbóth[1], Piroska Molnár-Bíróné[1], Ildikó Forgács[1], Judit Remenyik[1†] and Judit Dobránszki[2*†]

[1]Institute of Food Technology, Faculty of the Agricultural and Food Science and Environmental Management, University of Debrecen, Debrecen, Hungary, [2]Centre for Agricultural Genomics and Biotechnology, Faculty of the Agricultural and Food Science and Environmental Management, University of Debrecen, Nyíregyháza, Hungary

Melatonin is an ancient hormone whose physiological effects have been extensively studied in animals and human. We now know that it also plays a prominent role in the growth and development of plants. In our present experiment, the relationship between endogenous melatonin and the antioxidant system was investigated in potato plant grown *in vitro*. Changes in redox homeostasis under ultrasound stress were examined. The concentration of small molecule antioxidants and enzymes of the three-level antioxidant pathway was measured. ELISA method was used to determine the melatonin levels in plant tissues at each growth stage (0 h, 24 h, 48 h, 1 week, and 4 weeks after subculturing the explants) both in control and ultrasound-treated plants. Ultrasound stress activated the three-level defense system and decreased the endogenous melatonin levels. Melatonin was able to provide protection against membrane damage caused by drastic ultrasound treatment. Melatonin at the heart of the redox network is a key component regulating various biochemical, cellular, and physiological responses. It has a dual role, as it is able to act both as a growth regulator and an antioxidant. A close relationship was evidenced between the plant hormone indole-3-acetic acid and melatonin and ascorbic acid.

KEYWORDS

redox homeostasis, endogenous melatonin, glutathione, lipid peroxidation, indole-3-acetic acid

1 Introduction

Melatonin (MT) is a long-known (since the 1950s) hormone, and several research studies that have been published point out that it takes part, either directly or indirectly, in the regulation of almost every physiological process, including the circadian rhythm (Dijk and Czeisler, 1994). The new miracle of this old hormone was the discovery of its synthesis in plants, and like its multiple roles in vertebrates, it is also essential in them (Cassone, 1998; Arnao and Hernández-Ruiz, 2013; Arnao and Hernández-Ruiz, 2014; Arnao and Hernández-Ruiz, 2015; Battacharya and Jha, 2020).

Several research groups have started to study the effects of exogenous MT on the agricultural crops. It was studied in terms of how it can raise biomass by increasing stress tolerance (Erland et al., 2015). Experiments have proven that it inhibits chlorophyll degradation in leaves or their ageing (Erland et al., 2015). MT can enhance rooting, root regeneration, and the adaptation to different abiotic stress factors, thus tolerating salt stress and water shortage (Li et al., 2017). These effects directly contributed to improved yields and increased food production. Most of the world face malnutrition and increased food demand with low resources, so it is important to know how MT can play a significant role in improving crop yield. However, it is very important to investigate the possible and potential role of MT in detail, including with model systems such as *in vitro* plant tissue culture. This is important because MT has several functions (Arnao and Hernández-Ruiz, 2019), so it cannot be questioned that it may have a toxic concentration both on plants and on the other members of the food chain. We do not have yet convincing knowledge of its effect on bacteria and fungi, the microflora of soil and animals.

Although more and more data are available on the growth-stimulating effect of exogenous MT, little is known about its regulatory role in the presence and accumulation of endogenous MT. This is understandable since it is present in different amounts in different plant species and even varieties, but it is also known that the amount is different in different parts of the plant within a plant and depends also on the developmental stage (Van Tassel et al., 2001; Arnao and Hernández-Ruiz, 2015). Moreover, it is known that its concentration varies depending on the time of day (Arnao and Hernández-Ruiz, 2015). There is likewise the lack of a uniform, accepted test protocol facilitating the determination of endogenous melatonin levels.

In our present study, stress conditions were induced by different ultrasound treatments. Ultrasound is an abiotic stressor that can also be used to modify plant growth and development *in vitro*, and its use can be incorporated into existing micropropagation techniques easily (Teixeira da Silva and Dobránszki, 2014; Teixeira da Silva et al., 2020). The aim of our present experimental work was to study the mechanisms which help to understand the role of MT under stress conditions and its relationship with indole-3-acetic acid (IAA) metabolism. How can MT coordinate the growth and improve the stress response of plants *in vitro*? What cascade processes were induced by ultrasound stress, and how does the endogenous MT-IAA concentration change? How can MT protect photosynthesis *via* supporting chlorophyll synthesis during adaptation to abiotic (ultrasound) stress?

2 Materials and methods

2.1 Plant material and ultrasonication of *in vitro* plant explants

The plant material (*Solanum tuberosum* L. cv. Desirée, 4-week-old *in vitro* plantlets) and growing conditions *in vitro* were identical as described earlier in Teixeira da Silva et al. (2020). The *in vitro* single-node segments of stems excised from 4-week-old plantlets were ultrasonicated at 35 kHz, 20°C, and 70 W for 0 (control), 20, and 30 min by Elmasonic X-tra 30 H ultrasonicator and then cultured on Murashige and Skoog (1962) medium (MS medium) as described in detail earlier (Teixeira da Silva et al., 2020). In short, ultrasonication occurred in the ultrasonicator in 50-ml glass beakers, each containing 90 explants immersed in 40 ml liquid MS medium. The beakers were surrounded by distilled water in the ultrasonicator, and the temperature of the water was kept constant at 25°C. The explants were placed in 400-ml glass jars containing 50 ml of MS medium and 30 explants; in total, 750 explants were used for each treatment. The plant cultures were grown *in vitro* for 4 weeks at 22 ± 2°C under a 16-h photoperiod at a photosynthetic photon flux density of 63.5 µmol m^{-2} s^{-1}.

2.2. Sampling times and measurements of morphological parameters and chlorophyll content

Plant samples were taken at 0 h, 24 h, 48 h, 1 week, and 4 weeks after ultrasonication, and they were stored at -80°C until biochemical analysis. For sampling, at least 90 explants (at 0, 24, and 48 h) or plantlets (at 1 and 4 weeks) were used from three different jars.

At the end of the *in vitro* subculture (at 4 weeks), the length and fresh weight of shoots and roots and the number of nodes per plantlet were measured. The chlorophyll a (*chl a*), chlorophyll b (*chl b*), and *chl a* + *chl b* contents in shoots of 4-week-old plantlets were determined spectrophotometrically, and the ratio of *chl a*/*chl b* was calculated as described earlier (Dobránszki and Mendler-Drienyovszki, 2014; Dobránszki

et al., 2017). For morphological measurements and chlorophyll content analysis, plant samples taken from five jars, each of which contained 30 explants/plantlets, were used.

2.3 Biochemical analyses

2.3.1 Sample preparation

Three replicates of each plant sample were used for sample preparation, each containing 250 mg of plant material. Frozen (plant) samples were homogenized with mortar and pestle under liquid nitrogen and extracted in 3 ml of ice-cold 50 mmol sodium phosphate buffer. The received solution was centrifuged at 10,000 × *g* at 4°C for 20 min. The supernatant was collected and stored at -20°C until the experiments. Through measuring the glutathione (GSH), glutathione reductase (GR), superoxide dismutase (SOD), ascorbic acid peroxidase (APX), IAA, glutathione synthetase (GSS), and ascorbic acid (AA) levels, absorbance was determined by a BMG Labtech SpectroStar Nano microplate reader.

Moreover, 200 mg of samples was frozen at -70°C and lyophilized to determine the lipid-soluble antioxidant capacity (ACL) and the water-soluble antioxidant capacity (ACW). After dehydration, the samples were ground to fine powder. To measure ACL and ACW, 25–25 mg of dry powder was dissolved in 1 ml methanol and 1 ml dH_2O, respectively, during electromagnetic stirring for 60 s at 25°C. The homogenates were centrifuged at 10,000 × *g* at room temperature for 5 min. The supernatant was collected and stored at -20°C until the measurement. ACL and ACW were detected with Analytikjena PhotoChem.

2.3.2 Measurements

Commercially available kits were used for the determination of catalase (CAT; Abnova, Taipei, Taiwan), SOD (ACW:849-60002-0; SOD: SIGMA: S7571; Analytikjena AG, Jena, Germany), GSH (kit number: 703002 Cayman Chemical Ann Arbor, MI, USA), GR (kit number: ab83461; Abcam plc., Cambridge, UK), GST (Abcam plc.), APX (MyBiosource, Inc., San Diego, CA, USA), ACW (kit number: 846-60002-0; Analytikjena AG), ACL (kit number: 849-60004-0; Analytikjena AG), AA (kit number: ab65346; Abcam), indol-3-aceic acid (kit number: CEA737Ge; Cloud-Clone Corp. Huston, Texas), melatonin (kit number: ab213978; Abcam plc., Cambridge, UK), glutathione synthase (kit number: MBS9373764; MyBioSource, Inc., San Diego, CA, USA). The reaction mixtures in each measurement were prepared, and then calculations were performed as described in each protocol book.

2.3.2.1 Determination of SOD

SOD was determined with a commercially available ACW kit (ACW: 849-60002-0; SOD: SIGMA: S7571; Analytikjena AG, Jena, Germany). The SOD of samples ensures the removal of superoxide anion radicals ($O_2^{\bullet -}$) formed by the auto-oxidation of hemoglobin. Furthermore, 1,500 µl R1, 1,000 µl R2, and 25 µl R3 reagents of ACW kit were mixed for making blanks. Using at least five points with the standard of the SOD enzyme, a calibration was made between 0.02112 and 0.2112 nmol. For measurements, we used the supernatant of the samples. Moreover, 1,490 µl of R1, 1,000 µl of R2, 25 µl of R3, and 10 µl of the samples were included in the working solution. The results generated by PhotoChem were compared with the standard equation and re-counted to units per milliliter. The SOD activity of the samples was expressed in units per milliliter.

2.3.2.2 Determination of reduced glutathione and oxidized glutathione

The concentration of reduced glutathione and oxidized glutathione was determined using a commercially available assay kit (kit number: 703002 Cayman Chemical Ann Arbor, Michigan). In the assay, 5,5′-dithio-bis(2-nitrobenzoic acid) (DTNB) and GSH react and generate a yellow product (2-nitro-5-thiobenzoic acid). Under the assay conditions, GSSG was reduced, producing 2 mEq of GSH. The kit reagents were dissolved according to the "reagent preparation" chapter. The standard curve was prepared as described in the kit. Then, 50 µl of standards was added to the designated wells on the plate. Moreover, 50 µl of each sample was added to the sample wells. The assay cocktail contained 117.2 µl MES buffer, 4.70 µl cofactor mixture, 22 µl enzyme mixture, 24 µl dH_2O, and 4.67 µl reconstituted DTNB per well. In addition, 150 µl assay cocktail was added to each of the wells containing standards and samples. The plate was incubated at 25°C for 25 min in the dark. The measurement was started after the incubation immediately. The concentration of GSH and GSSG was determined by measuring the absorbance colorimetrically at 405 nm. The sample GSH concentration was compared with a GSH standard curve, and the concentration of GSH was expressed as plant GSH concentration (in µM). The sample GSSG concentration was compared with the GSSG standard curve, and the concentration of GSSG was expressed as plant GSSG concentration (in µM).

2.3.2.3 Determination of glutathione reductase

The GR activity was determined using a commercially available assay kit (kit number: ab83461; Abcam plc., Cambridge, UK). In this assay, GR forms GSH from GSSG; then, while GSH reacts with DTNB, 2-nitro-5-thiobenzoate anion (TNB^{2-}) is generated. By measuring the change in absorbance at 405 nm, the GR activity can be determined. The kit reagents were dissolved as described in the protocol book. The samples were pre-treated first. Next, 5 µl 3% H_2O_2 was added to 100 µl of each sample. The samples were incubated at 25°C for 5 min. Then, 5 µl of CAT was added to the samples, and

the samples were incubated at 25°C for another 5 min. After the pre-treating procedure, 50 µl of the pre-treated samples was added into the sample wells. The standard curve was prepared as described in the kit, and 50 µl of the diluted standard solution was added into the correct wells. The reaction mixture was prepared as described in the protocol book. The mix contained 40 µl GR assay buffer, 2 µl DTNB solution, 2 µl NADPH solution, and 6 µl GSSG solution per well, except the standard wells. Furthermore, 50 µl of the reaction mixture was added to the samples. The microplate reader was set to take one reading every 5 min for 30 min for GR activity measurement. The measurement was started immediately after the addition of the reaction mixture. The kinetics of the reaction was read to ensure that A_1 and A_2 were in a linear reaction range, and $\Delta A_{405nm} = A_2 - A_1$ (A_2 is the absorbance data in the second reading, and A_1 is the absorbance data in the first reading). The TNB standard curve was plotted, and ΔA_{405nm} was applied to this curve to obtain ΔB nmol of TNB. The obtained result was substituted into the equation described in the kit's instruction:

GR activity = $\frac{\Delta B}{(T_2 - T_1) \quad 0.9V}$ D = nmol/min/mL = mU/mL [ΔB is the TNB amount from the TNB standard curve (in nmol)]. T_1 is the time of the first reading (A_1) (in min). T_2 is the time of the second reading (A_2) (in min). V is the pre-treated sample volume added into the reaction well (in ml); 0.9 is the sample volume change factor during the sample pre-treatment procedure; D is the dilution factor, as suggested in the kit's description. The GR activity was expressed as plant GR activity (in nmol/min/ml = mU/ml).

2.3.2.4 Determination of GPX

The glutathione peroxidase (GPX) activity was determined using a commercially available assay kit (kit number: ab102530; Abcam plc.). In this assay, GPX generates GSSG from GSH during H_2O_2 reduction, and that generated GSSG reduced back to GSH by GR during the consumption of nicotinamide adenine dinucleotide phosphate (NADPH). The NADPH reduction is proportional to the GPX activity and can be measured colorimetrically at 340 nm. The kit reagents were dissolved as described in the protocol book. The standard curve was prepared as described in the kit, and 90 µl of the diluted standard solutions was added into the correct wells. Then, 50 µl of samples, positive control, and reagent control was added to the plate into the correct well. The reaction mixture was as described in the protocol book. The mix contained 33 µl assay buffer, 3 µl 40 mM NADPH solution, 2 µl GR solution, and 2 µl GSH solution per well except the standard wells. Then, 40 µl of the reaction mix was added to the samples, positive control, and reagent control. The plate was incubated at room temperature for 15 min. After incubation, the absorbance was measured. If the absorbance value of the samples was lower than 1.0, then 1 µl of 40 mM NADPH was added to the sample. Moreover, 1 µl of 40 mM NADPH gives a ~0.5 increase of absorbance at 340 nm. After this step, 10 µl of cumene hydroperoxyde was added to the samples, positive control, and reagent control wells to start the GPX reaction. The microplate reader was set to take one reading every 5 min for 30 min for GR activity measurement. The measurement was started immediately after the addition of the cumene hydroperoxide at ΔA_{340nm} [ΔA_{340nm} = (sample A_1 – sample A_2) - (reagent control A_1 - reagent control A_2) (A_1 is the absorbance value in the first reading, and A_2 is the absorbance data in the second reading)]. The NADPH standard curve was plotted, and ΔA_{340nm} was applied to this curve to obtain ΔB nmol of NADPH. The obtained result was substituted into the equation:

GPX activity = $\frac{\Delta B}{(T_2 - T_1) \quad V}$ D = nmol/min/mL = mU/mL [ΔB = NADPH amount that was decreased between T_1 and T_2 (in nmol), T_1 = time of the first reading (A_1) (min), T_2 = time of second reading (A_2) (min), V = pre-treated sample volume added into the reaction well (ml), and D = sample dilution factor]. The NADPH standard curve was plotted, and the equations suggested by the kit were used. The activity of GPX was expressed as a plant GPX activity (mU/ml).

2.3.2.5 Determination of glutathione-S-transferase

The glutathione-S-transferase (GST) activity was determined by a commercially available kit (Abcam plc.). The assay is based on the reaction between GSH and 1-chloro-2,4-dinitrobenzene (CDNB), of which the reaction depends on the presence of the active GST under certain conditions. The kit reagents were dissolved as described in the protocol book. Then, 50 µl of the samples, diluted positive control, and negative control was added into the correct wells. The reaction mixture was as described in the protocol book. The mix contained 49 µl GST assay buffer and 1 µl GST substrate (CDNB) solution per well. In addition, 50 µl of the reaction mixture was added to each well. The microplate reader was set to take one reading every 2 min for 16 min for GST activity measurement. The measurement was started immediately after the addition of the GST reaction mix. The changes of the absorbance were measured at 340 nm.

$$\Delta A340nm = \frac{\Delta A340 \quad (\text{time2}) - \Delta A340 \quad (\text{time1})}{\text{Time} \quad 2 \quad (\text{min}) - \text{Time} \quad 1 \quad (\text{min})}$$

(A_1 is the absorbance value in the first reading, and A_2 is the absorbance data in the second reading) was determined for all samples. The obtained result was substituted into the equation:

GST activity = $\frac{\Delta A340\ \text{nm}}{(0.0096) \quad (0.2893) \quad (D/A)}$ [0.0096 µmol^{-1} cm^{-1} is the extinction coefficient of the glutathione-DNB adduct, A = sample volume added into the reaction well (ml), D = sample dilution factor, V = sample volume added to the well (ml), and

0.2893 cm is the light path of the 0.1 ml reaction volume in a Greiner Bio One 655101 96-well plate (cm)]. The GST activity of the samples was expressed as plant GST activity (in mU/ml).

2.3.2.6 Determination of APX

APX was determined using a commercially available kit (MyBiosource, Inc., San Diego, CA, USA). The kit is based on double-sandwich ELISA where the substrate (TMB) finally turns into a yellow product and the depth of the yellow color was measurable at 450 nm and positively correlated with APX activity. The kit reagents were dissolved as described in the protocol book. The standard curve was prepared as described in the kit, and the diluted standard solutions were added into the correct wells. First, samples, blank, and different concentrations of standards were added to the corresponding wells (100 µl for each well). The reaction wells were sealed with adhesive tapes and incubated at 37°C for 90 min. After this step, the plate was washed three times with 350 µl diluted washing buffer. Thereafter, 100 µl of biotinylated plant APX antibody liquid was added to each reaction well. The reaction wells were sealed with adhesive tapes, and the plate was incubated at 37°C for 60 min. After incubation, the plates were washed as described previously. Then, 100 µl of enzyme–conjugate liquid was added to each well, except the blank wells. The reaction wells were sealed with adhesive tapes and incubated at 37°C for 30 min. The plate was washed five times as described. Then, 100 µl of Colour Reagent was added to each well. The reaction wells were sealed with adhesive tapes and incubated at 37°C for 30 min. In the last step, 100 µl of Colour Reagent C was added to each well, and the absorbance was measured at 450 nm. The concentration of APX in the samples was determined by comparing the absorbance values of the samples to a standard curve. The APX concentration was expressed as plant APX concentration (in ng/ml).

2.3.2.7 Determination of the antioxidant capacity of water-soluble compounds

ACW was determined using a commercially available ACW kit (kit number: 846-60002-0; Analytikjena AG). Radicals are generated photo-chemically by UV irradiation of a photosensitizer compound. The PhotoChem measures the inhibition of radicals by the sample ACW content.

The ACW kit contained R1, R2, R3, and R4 reagents. R1 and R2 were ready for use and stored at 2–8°C. R3 was lyophilized and stored at -20°C until use. Furthermore, 750 µl of R2 reagent was added into R3 and was ready to use. A stock solution was made from R4 reagent; 490 µl of R1 reagent and 10 µl of H_2SO_4 were added into R4 reagent. Ten-fold dilutions were done from the stock solution (10 µl of R4 stock solution + 990 µl of R1 solution). First, the blank was made: 1,500 µl of R1, 1,000 µl of R2, and 25 µl of R3 were mixed. The calibration was made between 0, 1, and 2 nmol (at least five points) with L-ascorbic acid standard. Moreover, 25 mg of the lyophilized sample was dissolved in dH_2O and mixed for 90 s after the sample was centrifuged at 10,000 rpm for 5 min. The supernatant of the prepared samples was used for the measurement. The working solution contained 1,490 µl of R1, 1,000 µl of R2, 25 µl of R3, and 10 µl of the samples. The calculation for the lyophilized sample was as follows:

$$\text{Concentration} = \frac{(\text{results})\,(\text{dilution})\,(176.13)}{(\text{sample volume})\,(\text{used lyophilized quantity})}$$

The result by the PhotoChem; 176.13: vitamin C molecular weight; sample volume: pipetted volume (in µl), lyophilized sample quantity (in mg). The final result was added in microgram per milligram (µg/mg) ascorbic acid equivalent.

2.3.2.8 Determination of antioxidative capacity of lipid compounds

The antioxidative capacity of lipid compounds (ACL) was determined using a commercially available ACL kit (kit number: 849-60004-0; Analytikjena AG). The methodology is similar as that which was used for the ACW test. The ACL kit contained R1, R2, R3, and R4 reagents. R1 and R2 were ready for use and stored at 2–8°C. R3 was lyophilized and stored at -20°C until use. Moreover, 750 µl of R2 reagent was added into R3 and was ready to use. The stock solution was made from R4 reagent, 500 µl of R1 reagent was added into R4 reagent, and there were 10-fold dilutions obtained from the stock solution (10 µl of R4 stock solution + 990 µl of R1 solution. First, the blank was made: 2,300 µl of R1, 200 µl R2, and 25 µl R3 were mixed. The calibration was made between 0.2 and 3 nmol (at least five points) with trolox standard. Then, 25 mg of the lyophilized sample was dissolved in 1 ml of methanol and mixed for 90 seconds after the sample was centrifuged at 10,000 × *g* for 5 min. The supernatant of the prepared samples was used for the measurement. The working solution contained 2,290 µl of R1, 200 µl of R2, 25 µl of R3, and 10 µl of the samples. The calculation for lyophilized sample is as follows:

$$\text{Concentration} = \frac{(\text{results})\,(\text{dilution})\,(250.3)}{(\text{sample volume})\,(\text{used lyophilized quantity})}$$

The result by PhotoChem; 250.3: trolox molecular weight; sample volume: pipetted volume (in µl), lyophilized sample quantity (in mg). The final result was added in µg/mg trolox equivalent.

2.3.2.9 Determination of ascorbic acid (vitamin C)

The ascorbic acid (AA) concentration was determined using a commercially available assay kit (kit number: ab65346; Abcam plc.). In this assay, a proprietary catalyst oxidizes AA to produce products that interact with the AA probe, generating color. The

kit reagents were dissolved as described in the protocol book. The standard curve was prepared as described in the kit, and the diluted standard solutions were added into the correct wells (120 µl); 120 µl of the blank and samples, respectively, was added to the correct well. The reaction mix was prepared according to the protocol book. Moreover, 50 µl of the reaction mix was added to each well. The color was developed within 3 min and stable for an hour. Absorbance was measured at 570 nm. An AA standard curve was plotted, and the equation Concentration = $\frac{As}{Sv}$ (where As is ascorbic acid amount from the standard curve, and Sv is the sample volume added in the sample wells) was used as suggested in the kit's description. The results were multiplied by the molecular weight of AA (176.12 g). The AA concentration of samples was expressed as plant AA concentration (in ng/µl) [1].

2.3.2.10 Determination of melatonin

Melatonin was determined using a commercially available assay kit (kit number: ab213978; Abcam plc.). The determination of melatonin is independent of species. All reagents and samples were prepared as described in the protocol book. To determine the melatonin concentration, 500 mg of sample was ground in liquid nitrogen. The dried and ground samples were dissolved in 125 µl of stabilizer solution, and then 750 µl cold ethyl acetate was added. The sample solutions were vortexed for 30 s and were placed on ice for 3 min. After this, they were vortexed again as mentioned previously and were placed on ice for 2 min. The solutions were placed in ultrasonic bath for 5 min. All samples were centrifuged at 4°C 1,000 × *g* for 10 min. The upper phase was removed, and the lower phase was dried with vacuum centrifuge. In this assay, the samples (100 µl), standards (100 µl), and stabilizer (100 and 150 µl) were added to 96 wells coated with IgG antibody specific to free melatonin. A solution of a biotin-labeled melatonin tracer (50 µl) was also added to the plate, and it was sealed. The plate was incubated for 1 h at 500 rpm and room temperature. Under these conditions, the specific antibody binds to melatonin in the sample or to the tracer. The plate was washed three times with 400 µl of wash solution after the incubation. The wells were empty after the wash procedure. Furthermore, 200 µl of melatonin conjugate was added into all wells, except the blank wells, which binds to the biotinylated tracer. The plate was sealed and incubated for 30 min at 500 rpm and room temperature. The plate was washed as detailed previously. Then, 200 µl of TMB substrate was added into each well. The plate was sealed and incubated for 30 min at 500 rpm and room temperature. Under these conditions, blue color is generated. Moreover, 50 µl of stop solution was added to stop the substrate reaction. The color was changed to yellow, and it was measured at 450 nm. The standard curve was plotted, and the concentrations were calculated with MARS software as mentioned in the protocol book.

2.3.2.11 Determination of GSS

The concentration of GSS was measured by a commercially available ELISA kit (kit number: MBS9373764; MyBioSource, Inc. San Diego, CA, USA). The reagents were prepared as mentioned in the protocol book. Then, 50 µl of standards, samples, and blank, respectively, was added into the wells in duplicate. Horseradish peroxidase–conjugate reagent (50 µl) was added to each well. The plate was covered with a closure plate membrane and was incubated for 60 min at 37°C. The incubation mixtures of the wells were dumped into the proper waste container. Then, 350 µl of wash solution was added into each well, and after 1 min, the solution was aspirated. This step was repeated three more times for a total of four washes. Next, 50 µl of chromogen A and chromogen B, respectively, was added to each well. The plate was sealed and incubated for 15 min at 37°C. Then, 50 µl of stop solution was added to each well, and the optical density (OD) was measured at 450 nm. The standard curve was plotted, and the concentrations were calculated with MARS software as mentioned in the protocol book.

2.3.2.12 Determination of IAA

The concentration of IAA was measured with a commercially available ELISA kit ((kit number: CEA737Ge; Cloud-Clone Corp., Houston, TX, USA). All reagents and solutions were prepared as described in the protocol book. Then, 50 µl of standards, samples, and blank, respectively, was added into the determined wells, and then 50 µl of detection reagent A was added to each well immediately. The plate was sealed, shaken gently, and incubated for 1 h at 37°C. The solution in the wells was aspirated. The wells were washed with 350 µl of wash solution three times. Then, 100 µl of detection reagent B working solution was added to each well. The plate was sealed and incubated for 30 min at 37°C. The wash procedure was repeated for a total of five times as described previously. Moreover, 90 µl of substrate solution was added to each well. The plate was sealed and incubated for 10 min at 37°C. Then, 50 µl of stop solution was added to each well, and the OD was measured at 450 nm. The standard curve was plotted, and the concentrations were calculated with MARS software as mentioned in the protocol book.

2.4 Statistical analyses

The morphological parameters and chlorophyll content data of plantlets were analyzed by one-way ANOVA followed by Tukey's test at $p < 0.05$ using SPSS for Windows software (SPSS®, version 21.0). The antioxidant parameters were analyzed by one-way ANOVA followed by Tukey's test (at $p < 0.05$) for multiple comparisons using GraphPad Prism (version 9), and the results are presented as mean ± SEM. The correlation between

biochemical parameters was analyzed by Pearson correlation ($p< 0.05$).

3 Results

3.1 After-effects of ultrasonication on the growth parameters and chlorophyll content of *in vitro* potato plantlets

The morphological parameters and chlorophyll content of *in vitro* shoots were measured 4 weeks after ultrasonication, at the end of the subculture. Except for the number of nodes per plantlet (NN), which was not affected by the ultrasound (US) treatments, all other measured morphological parameters and the chlorophyll content of the 4-week-old plantlets were modified in response to ultrasonication by the end of the subculture (Table 1). The length of shoots (SL) decreased after ultrasonication; however, with increase in the exposure time to 30 min, the decrease was significantly lower than after the shorter exposure time (20 min). The length of the roots and the fresh weight of shoots were increased by ultrasonication but independently of the exposure time. However, the fresh weight of roots (RFW) was increased only after a shorter exposure time (20 min), while extending the exposure time of ultrasound treatment did not cause a significant change in the RFW compared with the control.

Both the *chl a* and the *chl b* contents decreased after ultrasonication. The extension of the exposure time caused a significant further decrease in both parameters. The extent of the decrease was more pronounced in *chl b* than in *chl a*. The *chl a* content was reduced by 20 and 33% after exposure to ultrasound for 20 and 30 min, respectively, compared with the control, while the decrease of *chl b* was 48 and 58% after each respective US treatment (Table 1).

3.2 Changes in the concentration of small molecule antioxidants and the activity of antioxidant pathway enzymes, melatonin, and IAA levels

Comparing the water-soluble antioxidant capacity (ACW) and the lipid-soluble antioxidant capacity (ACL) of control plants (Figure 1), we found that ACL was a multiple of ACW. Significant differences were noted only in ACL values which were similar to those of a former study that included another ultrasound treatment (Dobránszki et al., 2017). In the intensive growth phases, in 24-h- and 1-week-old plantlets, the metabolic stress triggered by growth and development was so significant that the ACL values largely decreased. The US treatments for 20 and 30 min did not influence this tendency, and a large amount of prooxidant was produced because of the intensive anabolic processes, which largely decreased the antioxidant capacity; however, the applied stress factor did not decrease it. It cannot be seen that the degradation of molecules, which eliminated prooxidants caused by metabolic and abiotic stress, was composed additively (Figure 1).

By studying the SOD activity (Figure 1), we found that it increased significantly at 24 and 48 h compared with 0 h in the control group. In 1-week-old plantlets, the SOD activity decreased, and then a further decrease could be seen in the 4-week-old plantlets. This tendency did not change significantly if the plant material was ultrasonicated for 20 min. However, in 48-h-old plants, the SOD activity did not increase in response to the 30-min-long US treatment. A significant increase of SOD activity could be detected in 1-week-old plantlets, but it did not change significantly in 4-week-old samples.

The GSH concentration of the control plant gradually increased in certain growth phases, and then in the 1-week-old plant, it significantly decreased. In this phase, the radicle transforms into root and the axillary buds transform into

TABLE 1 Morphological parameters and chlorophyll (*chl*) content of *in vitro* plantlets 4 weeks after exposure to different ultrasound (US) treatments.

	Control[a] (non-ultrasonicated)	20-min US[a]	30-min US
Shoot length (mm)	74.11 ± 1.53 a	59.15 ± 1.77 c	67.44 ± 1.69 b
Number of nodes/plantlets	6.91 ± 0.09 a	6.84 ± 0.14 a	7.09 ± 0.35 a
Shoot weight (g/vessel)	3.96 ± 0.27 b	5.09 ± 0.16 a	5.38 ± 0.18 a
Root length (mm)	48.97 ± 1.29 b	58.38 ± 2.12 a	58.83 ± 1.99 a
Root weight (g/vessel)	2.84 ± 0.28 b	4.79 ± 0.23 a	3.27 ± 0.25 b
chl a content (μg/g FW)	840.1 ± 68.8 a	677.7 ± 31.7 b	439.7 ± 38.6 c
chl b content (μg/g FW)	232.9 ± 18.3 a	155.7 ± 7.9 b	97.5 ± 8.5 c
chl a + *chl b* content (μg/g FW)	1,074.9 ± 87.1 a	834.9 ± 39.6 b	538.0 ± 42.3 c
chl a/*chl b*	3.60 ± 0.05 c	4.36 ± 0.04 b	4.52 ± 0.11 a

[a]Data from control and 20-min US were presented in a recent publication (Teixeira da Silva et al., 2020) in another context. Mean values (± standard error) followed by different letters in each row indicate significantly (P< 0.05) different values between treatments according to ANOVA followed by the Tukey test.
FW, fresh weight.

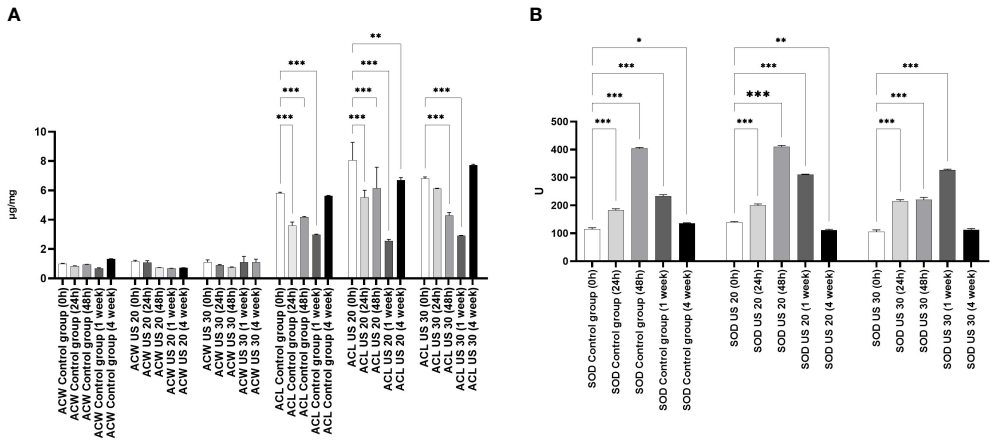

FIGURE 1
Effect of the sampling time and ultrasound treatments on the water soluble antioxidant capacity (ACW) and the lipid-soluble antioxidant capacity (ACL) **(A)** and the SOD activity **(B)**. *, **, *** mean the significant differences at $P < 0.05$, $P < 0.01$, $P < 0.001$, respectively.

leaves. Similar to our former experimental results (Dobránszki et al., 2017), GSH was needed to eliminate the intensive radicle production in this phase, which can explain the decrease of its concentration (Figure 2). As a result of the US treatments, its concentration increased in the different sampling times; the US treatment for 30 min also resulted in its very high concentration in the 4-week-old plant. At the background of these changes, there can be a change of activity of GSS because its activity and

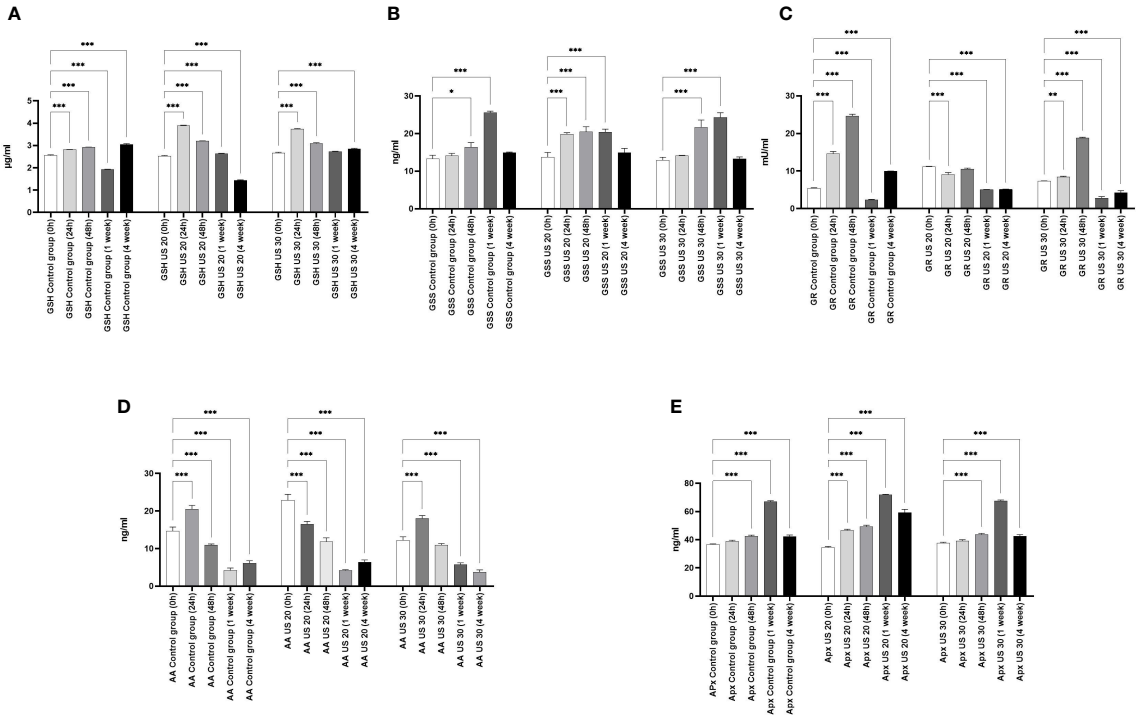

FIGURE 2
Effect of the sampling time and ultrasound treatments on reduced glutathione (GSH) concentrations **(A)**, glutathione synthetase (GSS) concentration **(B)**, glutathione reductase (GR) activity **(C)**, ascorbic acid (AA) concentration **(D)**, and ascorbic acid peroxidase (APX) concentration **(E)**. *, **, *** mean the significant differences at $P < 0.05$, $P < 0.01$, $P < 0.001$, respectively.

10.3389/fpls.2022.979141

the amount of GSH are inverses of each other. GR is responsible for maintaining the glutathione pool by splitting the conjugated glutathione. Our results are not surprising. In the control group, it follows the change of the GSH concentration. The US treatment for 20 min did not influence the direction of the quantitative changes; however, the GR activity decreased significantly. The US treatment for 30 min, which was a strong abiotic stress, increased the GR activity 48 h after ultrasonication, but in the following growth phases, it could not increase the enzyme activity compared with the control (Figure 2).

Besides the glutathione pool, ascorbic acid (AA) plays an important role in maintaining the redox homeostasis both in the detoxification phase and in the regeneration phase. At 24 h, its concentration in the control group increased; after that, a gradual decrease can be seen in the following growth phases (Figure 2). It is very considerable that, besides the metabolic stress caused by growth and development, the applied abiotic stress, *i.e.*, ultrasonication, did not change its concentration significantly in plants.

The IAA concentration did not change in the first 24 h, but in the other growth phases, it decreased in non-ultrasonicated plantlets (Figure 3). It did not decrease significantly in the 1-week-old plantlets compared with the initial stage. However, the US treatment produced its modulatory effect. The ultrasound treatment for 20 min significantly increased its concentration in the 4-week-old plantlets. Ultrasonication for 30 min did not cause an increase in the 1-week-old plantlets, but it caused a significant increase in all the other phases.

The MT concentration of the control group is significantly different in every growth phase (Figure 3). At 24 h, the MT concentration increased, then it decreased in 48-h-old and 1-week-old samples compared with the 0-h samples; in 4-week-old plantlets, however, its concentration increased significantly. Both the 20- and 30-min-long US treatments decreased the MT concentration in the plant samples compared with the control in every sampling time. After a 20-min-long ultrasonication, the MT level increased in the 24-h-old samples compared with the 0-h ones, while it decreased as a response to the 30-min-long US treatment. Both 20- and 30-min-long US treatments decreased the MT concentration in the later growth phases (48 h and 1 week), but then they increased it in 4-week-old plantlets.

4 Discussion

The *in vitro* plant tissue culture technique has a unique role in sustainable and competitive agriculture, horticulture, and forestry and has been successfully applied in plant breeding. Plant tissue culture has become an integral part of plant production and plant breeding. Plant tissue culture and micropropagation are playing an increasingly important role in green biotechnology. It can be an opportunity for producing excellent-quality, disease-free, and uniform plants. Various physical and chemical alternatives are searched to encourage the intensive growth of plants. Although the number of examinations is still restricted, there are evidence that ultrasonic treatment can increase the growth and development, including *in vitro* organogenesis as well (Teixeira da Silva and Dobránszki, 2014). However, there is no data on its exact mechanisms. Ultrasonication can result in cavitation and acoustic microflow, which can modify the ultrastructure of cells, enzyme activity, and cell growth. It can cause fractures in extracellular polymers, release DNA from the nucleus, decrease the stability of cells, change the permeability of the cell membrane, and modify the charges on the cell surface (Rokhina et al., 2009). It is necessary that, as a stress factor, it

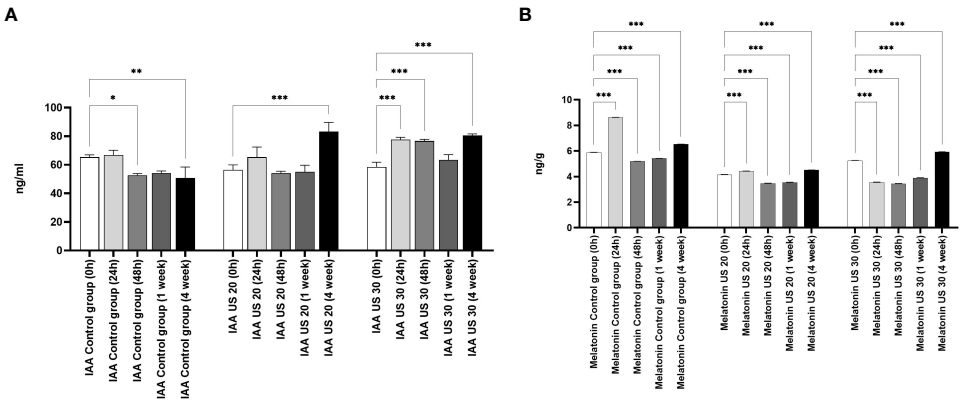

FIGURE 3
Effect of the sampling time and ultrasound treatments on the concentration of indole-3-acetic acid (IAA) **(A)**, and melatonin **(B)**. *, **, *** mean the significant differences at $P < 0.05$, $P < 0.01$, $P < 0.001$, respectively.

activates the three-level antioxidant protection system (Dobránszki et al., 2017). The ultrasonic treatment of plants also opens other routes and can be suitable for studying the role of melatonin in stress processes.

The increasing number of investigations has recently found that MT is essential in the regulation of both developmental processes and stress responses in plants (Van Tassel et al., 2001; Murch and Saxena, 2002; Arnao and Hernández-Ruiz, 2006; Wang et al., 2012; Arnao and Hernández-Ruiz, 2013; Arnao and Hernández-Ruiz, 2014; Arnao and Hernández-Ruiz, 2015; Reiter et al., 2016; Fan et al., 2018; Wang et al., 2018; Arnao and Hernández-Ruiz, 2019; Battacharya and Jha, 2020; Khan et al., 2020). The photoperiod and circadian rhythm controlling the role of MT is less relevant in plant tissue cultures than in *ex vitro* plants considering that the cultures *in vitro* are not autotroph but mixotroph (George and Davies, 2008). Our previous transcriptomic examinations (Teixeira da Silva et al., 2020) supported our present results and can give a possible explanation as to why the chlorophyll concentration decreased in response to the US treatments. Upregulation of the gene responsible for chlorophyllase was recently detected 24 h after the 20-min-long US treatment of single-node *in vitro* potato explants, which suggested the potential degradation of *chl a* and *chl b* (Teixeira da Silva et al., 2020). Our current measurements of chlorophyll content (Table 1) confirmed our earlier hypothesis based on a transcriptomic study (Teixeira da Silva et al., 2020) and proved that ultrasonication (35 kHz and 70 W for 20 min) by a liquid-based ultrasonicator caused the degradation of both *chl a* and *chl b*. In addition, the extension of the exposure period from 20 to 30 min led to a further decrease in the chlorophyll content of the 4-week-old plantlets in our present study. Exploring the real cause of the further decreases in the chlorophyll content by extending the exposure time of ultrasonication requires further investigation, but this may be due to either a further increase in the expression level of the gene responsible for chlorophyllase or alterations in the expression level of other genes responsible for the synthesis or degradation of chlorophyllase.

4.1 Endogenous melatonin as an antioxidant

In our previous experimental work (Dobránszki et al., 2017), when we applied a gentler US treatment, the results showed that the three-level antioxidant system was activated for the elimination of prooxidants. GSH was available for the glutathione-dependent enzymes of the enzymatic route. The GSH concentration increased for the effect of stress (for example, in the 4-week-old plants, it was 25 uM/ml) compared with the control group (Figure 2). AA, essential for GSH regeneration, was 40 ng/ml in the 4-week-old plantlets. If a much stronger ultrasound stress was applied (Dobránszki et al., 2020), as presented in this work, it could badly disturb the membrane integrity according to the literature (Rokhina et al., 2009), but we have got unexpected plant responses. The concentration of small molecule antioxidants was not increased compared with the control plants. These results suggest that, although the antioxidant protection system was activated, the small molecule antioxidants could not adjust the prooxidant–antioxidant balance. Therefore, another protection system was needed, which helps in eliminating the lipid peroxidation processes and supports the plant for it not to die from stress (Figure 4).

As was recently investigated, the gene expression of some enzymes related to the biosynthesis of MT and IAA changed when single-node *in vitro* explants of potato were exposed to ultrasonication for 20 min (Teixeira da Silva et al., 2020). Immediately after the 20-min-long US treatment, the genes for tryptophan (Trp) synthase (EC 4.2.1.20) were upregulated, causing an increased level of Trp, as a direct consequence of the US treatment. Trp is the precursor of both IAA and MT biosynthesis (Posmyk and Janas, 2009; Fan et al., 2018). Its downregulation was detected only 48 h after a 20-min-long ultrasonication. The measured MT level of the ultrasonicated samples, independently of the exposure time, was lower at 24 h, 48 h, and 1 week after ultrasonication compared with the control, presumably due to its use in stress mitigation caused by ultrasonication. However, by the end of the subculture, the MT level was significantly the highest after a 20-min-long ultrasonication, while its level remained significantly lower than in the control when ultrasonication was carried out for 30 min. However, the experimental results show no increase in MT levels after US treatment except for the 4-week-old plant but rather an increase in IAA concentration. This suggests that an increase in the expression of the genes for Trp synthase confirms the pathway for IAA synthesis, and the endogenous MT levels are generally constant and low in potato plants grown *in vitro*.

In plant tissue cultures, the low yield of the secondary metabolites can be explained with the lack of cell differentiation (Verpoorte et al., 2002). As a consequence, the concentrations of both the lipid-soluble (ACL) and especially the water-soluble antioxidants (ACW) are very low. However, the MT concentration was constant, which referred to its important role in maintaining the redox homeostasis during plant growth. The applied US treatment decreased its concentration, which can be explained by the fact that MT is an amphipathic molecule and can directly eliminate free radicals. Unlike the other radical catchers, it is a multifunctional antioxidant; it can easily get through the cell membranes because of its high lipophilicity and hydrophilicity (Hardeland, 2016). Unlike the other small-molecule biological antioxidants such as ascorbic acid, α-tocopherol, lipoic acid, *etc.*, MT does not go through a redox cycle; it can be considered a terminal antioxidant. It suffers a molecular transformation while efficiently eliminating free electrons from the system. All the products of this transformation are also strong antioxidants

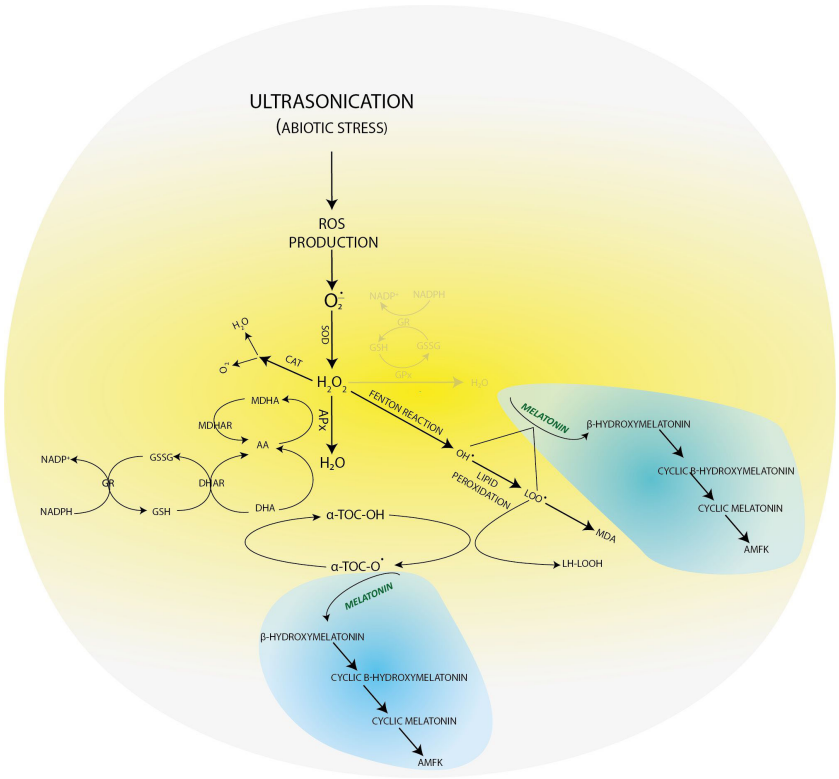

FIGURE 4
Molecular transformations of melatonin and its role in reactive oxygen species elimination. All products of its molecular transformation result in strong antioxidants (in blue bubbles), and they, as radical catchers, eliminate free electrons after exposure of the plant to different stresses.

themselves (for example, cyclic 3-hydroxi-melatonin, 2-formil-5-methoxyquinuramine, and *N*-acetil-5-methoxyquinuramine) (Davanipour et al., 2009). These metabolites (Figure 4) work as radical catchers sometimes more aggressively than the MT itself regarding ROS neutralization. Besides this, most of these processes have one more ROS in every step, so one MT molecule can bond 10 ROS, in contrast with the classical antioxidants. It was found that MT promotes to repair the oxidized DNA. This can be due to the fact that MT can transform the guanosine radical into guanosine with electron transfer. It was shown that MT decreased the production of 8-hydroxi-2′-dezoxiguanosine, a damaged DNA product, which is 60–70 times efficient than certain classical antioxidants (ascorbic acid and α-tocopherol) (Qi et al., 2000; Reiter et al., 2016). The synthesis of superoxide anions mainly takes places in mitochondria during the oxidative phosphorylation. The superoxide anions quickly enzymatically transform into H_2O_2 for the effect of SOD. Then, H_2O_2 transforms into water or a very poisonous hydroxyl radical. Although hydroxyl radical formation can take place in many ways; the *in vivo* degradation of superoxide anion and hydrogen peroxide catalyzed by transition metal is the most important mechanism. Hydroxyl radicals form from hydrogen peroxide during the oxygen metabolism of the cell and the Fenton and the Haber–Weiss reactions in the presence of free iron and copper ions (Manchester et al., 2015). OH• forms in the Fenton reaction, when hydrogen peroxide interacts with the transition metals (Fe^{2+}, Cu^{1+}, *etc.*).

If in certain growth cycles only metabolic stress affected the plant, the MT level correlated to the IAA level. The prooxidants, which form on the biosynthetic routes, were eliminated by the redox system from plant cells. If abiotic stress, the ultrasonication, which changes the integrity of the membrane system, was applied, the level of the measurable MT isomer decreased because hydroxy-melatonin derivatives possibly form. These compounds are used for eliminating the hydrogen peroxides which form from the superoxide anion in enzymatic processes during the relief of the redox system. It can be seen that the MT level negatively correlated with the redox enzymes and glutathione. The severe US treatment (30-min-long ultrasonication) did not cause very drastic changes in the redox homeostasis of the plants, which could not have been compensated (Figure 5).

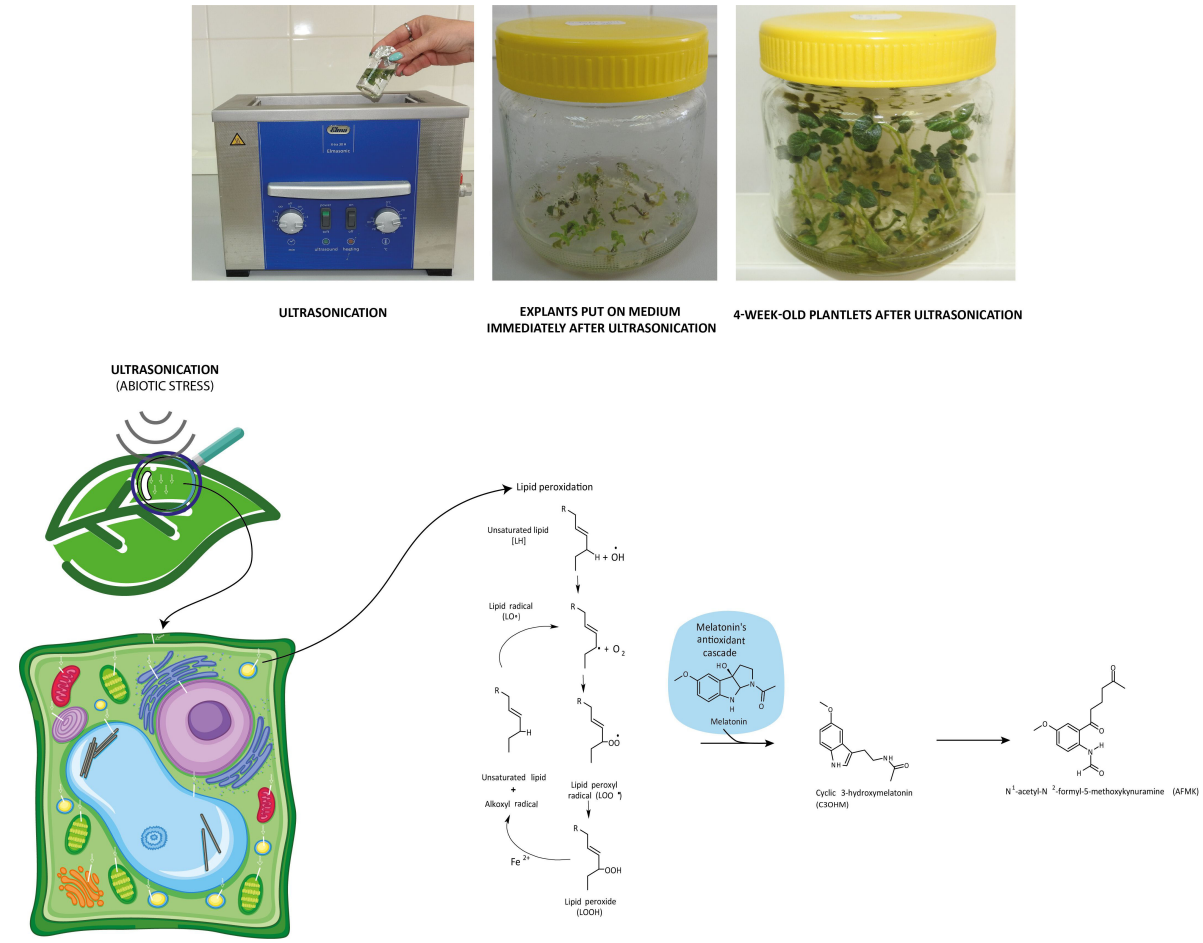

FIGURE 5
Ultrasonication of *in vitro* single-node potato explants and role of melatonin in the recovery of redox homeostasis after lipid peroxidation triggered by ultrasonication.

4.2 Endogenous melatonin as a growth regulator

The gene expression of indole pyruvate decarboxylase (EC 4.1.1.74), the key enzyme of the IAA biosynthesis (Koga, 1995), was upregulated 24 h after exposure to US for 20 min. At the same time (24 h), the expression intensity of tryptophan-tRNA ligase (EC 6.1.1.2) producing L-tryptophanyl-tRNA from Trp significantly decreased. Their downregulation was detected only 1 and 4 weeks after ultrasonication, respectively (Teixeira da Silva et al., 2020). This suggested that the 20-min-long ultrasonication supports the biosynthesis of IAA 24 h after the US treatment. Although data on the morphological parameters, like increasing fresh weight of shoots and roots and root length, may refer to auxin predominance in plantlets, the exact measurements of IAA content did not show a significantly increased level of IAA compared with the control after a 20-min-long exposure time of US. However, when the explants were treated with ultrasound for 30 min, the IAA level significantly increased 48 h and 1 week after ultrasonication.

The decrease in the shoot length of 4-week-old plantlets after ultrasonication of explants for 20 min may be connected to the earlier results that came from a transcriptomic study (Teixeira da Silva et al., 2020). In this study, the upregulation of the gene coding for gibberellin 2β-dioxygenase (EC 1.14.11.13) was detected 24 h after ultrasonication, which could result in catabolites of gibberellic acid. The SL value of the plantlets significantly increased after a 30-min-long ultrasonication compared with the shorter US treatments but remained significantly lower than that of the control. The background processes of these results require further investigations.

It is long known that the different phytohormones have a significant role in every aspect of plant physiology during growth and development. The effects of the application of cytokinin, GA_3, ABA, auxin, brassinosteroides, and jasmonic acid on plants have been revealed. Tryptophan is the frequent precursor of the

biosynthesis of MT and IAA (Posmyk and Janas, 2009; Erland et al., 2015; Erland and Saxena, 2018; Khan et al., 2020), which may result in these compounds having similar regulatory functions in plant growth and development (Shi et al., 2015). The connections between MT and a lot of other hormones have directly and indirectly been studied, but few signal transmission models were suggested in the adaptation to US stress as to how it protects photosynthesis with chlorophyll synthesis. In contrast with other long-studied abiotic stresses, our present investigation confirmed that US stress does not decrease the IAA concentration in plants; rather, it increases it (Shakeel et al., 2021).

Another indirect effect of MT is connected to the regulation of the activity of antioxidant enzymes, like GPX, GR, SOD, and CAT, and it is able to stimulate the synthesis of GSH (Rodriguez et al., 2004; Erland and Saxena, 2018). Taking into account its multifunctionality in plants, melatonin has recently been considered to be not only a plant hormone but also a master regulator in plants (Arnao and Hernández-Ruiz, 2019).

Concentrations of endogenous MT correlate with IAA levels (Figure 6). In addition, it shows a positive correlation with AA levels. The IAA levels also correlate positively with AA levels. Although there are common biosynthetic pathways for MT and IAAs in plants, the amount and the extent of their synthesis may be also determined by the concentration of AA. The question arises as to whether AA may have a regulatory role in the synthesis of tryptophan-dependent IAA formed by the other tryptophan-independent pathway. After 20 min of US treatment, MT shows a negative correlation at several points in the antioxidant system, including the concentration of GSH or SOD enzyme activity among the small-molecule antioxidants in addition to AA. A strong positive relationship was found with the amount of ACL. This suggests that MT and the MT derivatives formed during its catabolism strengthen the group of compounds with lipid-soluble antioxidant capacity. This does not change even if the stronger US treatment was applied. It is possible that MT directs the elimination of excess H_2O_2 by increasing the activity of SOD and by the synthesis of AA. Similar results were obtained by Kostopoulou et al. (2015) when exogenous MT and AA treatment was applied in citrus fruits.

5 Conclusion

MT appears to play a clear role in plant abiotic or metabolic stress adaptation in collaboration with other plant hormones. Its association with ROS provides evidence that MT is a key component at the center of the redox network from which various biochemical, cellular, and physiological responses are regulated. MT-ROS are self-regulating through the regulation of directly interacting systems and the biosynthesis of their own biosynthesis and catabolic genes. There is a close relationship between the plant hormone IAA and MT and AA. MT has a dual role in plants, acting both as an antioxidant and a growth regulator. It would also be important to examine how the activity of the redox system changes in different photoperiods and whether MT has a regulatory role in activating the system itself.

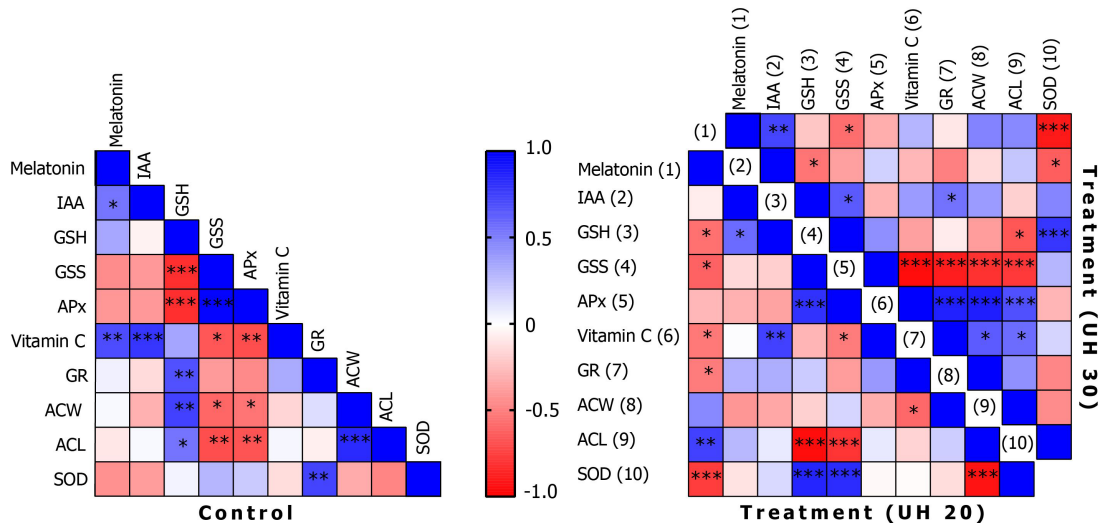

FIGURE 6
Correlations of biochemical parameters in the control group and after ultrasonication for 20 min (treatment, UH 20) and 30 min (treatment, UH 30), respectively. *, **, *** mean the significant differences at $P < 0.05$, $P < 0.01$, $P < 0.001$, respectively.

Data availability statement

The original contributions presented in the study are included in the article/Supplementary Material. Further inquiries can be directed to the corresponding author.

Author contributions

JD and JR devised the experimental design. JD conducted the ultrasonication experiments as well as collected and evaluated the growth data. GP-A, IF, and PM-B conducted the biochemical analyses under the supervision of JD and JR. All authors analyzed the data, wrote or contributed to all drafts of the manuscript, and take public responsibility for the data. All authors contributed to the article and approved the submitted version.

Funding

Project no. TKP2021-EGA-20 (Biotechnology) has been implemented with the support provided from the National Research, Development, and Innovation Fund of Hungary, financed under the TKP2021-EGA funding scheme.

Conflict of interest

The authors declare that the research was conducted in the absence of any commercial or financial relationships that could be construed as a potential conflict of interest.

Publisher's note

All claims expressed in this article are solely those of the authors and do not necessarily represent those of their affiliated organizations, or those of the publisher, the editors and the reviewers. Any product that may be evaluated in this article, or claim that may be made by its manufacturer, is not guaranteed or endorsed by the publisher.

References

Arnao, M. B., and Hernández-Ruiz, J. (2006). The physiological function of melatonin in plants. *Plant Signal. Behav.* 1 (3), 89–95. doi: 10.4161/psb.1.3.2640

Arnao, M. B., and Hernández-Ruiz, J. (2013). Growth conditions determine different melatonin levels in *Lupinus albus* l. *J. Pineal Res.* 55, 149–155. doi: 10.1111/jpi.12055

Arnao, M. B., and Hernández-Ruiz, J. (2014). Melatonin: plant growth regulator and/or biostimulator during stress? *Trends Plant Sci.* 19, 789–797. doi: 10.1016/j.tplants.2014.07.006

Arnao, M. B., and Hernández-Ruiz, J. (2015). Functions of melatonin in plants: A review. *J. Pineal Res.* 59, 133–150. doi: 10.1111/jpi.12253

Arnao, M. B., and Hernández-Ruiz, J. (2019). Melatonin: A new plant hormone and/or a plant master regulator? *Trends Plant Sci.* 24 (1), 38–48. doi: 10.1016/j.tplants.2018.10.010

Battacharya, P., and Jha, S. (2020). "Melatonin: An alternative signal to antioxidant enzyme modulation in plants," in *Neurotransmitters in plant signaling and communication, sinaling and communication in plants*. Ed. F. Baluška, S. Mukherjee and A. Ramakrishna, (Cham: Springer). pp 241–251.

Cassone, V. M. (1998). Melatonin's role in vertebrate circadian rhythms. *Chronobiol. Int.* 15 (5), 457–473. doi: 10.3109/07420529808998702

Davanipour, Z., Poulsen, H. E., Weimann, A., and Sobel, E. (2009). Endogenous melatonin and oxidatively damaged guanine in DNA. *BMC Endocr. Disord.* 9, 22. doi: 10.1186/1472-6823-9-22

Dijk, D. J., and Czeisler, C. A. (1994). Paradoxical timing of the circadian rhythm of sleep propensity serves to consolidate sleep and wakefulness in humans. *Neurosci. Lett.* 166 (1), 63–68. doi: 10.1016/0304-3940(94)90841-9

Dobránszki, J., Asbóth, G., Homoki, D., Bíró-Molnár, P., Teixeira da Silva, J. A., and Remenyik, J. (2017). Ultrasonication of *in vitro* potato single node explants: Activation and recovery of antioxidant defence system and growth responses. *Plant Physiol. Biochem.* 121, 153–160. doi: 10.1016/j.plaphy.2017.10.022

Dobránszki, J., Hidvégi, N., Gulyás, A., Tóth, B., Teixeira da Silva, J. A., and Dobránszki, J. (2020). Abiotic stress elements in *in vitro* potato (*Solanum tuberosum* l.) exposed to air-based and liquid-based ultrasound: A comparative transcriptomic assessment. *Prog. Biophysics Mol. Biol.* 1559 (158), 47–56. doi: 10.1016/j.pbiomolbio.2020.09.001

Dobránszki, J., and Mendler-Drienyovszki, N. (2014). Cytokinin-induced changes in the chlorophyll content and fluorescence of *in vitro* apple leaves. *J. Plant Physiol.* 171, 1472–1478. doi: 10.1016/j.jplph.2014.06.015

Erland, L. A., Murch, S. J., Reiter, R. J., and Saxena, P. K. (2015). A new balancing act: The many roles of melatonin and serotonin in plant growth and development. *Plant Signal. Behav.* 10, e1096469. doi: 10.1080/15592324.2015.1096469

Erland, L. A. E., and Saxena, P. (2018). Auxin driven indoleamine biosynthesis and the role of tryptophan as an inductive signal in hypericum perforatum (L.). *PloS One* 14 (10), e0223878. doi: 10.1371/journal.pone.0223878

Fan, J., Xie, Y., Zhang, Z., and Chen, L. (2018). Melatonin: A multifunctional factor in plants. *Int. J. Mol. Sci.* 19, 1528. doi: 10.3390/ijms19051528

George, E. F., and Davies, W. (2008). "Effects of physical environment," in *Plant propagation by tissue culture 3rd edition*, vol. 1 . Eds. E. F. George, M. A. Hall and G.-J. De Klerk (Dordrecht, The Nederlans: Springer), 423–464.

Hardeland, R. (2016). Melatonin in plants – diversity of levels and multiplicity of functions front. *Plant Sci.* 7. doi: 10.3389/fpls.2016.00198

Khan, A., Numan, M., Khan, A. L., Lee, I.-J., Imran, M., Asaf, S., et al. (2020). Melatonin: Awakening the defense mechanisms during plant oxidative stress. *Plants* 9, 407. doi: 10.3390/plants9040407

Koga, J. (1995). Structure and function of indolepyruvate decarboxylase, a key enzyme in indole-3-acetic acid biosynthesis. *Biochim. Biophys. Acta* 1249, 1–13. doi: 10.1016/0167-4838(95)00011-i

Kostopoulou, Z., Therios, I., Roumeliotis, E., Kanellis, A. K., and Molassiotis, A. (2015). Melatonin combined with ascorbic acid provides salt adaptation in *Citrus aurantium* l. seedlings. *Plant Physiol. Biochem.* 86, 155–165. doi: 10.1016/j.plaphy.2014.11.021

Li, H., Chang, J., Chen, H., Wang, Z., Gu, X., Wei, C., et al. (2017). Exogenous melatonin confers salt stress tolerance to watermelon by improving photosynthesis and redox homeostasis. *Front. Plant Sci.* 8. doi: 10.3389/fpls.2017.00295

Manchester, L. C., Coto-Montes, A., Boga, J. A., Andersen, L. P. H., Zhou, Z., Galano, A., et al. (2015). Melatonin: An ancient molecule that makes oxygen metabolically tolerable. *J. Pineal Res.* 59 (4), 403–419. doi: 10.1111/jpi.12267

Murashige, M., and Skoog, F. (1962). A revised medium for rapid growth and bioassay with tobacco tissue culture. *Physiol. Plant* 15, 473–497. doi: 10.1111/j.1399-3054.1962.tb08052.x

Murch, S. J., and Saxena, P. K. (2002). Melatonin: a potential regulator of plant growth and development? *Vitro Cell. Dev. Biol. Plant* 38, 531.

Posmyk, M. M., and Janas, K. M. (2009). Melatonin in plants. *Acta Physiol. Plant* 31, 1. doi: 10.1007/s11738-008-0213-z

Qi, W., Reiter, R. J., Tan, D. X., Manchester, L. C., Siu, A. W., and Garcia, J. J. (2000). Increased levels of oxidatively damaged DNA induced by chromium(III) and H_2O_2: protection by melatonin and related molecules. *J. Pineal Res.* 29 (1), 54–61. doi: 10.1034/j.1600-079x.2000.290108.x

Reiter, R. J., Mayo, J. C., Tan, D.-X., Sainz, R. M., Alatorre-Jimenez, M., and Qin, L. (2016). Melatonin as an antioxidant: Under promises but over delivers. *J. Pineal Res.* 61, 3, 253–278. doi: 10.1111/jpi.12360

Rodriguez, C., Mayo, J. C., Sainz, R. M., Antolin, I., Herrera, F., Martin, V., et al. (2004). Regulation of antioxidant enzymes: A significant role for melatonin. *J. Pineal Res.* 36, 1–9. doi: 10.1046/j.1600-079x.2003.00092.x

Rokhina, E. V., Lens, P., and Virkutyte, J. (2009). Low-frequency ultrasound in biotechnology: State of the art. *Trends Biotechnol.* 27, 298–306. doi: 10.1016/j.tibtech.2009.02.001

Shakeel, A., Kamran, M., Zhou, X., Irshad, A., Meng, X., Javed, T., et al. (2021). Melatonin improves the seed filling rate and endogenous hormonal mechanism in grains of summer maize. *Physiol. Plantarum.* 172 (2), 1059–1072. doi: 10.1111/ppl.13282

Shi, H., Jiang, C., Ye, T., Tan, D.-X., Reiter, R. J., Zhang, H., et al. (2015). Comparative physiological, metabolomic, and transcriptomic analyses reveal mechanisms of improved abiotic stress resistance in bermudagrass [Cynodon dactylon (L). pers.] by exogenous melatonin. *J. Exp. Bot.* 66 (3), 681–694. doi: 10.1093/jxb/eru373

Teixeira da Silva, J. A., and Dobránszki, J. (2014). Sonication and ultrasound: Impact on plant growth and development. *Plant Cell. Tissue Organ Cult. (PCTOC)* 117 (2), 131–143. doi: 10.1007/s11240-014-0429-0

Teixeira da Silva, J. A., Hidvégi, N., Gulyás, A., Tóth, B., and Dobránszki, J. (2020). Transcriptomic response of *In vitro* potato (*Solanum tuberosum* l.) to piezoelectric ultrasound. *Plant Mol. Biol. Rep.* 38, 404–418. doi: 10.1007/s11105-020-01204-3

Van Tassel, D. L., Roberts, N., Lewy, A., and O'neill, S. D. (2001). Melatonin in plant organs. *J. Pineal Res.* 31, 8–15. doi: 10.1034/j.1600-079x.2001.310102.x

Verpoorte, R., Contin, A., and Memelink, J. (2002). Biotechnology for the production of plant secondary metabolites. *Phytochem. Rev.* 1, 13–25. doi: 10.1023/A:1015871916833

Wang, Y., Reiter, R. J., and Chan, Z. (2018). Phytomelatonin: a universal abiotic stress regulator. *J. Exp. Bot.* 69 (5), 963–974. doi: 10.1093/jxb/erx473

Wang, P., Yin, L., Liang, D., Li, C., Ma, F., and Yue, Z. (2012). Delayed senescence of apple leaves by exogenous melatonin treatment: Toward regulating the ascorbate-glutathione cycle. *J. Pineal Res.* 53, 11–20. doi: 10.1111/j.1600-079X.2011.00966.x

frontiers | Frontiers in Plant Science

TYPE Original Research
PUBLISHED 29 September 2022
DOI 10.3389/fpls.2022.944894

OPEN ACCESS

EDITED BY
Alessandra Boccaccini,
Università di Tor Vergata,
Italy

REVIEWED BY
Samar Gamal Thabet,
Fayoum University, Egypt
María Pilar Cordovilla,
University of Jaén, Spain

*CORRESPONDENCE
Xueli Wu
xueli0510qau@163.com

SPECIALTY SECTION
This article was submitted to Plant Physiology, a section of the journal Frontiers in Plant Science

RECEIVED 16 May 2022
ACCEPTED 06 September 2022
PUBLISHED 29 September 2022

CITATION
Jiang K, Yang Z, Sun J, Liu H, Chen S, Zhao Y, Xiong W, Lu W, Wang Z-Y and Wu X (2022) Evaluation of the tolerance and forage quality of different ecotypes of seashore paspalum. *Front. Plant Sci.* 13:944894. doi: 10.3389/fpls.2022.944894

Evaluation of the tolerance and forage quality of different ecotypes of seashore paspalum

Kai Jiang[1], Zhimin Yang[2], Juan Sun[1], Huancheng Liu[1], Shenmiao Chen[1], Yongzhuo Zhao[1], Wangdan Xiong[1], Wenjie Lu[1], Zeng-Yu Wang[1] and Xueli Wu[1]*

[1]College of Grassland Science, Qingdao Agricultural University, Qingdao, China, [2]College of Grassland Science, Nanjing Agricultural University, Nanjing, China

Seashore paspalum is a halophytic, warm-season grass with wide applications. It is noted for its superior salt tolerance in saline environments; however, the nutritive value of seashore paspalum and the effect of salinity remains to be determined. Therefore, this study aimed to evaluate the relationship between agronomic traits and forage quality and identified the effects of short-term high-salt stress (1 week, 700 mM NaCl) on the growth and forage nutritive value of 16 ecotypes of seashore paspalum. The salt and cold tolerances of the seashore paspalum ecotypes were assessed based on the survival rate following long-term high-salt stress (7 weeks, 700 mM NaCl) and exposure to natural low temperature stress. There were significant genetic (ecotype-specific) effects on plant height, leaf–stem ratio, and survival rate of seashore paspalum following salt or low temperature stress. Plant height was significantly negatively correlated with the leaf–stem ratio (r = −0.63, P<0.01), but the heights and leaf–stem ratios were not significantly correlated with the fresh weight (FW) and dry weight (DW) of the shoots. High salinity decreased the FW and DW of the shoots by 50.6% and 23.6%, respectively, on average. Seashore paspalum exhibited outstanding salt tolerance and forage quality at high salinity. The survival rate of the different ecotypes of seashore paspalum varied from 6.5% to 49.0% following treatment with 700 mM NaCl for 7 weeks. The crude protein (CP) content of the control and treatment groups (700 mM NaCl) was 17.4% and 19.3%, respectively, of the DW on average, and the CP content of most ecotypes was not significantly influenced by high salinity. The average ether extract (EE) content ranged from 4.6% to 4.4% of the DW under control and saline conditions, respectively, indicating that the influence was not significant. The neutral detergent fiber (NDF) and acid detergent fiber (ADF) contents of the control group were 57.4% and 29.8%, respectively, of the DW on average. Salt stress reduced the content of NDF and ADF to 50.2% and 25.9%, respectively, of the DW on average. Altogether, the results demonstrated that stress did not have any significant effects on the CP and EE content of most ecotypes, but reduced the NDF and ADF content and improved relative feed value (RFV). The results obtained herein support the notion that seashore paspalum is a good candidate for improving the forage potential of saline soils and can provide useful guidelines for livestock producers.

KEYWORDS
seashore paspalum, forage quality, crude protein contents, salinity, low temperature

Introduction

Soil salinization is a major environmental concern affecting global agricultural production and the ecological environment (Anderson et al., 2015; Yin et al., 2019). Salinization affects approximately 7% of the land surface worldwide, threatens nearly 20% of global irrigated land, and the proportion of saline soils is increasing (Li et al., 2014; Gangwar et al., 2020; Mora et al., 2020). The total area of saline soil in China is approximately 3.6×10^7 ha, which accounts for 4.88% of the total available land area of the country (Dong et al., 2019; Zhang et al., 2022). Saline-alkali lands are one of the limiting factors for crop production and ecological construction. Soil salinity and low temperature are the major environmental constraints that severely affect the growth and productivity of crop plants (Robinson et al., 2004; Moustafa et al., 2021). Plants growing under salt-stressed conditions are challenged by ionic imbalance, impaired photosynthesis, osmotic stress, and nutrient deficiency, which seriously inhibit plant growth and quality (Huang et al., 2015; Munns and Gilliham, 2015; Oney-Birol, 2019). However, these lands can be used as an important reserve land resource (Munir et al., 2022). Soil engineering and agronomic solutions for alleviating soil salinity are ineffective to date, and growing salinity-tolerant plants can improve the utilization rate of saline-alkali lands (Gu et al., 2019). The protection of arable lands and the development of saline-alkali lands will be important measures for ensuring food security and economic and population growth. The development of animal husbandry in saline areas is an important measure for multifunctional ecological agriculture. But, the supply of forage is an important limiting factor for the development of animal husbandry in saline-alkali areas. Owing to poor salt tolerance, the yield and quality of traditional forage plants, including alfalfa (*Medicago sativa* L.) (Campanelli et al., 2013; Badran et al., 2015; Monirifar et al., 2020), sweet sorghum (*Sorghum bicolor* L. Moench) (Yang et al., 2020), and forage kochia (*Bassia prostrata* L.) (Waldron et al., 2020), are affected by salt stress. However, halophytes can grow well at high salt concentrations (200 mM NaCl and higher) as they possess highly special mechanisms of salt resistance (Yuan et al., 2019; Shoukat et al., 2020). Halophytic forage plants or grasses can provide a basis for the development of halophyte-based agricultural practices with the aim of increasing the security and yield of agricultural and livestock products (Norman et al., 2019; Munir et al., 2022).

Seashore paspalum (*Paspalum vaginatum* O. Swartz) is a halophytic, warm-season grass that is commonly grown on athletic fields, golf courses, and landscape areas. Seashore paspalum grows extensively in saline regions of the landscape and has an immense potential to be used under harsh and stressful environmental conditions (Pessarakli, 2018). The plant is favored owing to its high tolerance to salt, drought, water logging, low soil pH, and adaptation to conditions of low irradiance and weak shade (Pompeiano et al., 2016; Karimi et al., 2018). Evaluation of the salt tolerance of seashore paspalum and other species of grass indicates the superior salt tolerance of seashore paspalum (Marcum and Murdoch, 1994). Seashore paspalum has better ion regulation abilities that are mediated *via* its ability to maintain a high concentration of K^+ in shoots and the reduced transfer of Na^+ from roots to shoots, which leads to the maintenance of a high K^+/Na^+ ratio. Therefore, seashore paspalum is capable of evading ion-specific damage resulting from salt stress (Schiavon et al., 2012; Wu et al., 2018). Moreover, the plant has an enhanced Ca^{2+} signaling transduction pathway resulting from Na^+ accumulation, which aids in maintaining the activities of the major antioxidant enzymes (Wu et al., 2020).

Seashore paspalum has the second largest number of cultivars in the *Paspalum* genus, of which the majority of cultivars have been developed in the USA, particularly at the University of Georgia (Acuña et al., 2019). Molecular markers are used for the effective identification of phenotypic variations and genetic differences among ecotypes during the collection and evaluation of germplasm resources. Microsatellite sequence markers are usually species-specific; however, few such markers are available for *P. vaginatum* (Cidade et al., 2013). Using 43 simple sequence repeat (SSR) markers, a previous study determined the relationship between *P. vaginatum* and *P. distichum*, and determined their genetic diversity and ploidy levels (Eudy et al., 2017). Previous studies have analyzed the diversity and variations among different ecotypes of seashore paspalum using random amplified polymorphic DNA (RAPD) markers (Liu et al., 1994), amplified fragment length polymorphisms (AFLPs) (Chen et al., 2005), and SSR markers

Abbreviations: Pn, net photosynthetic rate; Ci, intercellular CO_2 concentration; Tr, transpiration rate; Gs, stomatal conductance; FW, fresh weight; DFR, dry-fresh weight ratio; DW, dry weight; CP, crude protein; EE, ether extract; NDF, neutral detergent fiber; ADF, acid detergent fiber; DDM, digestible dry matter; DMI, dry-matter intake; RFV, relative feed value.

(Wang et al., 2006). A previous study developed several thousand single-nucleotide polymorphism (SNP) markers that segregated in an F1 population, generated from a cross between ecotypes 509022 and HI33 of seashore paspalum. The markers were subsequently used to construct the first genetic maps for this plant (Qi et al., 2019). Although seashore paspalum has been utilized for almost a hundred years and numerous cultivars have been developed, few genetic resources are available for this plant to date (Qi et al., 2019). There is a major difference between the salt- and cold-tolerant varieties of seashore paspalum (Cardona et al., 1997). 'SI92' and 'SI93-1' are salt-tolerant varieties, while 'SI95' and 'Adalayd' have the worst salt tolerance (Lee et al., 2004). Several recent studies have evaluated stress (salt, drought, etc.) tolerance (Karimi et al., 2018; Tran et al., 2018) and determined the underlying regulatory mechanism in different varieties of seashore paspalum (Cyril et al., 2002; Pompeiano et al., 2016; Serena et al., 2018; Wu et al., 2018). Seashore paspalum has remarkable salt tolerance properties; but its low tolerance to cold environments seriously affects its application in regions with low temperatures. However, there is a scarcity of studies evaluating the nutritive value of seashore paspalum during salt response.

The cultivation of halophytes for agriculture and animal husbandry development needs is recommended due to their ability to grow in saline-degraded lands, which provides environmental and economic benefits to society (Himabindu et al., 2016). However, most studies on salt-tolerant forage plants have emphasized evaluating biomass growth and physiological mechanisms, whereas few studies have focused on determining the effect of salinity on the forage quality of halophyte species. Therefore, further studies are necessary to evaluate the effect of salinity on the forage quality of halophytes (Norman et al., 2013; Waldron et al., 2020). Seashore paspalum is a natural inhabitant of saline soils and has numerous potential applications for sustaining excellent forage productivity, which can improve forage yield and, in particular, improve the usage rate of saline lands. Seashore paspalum is noted for its high salt tolerance ability. However, the forage quality and effect of salinity on its nutritive value remain to be determined. Therefore, this study determined the effect of salinity on the forage quality of seashore paspalum. In this study, we evaluated the low temperature and high salt tolerance of seashore paspalum, determined the relationship between biomass and photosynthesis, and investigated the forage nutritive value of seashore paspalum under salinity conditions. In this study, cold- and salt-tolerant ecotypes of seashore paspalum with high biological yield and high nutritional quality were selected to provide a basis for agriculture and animal husbandry development needs in saline lands.

Materials and methods

Plant growth and treatments

In this study, 16 ecotypes of seashore paspalum were collected from coastal environments and golf courses (Table 1). The 16 ecotypes showed genetic divergence in terms of various characteristics, including plant height, length and width of leaves, tillers/plant, leaf color, spreading growth pattern, plant density, and tolerance. For instance, we observed that 509022 and 614678 plants were taller, had longer leaves, and faster growth rates than the other ecotypes. Contrarily, T25 plants were short, and their leaves were short and soft. The leaf color of 647907 and T25 plants was darker than that of the other ecotypes (Figure 1). The 16 seashore paspalum ecotypes were planted in soil containing a mixture of peat and perlite (3:1) in isolated plastic pots. Each ecotype was multiplied by vegetative propagation in nine uniform plastic pots, and 50 stem segments were planted per pot. The plants were fully irrigated and grown in a greenhouse under natural light. Throughout the experiment, the day and night temperatures were maintained at 30°C and 25°C, respectively, and the relative humidity was maintained at 50% during the day and 70% during the night.

The stress treatments were initiated when the plants had been growing in the greenhouse for 8 weeks, and various indicators were measured. For each ecotype, three pots of plants were designated as the control, which were routinely maintained under normal growth conditions. For measuring

TABLE 1 The sources of 16 seashore paspalum ecotypes.

Entry	Origin	Entry	Origin
SP002	China	PI 647896	United States of America
SP007	China	PI 647900	United States of America
T25	China	PI 647902	United States of America
PI 509022	United States of America	PI 647903	United States of America
PI 509023	United States of America	PI 647907	United States of America
PI 614678	United States of America	PI 647909	United States of America
PI 647891	United States of America	PI 647914	United States of America
PI 647894	United States of America	PI 647921	United States of America

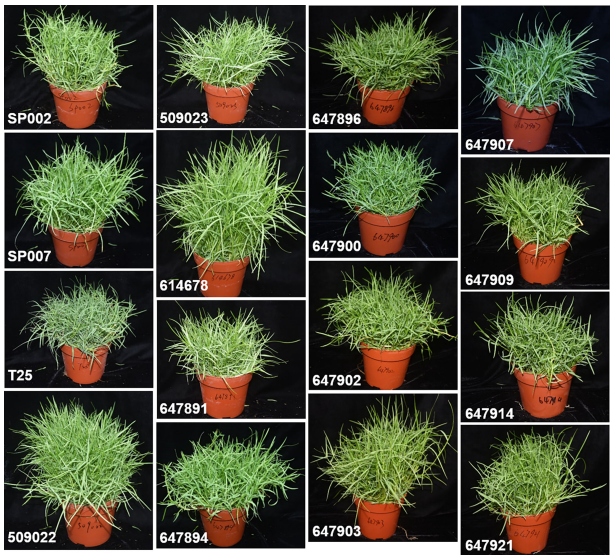

FIGURE 1
Characterization of 16 seashore paspalum ecotypes under normal condition for 40 d.

plant height, three of the tallest tillers were selected randomly per ecotype, and the height was measured in cm from the level of the soil to the tip of the tallest leaf with a ruler. The tillers were manually separated into leaves and stems, and subsequently oven dried at 65°C for 96 h to determine the DW for estimation of the leaf–stem ratio. The second fully developed leaves from the top were used for measuring the chlorophyll content and determining the photosynthesis-related parameters in three replicates. For measurement of the chlorophyll content, the leaves (0.1 g) were fully extracted for 48 h in 10 ml of 95% ethanol (v/v) in the dark. The absorbance at 645 nm and 663 nm was determined using a spectrophotometer as previously described (Wu et al., 2018). The net photosynthetic rate (Pn), intercellular CO_2 concentration (Ci), transpiration rate (Tr), and stomatal conductance (Gs) were measured using the LI-6400-40 portable photosynthesis system at 25°C and 400 ppm CO_2.

For salinity treatments, three pots of plants per ecotype were irrigated with 400 mM NaCl solution for 3 days (d) and then with 700 mM NaCl for 1 week. All the tillers in the pots were clipped to a height of 5 cm from the soil surface. The relative growth of the plants was calculated under control conditions using the formula: fresh weight (FW)/duration of growth (d). The FW was recorded separately under control and saline conditions. For determination of the DW, herbage mass, and forage nutritive value, the harvested samples were dried in a forced air oven at 105°C for 30 min and then at 65°C until a constant weight was reached. The water content (WC) and dry-fresh weight ratio (DFR) of the plants were measured under control and salinity treatment conditions. The WC was calculated using the following formula: WC = [(FW − DW)/FW] × 100% (Gitau et al., 2017). The DFR was calculated using the formula: DFR = FW/DW. The dried shoot samples were ground to a particle size of 1 mm using an automatic grinding machine for analysis of forage nutritive value. The analyses were performed in triplicate for each sample.

Assessment of forage nutritive value

The forage nutritive value was determined in triplicate based on the DW. The total concentration of N and C was determined by dry combustion using a Vario EL cube elemental analyzer (Elementar, Germany), and the crude protein (CP) content (% DW) was calculated as 6.25 × N concentration. The ether extract (EE) content was determined according to the Chinese Standard GB/T 6435-1986. Briefly, the samples (1.0 g) were placed in individual test bags and sealed, following which they were dried at 65°C for 3 h. Petroleum ether was added to an ANKOM XT15 automatic fat analyzer (ANKOM Technology, USA) for extraction and determination. The crude fat content was calculated from the changes in weight (Ji and Wang, 2002). The contents of the neutral detergent fiber (NDF; % DW) and acid detergent fiber (ADF; % DW) were sequentially determined using an ANKOM A2000i automatic fiber analyzer (ANKOM Technology, USA). Briefly, the samples (0.5 g) were placed in dedicated filter bags (F57 or F58, ANKOM Technology, USA) and sealed. The NDF and ADF contents were measured using the filter bag technology, according to the detailed instructions

in the ANKOM A2000i manual. The digestible dry matter (DDM; % DW), dry-matter intake (DMI; % DW), and the relative feed value (RFV; % DW) were calculated on a DW basis using the following formulas (Kim and Anderson, 2015):

$$DDM = 88.9 - (0.779 \times ADF)$$

$$DMI = 120 / NDF$$

$$RFV = (DDM \times DMI) / 1.29$$

Assessment of salt and cold tolerance

The salt and cold tolerance of the plants was also evaluated from the survival rate. The NaCl concentration was increased to 700 mM for 7 weeks, and the samples were photographed after harvesting. The survival rate was subsequently calculated after salt treatment by watering for 7 d to wash out the salt. The survival rate (%) was calculated as: (number of plants that survived after watering/the total number of plants) × 100.

To evaluate cold tolerance, three pots of plants were removed per ecotype from the greenhouse and maintained at natural low temperatures for 9 d and 15 d at Qingdao Agricultural University, situated in southeast Shandong on the northern shore of the Huanghai Sea (37° 09' N, 119° 30' E). The area has a temperate monsoon climate, and the average annual temperature of this area is 12.7°C. The temperature during cold treatment was recorded. The survival rate (%) was calculated as: (number of plants that survived after returning to 25°C/total number of plants) × 100.

Data analyses

Data from three replicates were analyzed by one-way analysis of variance (ANOVA). The results are presented as the mean ± standard error of biological replications. The means were separated using Duncan's multiple range test (P<0.05). Statistical analyses were performed using the Statistical Package for the Social Sciences (SPSS; version 17.0). The correlations among the features were estimated with Pearson's correlation coefficient test, performed using the appropriate method in SPSS.

Results

Analysis of agronomic traits and photosynthesis-related parameters

Analyses of the agronomic traits revealed significant genetic (ecotype-specific) differences in plant height and leaf–stem ratio. Plant height is one of the important traits that affect the yield, and in this study, the height of the plants was significantly negatively correlated with the leaf–stem ratio (r = −0.63, P< 0.01) (Table 2). For instance, we observed that 509022 and 614678 plants were significantly taller and had significantly lower leaf–stem ratios than those of 647902 and 647921 plants. The heights of the plants in the different ecotypes ranged from 47.10 cm for 509022 plants to 9.10 cm for 509023 plants. The 509022, 614678, and 647903 plants were significantly taller than SP002, SP007, T25, 509023, 647894, 647896, 647900, 647902, 647909, 647914, and 647921 plants. Leaf proportion has important effects on forage nutritive value, and it was found to be affected by the ecotype of the plants. The leaf–stem ratio of 647921 plants was significantly higher than that of 647903 plants (0.92 vs. 0.22, P< 0.05). The 647921 plants had a more horizontal and prostrate growth pattern compared to that of 647903 plants, and the shorter canopy height of 647921 resulted in an increased leaf proportion and decreased stem elongation (Figures 2A, C). The relative growth of the 16 ecotypes of seashore paspalum ranged from 0.17 to 0.47 (Figure 2B) and was not significantly correlated with the quantitative traits in Table 2, according to Pearson's correlation coefficient test.

The chlorophyll content of the different ecotypes ranged from 1.04 mg/g for SP007 plants to 1.98 mg/g for 509023 plants. The 509023 plants had the highest chlorophyll content,

TABLE 2 Pearson's correlation coefficients between pairs of traits.

	Relative growth of plant	Leaf–stem ratio	Plants height	Chlorophyll contents	Pn	Ci	Tr	Gs
Relative growth of plant	–	0.34	−0.22	−0.21	0.03	−0.06	−0.02	−0.08
Leaf–stem ratio		–	**−0.63****	0.03	0.21	−0.46	−0.18	−0.18
Plants height			–	−0.11	−0.07	0.13	−0.18	−0.17
Chlorophyll contents				–	0.41	−0.42	0.29	0.19
Pn					–	**−0.69****	**0.60***	**0.62***
Ci						–	0.03	0.06
Tr							–	**0.97****
Gs								–

*P<0.05, **P<0.01 represent significant values that been bold in tables.
Pn, net photosynthetic rate; Ci, intercellular CO_2 concentration; Tr, transpiration rate; Gs, stomatal conductance.

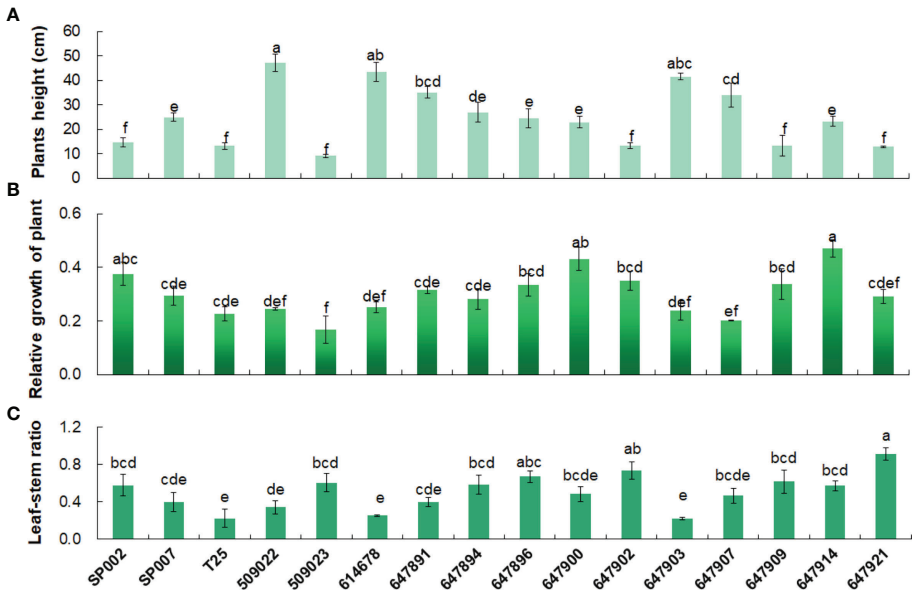

FIGURE 2
Agronomic traits analysis of 16 seashore paspalum ecotypes. Plants height **(A)**, Relative growth of plant **(B)** and Leaf–stem ratio **(C)** of 16 seashore paspalum ecotypes were measured when plants grown in the greenhouse for 8 weeks. Means of three replicates and standard errors are presented; the same letter above the column indicates no significant difference at $P<0.05$.

which was significantly higher than that of SP007, T25, 509022, 614678, 647891, 647896, 647909, and 647921 plants (Figure 3A). The results of Pearson's correlation coefficient test revealed that the correlation between the chlorophyll content and Pn was not significant (r = 0.41, P >0.05) (Table 2). However, chlorophyll is an important pigment that is necessary for photosynthesis in plants, and the chlorophyll content can reflect the degree of photosynthesis. For instance, the chlorophyll content and Pn of 509022 plants were significantly lower than those of 509023 plants, and a similar trend was observed in the chlorophyll content and Pn (Figures 3A, B). Photosynthesis provides energy for plant growth and development and is an important criterion for evaluating plant productivity. The photosynthetic parameters that represent photosynthetic ability and efficiency were monitored under normal conditions. It was observed that the Pn varied between 0.47 and 3.90 μmol $m^{-2}s^{-1}$, and there were minor differences in the Pn among the majority of ecotypes studied herein. For instance, we observed that the Pn of T25 and 509022 plants was significantly lower than that of SP002, 509023, and 614678 plants (Figure 3B). The Pn was strongly negatively correlated with the Ci (Figure 3C) (r = −0.69, P<0.01) but positively correlated with the Tr (Figure 3D) (r = 0.60, P<0.05) and Gs (Figure 3E) (r = 0.62, P<0.05) (Table 2).

Effect of salt stress on shoot biomass parameters

Salt stress significantly reduced the FW of the plants, with the exception of T25, 509023, and 647907 plants. The FW of the plants was 16.53 g on average under control conditions and 7.99 g on average following salt treatment (Figure 4A). The FWs of the plants were strongly positively correlated with the WC but negatively correlated with the DFR. The DW was strongly correlated with the FW only under control conditions (r = 0.674, P< 0.01) (Table 3). For instance, the FW (25.89 g) and WC (79.85%) were high in 647914 plants, but the DFR was low (0.20) in all the ecotypes under control conditions (Figures 4A, C, D). The DW of the majority of ecotypes decreased under salt treatment, with the exception of SP007 and 647907 plants, in which the DWs were not significantly different but increased only slightly (Figure 4B). The results of Pearson's correlation coefficient test revealed that the DFRs of plants under control and saline conditions were highly significantly correlated (r = 0.625, P<0.01) (Table 3). The DFR significantly increased in most ecotypes following salt treatment, but there was no significant difference in the DFRs of T25 and 647909 plants (Figure 4D). This was primarily attributed to the reduction in FW caused by water loss from the plants under saline conditions.

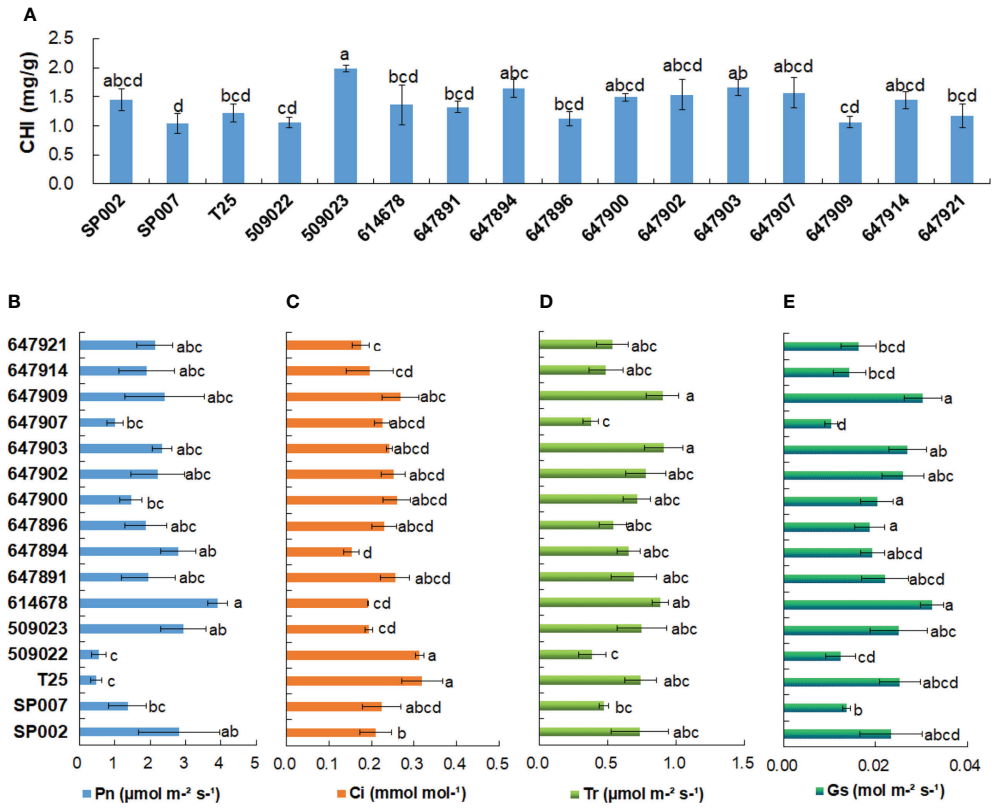

FIGURE 3
Chlorophyll contents and photosynthesis-related parameters analysis of 16 seashore paspalum ecotypes. Chlorophyll contents **(A)**, net photosynthetic rate (Pn) **(B)** and intercellular CO_2 concentration (Ci) **(C)**, transpiration rate (Tr) **(D)**, and stomatal conductance (Gs) **(E)** were measured by LI-6400-40 portable photosynthesis system when 16 seashore paspalum ecotypes grown in the greenhouse for 8 weeks. Means of three replicates and standard errors are presented; the same letter above the column indicates no significant difference at $P<0.05$.

Effect of salt stress on forage nutritive value

The CP content of the different ecotypes ranged from 9.04% to 23.04% of the DW, and the average CP content was 17.42% of the DW under control conditions. The results demonstrated that salt stress did not have any significant effects on the CP content of most varieties (19.31% of DW on average), but significantly increased the CP content of SP002, 509023, and 647909 plants (Figure 5A). Additionally, the C/N ratio of the majority of ecotypes was not significantly affected by salinity (17.34 and 13.08 on average under control and saline conditions, respectively), with the exception of SP002 and 509023 plants. The C/N ratio of SP002 and 509023 plants decreased significantly from 34.91 and 40.88, respectively, under control conditions, to 12.71 and 15.90, respectively, under saline conditions (Figure 5B). The EE and CP contents of 647907 plants were high among the 16 ecotypes, being 5.70% and 23.04%, respectively, of the DW, while those of 509023 plants were low, being 1.93% and 9.04%, respectively, of the DW under control conditions (Figures 5A, C). The average EE content ranged from 4.69% to 4.44% of the DW under control and saline conditions, respectively, indicating that the saline environment had no significant influence on the EE content of the plants, with the exception of 509022 plants, in which the EE content decreased significantly under saline conditions (Figure 5C).

All the ecotypes had a higher content of NDF (57.4% of DW on average) under control conditions. Salt stress significantly decreased the NDF content to 50.2% of DW on average, with the exception of SP007, 509022, 647896, 647900, 647903, and 647909 plants (Figure 6A). There were no significant differences in the ADF content between control and saline conditions, with the exception of 509023, 647894, 647907, and 647921 plants. However, as an advanced forage breeding ecotype, 647907 had a high forage nutritive value, indicated by the high values of ADF, NDF, CP, and EE (Figures 5A, C, 6A, B). The forage quality parameters, including DDM, DMI, and RFV, calculated from the content of ADF and NDF, increased in all

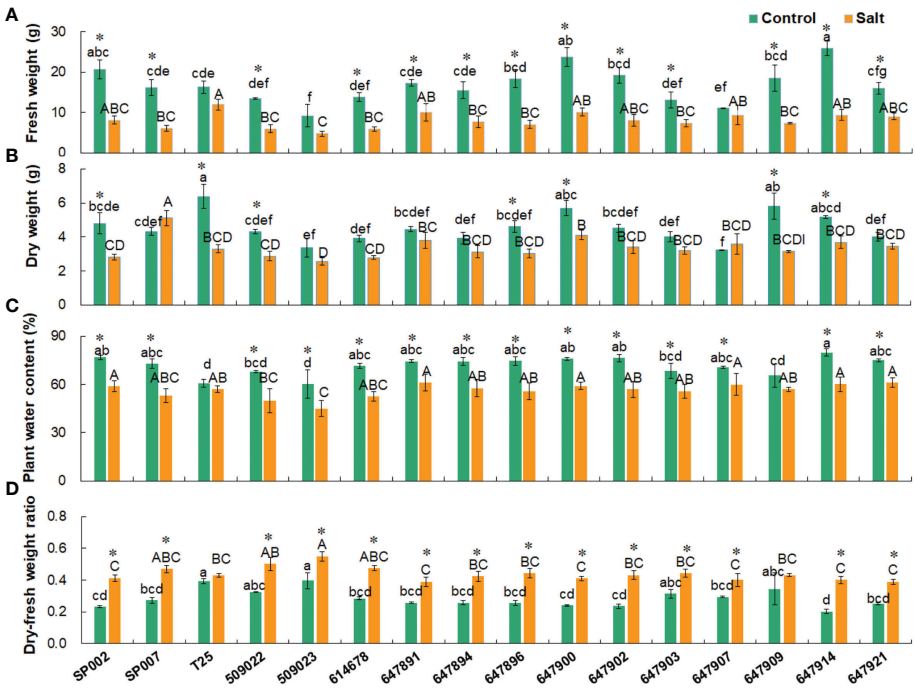

FIGURE 4
Effect of salt stress on shoot biomass parameters of 16 seashore paspalum ecotypes. Shoots were sampled for measurement of fresh weight **(A)**, dry weight **(B)**, water content **(C)**, and dry- fresh weight ratio **(D)** before treatment (control) and after NaCl treatment for 10 d (salt). Means of three independent experiments and standard errors are presented; the same letter above the column indicates no significant difference at $P<0.05$. Lowercase letters and uppercase letters respectively indicate significant comparisons among different ecotypes in the control group and treatment group. * indicates significant difference at $P<0.05$ by T-test between salt treatment and control for 16 ecotypes.

ecotypes under saline conditions (68.7%, 2.4%, and 128.2%, respectively, on average). There was a small difference in the DDM, DMI, and RFV of the majority of ecotypes, which were 65.7%, 2.1%, and 106.7%, respectively, on average, under control conditions. The DDM ranged from 58.9% (647907) to 69.8% (509023), while the DMI ranged from 2.0% (647907) to 2.18% (647900), and the RFV varied between 91.5% (647907) and 115.0% (SP002) across the 16 ecotypes (Figures 6C–E).

TABLE 3 Pearson's correlation coefficients between pairs of traits.

	FW control	DW control	W Ccontrol	DFR control	F Wsalt	DW salt	WC salt	DFR salt
FW control	–	**0.67****	**0.67****	**−0.67****	0.46	0.33	**0.57***	**−0.57***
DW control		–	−0.04	0.04	0.55*	0.17	0.31	−0.31
WC control			–	**−0.99****	0.19	0.35	0.60*	-0.60*
DFR control				–	−0.21	−0.37	**−0.62****	**0.62****
FW salt					–	0.29	**0.79****	**−0.78****
DW salt						–	0.34	−0.33
WC salt							–	**−0.99****
DFR salt								–

*P<0.05, **P<0.01 represent significant values that been bold in tables.
FW, fresh weight; DW, dry weight; WC, water content; DFR, dry-fresh weight ratio.

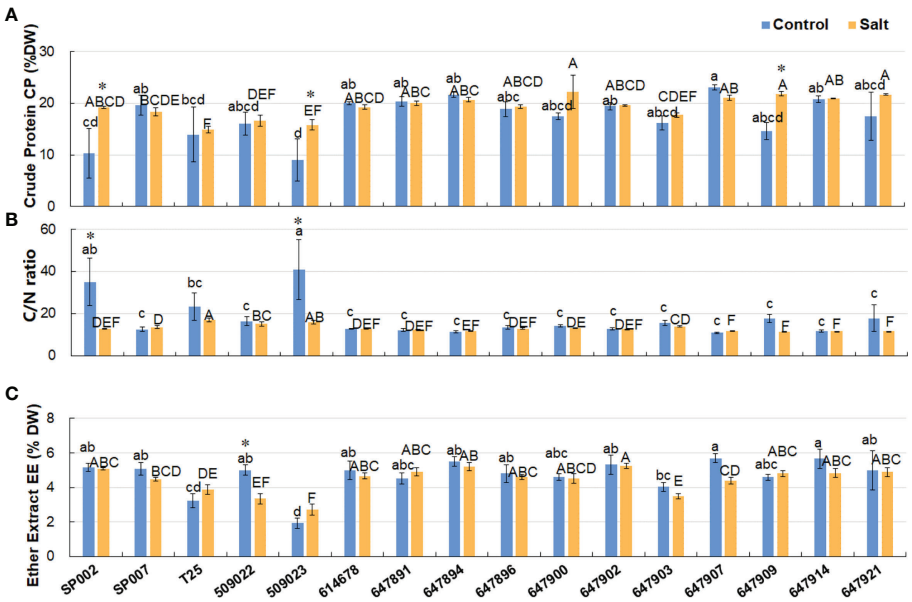

FIGURE 5
Effect of salt stress on crude protein, C/N ratio, and ether extract of 16 seashore paspalum ecotypes. The Crude Protein CP **(A)**, C/N ratio **(B)**, and Ether Extract EE **(C)** of shoots were measured before treatment (control) and after NaCl treatment for 10 d (salt). Means of three independent experiments and standard errors are presented; the same letter above the column indicates no significant difference at $P<0.05$. Lowercase letters and uppercase letters respectively indicate significant comparisons among different ecotypes in the control group and treatment group. * indicates significant difference at $P<0.05$ by T-test between salt treatment and control for 16 ecotypes.

Analysis of salt and cold tolerance

The effect of short-term high-salt stress (1 week, 700 mM NaCl) on the growth and forage nutritive value of seashore paspalum was evaluated in this study. The salt tolerance of the seashore paspalum ecotypes was subsequently evaluated by determining the survival rate after long-term high-salt stress (7 weeks, 700 mM NaCl). The evaluation of survival rate is a fundamental strategy for selecting grasses that can be grown in areas with saline land and low temperature conditions. The survival rates after salt and low temperature stress were significantly influenced by the ecotype of the plants. The survival rate of the 16 seashore paspalum ecotypes varied from 49.0% for 647921 plants to 6.5% for T25 plants under long-term high-salt stress (Figures 7A, B).

To evaluate cold tolerance, the plants were subjected to short-term (9 d) and long-term (15 d) natural low-temperature treatments, where the temperature ranged from −5 °C to 9 °C (Figure 8A). The survival rate at low temperatures was influenced by the ecotypes of the plants, and ranged from 23.3% (647902) to 88.6% (T25) under short-term low temperature stress, but the effect of the ecotype was not a significant influencing factor for most plants (59.5% on average), with the exception of 647897 and 647902 plants under short-term low temperature stress. Long-term low temperature stress significantly decreased the survival rate of the plants by 14.4% on average, with the exception of 614678, 647891, 647894, 647900, 647902, and 647909 plants (Figures 8B, C). The survival rate of the plants during short-term and long-term natural low-temperature treatments was significantly positively correlated ($r = 0.534$, $P<0.05$).

Discussion

Freshwater resources and agricultural prime lands should be allocated for growing food crops for the increasing human population. However, saline lands can be used for the cultivation of halophytes for ecological benefits. Halophytes are expected to have an increasingly important role as genetic resources for the re-vegetation of saline lands (Flowers and Colmer, 2015). Seashore paspalum can produce feed for livestock and grow on poor-quality soils that are unfit for growing crops or for traditional pasture production and can serve as a forage grass for value-added development of saline lands. An early study evaluating the yield and quality of seashore paspalum under saline conditions demonstrated that seashore paspalum has the highest ash content (15.5%) and DW yield, which are almost unaffected by soil salinity. The study revealed that seashore paspalum could show promise in forage production under conditions of high salinity (Pasternak et al., 1993).

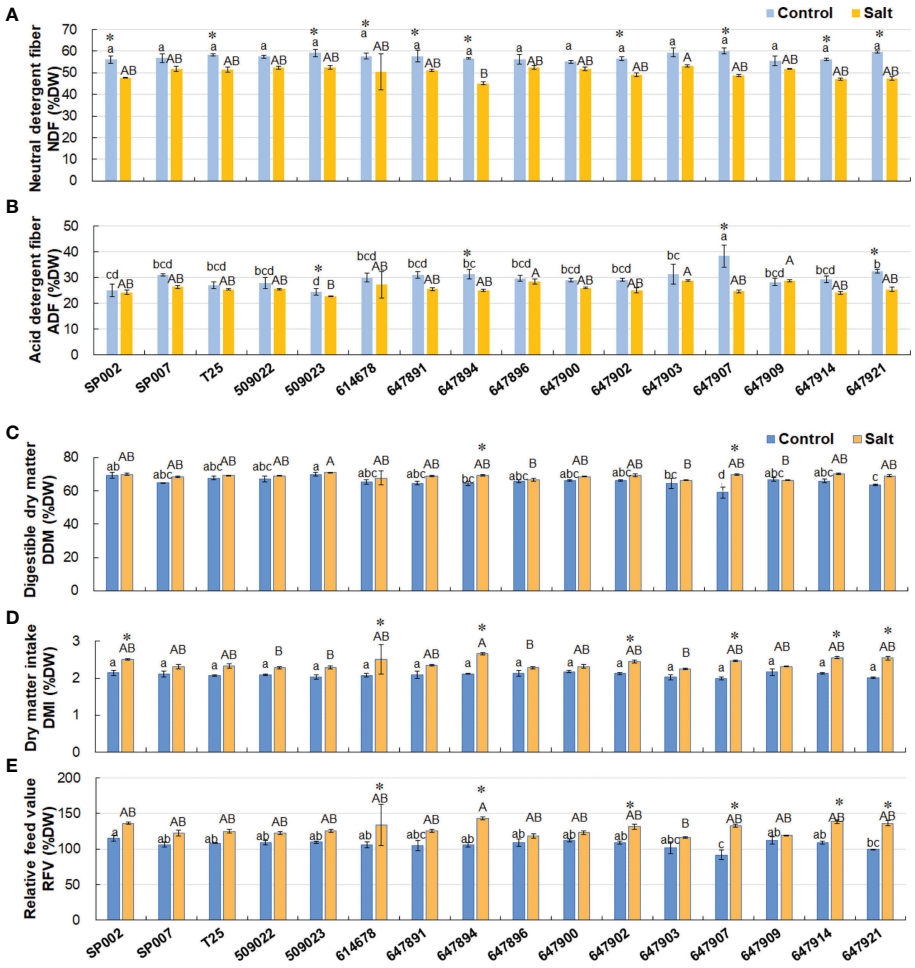

FIGURE 6
Effect of salt stress on forage nutritive value of 16 seashore paspalum ecotypes. The neutral detergent fiber NDF (% DW) **(A)** and acid detergent fiber ADF (% DW) **(B)** were measured before treatment (control) and after NaCl treatment for 10 d (salt); then digestible dry matter, DDM (% DW) **(C)**, dry-matter intake, DMI (% DW) **(D)**, and relative feed value (RFV) **(E)** were determined. Means of three independent experiments and standard errors are presented; the same letter above the column indicates no significant difference at $P<0.05$. Lowercase letters and uppercase letters respectively indicate significant comparisons among different ecotypes in the control group and treatment group. * indicates significant difference at $P<0.05$ by T-test between salt treatment and control for 16 ecotypes.

Relationship between agronomic traits and forage quality

Compared with cold-season grasses, perennial warm-season grasses typically have the potential to produce higher biomass yields (Anderson et al., 2015). In a previous study, the forage yield of meadow bromegrass (*Bromus riparius* Rehm) was correlated with plant height and branching ability (de Araujo and Coulman, 2002). In the present study, we selected the warm-season grass, seashore paspalum, owing to its higher biomass yields and tolerance to soil salinity. We observed that the plant heights and leaf–stem ratios were significantly affected by the ecotype of the plants. However, the height and leaf–stem ratio of seashore paspalum plants were not important factors in determining the yield and had no significant correlation with the FW or DW of the plants. There were no significant differences between the chlorophyll content and Pn of the majority of ecotypes studied herein. Consequently, the forage yield of seashore paspalum was more likely determined by the tillering ability than the genetic makeup of each ecotype. This finding differed from the results of some studies which demonstrated that the fresh and dry forage yields of alfalfa cultivars are mostly attributed to high leaf to shoot ratio, plant height, and chlorophyll content (Monirifar et al., 2020). The improvement of chlorophyll content and photosynthetic capacity is an important factor that influences the yield of alfalfa (Cornacchione and Suarez, 2017). Generally, leaf tissues have higher forage quality than stem tissues, and a marked

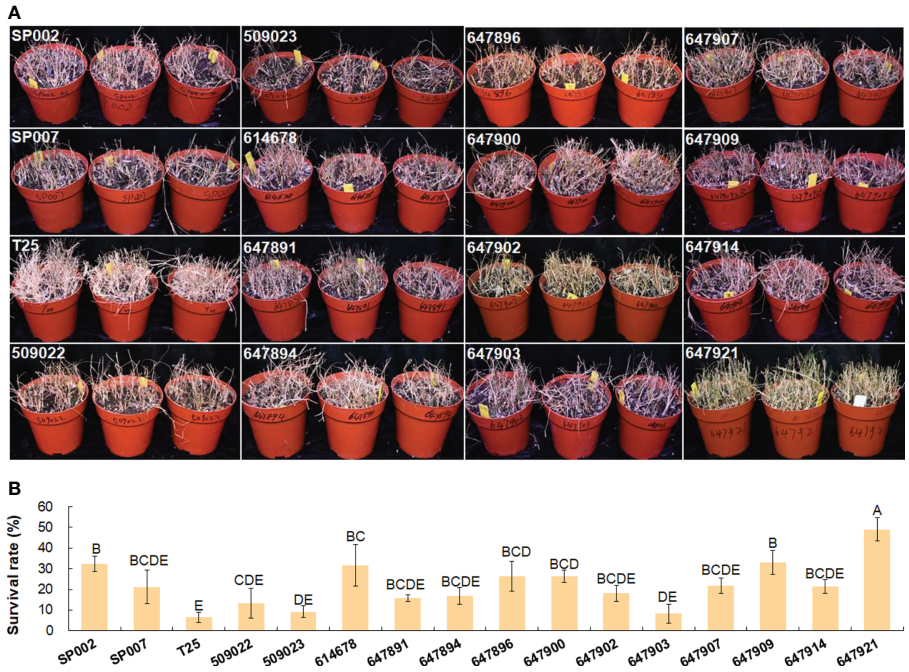

FIGURE 7
Analysis of salt tolerance in 16 seashore paspalum ecotypes. Photographs were taken when NaCl concentration was increased to 700 mM for 7 weeks **(A)**; then survival rates were calculated after salt treatment by watering to wash salt for 7 d **(B)**. Means of three replicates and standard errors are presented; the same letter above the column indicates no significant difference at $P<0.05$.

increase in the leaf–stem ratio of forage grasses is expected to improve forage quality (Casler et al., 2014; Sanchez et al., 2018). A higher leaf–stem ratio significantly affects the CP content of rhizome peanut (*Arachis glabrata* Benth.) ecotypes (Alencar et al., 2019) and alfalfa (Hakl et al., 2016). However, the results of this study suggested that the leaf–stem ratio and the forage nutritive value, indicated by the CP content, EE content, NDF, and ADF, were not significantly correlated. This could be attributed to the low density and lignification of the stem in seashore paspalum.

Effect of salinity on forage yield and CP content

Despite the excellent salt tolerance ability of seashore paspalum, the FW, DW, and DFR of the majority of ecotypes were influenced by high salinity. Salt stress significantly decreased the FW of most ecotypes. A previous study demonstrated that the dry mass of the shoot of two halophytic grasses, puccinellia (*Puccinellia ciliata* Bor. cv. Menemen) and tall wheatgrass (*Thinopyrum ponticum* Podp.), decreased by 50% following treatment with 300 mM NaCl, and both grasses barely survived under 600 mM NaCl (Jenkins et al., 2010). The growth of switchgrass (*Panicum virgatum* L.) EG 2101 has been shown to be severely affected by increasing levels of salinity, but it produces more biomass than populations of prairie cordgrass (*Partina pectinata* Link) under moderate salinity (5 dS m^{-1}) (Anderson et al., 2015). In this study, high salinity (700 mM NaCl) decreased the FW and DW of seashore paspalum shoots by 50.6% and 23.6%, respectively, on average. The survival rate of the seashore paspalum ecotypes varied from 6.5% to 49.0% following treatment with 700 mM NaCl for 7 weeks.

The results of this study suggest that seashore paspalum has outstanding salt tolerance and forage quality at high salinity. As the growth of alfalfa and tall wheatgrass is stunted by 600 mM NaCl, their forage quality at high levels of salinity (above 300 mM NaCl) cannot be evaluated owing to insufficient sample size (Shahba et al., 2012; Sagers et al., 2017; Waldron et al., 2020). The CP content of seashore paspalum was found to be higher than that of Rhodes grass (*Chloris gayana* Kunth.) (11.5%) and Bermuda grass (*Cynodon dactylon* L. Pers.) (16%) but lower than that of alfalfa (22%), *Agropyron cristatum* (36%), and *Lolium perenne* (34%) (Pasternak et al., 1993; Lee, 2018). A previous study on 15 cultivars of wheat (*Triticum aestivum* L.) reported that the CP content varied from 20% to 24% (Kim and Anderson, 2015), while an oat (*Avena sativa* L.) cultivar (Forage Plus and Ogle) was reported to have a CP content of 13%–15% (Coblentz and Cavadini, 2016). The mean CP content of sporobolus grass (*Sporobolus virginicus*), a halophytic grass,

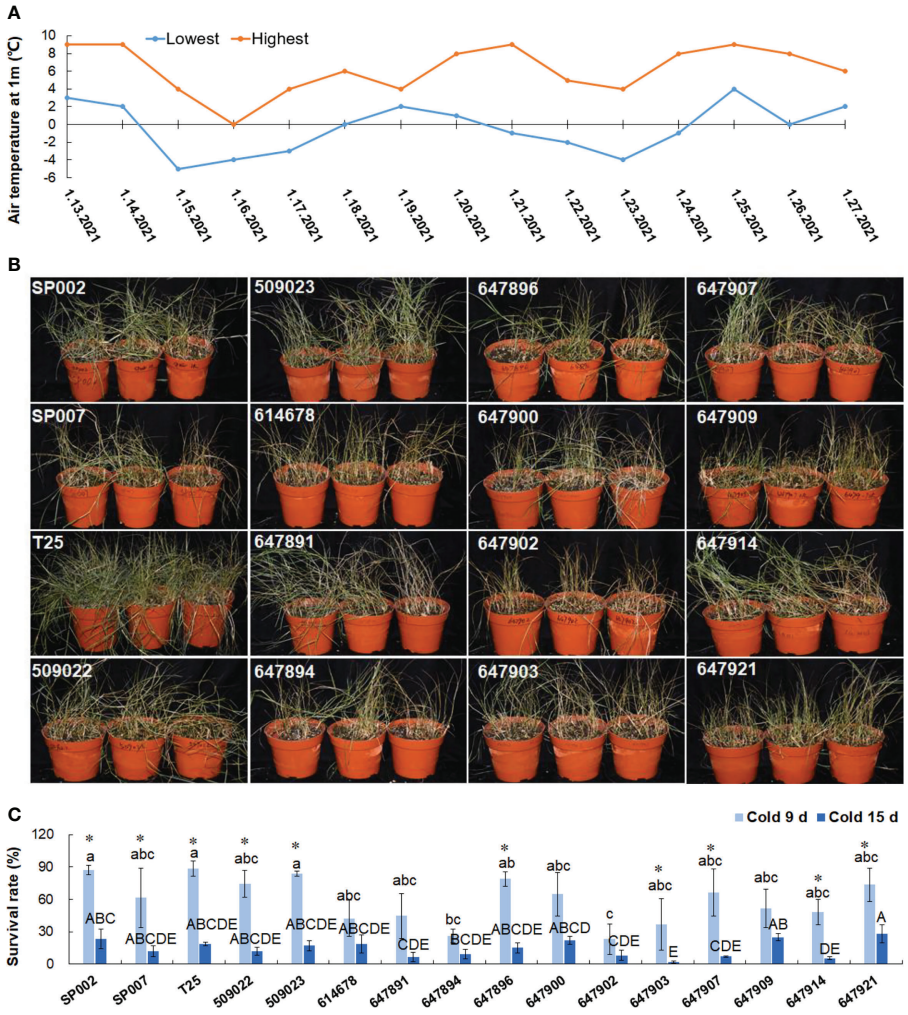

FIGURE 8
Analysis of low temperature tolerance in 16 seashore paspalum ecotypes. Temperature change diagram of plants treated with low temperature for 15 d **(A)**. Plants were photographed after 9 d under low temperature treatment **(B)**. Survival rates were respectively documented for 9 and 15 d **(C)**. Means of three replicates and standard errors are presented; the same letter above the column indicates no significant difference at $P<0.05$. Lowercase letters and uppercase letters respectively indicate significant comparisons among different ecotypes in cold 9 d and cold 15 d. * indicates significant difference at $P<0.05$ by T-test between cold 9 d treatment and cold 15 d treatment for 16 ecotypes.

was reported to be 8.7% of the dry matter, which was found to be higher than that of four other species of grass grown on the saline soils of Australia, with mean CP contents of 5%–8% of the dry matter. (Al-Shorepy et al., 2010; Norman et al., 2013). These findings indicate that there is no relationship between the CP content and soil salinity, and the effects of salinity on the CP content of grasses are inconsistent. The forage quality of the halophyte, forage kochia, is affected by the accumulation of salt when grown on saline soils containing nearly 300 mM of salt. A study demonstrated that the CP content of forage kochia following treatment with 600 mM NaCl decreased by 41% of that of the control (Waldron et al., 2020). The CP content of sporobolus grass was reported to increase from 6 to 9% when irrigated with increasingly saline water (Ashour et al., 1997). In this study, the CP content of seashore paspalum was not significantly affected at 700 mM NaCl. The CP content was 17.4% and 19.3% under control and saline (700 mM NaCl) conditions, respectively, with the exception of three ecotypes in which the CP content had increased significantly. The CP content of almost all the ecotypes of seashore paspalum was significantly higher than the recommended level for nursing calves (15% dry matter) and lactating cows (9%–12% dry matter) (Kim and Anderson, 2015). Furthermore, seashore paspalum can be an important source of antioxidants in saline environments. The results of this study are corroborated by those of several studies on various halophytes. Antioxidant enzymes play a key role in salt tolerance and improve plant growth by quenching reactive oxygen species and could

therefore serve as a good source of protein for livestock (Tlili et al., 2020).

Effect of salinity on fiber quality

The cell walls of forage plants contain large amounts of fiber that comprise NDF, ADF, and acid detergent lignin (ADL). NDF and ADF are very important indicators for determining the forage quality, and the contents of NDF and ADF are negatively correlated with forage digestibility by livestock (Surber et al., 2011; Xie et al., 2011; Sanz-Sáez et al., 2012). The NDF content is especially important when formulating feed rations for ruminant animals and correlates with forage intake (Buxton, 1996). High lignin content contributes to the low forage quality of some warm-season grasses (Giordano et al., 2014; Gitau et al., 2017). Statistical analyses have revealed that the mean values of NDF and ADF across all forage plants are 57% and 32%, respectively. The mean NDF and ADF content are highest in grasses, being 59% and 33%, respectively, and lowest in legumes, being 42% and 28%, respectively. Large variations in the values of NDF and ADF have been reported within species. The highest values of NDF measured in grasses are 39%–70% and 34%–62% in *Alopecurus pratensis* and *L. perenne*, respectively, while the highest values of ADF reported in grasses are 2%–35% and 18%–46% in *L. multiflorum* and *B. inermis*, respectively (Lee, 2018).

In this study, the ADF content was significantly correlated with the CP (r = 0.802, P<0.01) and EE (r = 0.548, P<0.05) contents under control conditions. This finding was different from the results of a study which reported that the ADF content is significantly negatively correlated with the CP content (de Araujo and Coulman, 2002). The average NDF and ADF contents of seashore paspalum were 57.4% and 29.8%, respectively, of the DW under control conditions, which were lower than those of the forage Bermuda grass. A study reported significant variations in the ADF (24.1% to 34.5%) and NDF (64.3% to 77.3%) contents of 168 plant introductions of forage Bermuda grass (Anderson et al., 2010). The ADF (20.6% to 24.3%) and NDF (39.4% to 46.5%) contents of wheat are markedly lower than those of seashore paspalum. The NDF content of old man saltbush (*Atriplex nummularia* L.) collected from diverse saline soils is also lower (30% to 45% of DW) than that of seashore paspalum. The ecotypes and salt stress had little influence on the RFV (91% to 115%) of seashore paspalum; however, it has been reported that the RFV of wheat (146% to 183%) is significantly affected by the variety. The superiority of the RFV is reflected in the lower values of ADF and NDF. However, higher values of RFV also result in the worst mean forage yield in some varieties of wheat (Kim and Anderson, 2015).

Forage plants undergo morphological and physiological changes that affect the NDF content and nutritive values (Arnold et al., 2019). However, the interactions between the salinity of the environment and the forage fiber value of grasses are not consistent (Norman et al., 2013). Our results suggest that short-term salt stress significantly affected the DW and reduced the NDF and ADF contents to a slight extent (50.2% and 25.9% of DW on average, respectively; P >0.05). The lower NDF content was beneficial for the higher dietary energy and improved livestock intake of seashore paspalum. It has been reported that the NDF contents of forage kochia are not affected by salinity (from 30% to 32.4%), while those of alfalfa and tall wheatgrass are only slightly affected by saline conditions (Waldron et al., 2020). Furthermore, a study demonstrated that there is no clear correlation between the NDF content and increasing salinity in river saltbush (Masters et al., 2010). These existing findings support the results of this study on seashore paspalum. The results of the present study further suggest that seashore paspalum has excellent salt tolerance ability and could also serve as a high-quality forage plant.

Conclusions

Seashore paspalum is a halophytic warm-season grass with superior salt tolerance. Although the plant is primarily used in athletic fields and landscape areas as lawn grass, seashore paspalum is an attractive potential feedstock that is used for livestock feed (for hay and grazing) owing to its superior ground cover, biomass accumulation, and salt tolerance. The majority of studies on salt-tolerant forage plants emphasize elucidating the agronomic traits and underlying physiological mechanisms. Fewer studies have aimed to elucidate the effects of salinity on the forage quality of halophyte species. This study is the first to investigate the nutritive value of seashore paspalum and the influence of salinity on its nutritive value. Altogether, the results demonstrated that there were significant genetic (ecotype-specific) effects on plant heights and leaf–stem ratios in seashore paspalum. Salt stress significantly decreased the FW of the majority of ecotypes. However, seashore paspalum exhibited outstanding salt tolerance and forage quality at high salinity. Salt stress did not significantly affect the CP and EE contents of most ecotypes, but slightly reduced the NDF and ADF contents and improved the RFV. The results supported the fact that seashore paspalum is a good candidate for improving the forage base of saline soils. Seashore paspalum can serve as an excellent forage plant, providing high quality forage in saline soils. The study also focused on improving the productivity of saline systems by selecting ecotypes with higher nutritive value and biomass. For instance, the ecotype of 647907 selected in this study had the highest EE and CP content; however, the DW of the plants increased only slightly under high salt stress. At the same time, the interactions between the ecotypes and their environment should be considered when selecting ecotypes with higher feeding values. The cold and salt tolerance of the

ecotypes was additionally evaluated herein, and the results could provide a basis for the selection of different ecotypes at different climates and salinities.

Data availability statement

The raw data supporting the conclusions of this article will be made available by the authors, without undue reservation.

Authors contributions

KJ conducted experiments. ZY, JS, HL, SC, YZ, WX, and WL give advice and assistance in this research. ZW revised manuscript. XW designed experiments and wrote manuscript. All authors contributed to the article and approved the submitted version.

Funding

This work was supported by the National Natural Science Foundation of China (32101423), the Foundation Project of Shandong Natural Science Foundation (ZR2021MC066), the Fundamental Research Funds for the Universities (6631120002), and the 'First Class Grassland Science Discipline' programme of Shandong Province.

Acknowledgments

The authors would like to acknowledge Meng Shi, Ying Chen, Rui Zhao, Xiaofan Wu, Wenjian Xu, and Dongyang Liu for their help on the article and also thank the National Foundation and the Key Laboratory of the Yellow River Delta Grassland Resources and Ecology of the Chinese Forestry and Grassland Administration for the support of this project.

Conflict of interest

The authors declare that the research was conducted in the absence of any commercial or financial relationships that could be construed as a potential conflict of interest.

Publisher's note

References

Acuña, C. A., Martínez, E. J., Zilli, A. L., Brugnoli, E. A., Espinoza, F., Marcón, F., et al. (2019). Reproductive systems in *Paspalum*: Relevance for germplasm collection and conservation, breeding techniques, and adoption of released cultivars. *Front. Plant Sci.* 10 (1377). doi: 10.3389/fpls.2019.01377

Alencar, N. M., Vendramini, J. M. B., Dubeux, J. C. B., Santos, A. C., Sanchez, J. M. D., Silva, H. M., et al. (2019). Impact of leaf and stem proportions on dry matter and crude protein *in situ* disappearance of rhizoma peanut genotypes. *Crop Sci.* 59, 1815–1821. doi: 10.2135/cropsci2019.02.0114

Al-Shorepy, S. A., Alhadrami, G. A., and Al-Dakheel, A. J. (2010). Growth performances and carcass characteristics of indigenous lambs fed halophyte sporobolus virginicus grass hay. *Asian Australas. J. Anim. Sci.* 23, 556–562. doi: 10.5713/ajas.2010.90094

Anderson, W. F., Dien, B. S., Jung, H.-J. G., Vogel, K. P., and Weimer, P. J. (2010). Effects of forage quality and cell wall constituents of bermuda grass on biochemical conversion to ethanol. *Bioenerg. Res.* 3, 225–237. doi: 10.1007/s12155-009-9063-9

Anderson, E. K., Voigt, T. B., Kim, S., and Lee, D. K. (2015). Determining effects of sodicity and salinity on switchgrass and prairie cordgrass germination and plant growth. *Ind. Crop Prod.* 64, 79–87. doi: 10.1016/j.indcrop.2014.11.016

Arnold, A. M., Cassida, K. A., Albrecht, K. A., Hall, M. H., Min, D., Xu, X., et al. (2019). Multistate evaluation of reduced-lignin alfalfa harvested at different intervals. *Crop Sci.* 59, 1799–1807. doi: 10.2135/cropsci2019.01.0023

Ashour, N. I., Serag, M. S., Abd El-Haleem, A. K., and Mekki, B. B. (1997). Forage production from three grass species under saline irrigation in Egypt. *J. Arid. Environ.* 37, 299–307. doi: 10.1006/jare.1997.0284

Badran, A. E., ElSherebeny, E. A. M., and Salama, Y. A. (2015). Performance of some alfalfa cultivars under salinity stress conditions. *J. Agr. Sci.* 7, p281. doi: 10.5539/jas.v7n10p281

Buxton, D. R. (1996). Quality-related characteristics of forages as influenced by plant environment and agronomic factors. *Anim. Feed. Sci. Tech.* 59, 37–49. doi: 10.1016/0377-8401(95)00885-3

Campanelli, A., Ruta, C., Morone-Fortunato, I., and Mastro, G. (2013). Alfalfa (Medicago sativa l.) clones tolerant to salt stress: *in vitro* selection. *Open Life Sci.* 8, 765–776. doi: 10.2478/s11535-013-0194-1

Cardona, C. A., Duncan, R. R., and Lindstrom, O. (1997). Low temperature tolerance assessment in paspalum. *Crop Sci.* 37, 1283–1291. doi: 10.2135/cropsci1997.0011183X003700040043x

Casler, M. D., Undersander, D. J., Papadopolous, Y. A., Bittman, S., Hunt, D., Mathison, R. D., et al. (2014). Sparse-flowering orchardgrass represents an improvement in forage quality during reproductive growth. *Crop Sci.* 54, 421–429. doi: 10.2135/cropsci2013.04.0227

Chen, Z. B., Kim, W., Newman, M., Wang, M. L., and Raymer, P. (2005). Molecular characterization of genetic diversity in the USDA seashore paspalum germplasm collection. *Int. Turf. Soc Res. J.* 10, 543–549.

Cidade, F. W., Vigna, B. B., Souza, F. H., Valls, J. F. M., Dall'Agnol, M., Zucchi, M. I., et al. (2013). Genetic variation in polyploid forage grass: assessing the molecular genetic variability in the *Paspalum* genus. *BMC Genet.* 14, 50. doi: 10.1186/1471-2156-14-50

Coblentz, W. K., and Cavadini, J. S. (2016). Effects of seeding rate on the dry matter yield and nutritive value of fall-grown oat. *Crop Forage Turf. Man.* 2, 1–7. doi: 10.2134/cftm2016.0004

Cornacchione, M. V., and Suarez, D. L. (2017). Evaluation of alfalfa (*Medicago sativa* l.) populations' response to salinity stress. *Crop Sci.* 57, 137–150. doi: 10.2135/cropsci2016.05.0371

Cyril, J., Powell, G. L., Duncan, R. R., and Baird, W. V. (2002). Changes in membrane polar lipid fatty acids of seashore paspalum in response to low temperature exposure. *Crop Sci.* 42, 2031–2037. doi: 10.2135/cropsci2002.2031

de Araujo, M. R. A., and Coulman, B. E. (2002). Genetic variation, heritability and progeny testing in meadow bromegrass. *Plant Breed.* 121, 417–424. doi: 10.1046/j.1439-0523.2002.739124.x

Dong, F., Tang, Y., Xing, X., Liu, Z., and Xing, L. (2019). Formation and evolution of soil salinization in shouguang city based on PMS and OLI/TM sensors. *Water* 11, 345. doi: 10.3390/w11020345

Eudy, D., Bahri, B. A., Harrison, M. L., Raymer, P., and Devos, K. M. (2017). Ploidy level and genetic diversity in the genus *Paspalum*, group disticha. *Crop Sci.* 57, 3319–3332. doi: 10.2135/cropsci2017.04.0241

Flowers, T. J., and Colmer, T. D. (2015). Plant salt tolerance: adaptations in halophytes. *Ann. Bot.-london* 115, 327–331. doi: 10.1093/aob/mcu267

Gangwar, P., Singh, R., Trivedi, M., and Tiwari, R. K. (2020). "Sodic soil: management and reclamation strategies," in *Environmental concerns and sustainable development* (Singapore: Springer Singapore), 175–190. doi: 10.1007/978-981-13-6358-0_8

Giordano, A., Liu, Z., Panter, S. N., Dimech, A. M., Shang, Y., Wijesinghe, H., et al. (2014). Reduced lignin content and altered lignin composition in the warm season forage grass paspalum dilatatum by down-regulation of a cinnamoyl CoA reductase gene. *Transgenic Res.* 23, 503–517. doi: 10.1007/s11248-014-9784-1

Gitau, M. M., Fan, J., Xie, Y., and Fu, J. (2017). Genetic diversity and association mapping of forage quality in diverse bermudagrass accessions. *Euphytica* 213, 234. doi: 10.1007/s10681-017-2024-z

Gu, C., Iwaasa, A. D., Wall, K., Gatzke, C., and Zhao, M. (2019). Seeding rate and fertility effects on AC saltlander forage production on saline soils. *Agron. J.* 111, 328–335. doi: 10.2134/agronj2018.06.0395

Hakl, J., Fuksa, P., Konečná, J., and Šantrůček, J. (2016). Differences in the crude protein fractions of lucerne leaves and stems under different stand structures. *Grass Forage Sci.* 71, 413–423. doi: 10.1111/gfs.12192

Himabindu, Y., Chakradhar, T., Reddy, M. C., Kanygin, A., Redding, K. E., and Chandrasekhar, T. (2016). Salt-tolerant genes from halophytes are potential key players of salt tolerance in glycophytes. *Environ. Exp. Bot.* 124, 39–63. doi: 10.1016/j.envexpbot.2015.11.010

Huang, L., Liang, Z., Suarez, D. L., Wang, Z., Ma, H., Wang, M., et al. (2015). Continuous nitrogen application differentially affects growth, yield, and nitrogen use efficiency of *Leymus chinensis* in two saline–sodic soils of northeastern China. *Agron. J.* 107, 314–322. doi: 10.2134/agronj14.0250

Jenkins, S., Barrett-Lennard, E. G., and Rengel, Z. (2010). Impacts of waterlogging and salinity on puccinellia (*Puccinellia ciliata*) and tall wheatgrass (*Thinopyrum ponticum)*: zonation on saltland with a shallow water-table, plant growth, and na+ and k+ concentrations in the leaves. *Plant Soil* 329, 91–104. doi: 10.1007/s11104-009-0137-4

Ji, Z. H., and Wang, Y. (2002). "Animal husbandry and veterinary bureau of the ministry of agriculture (national feed work office)," in *Compilation of feed industry standards* (Beijing: China Standard Press).

Karimi, I. Y. M., Kurup, S. S., Salem, M. A. M. A., Cheruth, A. J., Purayil, F. T., Subramaniam, S., et al. (2018). Evaluation of bermuda and paspalum grass types for urban landscapes under saline water irrigation. *J. Plant Nutr.* 41, 888–902. doi: 10.1080/01904167.2018.1431669

Kim, K.-S., and Anderson, J. D. (2015). Forage yield and nutritive value of winter wheat varieties in the southern great plains. *Euphytica* 202, 445–457. doi: 10.1007/s10681-014-1325-8

Lee, M. A. (2018). A global comparison of the nutritive values of forage plants grown in contrasting environments. *J. Plant Res.* 131, 641–654. doi: 10.1007/s10265-018-1024-y

Lee, G., Carrow, R. N., and Duncan, R. R. (2004). Photosynthetic responses to salinity stress of halophytic seashore paspalum ecotypes. *Plant Sci.* 166, 1417–1425. doi: 10.1016/j.plantsci.2003.12.029

Li, J., Pu, L., Han, M., Zhu, M., Zhang, R., and Xiang, Y. (2014). Soil salinization research in China: Advances and prospects. *J. Geogr. Sci.* 24, 943–960. doi: 10.1007/s11442-014-1130-2

Liu, Z. W., Jarret, R. L., Duncan, R. R., and Kresovich, S. (1994). Genetic relationships and variation among ecotypes of seashore paspalum (*Paspalum vaginatum*) determined by random amplified polymorphic DNA markers. *Genome.* 37, 1011–1017. doi: 10.1139/g94-143

Marcum, K. B., and Murdoch, C. L. (1994). Salinity tolerance mechanisms of six C_4 turfgrasses. *J. Am. Soc Hortic. Sci.* 119, 779–784. doi: 10.21273/JASHS.119.4.779

Masters, D., Tiong, M., Vercoe, P., and Norman, H. (2010). The nutritive value of river saltbush (Atriplex amnicola) when grown in different concentrations of sodium chloride irrigation solution. *Small Ruminant Res.* 91, 56–62. doi: 10.1016/j.smallrumres.2009.10.019

Monirifar, H., Mirmozaffari Roudsari, A., Ghassemi, S., and Tavasolee, A. (2020). Harvest time and cultivar effects on growth, physiological traits, yield and quality of alfalfa in saline condition. *Int. J. Plant Prod.* 14, 453–462. doi: 10.1007/s42106-020-00096-3

Mora, O., Le Mouël, C., de Lattre-Gasquet, M., Donnars, C., Dumas, P., Réchauchère, O., et al. (2020). Exploring the future of land use and food security: A new set of global scenarios. *PloS One* 15, e0235597. doi: 10.1371/journal.pone.0235597

Moustafa, E. S. A., El-Sobky, E.-S. E. A., Farag, H. I. A., Yasin, M. A. T., Attia, A., Rady, M. O. A., et al. (2021). Sowing date and genotype influence on yield and quality of dual-purpose barley in a salt-affected arid region. *Agronomy* 11, 717. doi: 10.3390/agronomy11040717

Munir, N., Hasnain, M., Roessner, U., and Abideen, Z. (2022). Strategies in improving plant salinity resistance and use of salinity resistant plants for economic sustainability. *Crit. Rev. Env. Sci. Tec.* 52, 2150–2196. doi: 10.1080/10643389.2021.1877033

Munns, R., and Gilliham, M. (2015). Salinity tolerance of crops – what is the cost? *New Phytol.* 208, 668–673. doi: 10.1111/nph.13519

Norman, H. C., Duncan, E. G., and Masters, D. G. (2019). Halophytic shrubs accumulate minerals associated with antioxidant pathways. *Grass Forage Sci.*, 74, 345–355. doi: 10.1111/gfs.12434

Norman, H. C., Masters, D. G., and Barrett-Lennard, E. G. (2013). Halophytes as forages in saline landscapes: Interactions between plant genotype and environment change their feeding value to ruminants. *Environ. Exp. Bot.* 92, 96–109. doi: 10.1016/j.envexpbot.2012.07.003

Oney-Birol, S. (2019). Exogenous l-carnitine promotes plant growth and cell division by mitigating genotoxic damage of salt stress. *Sci. Rep.* 9, 17229. doi: 10.1038/s41598-019-53542-2

Pasternak, D., Nerd, A., and De Malach, Y. (1993). Irrigation with brackish water under desert conditions IX. the salt tolerance of six forage crops. *Agr. Water Manage.* 24, 321–334. doi: 10.1016/0378-3774(93)90010-8

Pessarakli, M. (2018). Screening various cultivars of seashore paspalum (*Paspalum vagenitum* Swartz) for salt tolerance for potential use as a cover plant in combatting desertification. *Int. J. Water Resour. Arid Environ.* 7, 36–43.

Pompeiano, A., Di Patrizio, E., Volterrani, M., Scartazza, A., and Guglielminetti, L. (2016). Growth responses and physiological traits of seashore paspalum subjected to short-term salinity stress and recovery. *Agr. Water Manage.* 163, 57–65. doi: 10.1016/j.agwat.2015.09.004

Qi, P., Eudy, D., Schnable, J. C., Schmutz, J., Raymer, P. L., and Devos, K. M. (2019). High density genetic maps of seashore paspalum using genotyping-by-sequencing and their relationship to the *Sorghum bicolor* genome. *Sci. Rep.* 9, 12183. doi: 10.1038/s41598-019-48257-3

Robinson, P. H., Grattan, S. R., Getachew, G., Grieve, C. M., Poss, J. A., Suarez, D. L., et al. (2004). Biomass accumulation and potential nutritive value of some forages irrigated with saline-sodic drainage water. *Anim. Feed Sci. Tech.* 111, 175–189. doi: 10.1016/S0377-8401(03)00213-X

Sagers, J. K., Waldron, B. L., Creech, J. E., Mott, I. W., and Bugbee, B. (2017). Salinity tolerance of three competing rangeland plant species: Studies in hydroponic culture. *Ecol. Evol.* 7, 10916–10929. doi: 10.1002/ece3.3607

Sanchez, J. M. D., Vendramini, J. M. B., Silveira, M. L., Sollenberger, L. E., Dubeux, J. C. B., Moriel, P., et al. (2018). Genotype and regrowth interval effects on *in situ* disappearance of rhizoma peanut. *Crop Sci.* 58, 2174–2181. doi: 10.2135/cropsci2018.03.0200

Sanz-Sáez, Á., Erice, G., Aguirreolea, J., Muñoz, F., Sánchez-Díaz, M., and Irigoyen, J. J. (2012). Alfalfa forage digestibility, quality and yield under future climate change scenarios vary with *Sinorhizobium meliloti* strain. *J. Plant Physiol.* 169, 782–788. doi: 10.1016/j.jplph.2012.01.010

Schiavon, M., Leinauer, B., Serena, M., Sallenave, R., and Maier, B. (2012). Bermudagrass and seashore paspalum establishment from seed using differing irrigation methods and water qualities. *Agron. J.* 104, 706–714. doi: 10.2134/agronj2011.0390

Serena, M., Schiavon, M., Sallenave, R., and Leinauer, B. (2018). Nitrogen fertilization of warm-season turfgrasses irrigated with saline water from varying irrigation systems. 1. quality, spring green-up and fall colour retention. *J. Agro. Crop Sci.* 204, 252–264. doi: 10.1111/jac.12254

Shahba, M. A., Alshammary, S. F., and Abbas, M. S. (2012). Effects of salinity on seashore paspalum cultivars at different mowing heights. *Crop Sci.* 52, 1358–1370. doi: 10.2135/cropsci2011.06.0337

Shoukat, E., Ahmed, M. Z., Abideen, Z., Azeem, M., Ibrahim, M., Gul, B., et al. (2020). Short and long term salinity induced differences in growth and tissue specific ion regulation of *Phragmites karka*. *Flora* 263, 151550. doi: 10.1016/j.flora.2020.151550

Surber, L., Abdel-Haleem, H., Martin, J., Hensleigh, P., Cash, D., Bowman, J., et al. (2011). Mapping quantitative trait loci controlling variation in forage quality traits in barley. *Mol. Breed.* 28, 189–200. doi: 10.1007/s11032-010-9473-6

Tlili, A., Ghanmi, E., Ayeb, N., Louhaichi, M., Neffati, M., and Tarhouni, M. (2020). Revegetation of marginal saline rangelands of southern Tunisia using pastoral halophytes. *Afr. J. Range For. Sci.* 37, 151–157. doi: 10.2989/10220119.2020.1720293

Tran, T. V., Fukai, S., Giles, H. E., and Lambrides, C. J. (2018). Salinity tolerance among a large range of bermudagrasses (*Cynodon* spp.) relative to other halophytic and non-halophytic perennial C_4 grasses. *Environ. Exp. Bot.* 145, 121–129. doi: 10.1016/j.envexpbot.2017.10.011

Waldron, B. L., Sagers, J. K., Peel, M. D., Rigby, C. W., Bugbee, B., and Creech, J. E. (2020). Salinity reduces the forage quality of forage kochia: a halophytic chenopodiaceae shrub. *Rangeland Ecol. Manage.* 73, 384–393. doi: 10.1016/j.rama.2019.12.005

Wang, M. L., Chen, Z. B., Barkley, N. A., Newman, M. L., Kim, W., Raymer, P., et al. (2006). Characterization of seashore paspalum (*paspalum vaginatum* swartz) germplasm by transferred SSRs from wheat, maize and sorghum. *Genet. Resour. Crop Ev.* 53, 779–791. doi: 10.1007/s10722-004-5540-3

Wu, P., Cogill, S., Qiu, Y., Li, Z., Zhou, M., Hu, Q., et al. (2020). Comparative transcriptome profiling provides insights into plant salt tolerance in seashore paspalum (*Paspalum vaginatum*). *BMC Genomics* 21, 131. doi: 10.1186/s12864-020-6508-1

Wu, X., Shi, H., and Guo, Z. (2018). Overexpression of a *NF-YC* gene results in enhanced drought and salt tolerance in transgenic seashore paspalum. *Front. Plant Sci.* 9(1355). doi: 10.3389/fpls.2018.01355

Xie, J., Kong, X., Chen, J., Hu, B., Wen, P., Zhuang, J., et al. (2011). Mapping of quantitative trait loci for fiber and lignin contents from an interspecific cross oryza sativa × oryza rufipogon. *J. Zhejiang Univ. Sci. B* 12, 518–526. doi: 10.1631/jzus.B1000299

Yang, Z., Li, J.-L., Liu, L.-N., Xie, Q., and Sui, N. (2020). Photosynthetic regulation under salt stress and salt-tolerance mechanism of sweet sorghum. *Front. Plant Sci.* 10 (1722). doi: 10.3389/fpls.2019.01722

Yin, J., Jia, J., Lian, Z., Hu, Y., Guo, J., Huo, H., et al. (2019). Silicon enhances the salt tolerance of cucumber through increasing polyamine accumulation and decreasing oxidative damage. *Ecotox. Environ. Safe* 169, 8–17. doi: 10.1016/j.ecoenv.2018.10.105

Yuan, X., He, P., Zhu, Q., and Li, X. (2019). Adversarial examples: attacks and defenses for deep learning. *IEEE Trans. Neural Netw. Learn. Syst.* 30, 2805–2824. doi: 10.1109/TNNLS.2018.2886017

Zhang, Z., Liu, H., Liu, X., Chen, Y., Lu, Y., Shen, M., et al. (2022). Organic fertilizer enhances rice growth in severe saline–alkali soil by increasing soil bacterial diversity. *Soil Use Manage.* 38, 964–977. doi: 10.1111/sum.12711

frontiers | Frontiers in Plant Science

TYPE Original Research
PUBLISHED 09 November 2022
DOI 10.3389/fpls.2022.1010492

OPEN ACCESS

EDITED BY
Alessandra Boccaccini,
Universitàdi Tor
Vergata, Italy

REVIEWED BY
Prashant Mohan-Anupama Pawar,
Regional Centre for Biotechnology
(RCB), India
Birgit Classen,
University of Kiel, Germany

*CORRESPONDENCE
Toshihisa Kotake
kotake@mail.saitama-u.ac.jp

SPECIALTY SECTION
This article was submitted to
Plant Physiology,
a section of the journal
Frontiers in Plant Science

RECEIVED 03 August 2022
ACCEPTED 21 October 2022
PUBLISHED 09 November 2022

CITATION
Kikuchi A, Hara K, Yoshimi Y, Soga K, Takahashi D and Kotake T (2022) *In vivo* structural modification of type II arabinogalactans with fungal endo-β-1, 6-galactanase in Arabidopsis. *Front. Plant Sci.* 13:1010492. doi: 10.3389/fpls.2022.1010492

In vivo structural modification of type II arabinogalactans with fungal endo-β-1, 6-galactanase in Arabidopsis

Aina Kikuchi[1], Katsuya Hara[1], Yoshihisa Yoshimi[1,2], Kouichi Soga[3], Daisuke Takahashi[1] and Toshihisa Kotake[1,4]*

[1]Division of Life Science, Graduate School of Science and Engineering, Saitama University, Saitama, Japan, [2]Department of Biochemistry, University of Cambridge, Cambridge, United Kingdom, [3]Department of Biology, Graduate School of Science, Osaka Metropolitan University, Osaka, Japan, [4]Green Bioscience Research Center, Saitama University, Saitama, Japan

Arabinogalactan-proteins (AGPs) are mysterious extracellular glycoproteins in plants. Although AGPs are highly conserved, their molecular functions remain obscure. The physiological importance of AGPs has been extensively demonstrated with β-Yariv reagent, which specifically binds to AGPs and upon introduction into cells, causes various deleterious effects including growth inhibition and programmed cell death. However, structural features of AGPs that determine their functions have not been identified with β-Yariv reagent. It is known that AGPs are decorated with large type II arabinogalactans (AGs), which are necessary for their functions. Type II AGs consist of a β-1,3-galactan main chain and β-1,6-galactan side chains with auxiliary sugar residues such as L-arabinose and 4-*O*-methyl-glucuronic acid. While most side chains are short, long side chains such as β-1,6-galactohexaose (β-1,6-Gal_6) also exist in type II AGs. To gain insight into the structures important for AGP functions, *in vivo* structural modification of β-1,6-galactan side chains was performed in Arabidopsis. We generated transgenic Arabidopsis plants expressing a fungal endo-β-1,6-galactanase, Tv6GAL, that degrades long side chains specifically under the control of dexamethasone (Dex). Two of 6 transgenic lines obtained showed more than 40 times activity of endo-β-1,6-galactanase when treated with Dex. Structural analysis indicated that long side chains such as β-1,6-Gal_5 and β-1,6-Gal_6 were significantly reduced compared to wild-type plants. Tv6GAL induction caused retarded growth of seedlings, which had a reduced amount of cellulose in cell walls. These results suggest that long β-1,6-galactan side chains are necessary for normal cellulose synthesis and/or deposition as their defect affects cell growth in plants.

KEYWORDS

cellulose synthesis, cell wall, endo-β-1,6-galactanase, *in vivo* modification, type II arabinogalactan

Introduction

Plant cell walls are composed of various polysaccharides including cellulose, pectic polysaccharides, and hemicelluloses (Mohnen, 2008). Among them, type II arabinogalactan (AG) is one of the most complex polysaccharides present in the cell wall and on the plasma membrane (Seifert and Roberts, 2007). Because of its complex and heterogenous carbohydrate structure, molecular functions of type II AGs are unclear and remain to be elucidated.

Type II AGs are generally found as carbohydrate moieties of arabinogalactan-proteins (AGPs) that are conserved extracellular glycoproteins in plants (Fincher et al., 1983; Seifert and Roberts, 2007; Ma et al., 2018). Type II AGs are necessary for AGP functions. For example, a non-classical type of AGP, called xylogen, loses its activity to induce the differentiation of tracheary elements in zinnia (*Zinnia elegans*) cells by chemical deglycosylation (Motose et al., 2004). Generally, the basic structure of type II AG is β-1,3:1,6-galactan, in which β-1,6-galactan side chains are attached onto a β-1,3-galactan main chain (Figure 1). The β-1,6-galactan side chains are further decorated with L-arabinose (Ara) and other auxiliary sugars such as glucuronic acid (GlcA), 4-*O*-methyl-GlcA (MeGlcA), L-fucose (Fuc), and L-rhamnose (Rha). (Tan et al., 2010; Tryfona et al., 2010; Tryfona et al., 2012; Shimoda et al., 2014; Inaba et al., 2015). Although the structure of type II AG, in particular auxiliary sugars, is diverse, depending on plant species, tissues, and developmental stages, several common features can be found in the β-1,3:1,6-galactan (Tsumuraya et al., 1987; Tsumuraya et al., 1988). First, the substitution ratio of β-1,3-galactan with β-1,6-galactosyl side chains in type II AGs ranges from 46 to 58% in many angiosperms (Ito et al., 2020). Second, β-1,6-galactose (β-1,6-Gal) is the dominant side chain, but long side chains such as β-1,6-galactohexaose (β-1,6-Gal_6) also occur as minor side chains in type II AGs (Ito et al., 2020).

The physiological importance of AGPs has been extensively demonstrated with β-Yariv reagent that specifically binds to the β-1,3-galactan main chain of type II AG (Yariv et al., 1967a; Yariv et al., 1967b; Seifert and Roberts, 2007; Kitazawa et al., 2013). For example, the treatment with β-Yariv reagent results in disorganization and depolymerization of cortical microtubules, probably the reason for cell bulging in tobacco suspension-cultured cells (Sardar et al., 2006). However, since the binding is to β-1,3-galactan main chains irrespective of other carbohydrate structures (Kitazawa et al., 2013), it is not obvious how to identify other important carbohydrate structures through studies with β-Yariv reagent. Moreover, β-Yariv reagent may cause secondary and side effects by forming insoluble precipitates with AGPs (Olmos et al., 2017).

The carbohydrate structure of type II AG is primarily determined during its synthesis. In Arabidopsis, many glycosyltransferases (GTs) involved in the synthesis of type II AG have been identified (Silva et al., 2020). Among them, GALT29A (At1g08280) is presumed to have a function in the attachment of β-1,6-galactosyl residues onto the β-1,3-galactan main chain in Arabidopsis (Dilokpimol et al., 2014). However, the expected structural changes in β-1,6-galactan side chains in

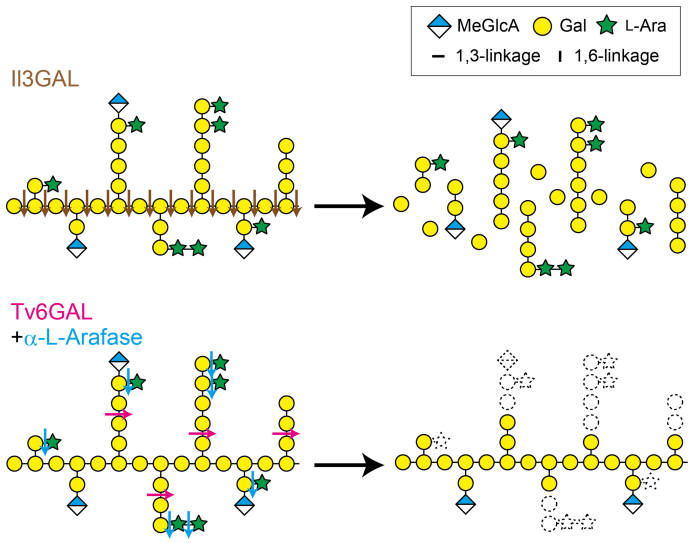

FIGURE 1
Il3GAL and Tv6GAL act differently on type II AG. Il3GAL specifically hydrolyzes the β-1,3-galactan main chain irrespective of the presence of β-1,6-galactan side chains. As a result of the action of Il3GAL, type II AG is degraded into oligosaccharides. Tv6GAL specifically hydrolyzes long β-1,6-galactan side chains of type II AG longer than β-1,6-Gal_2, leaving only short side chains.

type II AGs have not been observed in the loss-of-function mutant.

The carbohydrate structures are also changed through enzymatic degradation. Type II AGs undergo hydrolysis by endogenous glycoside hydrolases (GHs). Plant cells secret β-galactosidase, α-L-arabinofuranosidase (α-L-Arafase), β-L-arabinopyranosidase, and β-glucuronidase (β-GlcAase) to hydrolyze type II AGs (Kotake et al., 2005; Kotake et al., 2006; Eudes et al., 2008; Imaizumi et al., 2017). Because these plant GHs act only on non-reducing terminal residues, they do not drastically change type II AG structures. On the other hand, GHs secreted by fungi and bacteria hydrolyze type II AGs more efficiently than plant GHs. An exo-β-1,3-galactanase from *Irpex lacteus*, Il3GAL, hydrolyzes the β-1,3-galactan main chain bypassing β-1,6-galactan side chains, causing the degradation of type II AGs into oligosaccharides (Tsumuraya et al., 1990; Ichinose et al., 2005; Kotake et al., 2009; Matsuyama et al., 2020). An endo-β-1,6-galactanase from *Trichoderma viride* (*Hypocrea rufa*), Tv6GAL, specifically hydrolyzes β-1,6-galactan side chains in an endo-manner (Figure 1). The enzyme can specifically remove long β-1,6-galactan side chains from β-1,3:1,6-galactan, leaving only stubs of short side chains such as β-1,6-Gal on the main chain (Okemoto et al., 2003; Kotake et al., 2004) (Figure 1). Thus, these specific fungal GHs are reliable tools for structural and functional analysis of type II AGs (Kitazawa et al., 2013; Yoshimi et al., 2020).

We have recently developed a novel system to study type II AGs in Arabidopsis, in which type II AGs are specifically hydrolyzed into oligosaccharides by an exo-β-1,3-galactanase, Il3GAL, *in vivo* (Yoshimi et al., 2020). In *Dex::Il3GAL* plants, we have observed severe tissue disorganization caused by expression of the *Il3GAL* gene in hypocotyls and cotyledons, demonstrating the importance of type II AGs in the regulation of cell shape. On the other hand, we could not examine the importance of β-1,6-galactan side chains in type II AGs, as Il3GAL hydrolyzed type II AGs into oligosaccharides in this system. For the present study, we thus developed another system in which long β-1,6-galactan side chains are trimmed by the fungal endo-β-1,6-galactanase Tv6GAL in Arabidopsis. In the transgenic Arabidopsis, we observed high endo-β-1,6-galactanase activity and a significant decrease in long β-1,6-galactan side chains. Based on the retarded growth phenotype and changes in cell wall fractions of the transgenic plants, we discuss the physiological importance and involvement of long β-1,6-galactan side chains in cellulose synthesis and deposition.

Materials and methods

Transgenic Arabidopsis

Arabidopsis (*Arabidopsis thaliana*) ecotype Col-0 was used in this study. To generate transgenic Arabidopsis expressing *Tv6GAL* under the control of Dex, the Dex-inducible expression system with a binary vector, the pTA7001 plasmid, was used (Aoyama and Chua, 1997). The cDNA of *Tv6GAL* without signal sequence was amplified by PCR with specific primers Tv6GAL-F+BamHI and Tv6GAL-R+XbaI and cloned into pGEM-T-Easy vector (Promega) (Supplementary Table S1). For the generation of point-mutated Tv6GAL (Tv6GAL-PM), the mutation E210A replacing a putative catalytic residue Glu with Ala was introduced by PCR with a set of specific primers (Supplementary Figure S1; Supplementary Table S1). This residue is conserved for GH30 family enzymes including Tv6GAL. *Tv6GAL* and *Tv6GAL-PM* fragments were fused with a signal sequence of Arabidopsis *AGP4* amplified with AGP4signal+XhoI and AGP4signal-R+BamHI on pTA7001 (Supplementary Table S1) (Aoyama and Chua, 1997; Yoshimi et al., 2020). To generate *Dex::Tv6GAL* and *Dex::Tv6GAL-PM* plants, the plasmid constructs were introduced into Arabidopsis by Agrobacterium (*Rhizobium radiobacter*) mediated transformation (Clough and Bent, 1998). *Dex::Il3GAL* plants have been generated in our previous study (Yoshimi et al., 2020).

Plants were grown on Murashige-Skoog (MS)-agar media (Murashige and Skoog, 1962) in the presence of 10 μM Dex dissolved in DMSO. As the negative control for the treatment, the plants were treated with an equal amount of pure DMSO. For the assay of endo-β-1,6-galactanase activity of transgenic plants, the seeds were first incubated in the dark at 4°C for 2 days and grown under continuous light at 23°C for 2 weeks, whereas for the measurement of hypocotyl length, they were grown in the dark at 23°C for 5 days. Hypocotyl length was measured using ImageJ software.

Preparation of recombinant Tv6GAL protein

Tv6GAL and *Tv6GAL-PM* fragments without signal sequence were amplified by PCR and subcloned into the restriction sites EcoRI and XbaI of pPICZαC plasmid (Invitrogen, Waltham, MA, USA) as described previously (Takata et al., 2010). The methylotrophic yeast *Pichia pastoris* strain KM71 (Invitrogen) was then transformed by electroporation with the pPICZαC plasmids. The transformed *Pichia* yeasts were cultured in YPG medium containing 1% (w/v) yeast extract, 2% (w/v) peptone, and 1% (w/v) glycerol at 28°C with shaking at 90 rpm for 48 h. The cells were collected by centrifugation at 1,500 *g* for 5 min, washed with ice-cold water, and suspended in 50 ml of YP medium containing 1% (w/v) yeast extract and 2% (w/v) peptone. To induce the expression of recombinant Tv6GAL (rTv6GAL) or recombinant Tv6GAL-PM (rTv6GAL-PM), the yeast was cultured for another 4 days with addition of 1% (v/v) methanol each day. The rTv6GAL and rTv6GAL-PM proteins were collected in the supernatant of the culture medium by centrifugation at 1,500 *g* for 5 min and purified on a SP-Toyopearl HF 40F column (Tosoh, Tokyo, Japan) as described

previously (Takata et al., 2010). The purity of the recombinant enzymes was confirmed by SDS–PAGE (Laemmli, 1970).

Measurement of the mechanical properties of hypocotyls

Seedlings grown in the dark for 5 days were boiled for 10 min in 80% (v/v) ethanol and then stored in fresh 80% ethanol until analysis. Before measuring the mechanical properties of cell walls, seedlings fixed in 80% ethanol were rehydrated with several changes of water. The cell wall extensibility and the breaking load of the middle region of hypocotyls were measured using a tensile tester (Tensilon STB-1225S; A&D Co. Ltd., Tokyo, Japan). Hypocotyls were fixed between two clamps (distance between clamps was 1 mm) and stretched by raising the upper clamp at a speed of 20 mm/min until the hypocotyls broke. The cell wall extensibility (strain/load in units of μm/g) was determined by measuring the load's rate of increase from 1 to 2 g.

Determination of endo-β-1,6-galactanase activity

Endo-β-1,6-galactanase activity of rTv6GAL and rTv6GAL-PM was measured with a reaction mixture containing 0.5 mg/mL of algal β-1,6-galactan prepared from *Prototheca zopfii* that has long β-1,6-galactans together with short β-1,3-galactans (Okemoto et al., 2003), 50 mM sodium acetate buffer (pH 5.0) and enzyme at 37°C. The reducing sugars were measured colourimetrically by the Neocuproine method (Dygert et al., 1965). One unit of enzyme activity is capable of producing sugars equivalent to one μmol of glucose (Glc) from the substrate per minute.

To measure the activity of *Dex::Tv6GAL* and *Dex::Tv6GAL-PM* plants, the seedlings grown in the presence of 10 μM Dex were homogenized in 20 mM sodium acetate buffer (pH 5.0) containing 1 M NaCl with mortar and pestle. The homogenate was centrifuged at 10,000 *g*, and the resulting supernatant was collected and used as enzyme solution. The protein concentration was determined by the method of Bradford with bovine serum albumin as the standard (Bradford, 1976).

Measurement of cellulose content

The cellulose content of transgenic Arabidopsis was determined by using modified Updegraff method (Foster et al., 2010; Dampanaboina et al., 2021). The seedlings of transgenic Arabidopsis grown with 10 μM Dex under continuous light for 10 days were homogenized and treated with 50 mM Tris-HCl (pH 8.8), 0.5 mM ethylenediaminetetraacetic acid (EDTA), and 10% (w/v) SDS at 25°C. After washing by centrifugation with same buffer once and water twice, the precipitate was suspended in 70% (v/v) ethanol and heated at 70°C for 1 h. The precipitate was further washed with 70% (v/v) ethanol once, methanol once, and methanol/chloroform (1:1, v/v) once and divided into two fractions for the determination of total polysaccharides and cellulose. The fraction for cellulose was washed with acetone once and dried up. The polysaccharides other than cellulose in this fraction was hydrolyzed by the Updegraff reagent (73% (v/v) acetic acid and 9% (v/v) nitric acid) at 100°C for 30 min and removed. The remaining cellulose was washed with water twice, ethanol once, and diethyl ether once and dried up. These fractions were hydrolyzed with 72% (v/v) sulfuric acid at 25°C for 1 h and then 8% (v/v) sulfuric acid at 100°C for 4 h. The sugar amount of the fractions was measured by the phenol-sulfuric acid method (Dubois et al., 1956). The proportion of non-cellulosic polysaccharides and cellulose was calculated.

Structural analysis of type II AGs

Structural analysis by specific fragmentation with enzymes was performed as described (Ito et al., 2020). Type II AGs in the soluble fraction were dialyzed to remove mono- and oligosaccharides and hydrolyzed into Gal, L-Ara, MeGlcA, and β-1,6-galactooligosaccharides with exo-β-1,3-galactanase Il3GAL, endo-β-1,3-galactanase from *Flammulina velutipes*, β-GlcAase from *Aspergillus niger*, and α-L-Arafase from *Aspergillus niger* (Megazyme, Wicklow, Ireland) at 37°C for three hours (Supplementary Figure S2) (Konishi et al., 2008; Kotake et al., 2009; Yoshimi et al., 2017). The liberated β-1,6-galactooligosaccharides and monosaccharides were derivatized with *p*-aminobenzoic acid ethyl ester (ABEE) (Matsuura and Imaoka, 1988), and detected by an HPLC system as described previously (Ito et al., 2020; Yoshimi et al., 2020). Note that β-1,6-galactooligosaccharides liberated in this reaction respectively have one Gal residue that derives from the β-1,3-galactan main chain.

Results

In vitro modification of β-1,3:1,6-galactan

The endo-β-1,6-galactanase Tv6GAL had been identified and cloned from *T. viride* (*H. rufa*) in our previous study (Okemoto et al., 2003; Kotake et al., 2004). It differs from plant β-galactosidases in that it specifically acts on β-1,6-galactan in an endo-manner. For the present study, this specific action was confirmed *in vitro* using recombinant proteins. The rTv6GAL and rTv6GAL-PM were expressed in *Pichia* yeast and purified (Supplementary Figure S1). These recombinant proteins appeared as two protein bands with

relative molecular masses of 56 and 51 kDa on SDS-PAGE, whereas the calculated molecular weight for mature Tv6GAL is 50,589 (Figure 2A). It is presumed that differential *N*-glycosylation on these recombinant proteins in *Pichia* yeast is responsible for the difference (Gemmill and Trimble, 1999; Kotake et al., 2009; Strasser, 2016). The unmutated rTv6GAL showed strong hydrolytic activity (185 units/mg protein) on algal β-1,6-galactan used as substrate, but rTv6GAL-PM had extremely low activity (less than 1 unit/mg protein) (Figure 2B).

It has been shown that the removal of Ara residues remarkably enhances the hydrolysis of type II AG by Tv6GAL (Tsumuraya et al., 1988; Kotake et al., 2004). Here, we examined the hydrolysis of radish root AGP (Tsumuraya et al., 1988) by rTv6GAL alone, and by rTv6GAL combined with α-L-Arafase. The enzymatically modified AGPs were purified by size-exclusion chromatography to remove released mono- and oligosaccharides. Then, the product AGPs were subjected to structural analysis focusing on the length of β-1,6-galactan side chains. In this analysis, the type II AG was specifically hydrolyzed into β-1,6-galactooligosaccharides by combinational hydrolysis with Il3GAL, endo-β-1,3-galactanase (NcEn3GAL), β-GlcAase, and an α-L-Arafase (Konishi et al., 2008; Kotake et al., 2009; Kotake et al., 2011; Ito et al., 2020) (Supplementary Figure S2). The oligosaccharides were labeled with fluorescence and analyzed on HPLC. As shown in Figure 2C, the type II AG completely lost side chains longer than β-1,6-Gal_3 by combinational hydrolysis of rTv6GAL and α-L-Arafase: note that a β-1,6-Gal_3 side chain is detected as β-1,6-Gal_4 in this analysis as all oligosaccharides detected here have one Gal residue derived from the β-1,3-galactan main chain (Supplementary Figure S2). On the other hand, rTv6GAL alone did not efficiently act on β-1,6-galactan side chains. These results suggest that Tv6GAL can hydrolyze long β-1,6-galactan side chains of type II AG in combination with endogenous α-L-Arafase *in vivo*.

Transgenic Arabidopsis expressing fungal endo-β-1,6-galactanase

We generated transgenic Arabidopsis, *Dex::Tv6GAL* plants that express the *Tv6GAL* gene under the control of Dex-inducible promoter. For proper secretion of Tv6GAL, the original signal peptide of Tv6GAL was replaced with that from Arabidopsis AGP4 (AtAGP4) as had been done for *Dex::Il3GAL* plants (Yoshimi et al., 2020). We obtained six lines (#1, #3, #5, #6, #8, and #12) of *Dex::Tv6GAL* plants and two lines (#1 and #2) of *Dex::Tv6GAL-PM* plants as the negative control. The transgenic plants were grown in the presence of Dex to induce the expression of *Tv6GAL* or *Tv6GAL-PM* gene under continuous light.

To evaluate the transgenic lines, we first measured endo-β-1,6-galactanase activity of transgenic Arabidopsis using algal β-1,6-galactan as the substrate (Okemoto et al., 2003). Out of six lines of *Dex::Tv6GAL* plants, five lines (#3, #5, #6, #8, and #12) showed significantly higher activity (0.38, 3,52, 3,36, 0.95, and 0.82 units/g fresh weight) than wild-type (WT) Arabidopsis (0.08 units/g fresh weight) when treated with Dex (Figure 3). On the other hand, the activity of *Dex::Tv6GAL-PM* plants was comparable to WT plants. This indicates that Tv6GAL is properly synthesized in Arabidopsis and functions as endo-β-1,6-galactanase in this system. *Dex::Tv6GAL* plants #5 and #6 exhibited remarkably higher activity than the others, therefore these lines were mainly used in the following experiments. In line #5, leaky expression of *Tv6GAL* likely occurred without Dex treatment. Weak activity detected in WT plants is presumed to be endogenous β-galactosidase activity, as plant β-galactosidases also hydrolyze this algal β-1,6-galactan (Kotake et al., 2005).

In vivo modification of type II AGs

The main purpose of this study was to investigate the structural changes in β-1,6-galactan side chains of type II AGs *in vivo*. We did not express α-L-Arafase with Tv6GAL, because plants secret type II AG-active α-L-Arafases in cell walls (Kotake et al., 2006). To examine the *in vivo* structural change, type II AGs were extracted from light-grown *Dex::Tv6GAL* plants #5 and #6 and subjected to specific hydrolysis into β-1,6-galactooligosaccharides by a combination of enzymes followed by labeling with fluorescence and HPLC analysis as performed for the analysis of *in vitro* modification of type II AGs. Consistent with other plants such as spinach (*Spinacia oleracea*) and broccoli (*Brassica oleracea* var. italica) examined in a previous study (Ito et al., 2020), short side chains such as β-1,6-Gal and β-1,6-Gal_2 were very dominant over longer side chains including β-1,6-Gal_5 and β-1,6-Gal_6 in WT Arabidopsis (Figure 4A). Compared with WT plants, Dex-treated *Dex::Tv6GAL* plants #5 and #6 had a significantly reduced proportion of long β-1,6-galactan side chains such as β-1,6-Gal_5 and β-1,6-Gal_6 (Figure 4B). Consistent with endo-β-1,6-galactanase activity, Dex treatment did not significantly change β-1,6-galactan side chains in *Dex::Tv6GAL-PM* plants. In this study, β-1,6-galactan side chains longer than 1,6-Gal_7 could not be analyzed due to technical limits, however it is expected that these very long side chains were also hydrolyzed in the lines #5 and #6. Indeed, our previous study has identified β-1,6-Gal_{10} and β-1,6-Gal_{15} in type II AGs (Shimoda et al., 2014; Tsumuraya et al., 2019). Approximately half of the β-1,6-Gal_5 and β-1,6-Gal_6 remained in these lines treated with Dex. This may be caused by differential accumulation of Tv6GAL in the tissues and/or the decoration with other sugar residues that will be explained in the Discussion.

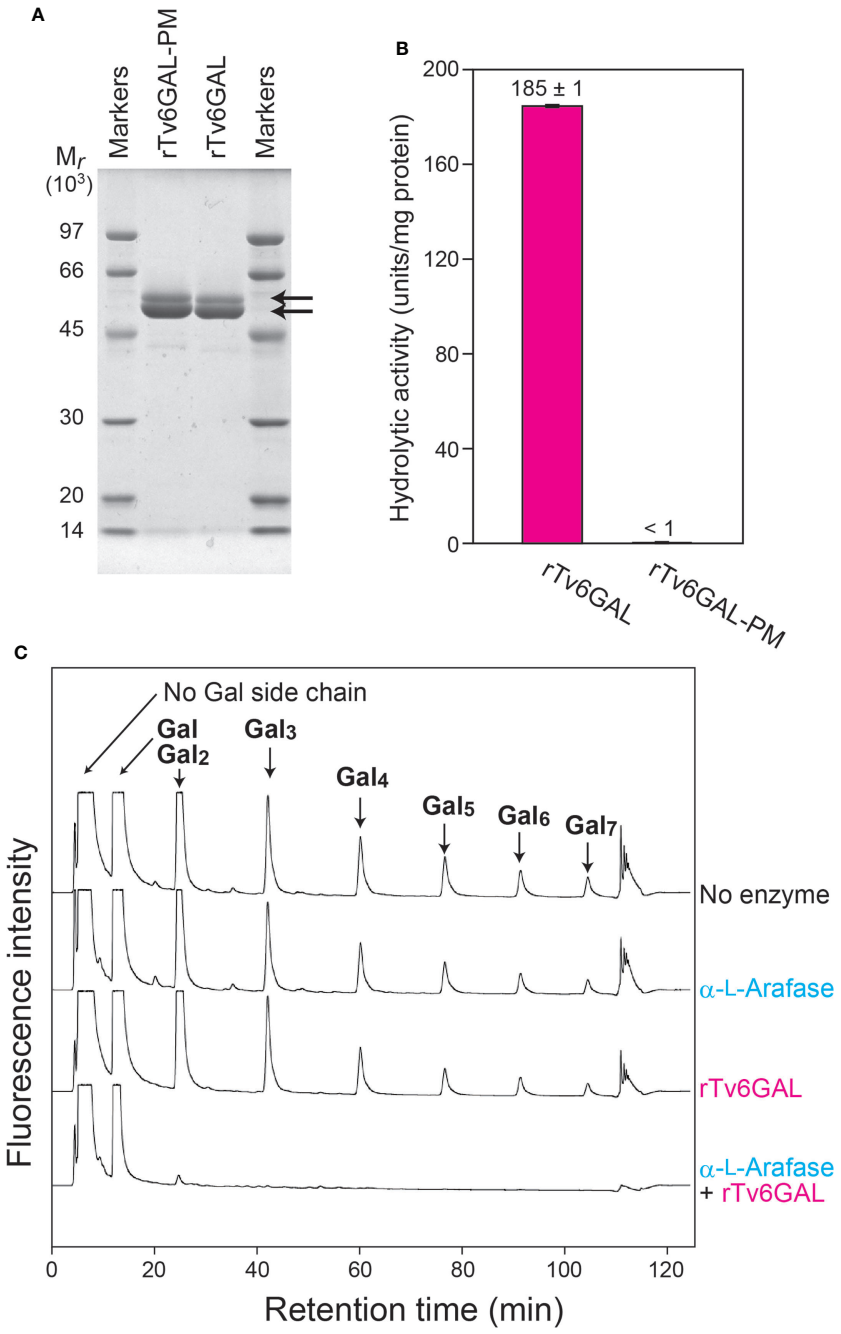

FIGURE 2
In vitro structural modification of β-1,3:1,6-galactan. **(A)** The expression of rTv6GAL and rTv6GAL-PM in *P. pastoris*. The purified rTv6GAL and rTv6GAL-PM were analyzed on SDS-PAGE. Proteins in the gel were stained with Coomassie Brilliant Blue R-250. Arrows indicate rTv6GAL and rTv6GAL-PM. **(B)** Hydrolytic activity of rTv6GAL and rTv6GAL-PM toward algal β-1,6-galactan. **(C)** Change in the length of β-1,6-galactan side chains. β-1,3:1,6-Galactan reacted with rTv6GAL was hydrolyzed into β-1,6-galactooligosaccharides using Il3GAL, NcEn3GAL, AnGlcAase, and α-L-Arafase (Supplementary Figure S2). The resulting mono- and oligosaccharides were derivatized with ABEE and analyzed on HPLC. Note that each β-1,6-galactooligosaccharide has one Gal derived from the β-1,3-galactan main chain. For example, a β-1,6-Gal_2 side chain is detected as 1,6-Gal_3 in this analysis. M_r, relative molecular mass.

10.3389/fpls.2022.1010492

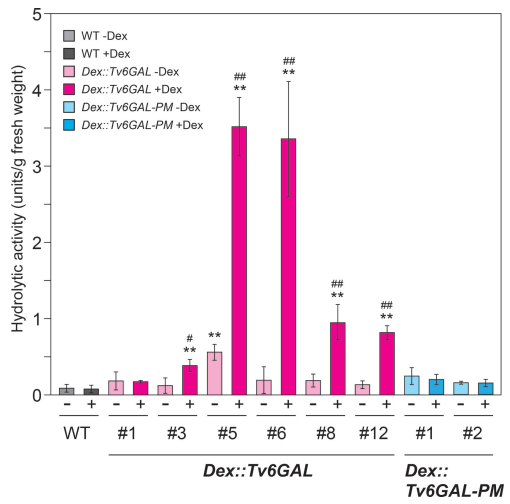

FIGURE 3
Enzymatic activity of *Dex::Tv6GAL* and *Dex::Tv6GAL-PM* plants. Endo-β-1,6-galactanase activity was measured using algal β-1,6-galactan as substrate. Endo-β-1,6-galactanase activity per g fresh weight is shown. Data are mean values with ± SD (n=3 biological replicates). Asterisks indicate differences from WT plants with Dex treatment (Student's *t*-test, **, $P<0.01$) and hash marks indicate significant differences between seedlings with and without Dex treatment (Student's *t*-test, #, $P<0.05$; ##, $P<0.01$).

Retarded growth of *Dex::Tv6GAL* plants

The physiological importance of AGPs in growth and development has been shown in Arabidopsis mutants and by treatment of plants with β-Yariv reagent (Silva et al., 2020; Kaur et al., 2021). In many cases, the perturbation of AGP functions results in reduced growth. In our previous study, *Dex::Il3GAL* Arabidopsis expressing the *Il3GAL* gene exhibited severe tissue disorganization with extremely bulged epidermal cells in light-grown seedlings and growth inhibition in dark-grown hypocotyls, demonstrating the physiological importance of type II AGs (Yoshimi et al., 2020). In this study, the influence of hydrolysis of long β-1,6-galactan side chains by Tv6GAL on the elongation growth of dark-grown hypocotyls was examined. Out of five lines of *Dex::Tv6GAL* plants, four lines (#3, #5, #6, and #12) exhibited significantly shorter hypocotyls (9, 60, 48, and 27% decrease, respectively) under Dex treatment than WT plants (Figure 5A). Consistent with endo-β-1,6-galactanase activity, the growth inhibition was more significant in lines #5 and #6 than in the other lines (Supplementary Figure S3). Growth inhibition was not observed in *Dex::Tv6GAL-PM* plants, although one line not treated with Dex had shorter hypocotyls than WT plants. The phenotypes of light-grown seedlings were also analyzed. Apparent dwarfism was seen in *Dex::Tv6GAL* plants #5 in the presence of Dex, while the growth phenotypes of line #6 were relatively weak compared with line #5 (Figure 5B). In addition, severe phenotypes occurred in *Dex::Il3GAL* plants including epidermal cell bulging and severe tissue disorganization were not observed in *Dex::Tv6GAL* plants.

The mechanical properties of dark-grown hypocotyls were determined by a tensile test. Together with *Dex::Il3GAL* plants #2, *Dex::Tv6GAL* plants #5, #6, and #12 showed significantly higher extensibility and lower breaking load when they were grown in the presence of Dex (Figure 6). On the other hand, *Dex::Tv6GAL-PM* plants #1 and #2 had properties comparable to those of WT plants. The changes in the mechanical properties may be the result of altered cell wall components and structure as well as tissue organization.

Decreased cellulose in *Dex::Tv6GAL* plants

The retarded growth and altered mechanical properties of *Dex::Tv6GAL* plants suggest that the decrease in long β-1,6-galactan side chains in type II AGs affected cell wall synthesis, modification, and/or metabolism. To investigate the influence of Tv6GAL expression on cellulose synthesis and deposition, we measured the cellulose content by the Updegraff method (Foster et al., 2010; Dampanaboina et al., 2021). The lines #5 and #6 of *Dex::Tv6GAL* plants grown in the presence of Dex had lower proportion of cellulose in total polysaccharides (25 and 31%, respectively) than WT (42%), indicating that type II AGs are necessary for proper cellulose synthesis and/or deposition. The changes in the lines #1 of *Dex::Tv6GAL-PM* plants were not observed. The reduced proportion of cellulose in the line #5 of *Dex::Tv6GAL* plants was also confirmed by cell wall fractionation into hot water (HW), EDTA, alkali, and cellulose fractions (Supplementary Figure S4). The line #5 showed a significant decrease in cellulose fraction and an increase in HW and EDTA fractions. Sugar composition analysis revealed that the line #5 had an increased proportion of Glc and a decreased proportion of GalA in HW fraction (Supplementary Table S2-S4). Interestingly, decreased cellulose and increased Glc in other fractions were observed for *Dex::Il3GAL* plants (Supplementary Figure S4), and have also been reported in the Arabidopsis temperature-sensitive *radial swelling 2* (*rsw2*, allelic to *korrigan*) mutant with a defect in cellulose synthesis (Lane et al., 2001).

Discussion

In vivo modification of β-1,6-galactan side chains

Type II AGs are the second most complex carbohydrates after pectin rhamnogalacturonan II in plants, as they have a heterogeneous β-1,3:1,6-galactan backbone, to which Ara, GlcA, MeGlcA, and other auxiliary sugars are attached. Type II AGs are conserved polysaccharides that can generally be found as glycan

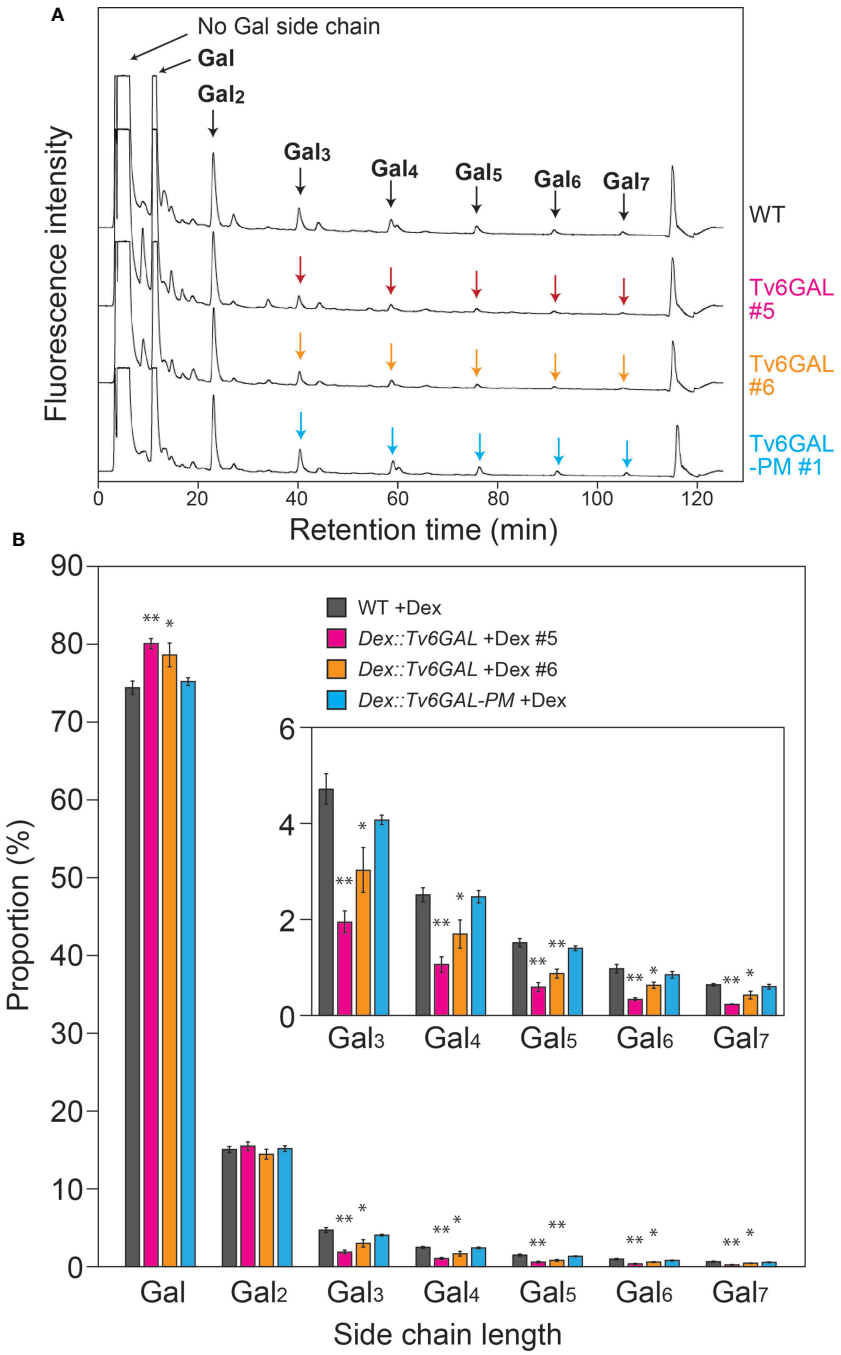

FIGURE 4
In vivo structural modification of type II AGs. **(A)** Representative chromatogram of β-1,6-galactooligosaccharides. Type II AGs were extracted from WT, *Dex::Tv6GAL* #5 and #6, and *Dex::Tv6GAL-PM* #1 plants grown in the presence of Dex and subjected to structural analysis as performed for *in vitro* modification to obtain the distribution of chain lengths of β-1,6-galactooligosaccharides (Supplementary Figure S2). In this chromatogram, β-1,6-galactooligosaccharides larger than β-1,6-Gal_2 were examined. **(B)** Distribution of Gal lengths of β-1,6-galactan side chains. The distribution of β-1,6-galactan side chains was calculated based on the peak areas of β-1,6-galactooligosaccharides. Data are mean values with ± SD (n=3 biological replicates). Asterisks indicate significant differences from WT plants (Student's *t*-test, *, $P<0.05$; **, $P<0.01$).

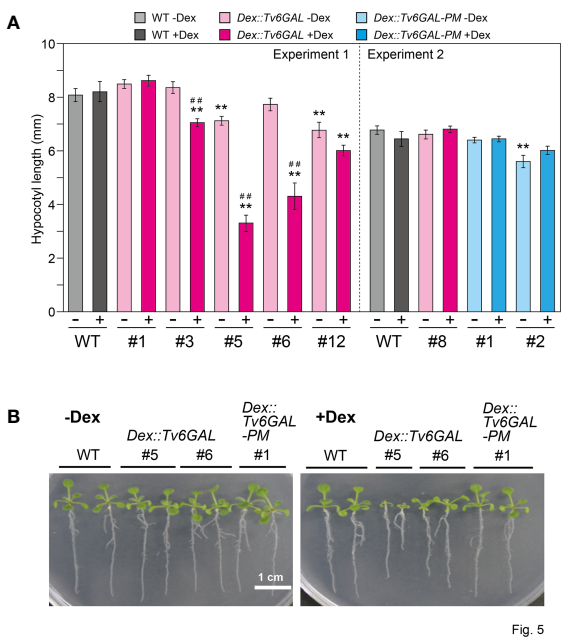

Fig. 5

FIGURE 5
Phenotypes of *Dex::Tv6GAL* plants. **(A)** Length of dark-grown hypocotyls. *Dex::Tv6GAL* and *Dex::Tv6GAL-PM* plants were grown on MS-agar plates with and without 10 μM Dex in the dark at 23°C for 5 days. The data show mean values with ± SD. n = 20. Asterisks indicate significant differences from WT plants (Student's *t*-test, **, $P<0.01$) and hash marks indicate significant differences between seedlings with and without Dex treatment (Student's *t*-test, ##, $P<0.01$). Representative plants are shown in Supplementary Figure S3. **(B)** Light-grown seedlings. The seedlings were grown on MS-agar plates with and without 10 μM Dex under continuous light at 23°C for 2 weeks. Representative plants were selected.

parts of AGPs in plants. Due to their heterogenicity and complexity, the identification of specific structures important for the functions of type II AGs is not easy. GHs acting on specific structures are reliable tools in the study of complex carbohydrates. Here we used a fungal endo-β-1,6-galactanase Tv6GAL to change β-1,6-galactan *in vivo* and observed a significant reduction of long β-1,6-galactan side chains in two lines of *Dex::Tv6GAL* plants for the first time (Figure 4). In these transgenic plants, the long side chains are presumably changed to short side chains such as β-1,6-Gal and β-1,6-Gal_2 by Tv6GAL. On the other hand, this *in vivo* hydrolysis of type II AGs was far from complete compared with *in vitro* modification of β-1,3:1,6-galactan. We suggest several possible reasons. First, there may be β-1,6-galactan side chains highly substituted with Ara residues that are resistant to Tv6GAL (Shimoda et al., 2014), although plants have high endogenous α-L-Arafase activity (Kotake et al., 2006). Tv6GAL requires removal of α-L-arabinofuranosyl residues for efficient hydrolysis of type II AGs (Kotake et al., 2004) (Figure 2). The presence of β-1,6-galactan highly substituted with Ara residues should be examined by using specific antibodies such as KM1 in a future study (Pfeifer et al., 2022). Second, not all tissues may have expressed the *Tv6GAL* gene at a high level because, for the expression of *Tv6GAL*, not only permeation by Dex but also accumulation in the same cell of the glucocorticoid receptor-fused transcription activation domain, which is transcribed from the transgene, is necessary. It is quite probable that the accumulation of Tv6GAL differed by tissues and developmental stages. Third, β-1,6-galactan side chains of type II AGs might be masked by the interaction with other cell wall components *in vivo*.

Functions of type II AGs in cellulose synthesis

For the functional analysis of type II AGs, Arabidopsis mutants with a defect in the synthesis of type II AGs are useful. The synthesis of type II AGs starts with Gal transfer from UDP-Gal onto hydroxyproline by the action of HPGT-GALT proteins. Then the chain elongation of the β-1,3-galactan main chain by β-1,3-galactosyltransferases, called CAGEs, occurs (Basu et al., 2013; Ogawa-Ohnishi and Matsubayashi, 2015; Nibbering et al., 2022). Importantly, an Arabidopsis *cage1 cage2* double mutant has been shown to have a significantly reduced amount of crystalline cellulose in shortened dark-grown hypocotyls (Nibbering et al., 2022). Because the protein levels of cellulose synthase catalytic subunits, CesAs, were significantly reduced in the double mutant while their expression levels were not changed, type II AGs are presumed to regulate CesAs by a post-transcriptional or post-translational mechanism. In addition, an Arabidopsis quintuple mutant of HPGT-GALTs also showed stunted growth and root swelling, which reminds us of the phenotypes of cellulose-deficient Arabidopsis mutants such as *cobra* and *korrigan* (Kaur et al., 2021). In the present study, the significantly reduced amount of cellulose fraction observed for *Dex::Tv6GAL*, as well as *Dex::Il3GAL* plants (Figure 7), suggests the participation of long β-1,6-galactan side chains in cellulose synthesis and/or deposition.

A recent study on Arabidopsis fasciclin-like AGP 11 (FLA11) and FLA12 has proposed that they perform a sensing function in the regulation of secondary cell wall synthesis in response to mechanical stress (Ma et al., 2022). In contrast with the studies on the *cage1 cage2* double mutant, the over-expression of the *FLA11* gene greatly affected the expression of CesA genes. Supporting the suggestion of a regulatory function of FLAs at the expression level, a drastic decrease in the expression level of the *CesA8* gene has also been observed in the Arabidopsis *fla16* mutant (Liu et al., 2020). Thus, molecular functions of AGPs in cellulose synthesis are still elusive, but it is highly probable that type II AGs including long β-1,6-galactan side chains have molecular functions different from those of core-protein domains such as the fasciclin-like domain.

No severe tissue disorganization was observed in *Dex::Tv6GAL* plants (Figure 5), which contrasts with *Dex::Il3GAL* plants (Yoshimi

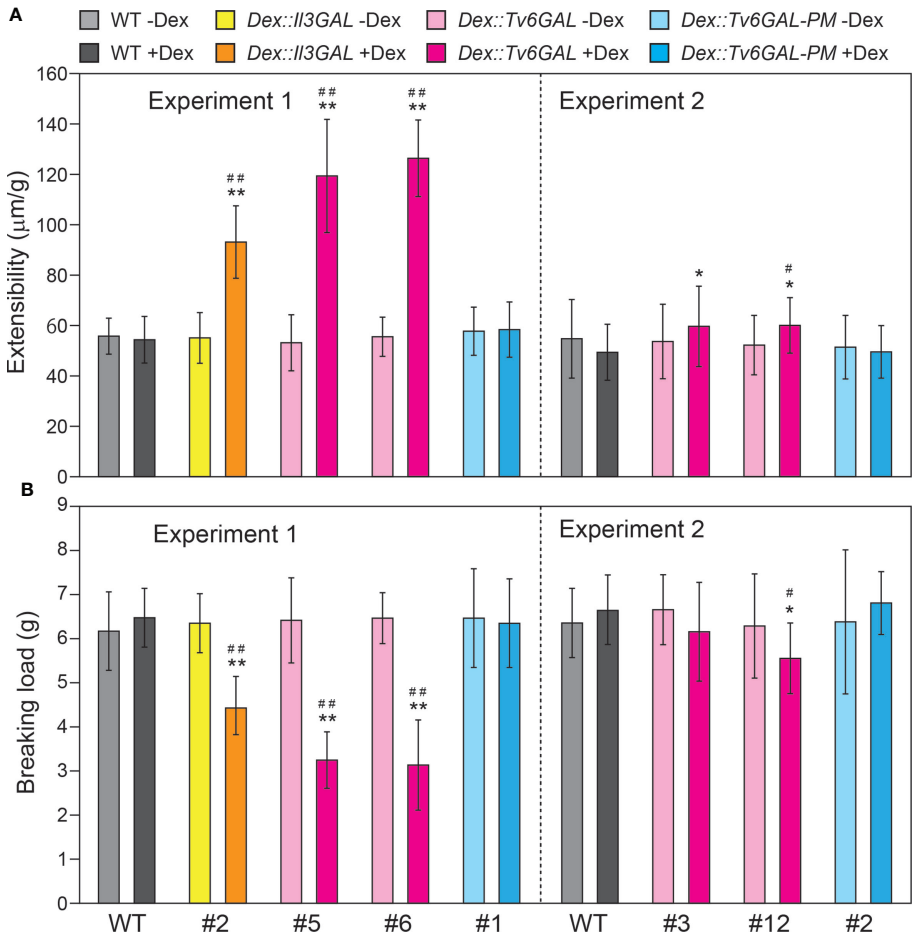

FIGURE 6
Mechanical properties of *Dex::Tv6GAL* plants. **(A)** Extensibility of hypocotyls. **(B)** Breaking load. The plants were grown on MS-agar plates with and without 10 μM Dex in the dark at 23°C for 5 days. The mechanical properties of the middle region of hypocotyls were measured by a tensile test. The data show mean values with ± SD, n = 20. Asterisks indicate significant differences from WT plants (Student's *t*-test, *, $P<0.05$; **, $P<0.01$) and hash marks indicate significant differences between plants with and without Dex treatment (Student's *t*-test, #, $P<0.05$; ##, $P<0.01$).

et al., 2020). In addition, the growth phenotypes of light-grown seedlings were weaker than those of *Dex::Il3GAL* plants. At this moment, we do not have a clear explanation for these differences. Given that Tv6GAL caused reduced function of long β-1,6-galactan side chains while Il3GAL perturbed the functions of type II AGs by releasing various β-1,6-galactan side chains from type II AG, severe tissue disorganization may occur only by the perturbation of type II AG functions. The phenotypes of these plants will be further analyzed in a future study.

Important carbohydrate structures for functions of type II AGs

For different physiological functions, different carbohydrate structures of type II AGs are required, although type II AGs are relatively minor components in cell walls. Indeed, GlcA and MeGlcA residues have been shown to be important for the Ca^{2+} capacitor function of AGPs through a study on Arabidopsis mutants defective in β-glucuronidation of type II AGs (Lopez-Hernandez et al., 2020). In Torenia (*Torenia fournieri*), MeGlcA-Gal was identified as an important structure for the signaling function of type II AGs in pollen tube guidance (Mizukami et al., 2016). This structure, called AMOR, makes pollen tubes responsive to the attractant peptide LURE. Interestingly, the methyl group of MeGlcA is indispensable for the function of AMOR. In the present study, we have identified long β-1,6-galactan side chains as important structures for the participation in cellulose synthesis or deposition. Through this function, long β-1,6-galactan side chains are presumed to affect cell elongation.

Our previous study has shown that the proportion of β-1,6-galactan side chains with a given Gal length is probably conserved in angiosperm. Consistent with five other plant species examined in that study (Ito et al., 2020), here the proportions of β-1,6-Gal_5

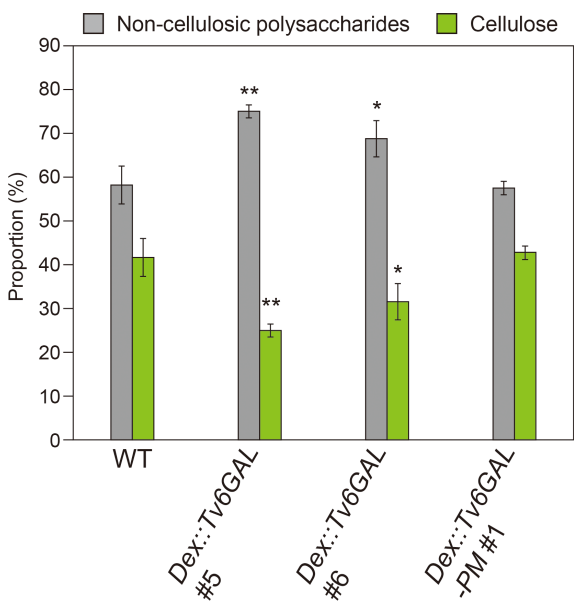

FIGURE 7
Proportion of cell wall fractions. Plants were grown on MS-agar media containing 10 μM Dex under continuous light for 10 days. Using the Updegraff method, the proportion of non-cellulosic polysaccharides and cellulose was determined. Data are mean values with ± SD (n = 3 biological replicates). Asterisks indicate significant differences from WT plants (Stud's *t*-test, *, $P<0.05$; **, $P<0.01$).

and β-1,6-Gal_6 were less than 2% each in Arabidopsis seedlings. These observations suggest that the long stretches of β-1,6-galactan occurring as minor side chains are conserved beyond plant species and physiologically important. Side chains much longer than β-1,6-Gal_7 likely exist in Arabidopsis. However, they must be very rare structures, as Gal and β-1,6-Gal_2 side chains did not largely increase when these very long side chains were converted to short side chains by Tv6GAL in *Dex::Tv6GAL* plants. However, we cannot exclude the possibility that the important β-1,6-galactan side chains are those that are much longer than β-1,6-Gal_5 and β-1,6-Gal_6. We note in this context that larch AG and gum arabic that lacks long side chains will not participate in cellulose synthesis.

Conclusion

In the present study, *in vivo* structural modification of long β-1,6-galactan side chains of type II AGs was performed for the first time. The phenotypes of transgenic plants expressing an endo-β-1,6-galactanase Tv6GAL suggested the importance of long β-1,6-galactan side chains and the involvement of type II AGs in cellulose synthesis or deposition. The present study also suggests that different carbohydrate structures are required for different physiological functions of type II AGs.

Data availability statement

The original contributions presented in the study are included in the article/Supplementary Material. Further inquiries can be directed to the corresponding author.

Author contributions

YY and TK designed the research. AK, KH, YY, KS, and TK performed the experiments and data collection. AK, KH, KS, DT, and TK analyzed the data. YY, KS, DT, and TK wrote the manuscript. All authors approved the final version of manuscript.

Funding

This research was supported by MEXT KAKENHI Grant-in-Aid for Scientific Research on Innovative Areas "Plant-Structure Optimization Strategy" to TK (no. 18H05495), by Grants-in-Aid for Scientific Research to TK (no. 19K06702) and to DT (no. 20K15494), and by a Broodbank Research Fellowship to YY (no. PD16178).

Acknowledgments

We thank Prof. Emeritus Yoichi Tsumuraya for technical advice and valuable discussion. We are also grateful to Mr. Tatsuya Kutsuno and Mr. Keita Higuchi for technical assistance.

Conflict of interest

The authors declare that the research was conducted in the absence of any commercial or financial relationships that could be construed as a potential conflict of interest.

Publisher's note

Supplementary material

The Supplementary Material for this article can be found online at: https://www.frontiersin.org/articles/10.3389/fpls.2022.1010492/full#supplementary-material

References

Aoyama, T., and Chua, N.-H. (1997). A glucocorticoid-mediated transcriptional induction system in transgenic plants. *Plant J.* 11, 605–612. doi: 10.1046/j.1365-313x.1997.11030605.x

Basu, D., Liang, Y., Liu, X., Himmeldirk, K., Faik, A., Kieliszewski, M., et al. (2013). Functional identification of a hydroxyproline-o-galactosyltransferase specific for arabinogalactan protein biosynthesis in arabidopsis. *J. Biol. Chem.* 288, 10132–10143. doi: 10.1074/jbc.M112.432609

Bradford, M. (1976). A rapid and sensitive method for the quantitation of microgram quantities of protein utilizing the principle of protein-dye binding. *Analytical Biochem.* 72, 248–254. doi: 10.1006/abio.1976.9999

Clough, S. J., and Bent, A. F. (1998). Floral dip: A simplified method for agrobacterium-mediated transformation of arabidopsis thaliana. *Plant J.* 16, 735–743. doi: 10.1046/j.1365-313x.1998.00343.x

Dampanaboina, L., Yuan, N., and Mendu, V. (2021). Estimation of crystalline cellulose content of plant biomass using the updegraff method. *J. Vis. Exp.* 171, e62031. doi: 10.3791/62031

Dilokpimol, A., Poulsen, C. P., Vereb, G., Kaneko, S., Schulz, A., and Geshi, N. (2014). Galactosyltransferases from arabidopsis thaliana in the biosynthesis of type II arabinogalactan: molecular interaction enhances enzyme activity. *BMC Plant Biol.* 14, 90. doi: 10.1186/1471-2229-14-90

Dubois, M., Gilles, K. A., Hamilton, J. K., Rebers, P. A., and Smith, F. (1956). Colorimetric method for determination of sugars and related substances. *Analytical Chem.* 82, 383–393. doi: 10.1021/AC60111A017

Dygert, S., Li, L. H., Florida, D., and Thoma, J. A. (1965). Determination of reducing sugar with improved precision. *Analytical Biochem.* 13, 367–374. doi: 10.1016/0003-2697(65)90327-1

Eudes, A., Mouille, G., Thévenin, J., Goyallon, A., Minic, Z., and Jouanin, L. (2008). Urification, cloning and functional characterization of an endogenous β-glucuronidase in arabidopsis thaliana. *Plant Cell Physiol.* 49, 1331–1341. doi: 10.1093/pcp/pcn108

Fincher, G. B., Stone, B. A., and Clarke, A. E. (1983). Arabinogalactan-proteins: structure, biosynthesis, and function. *Annu. Rev. Plant Physiol.* 34, 47–70. doi: 10.1146/ANNUREV.PP.34.060183.000403

Foster, C. F., Martin, T. M., and Pauly, M. (2010). Comprehensive compositional analysis of plant cell walls (Lignocellulosic biomass) part II: Carbohydrates. *J. Vis. Exp.* 37, e1837. doi: 10.3791/1837

Gemmill, T. R., and Trimble, R. B. (1999). Overview of n- and O-linked oligosaccharide structures found in various yeast species. *Biochim. Biophys. Acta (BBA) - Gen. Subj.* 1426, 227–237. doi: 10.1016/S0304-4165(98)00126-3

Ichinose, H., Yoshida, M., Kotake, T., Kuno, A., Igarashi, K., Tsumuraya, Y., et al. (2005). An exo-β-1,3-galactanase having a novel β-1,3-galactan-binding module from phanerochaete chrysosporium. *J. Biol. Chem.* 280, 25820–25829. doi: 10.1074/jbc.M501024200

Imaizumi, C., Tomatsu, H., Kitazawa, K., Yoshimi, Y., Shibano, S., Kikuchi, K., et al. (2017). Heterologous expression and characterization of an Arabidopsis β-l-arabinopyranosidase and α-d-galactosidases acting on β-l-arabinopyranosyl residues. *J. Exp. Bot.* 68, 4651–4661. doi: 10.1093/jxb/erx279

Inaba, M., Maruyama, T., Yoshimi, Y., Kotake, T., Matsuoka, K., Koyama, T., et al. (2015). L-fucose-containing arabinogalactan-protein in radish leaves. *Carbohydr. Res.* 415, 1–11. doi: 10.1016/j.carres.2015.07.002

Ito, K., Fukuoka, K., Nishigaki, N., Hara, K., Yoshimi, Y., Kuki, H., et al. (2020). Structural features conserved in subclass of type II arabinogalactan. *Plant Biotechnol.* 37, 459–463. doi: 10.5511/plantbiotechnology.20.0721a

Kaur, D., Held, M. A., Smith, M. R., and Showalter, A. M. (2021). Functional characterization of hydroxyproline-o-galactosyltransferases for arabidopsis arabinogalactan-protein synthesis. *BMC Plant Biol.* 21, 590. doi: 10.1186/s12870-021-03362-2

Kitazawa, K., Tryfona, T., Yoshimi, Y., Hayashi, Y., Kawauchi, S., Antonov, L., et al. (2013). β-galactosyl yariv reagent binds to the β-1,3-Galactan of arabinogalactan proteins. *Plant Physiol.* 161, 1117–1126. doi: 10.1104/pp.112.211722

Konishi, T., Kotake, T., Soraya, D., Matsuoka, K., Koyama, T., Kaneko, S., et al. (2008). Properties of family 79 β-glucuronidases that hydrolyze β-glucuronosyl and 4-o-methyl-β-glucuronosyl residues of arabinogalactan-protein. *Carbohydr. Res.* 343, 1191–1201. doi: 10.1016/j.carres.2008.03.004

Kotake, T., Dina, S., Konishi, T., Kaneko, S., Igarashi, K., Samejima, M., et al. (2005). Molecular cloning of a β-galactosidase from radish that specifically hydrolyzes β-(1→3)- and β-(1→6)-galactosyl residues of arabinogalactan protein. *Plant Physiol.* 138, 1563–1576. doi: 10.1104/pp.105.062562

Kotake, T., Hirata, N., Degi, Y., Ishiguro, M., Kitazawa, K., Takata, R., et al. (2011). Endo-β-1,3-galactanase from winter mushroom flammulina velutipes. *J. Biol. Chem.* 286, 27848–27854. doi: 10.1074/jbc.M111.251736

Kotake, T., Kaneko, S., Kubomoto, A., Haque, M. A., Kobayashi, H., and Tsumuraya, Y. (2004). Molecular cloning and expression in escherichia coli of a trichoderma viride endo-β-(1→6)-galactanase gene. *Biochem. J.* 377, 749–755. doi: 10.1042/BJ20031145

Kotake, T., Kitazawa, K., Takata, R., Okabe, K., Ichinose, H., Kaneko, S., et al. (2009). Molecular cloning and expression in pichia pastoris of a irpex lacteus exo-β-(1→3)-galactanase gene. *Bioscience Biotechnol. Biochem.* 73, 2303–2309. doi: 10.1271/bbb.90433

Kotake, T., Tsuchiya, K., Aohara, T., Konishi, T., Kaneko, S., Igarashi, K., et al. (2006). An α-L-arabinofuranosidase/β-D-xylosidase from immature seeds of radish (Raphanus sativus l.). *J. Exp. Bot.* 57, 2353–2362. doi: 10.1093/jxb/erj206

Laemmli, U. K. (1970). Cleavage of structural proteins during the assembly of the head of bacteriophage T4. *Nature* 227, 680–685. doi: 10.1038/227680a0

Lane, D. R., Wiedemeir, A., Peng, L., Höfte, H., Vernhettes, S., Desprez, T., et al. (2001). Temperature-sensitive alleles of RSW2 link the KORRIGAN endo-1,4-beta-glucanase to cellulose synthesis and cytokinesis in Arabidopsis. *Plant Physiol.* 123, 278–88. doi: 10.1104/pp.126.1.278

Liu, E., MacMillan, C. P., Shafee, T., Ma, Y., Ratcliffe, J., van de Meene, A., et al. (2020). Fasciclin-like arabinogalactan-protein 16 (FLA16) is required for stem development in arabidopsis. *Front. Plant Sci.* 11. doi: 10.3389/fpls.2020.615392

Lopez-Hernandez, F., Tryfona, T., Rizza, A., Yu, X. L., Harris, M. O. B., Webb, A. A. R., et al. (2020). Calcium binding by arabinogalactan polysaccharides is important for normal plant development. *Plant Cell* 32, 3346–3369. doi: 10.1105/tpc.20.00027

Ma, Y., MacMillan, C. P., de Vries, L., Mansfield, S. D., Hao, P., Ratcliffe, J., et al. (2022). FLA11 and FLA12 glycoproteins fine-tune stem secondary wall properties in response to mechanical stresses. *New Phytol.*, 233, 1750–1767. doi: 10.1111/nph.17898

Matsuura, F., and Imaoka, A. (1988). Chromatographic separation of asparagine-linked oligosaccharides labeled with an ultraviolet-absorbing compound, p-aminobenzoic acid ethyl. *Glycoconjugate J.* 5, 13–26. doi: 10.1007/BF01048328

Matsuyama, K., Kishine, N., Fujimoto, Z., Sunagawa, N., Kotake, T., Tsumuraya, Y., et al. (2020). Unique active-site and subsite features in the arabinogalactan-degrading GH43 exo-β-1,3-galactanase from phanerochaete chrysosporium. *J. Biol. Chem.* 295, 18539–18552. doi: 10.1074/jbc.RA120.016149

Ma, Y., Zeng, W., Bacic, A., and Johnson, K. (2018). AGPs through time and space. *Annu. Plant Rev.* 3, 767–804. doi: 10.1002/9781119312994.apr0608

Mizukami, A. G., Inatsugi, R., Jiao, J., Kotake, T., Kuwata, K., Ootani, K., et al. (2016). The AMOR arabinogalactan sugar chain induces pollen-tube competency to respond to ovular guidance. *Curr. Biol.* 26, 1091–1097. doi: 10.1016/j.cub.2016.02.040

Mohnen, D. (2008). Pectin structure and biosynthesis. *Curr. Opin. Plant Biol.* 11, 266–277. doi: 10.1016/j.pbi.2008.03.006

Motose, H., Sugiyama, M., and Fukuda, H. (2004). A proteoglycan mediates inductive interaction during plant vascular development. *Nature* 429, 873–878. doi: 10.1038/nature02613

Murashige, T., and Skoog, F. (1962). A revised medium for rapid growth and bioassay with tobacco tissue cultures. *Physiol. Plantarum* 15, 473–497. doi: 10.1111/j.1399-3054.1962.tb08052.x

Nibbering, P., Castilleux, R., Wingsle, G., and Niittylä, T. (2022). CAGEs are golgi-localized GT31 enzymes involved in cellulose biosynthesis in arabidopsis. *Plant J.* 110, 1271–1285. doi: 10.1111/tpj.15734

Ogawa-Ohnishi, M., and Matsubayashi, Y. (2015). Identification of three potent hydroxyproline O -galactosyltransferases in arabidopsis. *Plant J.* 81, 736–746. doi: 10.1111/tpj.12764

Okemoto, K., Uekita, T., Tsumuraya, Y., Hashimoto, Y., and Kasama, T. (2003). Purification and characterization of an endo-β-(1→6)-galactanase from trichoderma viride. *Carbohydr. Res.* 338, 219–230. doi: 10.1016/S0008-6215(02)00405-6

Olmos, E., García De La Garma, J., Gomez-Jimenez, M. C., and Fernandez-Garcia, N. (2017). Arabinogalactan proteins are involved in salt-adaptation and vesicle trafficking in tobacco by-2 cell cultures. *Front. Plant Sci.* 8. doi: 10.3389/fpls.2017.01092

Pfeifer, L., Utermöhlen, J., Happ, K., Permann, C., Holzinger, A., von Schwartzenberg, K., et al. (2022). Search for evolutionary roots of land plant arabinogalactan-proteins in charophytes: presence of a rhamnogalactan-protein in spirogyra pratensis (Zygnematophyceae). *Plant J.* 109, 568–584. doi: 10.1111/tpj.15577

Sardar, H. S., Yang, J., and Showalter, A. M. (2006). Molecular interactions of arabinogalactan proteins with cortical microtubules and f-actin in bright yellow-2 tobacco cultured cells. *Plant Physiol.* 142, 1469–1479. doi: 10.1104/pp.106.088716

Seifert, G. J., and Roberts, K. (2007). The biology of arabinogalactan proteins. *Annu. Rev. Plant Biol.* 58, 137–161. doi: 10.1146/annurev.arplant.58.032806.103801

Shimoda, R., Okabe, K., Kotake, T., Matsuoka, K., Koyama, T., Tryfona, T., et al. (2014). Enzymatic fragmentation of carbohydrate moieties of radish arabinogalactan-protein and elucidation of the structures. *Bioscience Biotechnol. Biochem.* 78, 818–831. doi: 10.1080/09168451.2014.910100

Silva, J., Ferraz, R., Dupree, P., Showalter, A. M., and Coimbra, S. (2020). Three decades of advances in arabinogalactan-protein biosynthesis. *Front. Plant Sci.* 11. doi: 10.3389/fpls.2020.610377

Strasser, R. (2016). Plant protein glycosylation. *Glycobiology* 26, 926–939. doi: 10.1093/glycob/cww023

Takata, R., Tokita, K., Mori, S., Shimoda, R., Harada, N., Ichinose, H., et al. (2010). Degradation of carbohydrate moieties of arabinogalactan-proteins by glycoside hydrolases from neurospora crassa. *Carbohydr. Res.* 345, 2516–2522. doi: 10.1016/j.carres.2010.09.006

Tan, L., Varnai, P., Lamport, D. T. A., Yuan, C., Xu, J., Qiu, F., et al. (2010). Plant O-hydroxyproline arabinogalactans are composed of repeating trigalactosyl subunits with short bifurcated side chains. *J. Biol. Chem.* 285, 24575–24583. doi: 10.1074/jbc.M109.100149

Tryfona, T., Liang, H.-C., Kotake, T., Kaneko, S., Marsh, J., Ichinose, H., et al. (2010). Carbohydrate structural analysis of wheat flour arabinogalactan protein. *Carbohydr. Res.* 345, 2648–2656. doi: 10.1016/j.carres.2010.09.018

Tryfona, T., Liang, H.-C., Kotake, T., Tsumuraya, Y., Stephens, E., and Dupree, P. (2012). Structural characterization of arabidopsis leaf arabinogalactan polysaccharides. *Plant Physiol.* 160, 653–666. doi: 10.1104/pp.112.202309

Tsumuraya, Y., Hashimoto, Y., and Yamamoto, S. (1987). An arabinogalactan and an arabinogalactan-containing proteoglycan from radish (Raphanus sativus) seeds. *Carbohydr. Res.* 161, 113–126. doi: 10.1016/0008-6215(87)84010-7

Tsumuraya, Y., Mochizuki, N., Hashimoto, Y., and Kovac, P. (1990). Purification of an exo-β-(1→3)-D-galactanase of irpex lacteus (Polyporus tulipiferae) and its action on arabinogalactan-proteins. *J. Biol. Chem.* 265, 7207–7215. doi: 10.1016/s0021-9258(19)39100-8

Tsumuraya, Y., Ogura, K., Hashimoto, Y., Mukoyama, H., and Yamamoto, S. (1988). Arabinogalactan-proteins from primary and mature roots of radish (Raphanus sativus l.). *Plant Physiol.* 86, 155–160. doi: 10.1104/pp.86.1.155

Tsumuraya, Y., Ozeki, E., Ooki, Y., Yoshimi, Y., Hashizume, K., and Kotake, T. (2019). Properties of arabinogalactan-proteins in European pear (Pyrus communis l.) fruits. *Carbohydr. Res.* 485, 107816. doi: 10.1016/j.carres.2019.107816

Yariv, J., Kalb, A. J., and Katchalski, E. (1967a). Isolation of an l-fucose binding protein from lotus tetragonolobus seed. *Nature* 215, 890–891. doi: 10.1038/215890a0

Yariv, J., Lis, H., and Katchalski, E. (1967b). Precipitation of arabic acid and some seed polysaccharides by glycosylphenylazo dyes. *Biochem. J.* 105, 1C–2C. doi: 10.1042/bj1050001c

Yoshimi, Y., Hara, K., Yoshimura, M., Tanaka, N., Higaki, T., Tsumuraya, Y., et al. (2020). Expression of a fungal exo-β-1,3-galactanase in arabidopsis reveals a role of type II arabinogalactans in the regulation of cell shape. *J. Exp. Bot.* 71, 5414–5424. doi: 10.1093/jxb/eraa236

Yoshimi, Y., Yaguchi, K., Kaneko, S., Tsumuraya, Y., and Kotake, T. (2017). Properties of two fungal endo-β-1,3-galactanases and their synergistic action with an exo-β-1,3-galactanase in degrading arabinogalactan-proteins. *Carbohydr. Res.* 453-454, 26–35. doi: 10.1016/j.carres.2017.10.013

frontiers | Frontiers in Plant Science

TYPE Mini Review
PUBLISHED 17 November 2022
DOI 10.3389/fpls.2022.1005991

OPEN ACCESS

EDITED BY
Qingfang He,
University of Arkansas at Little Rock, United States

REVIEWED BY
Alexei E. Solovchenko,
Lomonosov Moscow State University, Russia
Sanjeev Mishra,
Sardar Swaran Singh National Institute of Renewable Energy, India

*CORRESPONDENCE
Takuji Miyamoto
tmiyamoto@sake.nu.niigata-u.ac.jp
Norikuni Ohtake
ohtake@agr.niigata-u.ac.jp

†These authors have contributed equally to this work

SPECIALTY SECTION
This article was submitted to Plant Physiology, a section of the journal Frontiers in Plant Science

RECEIVED 28 July 2022
ACCEPTED 24 October 2022
PUBLISHED 17 November 2022

CITATION
Çakirsoy I, Miyamoto T and Ohtake N (2022) Physiology of microalgae and their application to sustainable agriculture: A mini-review. *Front. Plant Sci.* 13:1005991. doi: 10.3389/fpls.2022.1005991

Physiology of microalgae and their application to sustainable agriculture: A mini-review

Iffet Çakirsoy[1†], Takuji Miyamoto[2*†] and Norikuni Ohtake[1*]

[1]Graduate School of Science and Technology, Niigata University, Niigata, Japan, [2]Sakeology Center, Niigata University, Niigata, Japan

Concern that depletion of fertilizer feedstocks, which are a finite mineral resource, threatens agricultural sustainability has driven the exploration of sustainable methods of soil fertilization. Given that microalgae, which are unicellular photosynthetic organisms, can take up nutrients efficiently from water systems, their application in a biological wastewater purification system followed by the use of their biomass as a fertilizer alternative has attracted attention. Such applications of microalgae would contribute to the accelerated recycling of nutrients from wastewater to farmland. Many previous reports have provided information on the physiological characteristics of microalgae that support their utility. In this review, we focus on recent achievements of studies on microalgal physiology and relevant applications and outline the prospects for the contribution of microalgae to the establishment of sustainable agricultural practices.

KEYWORDS

microalga, sustainable agriculture, nutrient recycling, fertilizer alternative, CO_2-concentrating mechanism, membrane lipid remodeling

Introduction

With the increasing threat of mineral resource depletion through human activities, demand for renewable feedstocks is rising dramatically. The utilization of photosynthetic organisms, including land plants and algae, offers one promising solution. For example, lignocellulosic biomass, which is composed predominantly of plant secondary cell walls, represents an abundant and renewable feedstock for materials, chemicals, and fuels (Ragauskas et al., 2014; Umezawa, 2018; Miyamoto et al., 2020). Promoting the applications of photosynthetic organisms would contribute to the establishment of a sustainable human society.

In the context of agricultural sustainability, a renewable alternative to synthetic chemical fertilizers is urgently required. Enhanced utilization of synthetic chemical fertilizers in conjunction with the development of modern crop cultivars, in which the yield is highly responsive to intensive fertilization, has contributed to improved crop

productivity worldwide (Khush, 2001). For example, in soils a large portion of phosphorus (P), an essential macronutrient for plants, likely exists as non-available or poorly available forms for crops, which increases the importance of P fertilizer. However, because the raw material of P fertilizers, rock phosphate, is a finite resource distributed unevenly in limited areas of the world, depletion of the reserves is of grave concern (Desmidt et al., 2015). In addition, the manufacture of nitrogen (N) fertilizers requires the burning of fossil fuels to fix atmospheric N_2 and intensive use of N fertilizers enriches reactive N compounds, leading to soil acidification, water eutrophication, and atmospheric pollution (Hayashi et al., 2021). Thus, to establish a sustainable agricultural system worldwide, renewable alternatives to chemical fertilizers and the adoption of eco-friendly soil fertilization practices (Lin et al., 2019), as well as strategies to increase the nutrient use efficiency of crops (Hu et al., 2015; Wu et al., 2020; Ochiai et al., 2022), should be explored.

Microalgae are unicellular photosynthetic organisms commonly found in freshwater and marine ecosystems. They have been used in both experimental and real-world settings to biologically purify wastewater (Vadiveloo et al., 2021). Wastewater purification systems using microalgae represent a promising alternative to conventional wastewater treatment technologies that consume high amounts of energy, discharge sludge, and emit greenhouse gases (Qiao et al., 2020). Microalgae can rapidly grow and proliferate by efficiently acquiring carbon dioxide (CO_2) and nutrients, such as P and N, from water systems (Sukačová et al., 2020). Also, the use of microalgal biomass as a biofertilizer as well as a fuel resource can contribute to the enhanced recycling of nutrients (Das et al., 2019; Khan et al., 2019; Moges et al., 2020).

Previous works have revealed many physiological characteristics favorable to the use of microalgae in sustainable agriculture. In addition, empirical evidence on the effectiveness and characteristics of microalga-based fertilizers associated with their physiology has been reported. This review is focused on interactions between basic and applied studies of microalgae, providing insight into a strategy for the establishment of sustainable agriculture.

Carbon fixation capacity assisted by CO_2-concentrating mechanisms

The CO_2 assimilation capacity of photosynthetic organisms is critical to their growth. Ribulose 1,5-bisphosphate carboxylase/oxygenase (Rubisco) is a core enzyme involved in carbon fixation reactions. However, Rubisco generally shows a low affinity for CO_2 and the carboxylation reaction has a slow catalytic turnover rate. The oxygenase activity of Rubisco is also associated with CO_2-consuming photorespiration. These properties of Rubisco limit the efficiency of carbon fixation in photosynthetic organisms. In addition to the properties of Rubisco, aquatic conditions present further challenges for algal carbon fixation because the diffusion of CO_2 is substantially slower in water than in air. To overcome these problems, most algae develop CO_2-concentrating mechanisms (CCMs) that actively take up and enrich CO_2 and HCO_3^- in the pyrenoid, a chloroplast liquid-like non-membranous compartment rich in Rubisco (Hennacy and Jonikas, 2020). The pyrenoid of the algal model *Chlamydomonas reinhardtii* is penetrated by pyrenoid tubules, which are cylindrical structures of thylakoid membranes (Engel et al., 2015). The pyrenoid tubules may facilitate the rapid diffusion of small molecules, such as adenosine triphosphate (ATP) and sugars, between the chloroplast stroma and pyrenoid (Engel et al., 2015). A starch sheath composed of multiple starch granules forms around the pyrenoid in response to CO_2 limitation (Kuchitsu et al., 1988), which may prevent CO_2 diffusion from the pyrenoid.

Earlier reports on *C. reinhardtii* suggested that flexible CCM systems operate for adaptation to CO_2 limitation, i.e., low CO_2 (LC; approximately 0.03%–0.5%) and very low CO_2 (VLC; < 0.02%) environments (Wang and Spalding, 2014). Under LC conditions, CO_2 uptake mechanisms are predominantly activated. It has been suggested that the chloroplast protein limiting CO_2 inducible protein B (LCIB), which structurally resembles a β-type carbonic anhydrase (Jin et al., 2016), is indispensable for the stimulation of CO_2 uptake under LC conditions (Yamano et al., 2010; Wang and Spalding, 2014). It may be that LCIB captures CO_2 leaked from the pyrenoid by unidirectionally hydrating CO_2 to HCO_3^- under LC conditions (Yamano et al., 2022), though recombinant LCIB did not show carbonic anhydrase activity (Jin et al., 2016). LCIB proteins are dispersed uniformly in the chloroplast under LC conditions, whereas they migrate to the pyrenoid periphery under VLC conditions (Yamano et al., 2022). The starch sheath surrounding the pyrenoid is important in the localization of LCIB (Toyokawa et al., 2020). LCIB interacts with its homolog LCIC (Yamano et al., 2010). Additionally, LCIC accumulation is involved in LCIB migration (Yamano et al., 2022). These results suggest that an LCIB–LCIC complex plays a critical role in CCM regulation depending on the CO_2 concentration.

Although suppressed under LC conditions, HCO_3^- uptake is activated under VLC conditions. The ABC transporter high-light activated3 (HLA3) and anion channel LCIA, which are localized in the plasma membrane and chloroplast envelope, respectively, act cooperatively for the HCO_3^- uptake (Duanmu et al., 2009; Gao et al., 2015; Yamano et al., 2015).

It has been suggested that CCM-assisted carbon fixation is associated with nutrient availability (Raven et al., 2008). For example, a study using *C. reinhardtii*, *Chlamydomonas acidophila*, *Chlamydomonas pitschmannii*, and *Scenedesmus vacuolatus* observed different impacts of P limitation on their CCM, such as reduction of CO_2 and HCO_3^- uptake (Lachmann et al., 2017). Such impacts might be attributed to energy-

demanding processes driven by ATP in the CCMs (Su, 2021). Therefore, P uptake capacity is also crucial for the growth performance of microalgae in water systems. In addition, the P content of microalgal biomass may directly affect its effectiveness as a fertilizer, which will be described further below.

Phosphorus accumulation associated with membrane lipid remodeling

Nutrient availability substantially affects microalgal growth and lipid metabolism. Owing to their utility for lipid production, interactions between nutrient acquisition and lipid metabolism in microalgae have been extensively studied (Moore et al., 2013; Yaakob et al., 2021). However, for microalgal application in a wastewater purification system followed by fertilizer use, the lipid-metabolism-dependent nutrient uptake capacity of microalgae is of greater interest.

P starvation induces membrane lipid remodeling from phospholipids (e.g., phosphatidylethanolamine, phosphatidylcholine, and phosphatidylglycerol) to non-P-containing glycolipids (e.g., sulfoquinovosyldiacylglycerol, SQDG) and/or betaine lipids (e.g., diacylglyceroltrimethylhomoserine, DGTS), thus facilitating P reallocation to other biochemical and cellular processes (Moseley and Grossman, 2009; Rouached et al., 2010). In *Nannochloropsis oceanica*, the breakdown of phospholipids and the synthesis of DGTS and SQDG are stimulated in the exponential growth phase under P limitation (Mühlroth et al., 2017). Additionally, acyl-editing-mediated conversion of phospholipids to non-P-containing lipids is upregulated in the stationary growth phase (Mühlroth et al., 2017).

The lipid-remodeling-associated P uptake capacity is different in taxonomically diverse microalgae. For example, high P uptake occurs in *Nannochloropsis gaditana*, *Tetraselmis suecica*, and *Picochlorum atomus*, which can actively counterbalance phospholipids with betaine (non-P-containing) lipids under P limitation (Cañavate et al., 2017a; Cañavate et al., 2017b). Meanwhile, such high P uptake is practically absent in *Rhodomonas baltica*, *Chroomonas placoidea*, and *Chaetoceros gracilis*, which constitutively produce betaine lipids with fluctuating abundances of phospholipids depending on P supply levels (Cañavate et al., 2017a; Cañavate et al., 2017b). The diversity may be associated with distinct strategies of microalgae for adaptation to P limitation. Microalgal species displaying a high capacity for P uptake might be useful for the applications in P recycling from wastewater to farmland.

Given that P limitation induces membrane lipid remodeling also in land plants (Nakamura, 2013; Tawaraya et al., 2018; Hayes et al., 2022), information on the molecular mechanisms involved in microalgal lipid remodeling may be beneficial to enhance our understanding of low-P adaptation in land plants. The MYB transcription factor phosphorus starvation response1 (PSR1), a homolog of *Arabidopsis thaliana* phosphate starvation response regulator1 (PHR1), acts as a crucial regulator of the acquisition and reallocation of P in *C. reinhardtii* (Shimogawara et al., 1999; Wykoff et al., 1999; Bajhaiya et al., 2016). In a *N. oceanica* mutant deficient in the gene encoding PSR1, low-P-induced replacement of phospholipids with DGTS and SQDG is not observed (Murakami et al., 2020), further supporting the association of PSR1 with low-P-induced membrane lipid remodeling in microalgal species. In addition, the MYB transcription factor lipid remodeling regulator1 (LRL1), a homolog of AtMYB65 from *A. thaliana*, upregulates the expression of the gene encoding sulfoquinovosyl diacylglycerol2 (SQD2) involved in SQDG biosynthesis at an advanced stage of the low-P response of *C. reinhardtii* (Hidayati et al., 2019).

Applications of microalgae for nutrient recycling

Given the aforementioned physiological characteristics that support biomass productivity and nutrient uptake capacity, microalgae are a viable renewable and eco-friendly alternative for conventional wastewater treatment systems (Table 1). For example, *Chlorella vulgaris* and *Microcystis* sp. can recover 33 mg P L^{-1} (79%) and 37 mg P L^{-1} (88%), respectively, from an initial concentration of 41 mg P L^{-1} in wastewater in 14 days (Chu et al., 2021). With the escalation in the flow of P from terrestrial to water systems with increased industrialization (Liu et al., 2008; Schlesinger, 2012; Van Dijk et al., 2016), P recovery from wastewaters has become a mandatory practice (Peng et al., 2018). A large amount of P has been recovered annually from wastewater using microalgal biofilm techniques (Sukačová et al., 2020).

Further utilization of microalgal biomass recovered from wastewater treatment systems may facilitate the establishment of nutrient recycling (Table 2). The application of dried microalgal biomass can significantly increase total or plant-available nutrients (Dineshkumar et al., 2018; Dineshkumar et al., 2019; Saadaoui et al., 2019; Sharma et al., 2021) and organic carbon (Renuka et al., 2017) in soils. Deoiled dry biomass, which can be obtained as a residue of microalga-based oil production, improves crop productivity when used as a partial substitute for chemical fertilizers (Silambarasan et al., 2021). There are also reports on the positive effects of microalgal extracts and hydrolysates as a seed primer, foliar spray, and liquid fertilizer (Plaza et al., 2018; Kholssi et al., 2019; Supraja et al., 2020; Kusvuran, 2021). Interestingly, the potential of living microalgae to alleviate saline–alkaline stresses (Ma et al., 2022) and that of a soil-surface biofilm to suppress N loss through NH_3 volatilization (de Siqueira Castro et al., 2017) have been reported. Circular economy projects using microalgae for wastewater purification and farmland fertilization in a cattle farm (Lorentz et al., 2020) and winery company (Avila et al., 2022) have been tested.

TABLE 1 Biomass productivity and nutrient uptake capacity of microalgae in aquatic systems.

Microalgal species	Growth medium	Dry biomass yield (g L^{-1})	Nutrient uptake (mg L^{-1})	Reference
Chlamydomonas reinhardtii	BG11	0.4	not described	Farid et al., 2019
Chlorella minutissima	wastewater	0.4	N 26.4 P 4.4 K 2.2	Sharma et al., 2021
Chlorella vulgaris	BG11	0.8	not described	Dineshkumar et al., 2018
Chlorella vulgaris	BG11	0.2	not described	Farid et al., 2019
Chlorella vulgaris	wastewater	1.1	N 139.5 P 32.5	Chu et al., 2021
Chlorella sorokiniana	BG11	0.2	not described	Farid et al., 2019
Dunaliell salina	BG11	0.4	not described	Farid et al., 2019
Microcystis sp.	wastewater	1.1	N 161.2 P 36.5	Chu et al., 2021
Monoraphidium sp.	diluted anaerobic liquid digestate	0.7-0.8	$N\text{-}NH_4^+$ 16-32※ $P\text{-}PO_4^{3-}$ 0.8-2.3※	Jimenez et al., 2020
Spirulina platensis	Zarrouk	1.9	not described	Dineshkumar et al., 2018
microalgal consortia (*Scenedesmus* sp. & *Chlorella* sp.)	wastewater	1.8	Protein 175	Silambarasan et al., 2021
microalgal consortia (*Scenedesmus* sp. & *Chlorella* sp.)	wastewater	not described	$N\text{-}NH_4^+$ 4.7 $P\text{-}PO_4^{3-}$ 2.3	Avila et al., 2022

※*Monoraphidium* sp. removed 100% (ca. 16-32 mg L^{-1}) of $N\text{-}NH_4^+$ and 46.6-78.5% (ca. 0.8-2.3 mg L^{-1}) of $P\text{-}PO_4^{3-}$ from the diluted anaerobic liquid digestate (Jimenez et al., 2020).

It has also been reported that algal–bacterial aerobic granular sludge removes greater amounts of P and N from wastewater than does bacteria alone (Wang et al., 2021). Bacterial degradation of organic carbon may mitigate the issue of microalgal CO_2 acquisition in water systems, which was mentioned above. Additionally, the artificial augmentation of CO_2 in wastewater via supplementation with flue gas from combustion may also stimulate microalgal biomass productivity and nutrient uptake capacity, potentially resulting in enhanced nutrient recycling (He et al., 2012; Lara-Gil et al., 2016; Yadav et al., 2019).

Characteristics of microalga-based fertilizers

The application of dry biomass from *Chlorella minutissima* reduced the leaching of nitrate from farmland and increased leaf N content of spinach (*Spinacia oleracea*) plants (Sharma et al., 2022) (Table 2). The application of *Asterarcys quadricellulare* extracts significantly stimulated N assimilation and the nitrate reductase activity of potato (*Solanum tuberosum*) plants (Cordeiro et al., 2022). The applications of *C. vulgaris* biomass and chemical fertilizer resulted in comparable levels of shoot N uptake in wheat (*Triticum aestivum*) plants (Schreiber et al., 2018). These results demonstrate the effectiveness of the microalga-based fertilizer. However, the level of shoot P uptake was lower in the wheat plants grown under the microalgal treatment than in those grown under the chemical fertilizer treatment (Schreiber et al., 2018), suggesting that microalgal biomass acts as a slow-release P fertilizer. Microalgae can store P as polyphosphates (Delgadillo-Mirquez et al., 2016; Solovchenko et al., 2019; Chu et al., 2021), which are degraded slowly by soil microbes (Powell et al., 2011; Ray et al., 2013; Solovchenko et al., 2019). Furthermore, hydrothermal carbonization of microalgal biomass enhances its characteristics as a slow-release fertilizer, which increases the amount of moderately available P in soils more persistently compared with chemical fertilizer (Chu et al., 2021) (Table 2). Such fertilizer characteristics might increase the nutrient use efficiency of crops and/or reduce environmental pollution by suppressing the leaching of nutrients from farmland (Coppens et al., 2016; Jimenez et al., 2020; Sharma et al., 2022).

The application of microalgal extracts enriches essential macronutrients such as P, potassium, calcium, and magnesium in tomato plants (Suchithra et al., 2022) (Table 2). Microalga-based fertilizers also supply essential micronutrients as well as beneficial elements for plants (de Haes et al., 2012; Maurya et al., 2016; Wuang et al., 2016; Silva et al., 2019). In a wheat cultivation test, the application of microalgal biomass increased the contents of zinc, iron, copper, and manganese in plants (Rana et al., 2012; Prasanna et al., 2013; Renuka et al., 2017). Microalgal biomass rich in selenium, a beneficial element for plants, has been also suggested to serve as an effective fertilizer (Han et al., 2020).

Garcia-Gonzalez and Sommerfeld (2016) and Deepika and MubarakAli (2020) mentioned the occurrence in microalgal extracts of phytohormones that upregulate plant growth. It has been considered that microalgal components, including phytohormones, stimulate the production of antifungal

TABLE 2 Effects of microalga-based fertilizers on agricultural crops.

Microalgal species	Application forms	Nutrient content (%)	Crops	Effects	Reference
Arthrospira platensis, *Dunaliella salina*, & *Porphyridium* sp.	extracts (crude polysaccharides)	not described	*S. lycopersicum*	plant growth ↑; node number ↑	Rachidi et al., 2020
Asterarcys quadricellulare	extracts	not described	*S. tuberosum*	potato yield ↑; plant growth ↑; plant chlorophyll, amino acid, & sugar contents ↑; plant nitrate reductase enzyme activity↑; plant nitrogen assimilation ↑	Cordeiro et al., 2022
Chlorella minutissima	dried biomass	N 6.0 P 1.0 K 0.5	*Z. mays* & *S. oleracea*	soil nutrient content ↑; plant growth ↑ (vs. chemical fertilizer alone)	Sharma et al., 2021
Chlorella minutissima	dried biomass	N 6.0	*S. oleracea*	soil nitrate leaching ↓; leaf N content ↑ (vs. chemical fertilizer alone)	Sharma et al., 2022
Chlorella sorokiniana	dried biomass	N 6.1 P 1.2 K 8.9	*H. vulgare*	grain yield ↑ (vs. chemical fertilizer alone)	Suleiman et al., 2020
Chlorella vulgaris	hydrochar	N 6.2 P 4.3 K 0.9	*T. aestivum*	soil available P content ↑; plant P use efficiency ↑ (vs. chemical fertilizer alone)	Chu et al., 2021
Chlorella vulgaris	extracts	not described	*B. oleracea*	plant growth ↑; plant nutrient content ↑; plant phenolics & flavonoid contents ↑; plant antioxidant activity ↑ (under drought stress)	Kusvuran, 2021
Chlorella vulgaris	extracts	N 0.4 K 0.7	*S. lycopersicum*	fruit size ↑; fruit water content ↑; fruit soluble solid content ↑; fruit soluble sugar content ↑; fruit protein content ↑; fruit P, K, Ca, & Mg contents ↑	Suchithra et al., 2022
Chlorella vulgaris, *Chlorella sorokiniana*, & *Chlamydomonas reinhardtii*	extracts (crude polysaccharides)	polysaccharides 5.6-8.4	*S. lycopersicum*	plant β-1,3-glucanase activity ↑; plant phenylalanine ammonia lyase activity ↑; plant antioxidant activity ↑; plant fatty acid content ↑	Farid et al., 2019
Dunaliella salina	extracts (crude polysaccharides)	polysaccharides 199.8	*S. lycopersicum*	plant lipoxygenase activity ↑	Farid et al., 2019
Microcystis sp.	hydrochar	N 8.8 P 5.8 K 0.8	*T. aestivum*	soil available P content ↑; plant P use efficiency ↑; grain yield ↑ (vs. chemical fertilizer alone)	Chu et al., 2021
Monoraphidium sp.	dried biomass	N 3.3 P 0.9 K 0.5	*S. lycopersicum*	soil nitrate leaching ↓; plant growth → (vs. chemical fertilizer alone)	Jimenez et al., 2020
Nannochloropsis oculata	dried biomass	N 8.1 P 1.3 K 1.4	*S. lycopersicum*	leaf N & P contents →; fruit sugar content →; fruit carotenoid content → (vs. chemical fertilizer alone)	Coppens et al., 2016
Scenedesmus sp.	extracts	N 8.1 P 2.7 K 0.7	*T. aestivum*	plant nutrient uptake ↑; plant growth → (vs. chemical fertilizer alone)	Shaaban et al., 2010
Scenedesmus sp	dried biomass (deoiled)	N 7.5 P 1.6 K 0.7	*O. sativa*	plant growth ↑; tillering rate ↑; grain yield ↑ (vs. chemical fertilizer alone)	Nayak et al., 2019
Spirulina platensis	extract	N 7.8 P 0.8 K 1.6	*E. sativa*, *A. gangeticus*, *B. rapa*, & *B. oleracea*	plant growth →; seedling dry weight → (vs. chemical fertilizer alone)	Wuang et al., 2016

(Continued)

TABLE 2 Continued

Microalgal species	Application forms	Nutrient content (%)	Crops	Effects	Reference
Tetraselmis sp.	dried biomass	N 3.4 P 0.5 K 0.5	*P. dactylifera*	soil nutrient content →; plant growth →; plant chlorophyll content →; plant antioxidant activity → (vs. chemical fertilizer alone)	Saadaoui et al., 2019
microalgal bacterial flocs (*Klebsormidium* sp. & *Ulothrix* sp. are dominant)	dried biomass	N 2.4 P 0.6 K 0.2	*S. lycopersicum*	leaf N & P contents →; fruit sugar content →; fruit carotenoid content → (vs. chemical fertilizer alone)	Coppens et al.,2016
microalgal consortia (*Chlorella vulgaris* is dominant)	biomass	not described	*P. glaucum*	soil NH_3 volatilization ↓	de Siqueira Castro et al., 2017
microalgal consortia (*Chlorella* sp. & *Scenedesmus* sp.)	dried biomass (deoiled)	N 7.8 P 1.7 K 1.1	*S. lycopersicum*	plant growth ↑; plant nutrient content ↑; plant chlorophyll content ↑; fruit yield ↑ (vs. chemical fertilizer alone)	Silambarasan et al., 2021

Effects of microalga-based fertilizer application are described relative to a control or to those following complete and/or partial replacement with chemical fertilizer (vs. chemical fertilizer alone). Arrows indicate higher (↑), lower (↓), and comparable levels (→) of plant or soil parameters.

substances in plants (Spolaore et al., 2006; Coppens et al., 2016). In addition, crude polysaccharides obtained from microalgae have a biostimulant-like effect on plants (Farid et al., 2019; Rachidi et al., 2020) (Table 2). Plant morphological traits, such as plant height, leaf number, tillering rate, root length, and lateral root number, are positively affected by the application of a microalga-based fertilizer depending on its dosage (Wuang et al., 2016; Nayak et al., 2019; Deepika and MubarakAli, 2020) (Table 2). Commercially important components of fruit, such as carotenoids and sugars, increase in response to the application of microalga-based fertilizers (Kumari et al., 2011; Coppens et al., 2016; Mutale-Joan et al., 2020; Cordeiro et al., 2022). These changes might be partially due to the effect of plant growth regulators in microalgal biomass, although further investigation is required for verification.

Conclusions and prospects

To achieve rapid growth and efficient nutrient accumulation in water systems, microalgae developed mechanisms such as flexible CCMs and membrane lipid remodeling. Previous research has shed light on the sophisticated molecular interactions underlying the physiological characteristics of microalgae, which support its utility as a wastewater purification system and fertilizer. Applications of microalgae in a wastewater purification system followed by fertilizer use may facilitate the establishment of nutrient recycling. Many studies have shown that application of microalgal biomass can provide nutrients essential for plants and enrich organic carbons in soils. In addition, microalgal biomass contains slowly degradable forms of plant-essential nutrients, reducing the leaching of the nutrients from farmland. Furthermore, microalga-based fertilizers are regarded as suppliers of plant growth regulators. However, challenges remain in the expansion of microalga-based technologies. For example, a life cycle assessment highlighted the detrimental impact of electricity consumption required for microalgal cultivation (Diniz et al., 2017; de Souza et al., 2019). In addition, the application of a microalga-based fertilizer can stimulate the emission of greenhouse gases, such as N_2O and CO_2, from soils (Suleiman et al., 2020). Thus, further technological advances, as well as a more in-depth understanding of microalgal physiology, are required for wider implementation of microalgal applications for sustainable agriculture.

Author contributions

IC, TM, and NO wrote the manuscript. All authors contributed to the article and approved the submitted version.

Funding

This work was partially supported by the Japan Society for the Promotion of Science (JSPS) KAKENHI grant (JP#22K14876).

Conflict of interest

The authors declare that the research was conducted in the absence of any commercial or financial relationships that could be construed as a potential conflict of interest.

Publisher's note

References

Avila, R., Justo, Á., Carrero, E., Crivillés, E., Vicent, T., and Blánquez, P. (2022). Water resource recovery coupling microalgae wastewater treatment and sludge co-digestion for bio-wastes valorisation at industrial pilot-scale. *Bioresorce Technol.* 343, 126080. doi: 10.1016/j.biortech.2021.126080

Bajhaiya, A. K., Dean, A. P., Zeef, L. A. H., Webster, R. E., and Pittman, J. K. (2016). PSR1 is a global transcriptional regulator of phosphorus deficiency responses and carbon storage metabolism in *Chlamydomonas reinhardtii*. *Plant Physiol.* 170 (3), 1216–1234. doi: 10.1104/pp.15.01907

Cañavate, J. P., Armada, I., and Hachero-Cruzado, I. (2017a). Aspects of phosphorus physiology associated with phosphate-induced polar lipid remodelling in marine microalgae. *J. Plant Physiol.* 214, 28–38. doi: 10.1016/j.jplph.2017.03.019

Cañavate, J. P., Armada, I., and Hachero-Cruzado, I. (2017b). Interspecific variability in phosphorus-induced lipid remodelling among marine eukaryotic phytoplankton. *New Phytol.* 213 (2), 700–713. doi: 10.1111/nph.14179

Chu, Q., Lyu, T., Xue, L., Yang, L., Feng, Y., Sha, Z., et al. (2021). Hydrothermal carbonization of microalgae for phosphorus recycling from wastewater to crop-soil systems as slow-release fertilizers. *J. Clean. Prod.* 283, 124627. doi: 10.1016/j.jclepro.2020.124627

Coppens, J., Grunert, O., Van Den Hende, S., Vanhoutte, I., Boon, N., Haesaert, G., et al. (2016). The use of microalgae as a high-value organic slow-release fertilizer results in tomatoes with increased carotenoid and sugar levels. *J. Appl. Phycol.* 28 (4), 2367–2377. doi: 10.1007/s10811-015-0775-2

Cordeiro, E. C. N., Mógor, Á.F., Amatussi, J. O., Mógor, G., Marques, H. M. C., and de Lara, G. B. (2022). Microalga biofertilizer improves potato growth and yield, stimulating amino acid metabolism. *J. Appl. Phycol.* 34 (1), 385–394. doi: 10.1007/s10811-021-02656-0

Das, P., Quadir, M. A., Thaher, M. I., Alghasal, G. S. H. S., and Aljabri, H. M. S. J. (2019). Microalgal nutrients recycling from the primary effluent of municipal wastewater and use of the produced biomass as bio-fertilizer. *Int. J. Environ. Sci. Technol.* 16 (7), 3355–3364. doi: 10.1007/s13762-018-1867-8

Deepika, P., and MubarakAli, D. (2020). Production and assessment of microalgal liquid fertilizer for the enhanced growth of four crop plants. *Biocatal. Agric. Biotechnol.* 28 (1), 101701. doi: 10.1016/j.bcab.2020.101701

de Haes, H. A. U., Voortman, R. L., Bastein, T., Bussink, D. W., Rougoor, C. W., and van der Weijden, W. J. (2012) *Scarcity of micronutrients in soil, food and mineral reserves -urgency and policy options-. platform agriculture, innovation and society*. Available at: https://www.iatp.org/sites/default/files/scarcity_of_micronutrients.pdf.

Delgadillo-Mirquez, L., Lopes, F., Taidi, B., and Pareau, D. (2016). Nitrogen and phosphate removal from wastewater with a mixed microalgae and bacteria culture. *Biotechnol. Rep.* 11, 18–26. doi: 10.1016/j.btre.2016.04.003

de Siqueira Castro, J., Calijuri, M. L., Assemany, P. P., Cecon, P. R., de Assis, I. R., and Ribeiro, V. J. (2017). Microalgae biofilm in soil: Greenhouse gas emissions, ammonia volatilization and plant growth. *Sci. Total Environ.* 574, 1640–1648. doi: 10.1016/j.scitotenv.2016.08.205

Desmidt, E., Ghyselbrecht, K., Zhang, Y., Pinoy, L., van der Bruggen, B., Verstraete, W., et al. (2015). Global phosphorus scarcity and full-scale p-recovery techniques: A review. *Crit. Rev. Env. Tec. Sci.* 45 (4), 336–384. doi: 10.1080/10643389.2013.866531

de Souza, M. H. B., Calijuri, M. L., Assemany, P. P., de Siqueira Castro, J., and de Oliveira, A. C. M. (2019). Soil application of microalgae for nitrogen recovery: A life-cycle approach. *J. Clean. Prod.* 211, 342–349. doi: 10.1016/j.jclepro.2018.11.097

Dineshkumar, R., Kumaravel, R., Gopalsamy, J., Sikder, M. N. A., and Sampathkumar, P. (2018). Microalgae as bio-fertilizers for rice growth and seed yield productivity. *Waste Biomass Valor.* 9 (5), 793–800. doi: 10.1007/s12649-017-9873-5

Dineshkumar, R., Subramanian, J., Gopalsamy, J., Jayasingam, P., Arumugam, A., Kannadasan, S., et al. (2019). The impact of using microalgae as biofertilizer in maize (*Zea mays* l.). *Waste Biomass Valor.* 10 (5), 1101–1110. doi: 10.1007/s12649-017-0123-7

Diniz, G. S., Tourinho, T. C., Silva, A. F., and Chaloub, R. M. (2017). Environmental impact of microalgal biomass production using wastewater resources. *Clean Technol. Envir.* 19 (10), 2521–2529. doi: 10.1007/s10098-017-1433-y

Duanmu, D., Miller, A. R., Horken, K. M., Weeks, D. P., and Spalding, M. H. (2009). Knockdown of limiting-CO_2-induced gene *HLA3* decreases HCO_3^- transport and photosynthetic ci affinity in *Chlamydomonas reinhardtii*. *Proc. Natl. Acad. Sci. U.S.A.* 106 (14), 5990–5995. doi: 10.1073/pnas.0812885106

Engel, B. D., Schaffer, M., Kuhn Cuellar, L., Villa, E., Plitzko, J. M., and Baumeister, W. (2015). Native architecture of the chlamydomonas chloroplast revealed by *in situ* cryo-electron tomography. *eLife* 4, e04889. doi: 10.7554/eLife.04889

Farid, R., Mutale-Joan, C., Redouane, B., Mernissi Najib, E. L., Abderahime, A., Laila, S., et al. (2019). Effect of microalgae polysaccharides on biochemical and metabolomics pathways related to plant defense in solanum lycopersicum. *Appl. Biochem. Biotechnol.* 188 (1), 225–240. doi: 10.1007/s12010-018-2916-y

Gao, H., Wang, Y., Fei, X., Wright, D. A., and Spalding, M. H. (2015). Expression activation and functional analysis of HLA3, a putative inorganic carbon transporter in *Chlamydomonas reinhardtii*. *Plant J.* 82 (1), 1–11. doi: 10.1111/tpj.12788

Garcia-Gonzalez, J., and Sommerfeld, M. (2016). Biofertilizer and biostimulant properties of the microalga acutodesmus dimorphus. *J. Appl. Phycol.* 28 (2), 1051–1061. doi: 10.1007/s10811-015-0625-2

Han, W., Mao, Y., Wei, Y., Shang, P., and Zhou, X. (2020). Bioremediation of aquaculture wastewater with algal-bacterial biofilm combined with the production of selenium rich biofertilizer. *Water* 12 (7), 2071. doi: 10.3390/w12072071

Hayashi, K., Shibata, H., Oita, A., Nishina, K., Ito, A., Katagiri, K., et al. (2021). Nitrogen budgets in Japan from 2000 to 2015: Decreasing trend of nitrogen loss to the environment and the challenge to further reduce. *Environ. Pollut.* 286 (10), 117559. doi: 10.1016/j.envpol.2021.117559

Hayes, P. E., Adem, G. D., Pariasca-Tanaka, J., and Wissuwa, M. (2022). Leaf phosphorus fractionation in rice to understand internal phosphorus-use efficiency. *Ann. Bot.* 129 (3), 287–301. doi: 10.1093/aob/mcab138

Hennacy, J. H., and Jonikas, M. C. (2020). Prospects for engineering biophysical CO_2 concentrating mechanisms into land plants to enhance yields. *Annu. Rev. Plant Biol.* 71, 461–485. doi: 10.1146/annurev-arplant-081519-040100

He, L., Subramanian, V. R., and Tang, Y. J. (2012). Experimental analysis and model-based optimization of microalgae growth in photo-bioreactors using flue gas. *Biomass Bioenerg.* 41, 131–138. doi: 10.1016/j.biombioe.2012.02.025

Hidayati, N. A., Yamada-Oshima, Y., Iwai, M., Yamano, T., Kajikawa, M., Sakurai, N., et al. (2019). Lipid remodeling regulator 1 (LRL1) is differently involved in the phosphorus-depletion response from PSR1 in *Chlamydomonas reinhardtii*. *Plant J.* 100 (3), 610–626. doi: 10.1111/tpj.14473

Hu, B., Wang, W., Ou, S., Tang, J., Li, H., Che, R., et al. (2015). Variation in NRT1.1B contributes to nitrate-use divergence between rice subspecies. *Nat. Genet.* 47 (7), 834–838. doi: 10.1038/ng.3337

Jimenez, R., Markou, G., Tayibi, S., Barakat, A., Chapsal, C., and Monlau, F. (2020). Production of microalgal slow-release fertilizer by valorizing liquid agricultural digestate: Growth experiments with tomatoes. *Appl. Sci.* 10 (11), 3890. doi: 10.3390/app10113890

Jin, S., Sun, J., Wunder, T., Tang, D., Cousins, A. B., Sze, S. K., et al. (2016). Structural insights into the LCIB protein family reveals a new group of β-carbonic anhydrases. *Proc. Natl. Acad. Sci. U.S.A.* 113 (51), 14716–14721. doi: 10.1073/pnas.1616294113

Khan, S. A., Sharma, G. K., Malla, F. A., and Kumar, A. (2019). Microalgae based biofertilizers: A biorefinery approach of phycoremediate wastewater and harvest biodiesel and manure. *J. Clean. Prod.* 211, 1412–1419. doi: 10.1016/j.jclepro.2018.11.281

Kholssi, R., Marks, E. A., Miñón, J., Montero, O., Debdoubi, A., and Rad, C. (2019). Biofertilizing effect of chlorella sorokiniana suspensions on wheat growth. *J. Plant Growth Regul.* 38 (2), 644–649. doi: 10.1007/s00344-018-9879-7

Khush, G. S. (2001). Green revolution: The way forward. *Nat. Rev. Genet.* 2 (10), 815–822. doi: 10.1038/35093585

Kuchitsu, K., Tsuzuki, M., and Miyachi, S. (1988). Changes of starch localization within the chloroplast induced by changes in CO_2 concentration during growth of *Chlamydomonas reinhardtii*: Independent regulation of pyrenoid starch and stroma starch. *Plant Cell Physiol.* 29 (8), 1269–1278. doi: 10.1093/oxfordjournals.pcp.a077635

Kumari, R., Kaur, I., and Bhatnagar, A. K. (2011). Effect of aqueous extract of sargassum johnstonii setchell & Gardner on growth, yield and quality of *Lycopersicon esculentum* mill. *J. Appl. Phycol.* 23 (3), 623–633. doi: 10.1007/s10811-011-9651-x

Kusvuran, S. (2021). Microalgae (*Chlorella vulgaris* beijerinck) alleviates drought stress of broccoli plants by improving nutrient uptake, secondary metabolites, and antioxidative defense system. *Hortic. Plant J.* 7 (3), 221–231. doi: 10.1016/j.hpj.2021.03.007

Lachmann, S. C., Maberly, S. C., and Spijkerman, E. (2017). Species-specific influence of pi-status on inorganic carbon acquisition in microalgae (Chlorophyceae). *Botany* 95 (9), 943–952. doi: 10.1139/cjb-2017-0082

Lara-Gil, J. A., Senés-Guerrero, C., and Pacheco, A. (2016). Cement flue gas as a potential source of nutrients during CO_2 mitigation by microalgae. *Algal. Res.* 17, 285–292. doi: 10.1016/j.algal.2016.05.017

Lin, W., Lin, M., Zhou, H., Wu, H., Li, Z., and Lin, W. (2019). The effects of chemical and organic fertilizer usage on rhizosphere soil in tea orchards. *PloS One* 14 (5), e0217018. doi: 10.1371/journal.pone.0217018

Liu, Y., Villalba, G., Ayres, R. U., and Schroder, H. (2008). Global phosphorus flows and environmental impacts from a consumption perspective. *J. Ind. Ecol.* 12 (2), 229–247. doi: 10.1111/j.1530-9290.2008.00025.x

Lorentz, J. F., Calijuri, M. L., Assemany, P. P., Alves, W. S., and Pereira, O. G. (2020). Microalgal biomass as a biofertilizer for pasture cultivation: Plant productivity and chemical composition. *J. Clean. Prod.* 276, 124130. doi: 10.1016/j.jclepro.2020.124130

Ma, C., Cui, H., Ren, C., Yang, J., Liu, Z., Tang, T., et al. (2022). The seed primer and biofertilizer performances of living *Chlorella pyrenoidosa* on *Chenopodium quinoa* under saline-alkali condition. *J. Appl. Phycol.* 34 (3), 1621–1634. doi: 10.1007/s10811-022-02699-x

Maurya, R., Chokshi, K., Ghosh, T., Trivedi, K., Pancha, I., Kubavat, D., et al. (2016). Lipid extracted microalgal biomass residue as a fertilizer substitute for *Zea mays* l. *Front. Plant Sci.* 6. doi: 10.3389/fpls.2015.01266

Miyamoto, T., Tobimatsu, Y., and Umezawa, T. (2020). MYB-mediated regulation of lignin biosynthesis in grasses. *Curr. Plant Biol.* 24, 100174. doi: 10.1016/j.cpb.2020.100174

Moges, M. E., Heistad, A., and Heidorn, T. (2020). Nutrient recovery from anaerobically treated blackwater and improving its effluent quality through microalgae biomass production. *Water* 12 (2), 592. doi: 10.3390/w12020592

Moore, C. M., Mills, M. M., Arrigo, K. R., Berman-Frank, I., Bopp, L., Boyd, P. W., et al. (2013). Processes and patterns of oceanic nutrient limitation. *Nat. Geosci.* 6 (9), 701–710. doi: 10.1038/ngeo1765

Moseley, J. L., and Grossman, A. R. (2009). "Phosphorus limitation from the physiological to the genomic," in *The chlamydomonas source-book: Organellar and metabolic processes*, vol. 2 . Ed. D. B. Stern (San Diego: Academic Press), 189–215.

Mühlroth, A., Winge, P., El Assimi, A., Jouhet, J., Maréchal, E., Hohmann-Marriott, M. F., et al. (2017). Mechanisms of phosphorus acquisition and lipid class remodeling under p limitation in a marine microalga. *Plant Physiol.* 175 (4), 1543–1559. doi: 10.1104/pp.17.00621

Murakami, H., Kakutani, N., Kuroyanagi, Y., Iwai, M., Hori, K., Shimojima, M., et al. (2020). MYB-like transcription factor NoPSR1 is crucial for membrane lipid remodeling under phosphate starvation in the oleaginous microalga. *Nannochloropsis oceanica. FEBS Lett.* 594 (20), 3384–3394. doi: 10.1002/1873-3468.13902

Mutale-Joan, C., Redouane, B., Najib, E., Yassine, K., Lyamlouli, K., Laila, S., et al. (2020). Screening of microalgae liquid extracts for their bio stimulant properties on plant growth, nutrient uptake and metabolite profile of *Solanum lycopersicum* l. *Sci. Rep.* 10 (1), 1–12. doi: 10.1038/s41598-020-59840-4

Nayak, M., Swain, D. K., and Sen, R. (2019). Strategic valorization of de-oiled microalgal biomass waste as biofertilizer for sustainable and improved agriculture of rice (*Oryza sativa* L.) crop. *Sci. Total Environ.* 682, 475–484. doi: 10.1016/j.scitotenv.2019.05.123

Nakamura, Y. (2013). Phosphate starvation and membrane lipid remodeling in seed plants. *Prog. Lipid Res.* 52 (1), 43–50. doi: 10.1016/j.plipres.2012.07.002

Ochiai, K., Oba, K., Oda, K., Miyamoto, T., and Matoh, T. (2022). Effects of improved sodium uptake ability on grain yields of rice plants under low potassium supply. *Plant Dir.* 6 (4), e384. doi: 10.1002/pld3.387

Peng, L., Dai, H., Wu, Y., Peng, Y., and Lu, X. A. (2018). Comprehensive review of the available media and approaches for phosphorus recovery from wastewater. *Water Air Soil pollut.* 229 (4), 1–28. doi: 10.1007/s11270-018-3706-4

Plaza, B. M., Gómez-Serrano, C., Acién-Fernández, F. G., and Jimenez-Becker, S. (2018). Effect of microalgae hydrolysate foliar application (*Arthrospira platensis* and *Scenedesmus* sp.) on petunia x hybrida growth. *J. Appl. Phycol.* 30 (4), 2359–2365. doi: 10.1007/s10811-018-1427-0

Powell, N., Shilton, A., Pratt, S., and Chisti, Y. (2011). Phosphate release from waste stabilisation pond sludge: Significance and fate of polyphosphate. *Water Sci. Technol.* 63 (8), 1689–1694. doi: 10.2166/wst.2011.336

Prasanna, R., Babu, S., Rana, A., Kabi, S. R., Chaudhary, V., Gupta, V., et al. (2013). Evaluating the establishment and agronomic proficiency of cyanobacterial consortia as organic options in wheat–rice cropping sequence. *Exp. Agric.* 49 (3), 416–434. doi: 10.1017/S001447971200107X

Qiao, S., Hou, C., Wang, X., and Zhou, J. (2020). Minimizing greenhouse gas emission from wastewater treatment process by integrating activated sludge and microalgae processes. *Sci. Total Environ.* 732 (4), 139032. doi: 10.1016/j.scitotenv.2020.139032

Rachidi, F., Benhima, R., Sbabou, L., and El Arroussi, H. (2020). Microalgae polysaccharides bio-stimulating effect on tomato plants: Growth and metabolic distribution. *Biotechnol. Rep.* 25, e00426. doi: 10.1016/j.btre.2020.e00426

Ragauskas, A. J., Beckham, G. T., Biddy, M. J., Chandra, R., Chen, F., Davis, M. F., et al. (2014). Lignin valorization: Improving lignin processing in the biorefinery. *Science* 344 (6185), 1246843. doi: 10.1126/science.1246843

Rana, A., Joshi, M., Prasanna, R., Shivay, Y. S., and Nain, L. (2012). Biofortification of wheat through inoculation of plant growth promoting rhizobacteria and cyanobacteria. *Eur. J. Soil Biol.* 50, 118–126. doi: 10.1016/j.ejsobi.2012.01.005

Raven, J. A., Cockell, C. S., and La Rocha, C. L. (2008). The evolution of inorganic carbon concentrating mechanisms in photosynthesis. *Philos. Trans. R. Soc B-Biol. Sci.* 363 (1504), 2641–2650. doi: 10.1098/rstb.2008.0020

Ray, K., Mukherjee, C., and Ghosh, A. N. (2013). A way to curb phosphorus toxicity in the environment: Use of polyphosphate reservoir of cyanobacteria and microalga as a safe alternative phosphorus biofertilizer for Indian agriculture. *Environ. Sci. Technol.* 47 (20), 11378–11379. doi: 10.1021/es403057c

Renuka, N., Prasanna, R., Sood, A., Bansal, R., Bidyarani, N., Singh, R., et al. (2017). Wastewater grown microalgal biomass as inoculants for improving micronutrient availability in wheat. *Rhizosphere* 3 (2), 150–159. doi: 10.1016/j.rhisph.2017.04.005

Rouached, H., Arpat, A. B., and Poirier, Y. (2010). Regulation of phosphate starvation responses in plants: Signaling players and cross-talks. *Mol. Plant* 3 (2), 288–299. doi: 10.1093/mp/ssp120

Saadaoui, I., Sedky, R., Rasheed, R., Bounnit, T., Almahmoud, A., Elshekh, A., et al. (2019). Assessment of the algae-based biofertilizer influence on date palm (*Phoenix dactylifera* l.) cultivation. *J. Appl. Phycol.* 31 (1), 457–463. doi: 10.1007/s10811-018-1539-6

Schlesinger, W. H. (2012). *Biogeochemistry: An analysis of global change. 3rd ed* (New York, NY, USA: Elsevier/Academic Press).

Schreiber, C., Schiedung, H., Harrison, L., Briese, C., Ackermann, B., Kant, J., et al. (2018). Evaluating potential of green alga *Chlorella vulgaris* to accumulate phosphorus and to fertilize nutrient-poor soil substrates for crop plants. *J. Appl. Phycol.* 30 (5), 2827–2836. doi: 10.1007/s10811-018-1390-9

Shaaban, M. M., El-Saady, A. M., and El-Sayed, A. B. (2010). Green microalgae water extract and micronutrients foliar application as promoters to nutrient balance and growth of wheat plants. *J. Am. Sci.* 6 (9), 631–636. doi: 10.3923/pjbs.2001.628.632

Sharma, G. K., Khan, S. A., Shrivastava, M., Bhattacharyya, R., Sharma, A., Gupta, D. K., et al. (2021). Circular economy fertilization: Phycoremediated algal biomass as biofertilizers for sustainable crop production. *J. Environ. Manage.* 287 (4), 112295. doi: 10.1016/j.jenvman.2021.112295

Sharma, G. K., Khan, S. A., Shrivastava, M., Bhattacharyya, R., Sharma, A., Gupta, N., et al. (2022). Phycoremediated n-fertilization approaches on reducing environmental impacts of agricultural nitrate leaching. *J. Cleaner Production* 345 (5), 131120. doi: 10.1016/j.jclepro.2022.131120

Shimogawara, K., Wykoff, D. D., Usuda, H., and Grossman, A. R. (1999). *Chlamydomonas reinhardtii* mutants abnormal in their responses to phosphorus deprivation. *Plant Physiol.* 120 (3), 685–694. doi: 10.1104/pp.120.3.685

Silambarasan, S., Logeswari, P., Sivaramakrishnan, R., Incharoensakdi, A., Cornejo, P., Kamaraj, B., et al. (2021). Removal of nutrients from domestic wastewater by microalgae coupled to lipid augmentation for biodiesel production and influence of deoiled algal biomass as biofertilizer for *Solanum lycopersicum* cultivation. *Chemosphere* 268 (8), 129323. doi: 10.1016/j.chemosphere.2020.129323

Silva, G. H., Sueitt, A. P. E., Haimes, S., Tripidaki, A., van Zwieten, R., and Fernandes, T. V. (2019). Feasibility of closing nutrient cycles from black water by microalgae-based technology. *Algal. Res.* 44 (6), 101715. doi: 10.1016/j.algal.2019.101715

Solovchenko, A., Khozin-Goldberg, I., Selyakh, I., Semenova, L., Ismagulova, T., Lukyanov, A., et al. (2019). Phosphorus starvation and luxury uptake in green microalgae revisited. *Algal. Res.* 43, 101651. doi: 10.1016/j.algal.2019.101651

Spolaore, P., Joannis-Cassan, C., Duran, E., and Isambert, A. (2006). Commercial applications of microalgae. *J. Biosci. Bioeng.* 101 (2), 87–96. doi: 10.1263/jbb.101.87

Su, Y. (2021). Revisiting carbon, nitrogen, and phosphorus metabolisms in microalgae for wastewater treatment. *Sci. Total Environ.* 762 (1), 144590. doi: 10.1016/j.scitotenv.2020.144590

Suchithra, M. R., Muniswami, D. M., Sri, M. S., Usha, R., Rasheeq, A. A., and Preethi, B. A. (2022). Effectiveness of green microalgae as biostimulants and biofertilizer through foliar spray and soil drench method for tomato cultivation. *S. Afr. J. Bot.* 146 (14), 740–750. doi: 10.1016/j.sajb.2021.12.022

Sukačová, K., Vícha, D., and Dušek, J. (2020). Perspectives on microalgal biofilm systems with respect to integration into wastewater treatment technologies and phosphorus scarcity. *Water* 12 (8), 2245. doi: 10.3390/w12082245

Suleiman, A. K. A., Lourenço, K. S., Clark, C., Luz, R. L., da Silva, G. H. R., Vet, L. E., et al. (2020). From toilet to agriculture: Fertilization with microalgal biomass from wastewater impacts the soil and rhizosphere active microbiomes, greenhouse gas emissions and plant growth. *Resour. Conserv. Recycl.* 161, 104924. doi: 10.1016/j.resconrec.2020.104924

Supraja, K. V., Behera, B., and Balasubramanian, P. (2020). Efficacy of microalgal extracts as biostimulants through seed treatment and foliar spray for tomato cultivation. *Ind. Crop Prod.* 151, 112453. doi: 10.1016/j.indcrop.2020.112453

Tawaraya, K., Honda, S., Cheng, W., Chuba, M., Okazaki, Y., Saito, K., et al. (2018). Ancient rice cultivar extensively replaces phospholipids with non-phosphorus glycolipid under phosphorus deficiency. *Physiol. Plantarum* 163 (3), 297–305. doi: 10.1111/ppl.12699

Toyokawa, C., Yamano, T., and Fukuzawa, H. (2020). Pyrenoid starch sheath is required for LCIB localization and the CO_2-concentrating mechanism in green algae. *Plant Physiol.* 182 (4), 1883–1893. doi: 10.1104/pp.19.01587

Umezawa, T. (2018). Lignin modification *in planta* for valorization. *Phytochem. Rev.* 17 (6), 1305–1327. doi: 10.1007/s11101-017-9545-x

Vadiveloo, A., Foster, L., Kwambai, C., Bahri, P. A., and Moheimani, N. R. (2021). Microalgae cultivation for the treatment of anaerobically digested municipal centrate (ADMC) and anaerobically digested abattoir effluent (ADAE). *Sci. Total Environ.* 775 (3), 145853. doi: 10.1016/j.scitotenv.2021.145853

Van Dijk, K. C., Lesschen, J. P., and Oenema, O. (2016). Phosphorus flows and balances of the European union member states. *Sci. Total Environ.* 542, 1078–1093. doi: 10.1016/j.scitotenv.2015.08.048

Wang, J., Lei, Z., Tian, C., Liu, S., Wang, Q., Shimizu, K., et al. (2021). Ionic response of algal-bacterial granular sludge system during biological phosphorus removal from wastewater. *Chemosphere* 264, 128534. doi: 10.1016/j.chemosphere.2020.128534

Wang, Y., and Spalding, M. H. (2014). Acclimation to very low CO_2: Contribution of limiting CO_2 inducible proteins, LCIB and LCIA, to inorganic carbon uptake in *Chlamydomonas reinhardtii*. *Plant Physiol.* 166 (4), 2040–2050. doi: 10.1104/pp.114.248294

Wuang, S. C., Khin, M. C., Chua, P. Q. D., and Luo, Y. D. (2016). Use of spirulina biomass produced from treatment of aquaculture wastewater as agricultural fertilizers. *Algal. Res.* 15, 59–64. doi: 10.1016/j.algal.2016.02.009

Wu, K., Wang, S., Song, W., Zhang, J., Wang, Y., Liu, Q., et al. (2020). Enhanced sustainable green revolution yield *via* nitrogen-responsive chromatic modulation in rice. *Science* 367 (6478), eaaz2046. doi: 10.1126/science.aaz2046

Wykoff, D. D., Grossman, A. R., Weeks, D. P., Usuda, H., and Shimogawara, K. (1999). Psr1, a nuclear localized protein that regulates phosphorus metabolism in chlamydomonas. *Proc. Natl. Acad. Sci. U.S.A.* 96 (26), 15336–15341. doi: 10.1073/pnas.96.26.153

Yaakob, M. A., Mohamed, R. M. S. R., Al-Gheethi, A., Gokare, R. A., and Ambati, R. R. (2021). Influence of nitrogen and phosphorus on microalgal growth, biomass, lipid, and fatty acid production: An overview. *Cells* 10 (2), 393. doi: 10.3390/cells10020393

Yadav, G., Dash, S. K., and Sen, R. (2019). A biorefinery for valorization of industrial waste-water and flue gas by microalgae for waste mitigation, carbon-dioxide sequestration and algal biomass production. *Sci. Total Environ.* 688, 129–135. doi: 10.1016/j.scitotenv.2019.06.024

Yamano, T., Sato, E., Iguchi, H., Fukuda, Y., and Fukuzawa, H. (2015). Characterization of cooperative bicarbonate uptake into chloroplast storoma in the green alga *Chlamydomonas reinhardtii*. *Proc. Natl. Acad. Sci. U.S.A.* 112 (23), 7315–7320. doi: 10.1073/pnas.1501659112

Yamano, T., Toyokawa, C., Shimamura, D., Matsuoka, T., and Fukuzawa, H. (2022). CO_2-dependent migration and relocation of LCIB, a pyrenoid-peripheral protein in *Chlamydomonas reinhardtii*. *Plant Physiol.* 188 (2), 1081–1094. doi: 10.1093/plphys/kiab528

Yamano, T., Tsujikawa, T., Hatano, K., Ozawa, S., Takahashi, Y., and Fukuzawa, H. (2010). Light and low-CO_2-dependent LCIB-LCIC complex localization in the chloroplast supports the carbon-concentrating mechanism in *Chlamydomonas reinhardtii*. *Plant Cell Physiol.* 51 (9), 1453–1468. doi: 10.1093/pcp/pcq105

frontiers | Frontiers in Plant Science

TYPE Original Research
PUBLISHED 22 November 2022
DOI 10.3389/fpls.2022.1050355

OPEN ACCESS

EDITED BY
Alessandra Boccaccini,
Università di Tor Vergata,
Italy

REVIEWED BY
Lorenzo Ferroni,
University of Ferrara, Italy
Ginga Shimakawa,
Kwansei Gakuin University, Japan

*CORRESPONDENCE
Cornelia Spetea
cornelia.spetea.wiklund@bioenv.gu.se

SPECIALTY SECTION
This article was submitted to Plant Physiology, a section of the journal Frontiers in Plant Science

RECEIVED 21 September 2022
ACCEPTED 31 October 2022
PUBLISHED 22 November 2022

CITATION
Dukic E, Gollan PJ, Grebe S, Paakkarinen V, Herdean A, Aro E-M and Spetea C (2022) The Arabidopsis thylakoid chloride channel ClCe regulates ATP availability for light-harvesting complex II protein phosphorylation. *Front. Plant Sci.* 13:1050355. doi: 10.3389/fpls.2022.1050355

The Arabidopsis thylakoid chloride channel ClCe regulates ATP availability for light-harvesting complex II protein phosphorylation

Emilija Dukic[1], Peter J. Gollan[2], Steffen Grebe[2], Virpi Paakkarinen[2], Andrei Herdean[3], Eva-Mari Aro[2] and Cornelia Spetea[1]*

[1]Department of Biological and Environmental Sciences, University of Gothenburg, Gothenburg, Sweden, [2]Molecular Plant Biology Unit, Department of Life Technologies, University of Turku, Turku, Finland, [3]Climate Change Cluster, University of Technology Sydney, Ultimo, NSW, Australia

Coping with changes in light intensity is challenging for plants, but well-designed mechanisms allow them to acclimate to most unpredicted situations. The thylakoid K^+/H^+ antiporter KEA3 and the voltage-dependent Cl^- channel VCCN1 play important roles in light acclimation by fine-tuning electron transport and photoprotection. Good evidence exists that the thylakoid Cl^- channel ClCe is involved in the regulation of photosynthesis and state transitions in conditions of low light. However, a detailed mechanistic understanding of this effect is lacking. Here we report that the ClCe loss-of-function in *Arabidopsis thaliana* results in lower levels of phosphorylated light-harvesting complex II (LHCII) proteins as well as lower levels of the photosystem I-LHCII complexes relative to wild type (WT) in low light conditions. The phosphorylation of the photosystem II core D1/D2 proteins was less affected either in low or high light conditions. In low light conditions, the steady-state levels of ATP synthase conductivity and of the total proton flux available for ATP synthesis were lower in ClCe loss-of-function mutants, but comparable to WT at standard and high light intensity. As a long-term acclimation strategy, expression of the *ClCe* gene was upregulated in WT plants grown in light-limiting conditions, but not in WT plants grown in

standard light even when exposed for up to 8 h to low light. Taken together, these results suggest a role of ClCe in the regulation of the ATP synthase activity which under low light conditions impacts LHCII protein phosphorylation and state transitions.

KEYWORDS

Arabidopsis thaliana, ATP synthase, chloride channel (ClC), light-harvesting complex II (LHCII), low light acclimation, photosystem II, protein phosphorylation, proton motive force (PMF)

Introduction

Photosynthetic function is tightly coupled with growth and we need to understand how photosynthetic components are integrated to operate in a dynamic light environment. In low light, plants are limited in photosynthesis, and need mechanisms to maximize the light use efficiency. State transitions represent a reversible light acclimation mechanism for reconfiguring the photosynthetic light-harvesting apparatus to adjust excitation balance between photosystem II (PSII) and PSI and take place within a few minutes (Rantala et al., 2020). This is a way to maximize the efficiency of utilization of absorbed light energy under conditions when light is limiting for growth, by redistribution of a mobile pool of light-harvesting antenna (LHCII) trimers that can bind either to PSII (state 1) or to PSI (State 2). More specifically, in low light conditions favoring absorption by the PSII supercomplex, a part of LHCII (LHCB1 and LHCB2) are phosphorylated by the thylakoid bound STN7 kinase in the grana (Crepin and Caffarri, 2015). The phosphorylated LHCII (p-LHCII) dissociates from PSII, migrates to the grana margins and stroma lamellae where then associates with PSI, and functions as its light-harvesting antenna. Conversely, upon dephosphorylation, LHCII dissociates from PSI, migrates back to the grana and re-joins PSII. Noteworthy, while p-LHCB2 is essential for PSI-LHCI-LHCII complex formation (Crepin and Caffarri, 2015; 2018; Pan et al., 2018; Rantala et al., 2020), the p-LHCB1 is suggested to increase the mobility of PSII-LHCII supercomplexes and facilitate thylakoid remodelling (stacking, grana size) (Crepin and Caffarri, 2015). Importantly, a part of the mobile LHCII pool independently from phosphorylation is under most conditions associated with PSI (Croce, 2020). Grieco et al. (2015) brought evidence that, in addition to the phosphorylation-dependent movement of LHCII, entire complexes may migrate laterally to the grana margins in a LHCII antenna lake to allow for direct energy transfer from PSII to PSI under light that preferentially excites PSII. How LHCII and even large complexes like PSII and PSI move within the thylakoid membrane during state transitions is still unknown (Messant et al., 2021).

Three thylakoid-located ion channels/transporters, namely the thylakoid K^+/H^+ antiporter KEA3, the voltage-dependent Cl^- channel VCCN1 and the Cl^- channel ClCe have been unraveled in Arabidopsis to play important roles in the regulation of photosynthesis and light acclimation (Finazzi et al., 2015; Spetea et al., 2017; Szabo and Spetea, 2017). Deeper mechanistic understanding of how they work individually and in concert has evolved with the analyses of higher order loss-of-function mutants (Dukic et al., 2019; Hohner et al., 2019; Li et al., 2021). KEA3 and VCCN1 play a pivotal role in regulating the flow of K^+, H^+ and Cl^- ions across the thylakoid membrane, modulating the size and composition of the proton motive force (PMF), and in this way fine tuning photosynthetic electron transport and photoprotection, and indirectly many other chloroplast processes. The physiological role of ClCe is the least understood due to the weak photosynthetic phenotype of the Arabidopsis mutants (Dukic et al., 2019; Li et al., 2021). Nevertheless, ClCe loss-of-function in Arabidopsis altered the distribution of excitation energy between PSII and PSI during state transitions (Herdean et al., 2016a) and the electron transport in low light conditions (Dukic et al., 2019), but the mechanism remained unclear. Whether ClCe is a Cl^- channel or transporter is also not known due to unsuccessful heterologous expression. The activity as a Cl^-/H^+ exchanger for ClCf, which is the closest homologue of ClCe, has been demonstrated to be connected with the activity of the ATPase in Golgi membranes (Scholl et al., 2021). Here we aimed to

Abbreviations: Chl, chlorophyll; ClC, chloride channel; DIG, digitonin; DM, n-dodecyl-β-D-maltoside; F_v/F_m, maximum quantum yield of photosystem II photochemistry; GL, growth light; HL, high light; LEF, linear electron transport; LHC, light harvesting complex; LL, low light; NPQ, non-photochemical quenching; g_H^+, proton conductivity through ATP synthase; v_H^+, proton flux; PMF, proton motive force; PS, photosystem; qL, fraction of open PSII centers based on a lake model; Y(II), quantum yield of PSII photochemistry; Y(NO), quantum yield of non-regulated energy dissipation; Y(NPQ), quantum yield of regulated non-photochemical quenching.

decipher the mechanism behind altered state transitions in ClCe loss-of-function mutants by investigating if the LHCII phosphorylation and ATP synthase activity are affected. A compromised ATP synthesis is expected to perturb energy-dependent reactions such as LHCII protein phosphorylation with consequences for photosynthetic acclimation and plant growth. Based on analyses of *kea3, vccn1* and *clce* single, double, and triple mutants, we found lower levels of LHCII phosphorylation only in *clce* mutants and that this is caused by a reduced activity of the ATP synthase specifically under low light conditions. Moreover, the *clce* mutants displayed a lower photosynthetic performance and stronger shade avoidance traits relative to wild type when grown in light-limiting conditions.

Materials and methods

Plant material and growth conditions

Arabidopsis thaliana cv. Columbia-0 was used as wild type (WT). The mutant lines used in this study *clce-2 (c), kea3-1 (k), vccn1-1 (v), clce-2kea3-1 (ck), clce-2vccn1-1 (cv), kea3-1vccn1-1 (kv), and kea3-1vccn1-1clce-2* (*kvc*) were previously described (Dukic et al., 2019).

Plants used for phosphorylation experiments were grown in soil in growth chambers at 23°C and 60% relative humidity using 16 h light (100 µmol photons m^{-2} s^{-1})/8 h dark cycles (long-day) for 3 weeks or using 8 h light (120 µmol photons m^{-2} s^{-1})/16 h dark cycles (short-day) for 5 weeks. OSRAM PowerStar HQIT 400/D Metal Halide Lamps were used as light source. In some fluctuating light experiments, overnight dark-acclimated plants from short-day conditions were shifted to 15 µmol photons m^{-2} s^{-1} (LL1) conditions for 2 h, followed by 1000 µmol photons m^{-2} s^{-1} (HL) conditions for 2 h and back to 15 µmol photons m^{-2} s^{-1} (LL2) conditions for 2 h. Rosettes were harvested and frozen in liquid nitrogen after dark, 2 h in LL1, 2 h in HL, 15 min in LL2 and 2 h in LL2 conditions for later thylakoid isolations. Plants used for electrochromic shift (ECS) experiments were grown in soil for 6-8 weeks in a CLF PlantMaster chamber (Plant Climatics, Wertingen, Germany) using 8 h light (120 µmol photons m^{-2} s^{-1})/16 h dark cycles (short day) at 21°C/19°C, respectively, and 70% relative humidity. In some experiments, plants were grown using a short-day photoperiod in low light (15 µmol photons m^{-2} s^{-1}) for up to 8 months.

Thylakoid isolation and chlorophyll determination

Thylakoid isolations were performed with ice-cold reagents in cold room at 7°C. Fresh or frozen rosettes were ground in grinding buffer (50 mM HEPES–NaOH pH 7.5, 330 mM sorbitol, 5 mM $MgCl_2$, 0.05% (w/v) BSA, 0.065% (w/v) Na-ascorbate and 10 mM NaF) and filtered through Miracloth. Chloroplasts were collected by centrifugation at 4000 *g* for 6 min at 4°C and ruptured osmotically in shock buffer (50 mM HEPES–NaOH pH 7.5, 5 mM $MgCl_2$ and 10 mM NaF). Thylakoid membranes were collected by centrifugation at 4000 *g* for 6 min at 4°C and suspended in storage buffer (50 mM HEPES–NaOH pH 7.5, 100 mM sorbitol, 10 mM $MgCl_2$, and 10 mM NaF). Chlorophyll (Chl) concentrations were determined in 80% (v/v) buffered acetone according to Porra et al. (1989).

Gel electrophoresis and immunoblotting

For separation of native thylakoid protein complexes, large pore blue native polyacrylamide gel electrophoresis (lpBN-PAGE) was performed as described by Jarvi et al. (2011) with thylakoids solubilized in 1% (w/v) n-dodecyl-β-D-maltoside (DM) or 1% (w/v) digitonin (DIG). Additionally, thylakoid proteins were solubilized in Laemmli buffer (Laemmli, 1970) and separated by sodium dodecyl sulfate polyacrylamide gel electrophoresis (SDS-PAGE) in gels containing 15% (w/v) acrylamide and 6 M urea. For all gels, thylakoid samples were loaded on equal Chl basis.

For immunoblotting, proteins were transferred on PVDF membrane (Millipore) and recognized by specific antibodies for LHCB1 (1:5000, Agrisera), LHCB2 (1:5000, Agrisera), PsaB (1:3000, Agrisera), STN7 (1:1000, Agrisera), and CP47 (1:3000, gift from Prof. Roberto Barbato). Phosphorylated threonine residues were recognized with p-Thr antibody (1:3000, New England Biolabs) and phosphorylated LHCB1 (p-LHCB1, 1:10000, Agrisera) and LHCB2 (p-LHCB2, 1:10000, Agrisera). For detection, horseradish peroxidase-linked secondary antibody (Agrisera) and Amersham ECL Western blotting detection reagents (GE Healthcare) were used.

RNA isolation and quantitative RT-PCR

Total RNA was isolated from plant tissues of 6-week-old plants with an E.Z.N.A. R6827-01 Plant RNA kit (Omega Bio-Tek, GA, USA) and residual DNA was removed with E1091 DNAse (Omega Bio-Tek). cDNA was synthesized using 500 ng of total RNA through iScript cDNA synthesis Kit (Bio-Rad, Hercules, CA, USA). Quantitative real-time PCR analyses were conducted with a SsoAdvanced Universal SYBR Green Supermix on a CFX96 Touch Thermal Cycler (Bio-Rad). 50 ng of cDNA was used as qPCR template in 10 µl reactions. Amplifications were done in two-step PCR with the following conditions: initial denaturation for 2 min at 95°C, followed by 40 cycles of denaturation for 5 s at 95°C, annealing for 30 s at 60° and extension for 10 s at 72°C. After amplification, melt-curve analyses were performed for all primers.

Gene-specific primers used were ordered from Bio-Rad (Supplementary Table 1). ΔCq method ($2^{-\Delta Cq}$) was used to calculate relative expression using *PEX4* and *ACTIN8* as reference genes.

Kinetics of chlorophyll *a* fluorescence induction

In vivo Chl-*a* fluorescence in intact leaves of 30 min dark-acclimated plants was recorded using either a Handy-PEA, (Hansatech, UK) by applying saturating red actinic light of 3,500 μmol photons m^{-2} s^{-1} for 1 s or with a Dual-PAM 100 (Walz, Efeltrich, Germany) by applying a saturating pulse of 8,000 μmol photons m^{-2} s^{-1} for 700 ms and measuring light intensity<1.0 μmol photons m^{-2} s^{-1}. Initial F_0 and F_m fluorescence values were determined by the saturating pulse. The maximum quantum efficiency of PSII photochemistry (F_v/F_m) was calculated as $((F_m-F_0)/F_m)$ according to Genty et al. (1989).

Slow kinetics of Chl fluorescence from the upper surface of leaves on intact plants were recorded using a closed FluorCam 800 MF (Photon System Instruments, Drasow, Czech Republic). Plants were acclimated in dark condition for 20 min before recording Chl fluorescence kinetics using the following settings: 6 min actinic white light at 15, 100 or 650 μmol photons m^{-2} s^{-1} followed by 2 min darkness, saturating flash of white light at 4,000 μmol photons m^{-2} s^{-1} for 800 ms applied after every min of light/dark, shutter speed 10 μs, and sensitivity 50%. In addition to the maximum quantum yield of PSII photochemistry in the dark-acclimated state (F_v/F_m), the PSII quantum yield (Y(II)) and the non-photochemical quenching (NPQ) at 6 min of illumination were calculated according to Genty et al. (1989). The photochemical quenching of PSII (fraction of open PSII reaction centers based on a lake model, qL), the quantum yield of regulated NPQ (Y(NPQ)), and the quantum yield of non-regulated energy dissipation (Y(NO)) were calculated as described (Kramer et al., 2004) using the minimum fluorescence in the light (F_0') estimated according to Oxborough and Baker (1997).

Electrochromic band shift measurements

The proton motive force was estimated from ECS measured using the Dual-PAM 100 system equipped with a P515/535 module. Plants were first dark-acclimated for 30 min and then illuminated with actinic red light at 15, 100 or 650 μmol photons m^{-2} s^{-1} for 15 min. Before each measurement, three saturating single turnover 5-μs flashes at 200,000 μmol photons m^{-2} s^{-1} were applied to determine ECS_{ST}, which was used to normalize ECS_t. To determine the H^+ conductivity of the ATP synthase (g_H^+), the light was switched off at specific time points to record the ECS signal decay during 620-ms dark intervals. The g_H^+ parameter was calculated as 1/τ (time constant for decay during the first 100 ms (Cruz et al., 2005). The total proton flux available for ATP synthesis was calculated as $v_H^+ = PMF \times g_H^+$ (Cruz et al., 2001).

CO_2 fixation

Net rates of CO_2 fixation were determined using a Li-COR Li-6400 (Lincoln, Nebraska, USA). Plants were first light acclimated in the growth chamber for at least 1 h and then exposed in the gas exchange chamber to broad spectrum light generated with red, green and blue LEDs of fixed intensity (30, 150 and 700 μmol photons m^{-2} s^{-1}) in atmospheric CO_2 (440 μmol mol^{-1}) for approximately 5 min or until a steady state was reached. Since the leaf area was smaller than the chamber, data were normalized to leaf area determined using ImageJ.

Leaf starch analysis

For visualization of starch accumulation and breakdown, leaves from plants grown in short day at 15 μmol photons m^{-2} s^{-1} were harvested at the end of the light cycle (end of the day) and end of the dark cycle (end of the night). All leaves were bleached in 80% (v/v) ethanol at 80°C for 10 min, and the starch content was visualized by Lugol's staining for 10 min. After that, the leaves were rinsed and photographed on a light-table.

Statistical analyses

Presented data are means ± S.E.M. for 3-6 plants. Statistical analyses to compare the means between two groups were performed using the Student's *t*-test and among three or more groups using one-way ANOVA test. Statistically significant differences were considered at $P< 0.05$.

Results

LHCII and PSII core protein phosphorylation

LHCII and PSII core proteins undergo reversible phosphorylation in higher plants in a light intensity-dependent manner. Shift to high-light intensity induces strong phosphorylation of the PSII core and decreases LHCII phosphorylation. Shift to lower-light intensity, in turn, decreases the phosphorylation of PSII core, but strongly induces the phosphorylation of LHCII (Rintamaki et al., 1997; 2000; Tikkanen and Aro, 2014). Therefore, we first investigated the phosphorylation pattern in WT and *clce* in different light

conditions. Western blots of SDS-gels with a p-Thr antibody revealed lower levels of p-LHCII proteins in *clce* in low light conditions (as early as 15 min of illumination), but no difference from WT in high light conditions (Figure 1). The levels of p-D1/D2 proteins were only slightly lower as compared to WT in both low and high light.

Next, the WT plants and *clce* single, *clcevccn1, kea3clce, kea3vccn1* double, and *kea3vccn1clce* triple mutants were grown in either short- or long-day photoperiod. There was no visible difference in plant growth nor in the F_v/F_m parameter among the genotypes (Supplementary Figure 1). From these plants, we analyzed the photosynthetic complexes from thylakoids solubilized with either DIG (preferentially solubilizes stroma thylakoids and preserves supramolecular interactions of the thylakoid protein complexes) or with DM (solubilizes protein complexes from the entire thylakoid membrane and breaks the most labile interactions). Lp-BN gels of DM-solubilized thylakoids revealed a minor increase in the levels of the various types of PSII complexes between WT and different mutants suggesting that the functional architecture of PSII remained largely unchanged (Figures 2A–D). Nevertheless, in thylakoids solubilized with DIG also the less abundant LHCII-PSI supercomplexes were detected in lp-BN gels and their abundance was reduced both by the ClCe mutation and by the length of the day used during plant growth. Western blots with an antibody against p-LHCB2 of such gels revealed overall lower amounts of p-LHCB2 isoform in native complexes only for the ClCe-lacking lines, especially in plants grown in long-day conditions (Figures 2E, F). These blots clearly revealed the impact of reduced LHCB2 phosphorylation on the abundance of the PSI-LHCII supercomplex, in line with previous reports (Crepin and Caffarri, 2015; Pan et al., 2018). Even though PSII-LHCII-PSI megacomplexes contained less p-LHCB2, their abundance was not affected, suggesting that the formation of PSII-LHCII-PSI megacomplexes is independent of phosphorylation (Yokono et al., 2015).

Western blots presented in Figure 3 show that the steady-state levels of p-LHCB1 and particularly those of p-LHCB2 were lower in the *clce* lines, and this was not due to altered levels of the corresponding proteins. Furthermore, the levels of the STN7 kinase, the PSII CP47 subunit as well as the PSI PsaB subunit showed similar abundance in WT and mutant plants grown in short-day conditions, but slight reductions in PSII and PSI in long-day photoperiod were observed in the *kea3clce* and *clcevccn1* double and the *kea3vccn1clce* triple mutants. Taken together, these data provide evidence that the ClCe loss-of-function results in decreased levels of LHCII protein phosphorylation relative to WT in low light conditions.

Proton motive force, ATP synthase activity and CO_2 fixation

LHCII protein phosphorylation requires energy from ATP produced by the ATP synthase on the thylakoid membrane. Since the abundances of the LHCII substrate and responsible STN7 protein kinase were not different among the genotypes, to explain the differences in LHCII phosphorylation observed in the *clce* mutants we explored if the activity of the ATP synthase was affected. To this aim, the plants were grown in short day at 120 µmol photons m^{-2} s^{-1} (Supplementary Figure 2) and subjected to ECS measurements during illumination for 15 min at 15, 100 and 650 µmol photons m^{-2} s^{-1}, representing LL, GL, and HL conditions, respectively. From the ECS measurements, the thylakoid membrane total PMF size (estimated from ECSt), the conductivity to H^+ of the ATP synthase ($g_H{}^+$) and the proton flux ($v_H{}^+$) were calculated. The $g_H{}^+$ parameter indicates the rate at which cations (mainly H^+) move from the thylakoid lumen to the stroma mainly through the ATP synthase when briefly (100 ms) switching off the light. The $v_H{}^+$ parameter takes into account both PMF and $g_H{}^+$ and thus provides the total flux of H^+ available for ATP synthesis.

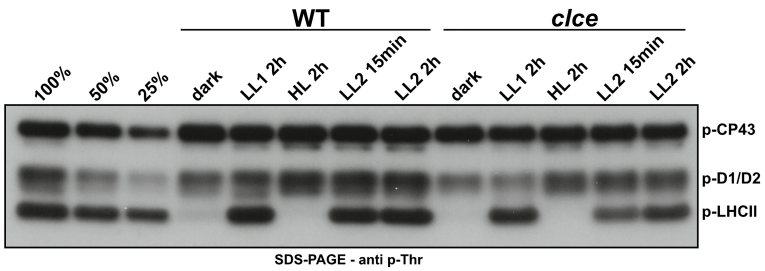

FIGURE 1
Phospho-Thr immunoblot of thylakoids from plants grown in short-day conditions. Wild-type plants (WT) and the *clce* mutant were grown using 8 h light (120 µmol photons m^{-2} s^{-1})/16 h dark cycles for 5 weeks. Overnight dark-acclimated plants were exposed to light at 15 µmol photons m^{-2} s^{-1} (LL1) for 2 h, followed by 1000 µmol photons m^{-2} s^{-1} (HL) for 2 h and back to 15 µmol photons m^{-2} s^{-1} (LL2) for 2 h. Thylakoids were isolated from leaves harvested at the given time points and light intensities. All thylakoids were loaded on equal chlorophyll basis of 0.5 µg. 100%, 50% and 25% WT sample after LL2 2h was used as loading control.

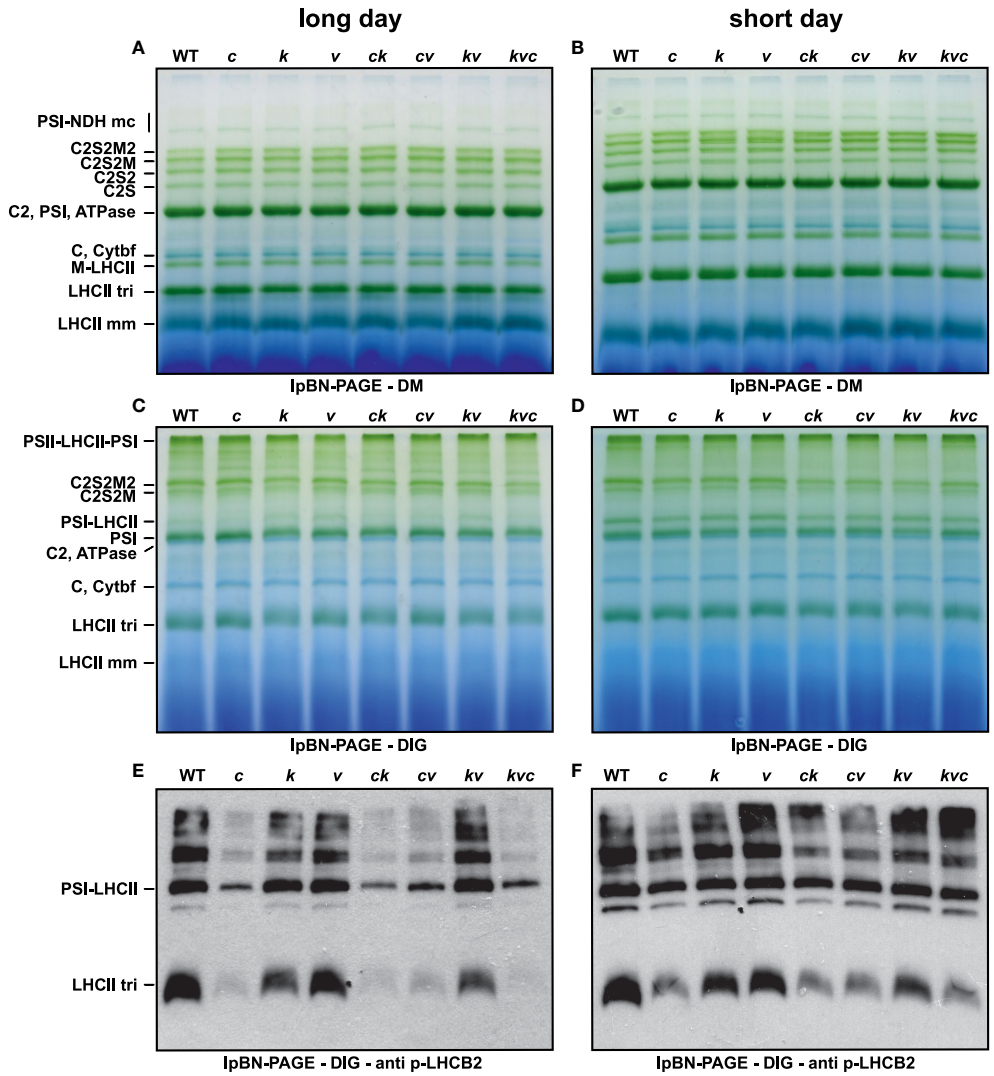

FIGURE 2
Levels of thylakoid protein complexes during long- and short-day conditions. Wild-type plants and mutants were grown using 16 h light (100 µmol photons m^{-2} s^{-1})/8 h dark cycles (long day) for 3 weeks **(A, C, E)** or 8 h light (120 µmol photons m^{-2} s^{-1})/16 h dark cycles (short day) for 5 weeks (**B, D, F**). **(A, B)** Large-pore blue-native gels (lpBN-PAGE) of thylakoids solubilized with 1% (w/v) n-dodecyl-β-D-maltoside (DM). **(C, D)** lpBN-PAGE of thylakoids solubilized with 1% (w/v) digitonin (DIG). **(E, F)** p-LHCB2 immunoblot from lpBN-PAGE of thylakoids solubilized with 1% (w/v) digitonin (DIG). Thylakoids were loaded on equal chlorophyll basis of 4 µg **(A–D)** and 1 µg **(E, F)**. WT – *Col-0*, *c* – *clce-2*, *k*– *kea3-1*, *v* – *vccn1-1*, *ck* – *clce-2kea3-1*, *cv* – *clce-2vccn1-1*, *kv* – *kea3-1vccn1-1*, and *kvc* – *kea3-1vccn1-1clce-2*.

Representative ECS recordings at two time points (210 s and 15 min) and three light intensities are shown for WT and *clce* in Supplementary Figure 3. Kinetics of PMF size and g_H^+ for the first 210 s are shown in Supplementary Figure 4. The complete kinetics are shown in Figure 4, and the steady-state values (at 15 min) in Figure 5.

LL was the condition where we observed a decreased level of LHCII phosphorylation in *clce* relative to WT (Figure 1). In LL we found a high total PMF at the onset of light up to 30 s in all genotypes (but slightly higher in the VCCN1-lacking mutants), then decreased and remained stable from 3 min until the end of illumination. There was no significant difference in PMF among the genotypes either at 210 s (Supplementary Figure 4, Supplementary Table 2) or 15 min (Figure 4). The g_H^+ parameter was low, stable, and similar among genotypes until 3 min (Supplementary Figure 4). The ATP synthase became gradually active up at 6 min and was fully functional until 15 min in WT (Figure 4). All ClCe-lacking mutants displayed a lower g_H^+ than WT during 6-15 min, suggesting a decreased ATP synthase activity. The plots in Figure 5 more clearly show

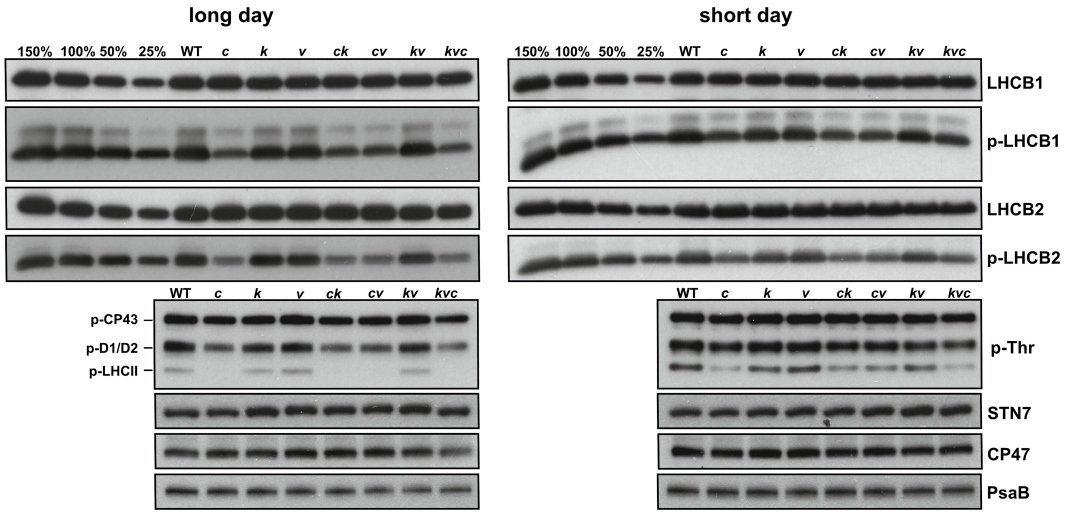

FIGURE 3
Thylakoid protein content and phosphorylation levels during long- and short-day conditions. Wild-type plants and mutants were grown using 16 h light (100 µmol photons m^{-2} s^{-1})/8 h dark cycles (long day) for 3 weeks or 8 h light (120 µmol photons m^{-2} s^{-1})/16 h dark cycles (short day) for 5 weeks. Immunoblots from thylakoids separated by SDS-PAGE and probed with LHCB1, p-LHCB1, LHCB2, p-LHCB2, p-Thr, STN7, CP47 (PSII) and PsaB (PSI) antibodies are shown. All thylakoids were loaded on equal chlorophyll basis of 0.5 µg, except 3 µg for STN7. 150%, 100%, 50% and 25% of WT samples were used as loading controls. WT – *Col-0*, *c* – *clce-2*, *k*– *kea3-1*, *v* – *vccn1-1*, *ck* – *clce-2kea3-1*, *cv* – *clce-2vccn1-1*, *kv* – *kea3-1vccn1-1*, and *kvc* – *kea3-1vccn1-1clce-2*.

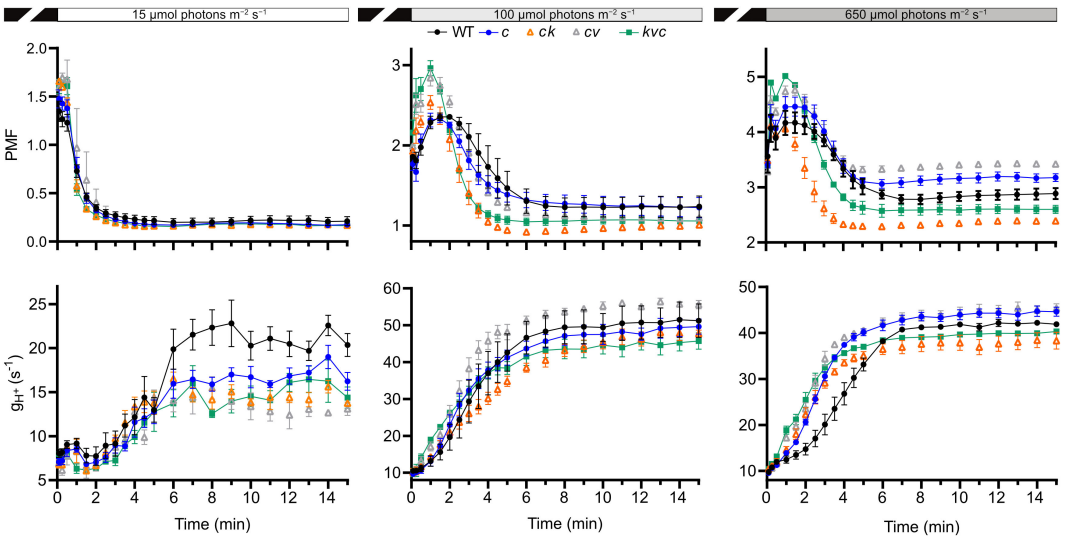

FIGURE 4
Kinetics of proton motive force and H^+ conductivity through ATP synthase. Electrochromic shift measurements (ECS) were performed on 30 min dark-acclimated wild-type and mutant plants grown in short-day conditions (120 µmol photons m^{-2} s^{-1}) and illuminated at the indicated intensities. Total proton motive force (PMF) and ATP synthase H^+ conductivity ($g_H{}^+$) were calculated from ECS decay kinetics as described in Methods. The plotted data are means ± S.E.M. (n = 6 plants). WT – *Col-0*, *c* – *clce-2*, *k*– *kea3-1*, *v* – *vccn1-1*, and *kvc* – *kea3-1vccn1-1clce-2*. Induction kinetics for the first 210 illumination are presented in Supplementary Figure 4.

10.3389/fpls.2022.1050355

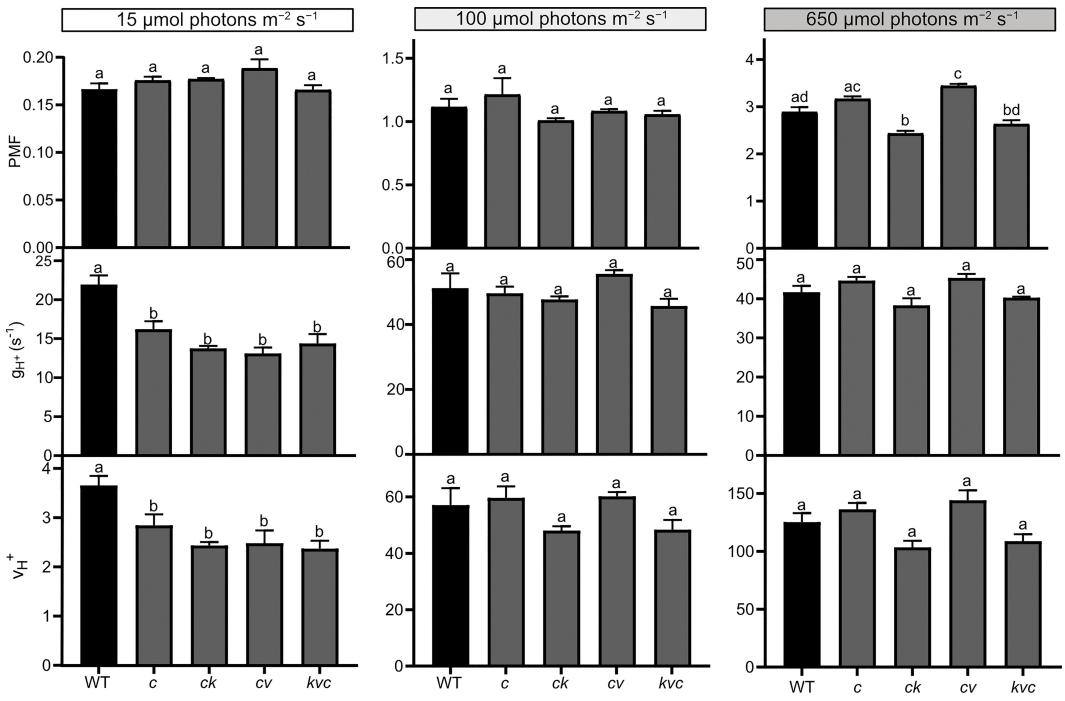

FIGURE 5
Steady-state proton motive force, H^+ conductivity and H^+ flux through the ATP synthase. Electrochromic shift measurements (ECS) were performed on 30 min dark-acclimated wild-type (WT) and mutant plants grown in short-day conditions (120 µmol photons m^{-2} s^{-1}) and illuminated for 15 min at the indicated intensities. Total proton motive force (PMF), ATP synthase H^+ conductivity ($g_H{}^+$) and H^+ flux ($v_H{}^+$) were calculated from ECS decay kinetics as described in Methods. The plotted data were obtained from Figure 4 and represent means ± S.E.M. (n = 6 plants). WT – *Col-0*, *c* – *clce-2*, *k*– *kea3-1*, *v* – *vccn1-1*, and *kvc* – *kea3-1vccn1-1clce-2*. Different letters denote statistically significant differences among genotypes according to ANOVA (P< 0.05).

that while there was no significant difference in PMF size, the $g_H{}^+$ in *clce* was significantly lower as compared to WT (by 40%), and that additional mutations in KEA3 and VCCN1 did not interfere with these patterns. We have also plotted the $v_H{}^+$ at the last time point of illumination (15 min) showing significantly lower values in the *clce* mutants in LL conditions.

Lower levels of LHCII phosphorylation were also observed in *clce* mutants relative to WT in GL conditions (Figure 3). The PMF size in GL was high until 2-3 min (Supplementary Figure 4), declined until 6 min and remained stable until the end of illumination (Figure 4). PMF size did not differ between WT and the *clce* single line throughout the illumination. Nevertheless, PMF size was higher up to 2 min in VCCN1-lacking mutants (*clcevccn1* and *kea3 vccn1clce*), lower between 2-6 min in the lines lacking KEA3 (*kea3clce* and *kea3vccn1clce)* and reached WT levels in all genotypes by the end of illumination. The PMF size was significantly lower in KEA3-lacking lines at 210 s (Supplementary Table 2), and like WT at the end of illumination (Figure 5). By the time PMF size became low and stable (6 min), the $g_H{}^+$ raised and reached maximal steady state levels, which were not significantly different among the genotypes (Figure 5). Also, the steady state $v_H{}^+$ was like WT in all mutants in GL conditions (Figure 5).

Even though LHCII phosphorylation does not take place in HL, PSII core protein phosphorylation occurs under these conditions (Figure 1), prompting us to record ECS for comparison with LL and GL. All genotypes displayed a high PMF for 2-3 min (Supplementary Figure 4), declined until 6 min and remained stable until the end of illumination (Figure 4). However, the VCCN1-lacking lines (*clcevccn1* and *kea3 vccn1clce*) displayed higher PMF in the first min and the KEA3-lacking lines (*kea3clce* and *kea3 vccn1clce*) had lower PMF throughout the illumination. In fact, intermediate levels were observed in the triple mutant relative to *clcevccn1* and *clcekea3*. The $g_H{}^+$ was significantly higher in all *clce* mutants than in WT at the beginning of illumination (Supplementary Figure 4, Supplementary Table 2). The $g_H{}^+$ continued to be higher up to 6 min when it became stable and similar to WT (Figure 4). The observed discrepancies between differences in PMF and $g_H{}^+$ at HL indicate that additional mechanisms for H^+ efflux across thylakoids may be functional in *clce* mutants under these light conditions before the ATP synthase becomes fully

active. The lack of significant differences in g_H^+ and v_H^+ among the genotypes at 15 min (Figure 5) are in line with the similar PSII core phosphorylation levels observed as early as at 15 min of illumination (Figure 1). Taken together, our data suggest that specifically ClCe loss-of-function significantly slows down H^+ efflux through the ATP synthase in the LL conditions, without impacting PMF size, and thus less ATP may become available for LHCII phosphorylation.

Inside the chloroplast, in addition to protein phosphorylation, ATP drives the highly energy-demanding CO_2 fixation. To investigate if a deficit of ATP affected this process, plants grown at 120 µmol photons m^{-2} s^{-1} were illuminated at 30, 150 and 700 µmol photons m^{-2} s^{-1} for 5, 15, 30 min, 1 h, 2 h, 5 h and 8 h. We did not observe any differences in net photosynthesis (A_n) among the genotypes at none of the tested light intensities and time points (Supplementary Figure 5), implying that the observed variation in H^+ efflux through the ATP synthase in the *clce* lines (Figure 5) did not impact CO_2 fixation. This result is in line with the WT-like growth of all mutants when grown in standard light (Supplementary Figures 1, 2).

Phenotypic analyses of plants grown in light-limiting conditions

Since the ATP synthase activity of *clce* was reduced in LL, the main emphasis was put on the growth and photosynthetic phenotype of plants grown in light-limiting conditions. The *clce* plants grown for 5-8 months at 15 µmol photons m^{-2} s^{-1} displayed smaller leaves with elongated petioles and significantly longer stem as compared to WT (Supplementary Figures 6A–E). The elongated stem likely represents a shade avoidance trait that plants normally develop when growing in limiting light (Franklin, 2008). Even though also observed in WT, this growth phenotype was more pronounced in the *clce* mutant, likely as a trade-off to get closer to the light source and absorb more light. The maximum PSII efficiency in the dark-acclimated state measured with Handy-PEA was slightly but significantly lower in *clce* than in WT (Supplementary Figure 6F).

Due to the small leaf size of plants grown at 15 µmol photons m^{-2} s^{-1}, we could not perform Chl fluorescence induction nor ECS kinetics in the light-acclimated state with the Dual-PAM 100. Instead, we used an Imaging FluorCam and further assessed the photosynthetic performance of *clce* plants relative to WT at 6 min of illumination at 15, 100 and 650 µmol photons m^{-2} s^{-1}. The maximum PSII efficiency in the dark state (F_v/F_m) was significantly lower in *clce* as compared to WT (Table 1) in line with the data obtained with Handy-PEA (Supplementary Figure 6F). During illumination, PSII efficiency (Y(II)) decreased with increasing light intensity and was significantly lower in *clce* than in WT at 15 µmol photons m^{-2} s^{-1}. The yield of non-regulated energy dissipation (Y(NO)) increased with increase in light intensity and was significantly higher in *clce* than in WT at 15 µmol photons m^{-2} s^{-1}. The yield of regulated NPQ (Y(NPQ)) increased with increasing light intensity and was not significantly different between WT and *clce*. Similar results were obtained for the NPQ parameter. Estimation of the fraction of open PSII centers, qL (Kramer et al. (2004), showed a clear decline with increase in light intensity and was significantly lower in *clce* compared to WT at 15 µmol photons m^{-2} s^{-1}.

Since assimilated CO_2 is transiently stored as starch in leaf chloroplasts during the day and is broken down during the night to supply energy for metabolism and growth, we next investigated the starch accumulation at the end of the day and night in WT plants and the *clce* mutant grown at 15 µmol photons m^{-2} s^{-1}. As shown in Supplementary Figure 7A, higher levels of starch (darker coloration) accumulated in the *clce* at the end of the light cycle. Moreover, *clce* also showed less depletion of starch at the end of the dark period relative WT

TABLE 1 Chlorophyll fluorescence parameters of plants grown in light-limiting conditions.

Parameter	15 µmol photons m^{-2} s^{-1}		100 µmol photons m^{-2} s^{-1}		650 µmol photons m^{-2} s^{-1}	
	WT	*clce*	WT	*clce*	WT	*clce*
F_v/F_m	0.823 ± 0.003	0.802 ± 0.005*				
Y(II)	0.741 ± 0.017	0.712 ± 0.014*	0.282 ± 0.035	0.312 ± 0.077	0.158 ± 0.044	0.137 ± 0.019
Y(NO)	0.216 ± 0.018	0.249 ± 0.024*	0.364 ± 0.019	0.353 ± 0.019	0.410 ± 0.019	0.408 ± 0.027
Y(NPQ)	0.043 ± 0.008	0.039 ± 0.023	0.354 ± 0.029	0.335 ± 0.061	0.432 ± 0.028	0.456 ± 0.019
NPQ	0.199 ± 0.043	0.165 ± 0.097	0.977 ± 0.096	0.944 ± 0.143	1.055 ± 0.073	1.124 ± 0.144
qL	0.693 ± 0.048	0.607 ± 0.035*	0.161 ± 0.025	0.210 ± 0.062	0.099 ± 0.028	0.091 ± 0.012

Wild type (WT) plants and the *clce* mutant were grown in short-day conditions at 15 µmol photons m^{-2} s^{-1} for 8 months. Plants were acclimated for 20 min in darkness and then illuminated at the given intensities for 6 min in a closed FluorCam. Chlorophyll fluorescence was recorded during illumination and the following parameters were calculated as described in Methods: F_v/F_m – the maximum PSII quantum yield, Y(II) – the PSII quantum yield in the light, Y(NO) – the quantum yield of non-regulated energy dissipation, Y(NPQ) – the quantum yield of regulated non-photochemical quenching, NPQ – non-photochemical quenching, and qL – the fraction of open PSII centers based on a lake model. Data are the means ± S.E.M. (n ≥ 4 leaves). Asterisks denote statistically significant differences between WT and *clce* according to Student's t-test (P< 0.05).

(Supplementary Figure 7B), indicating decreased rates of breakdown. Comparing the dark and light periods, starch was not at all degraded during the night in *clce*, whereas there was clearly more starch in light than in dark in the WT. Taken together, these data provide evidence that the ClCe loss-of-function in plants grown in light limiting conditions results in decreased photosynthetic performance, altered starch metabolism and growth.

ClCe expression levels and upregulation of other genes

We also investigated if *ClCe, KEA3* and *VCCN1* gene expression changes in WT versus *clce, kea3* and *vccn1* single mutants grown in standard GL light and exposed at three intensities (GL, LL and HL) over a time course of 3 and 8 h. The relative expression of *CLCe* did not change in WT over time nor in different light conditions versus darkness (Figure 6A and Supplementary Figure 8A). *KEA3* expression in WT did not differ between LL and GL relative to darkness, but it was significantly higher at 3 h in HL (3-fold), while *KEA3* expression in *clce* was upregulated to similar levels in comparison to darkness (5-fold) at all three light intensities (Figure 6A and Supplementary Figures 8A, B). *VCCN1* expression in WT did not significantly differ between LL and GL relative to darkness, however HL significantly upregulated it (6-fold, Figure 6A). In *clce*, the expression of *VCCN1* was upregulated 5-fold in LL and GL relative to darkness and 10-fold in HL (Figure 6A). The expression of *ClCe* was not altered relative to darkness in *kea3* and *vccn1* mutants at any of the three studied light intensities (Supplementary Figures 8C, D). The expression of *VCCN1* gene was upregulated after 8 h in HL in the *kea3* mutant, and of *KEA3* expression in the *vccn1* mutant.

In plants grown at 15 µmol photons m^{-2} s^{-1}, the expression of *ClCe* in WT leaves was upregulated 3-fold relative to darkness (Figure 6B), supporting the importance of ClCe in this light condition. The upregulation of *CLCe* expression may be a long-term acclimation strategy during growth in light-limiting conditions since no such effect was observed in WT leaves after up to 8 h exposure to LL (Figure 6A). The expression of *KEA3* gene was similar in WT and *clce* (3-4-fold upregulation versus darkness), whereas *VCCN1* expression was higher in *clce* (5-fold) versus WT (3-fold) (Figure 6B). Notably, when comparing the fold changes in Figures 6A, B, the upregulation of *KEA3* and *VCCN1* in *clce* was maximal in LL already at 3 h, since no large changes happened during growth in such light-limiting conditions.

Discussion

ClCe functions in the thylakoid membrane where also VCCN1 and KEA3 are active, although in different light conditions and with different kinetics. KEA3 and VCCN1 are particularly important in photosynthetic acclimation in the first minutes of constant illumination and under fluctuating light conditions (Dukic et al., 2019; Li et al., 2021). Good evidence exists that ClCe regulates electron transport through photosystems during illumination in constant light later in time than VCCN1 and KEA3 (Dukic et al., 2019) and during state transitions (Herdean et al., 2016a), but the mechanism has remained unclear. Previous studies investigating KEA3 (Correa Galvis et al., 2020), VCCN1 (Herdean et al., 2016b) and ClCe (Herdean et al., 2016a) found that VCCN1 and ClCe affected the PMF and the ATP synthase activity in high light conditions. Here we show that ClCe regulates ATP availability for LHCII phosphorylation and in this way maximizes photosynthetic performance particularly under light-limiting conditions.

Role of ClCe in the regulation of electron transport and ATP production

The growth and F_v/F_m of *clce* in standard light (100-120 µmol photons m^{-2} s^{-1}) were like WT (Supplementary Figures 1, 2). When grown in limiting light (15 µmol photons m^{-2} s^{-1}), there were differences in growth (Supplementary Figure 6) and slightly, but significantly lower F_v/F_m, lower Y(II) and higher Y (NO) for *clce* plants (Table 1), suggesting that ClCe plays a role in regulation of electron transport in low light. We could not perform ECS measurements due to the small leaf size of these plants. Nevertheless, when plants grown in standard GL light were exposed for 10 min to LL, the g_H^+ as well as v_H^+ of *clce* significantly decreased (by 40%) relative to WT (Figure 5). The total PMF which drives ATP synthesis did not differ between WT and mutants, excluding the PMF size as a cause for the observed reduction in g_H^+. We do not know at present how the overall higher relative expression of *VCCN1* and *KEA3* in the *clce* mutant than in WT (Figure 6) could account for the observed differences in PMF and g_H^+ (Figure 5). Moreover, additional mutations in KEA3 and VCCN1 did neither enhance or reduce the effect on g_H^+ and v_H^+ in *clce*, suggesting that ClCe alone is a regulator of ATP synthase activity in low light conditions.

To dissect the mechanism behind the effect on ATP synthase activity, it is necessary to consider its possible regulators in low light. Kohzuma et al. (2017) proposed that the PMF generated already at very low light intensity (10 µmol photons m^{-2} s^{-1}) is far above to what is needed to activate the ATP synthase, suggesting that PMF acts more as a dark-light switch rather than a finetuning mechanism. Another important modulator is the NADPH-dependent thioredoxin reductase C (NTRC) affecting the redox state of the ATP synthase γ-subunit thiols (Nikkanen et al., 2016). Like *clce*, the *ntrc* mutants had a lower g_H^+ than WT in low light, but in contrast to *clce*, *ntrc* displayed a high PMF, higher NPQ and lower electron transport rate than WT (Carrillo et al., 2016), excluding that the NTRC activity was affected in our mutants. Kanazawa and Kramer (2002) postulated that the g_H^+ is modulated

10.3389/fpls.2022.1050355

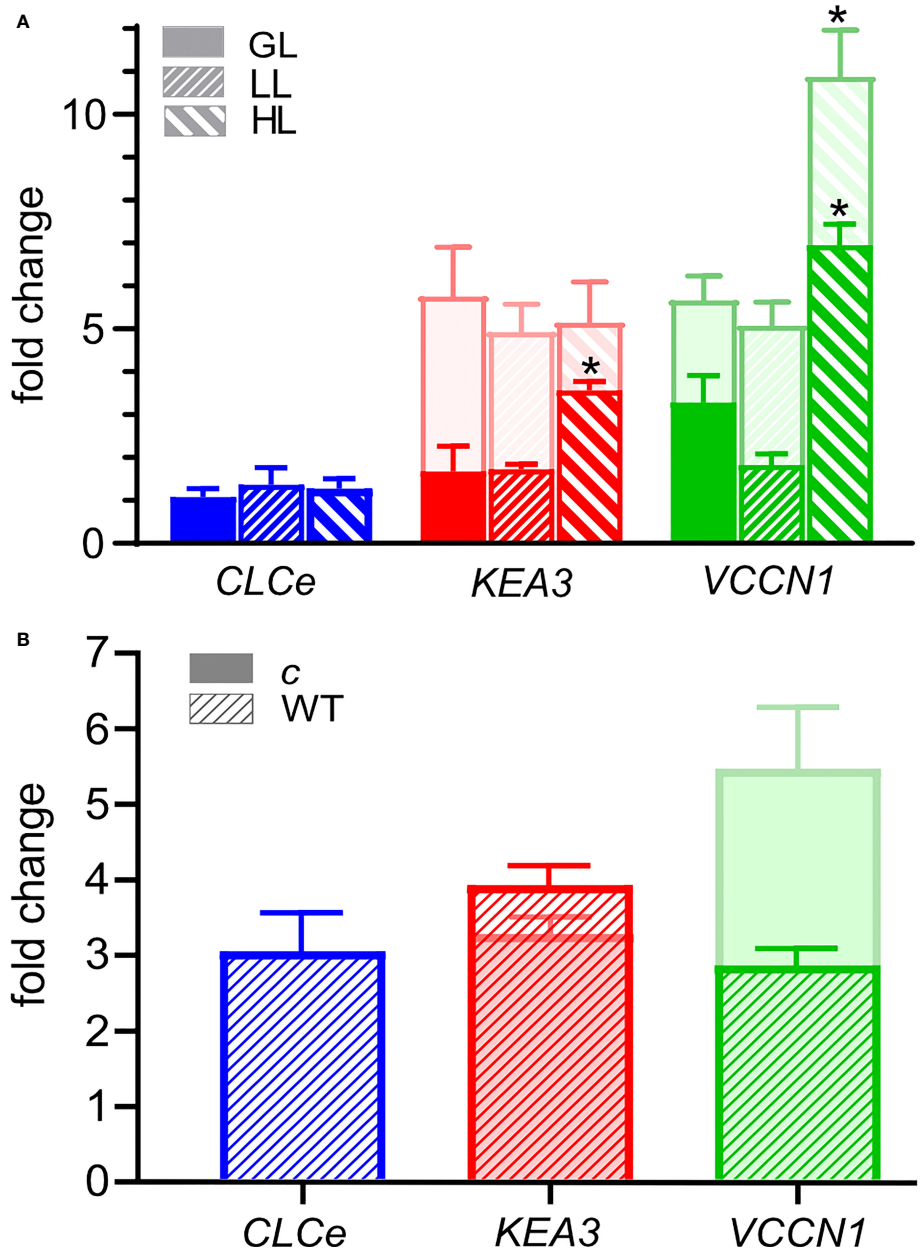

FIGURE 6
Fold change in the expression of *CLCe*, *KEA3* and *VCCN1* genes. **(A)** Wild type plants (WT, front bars) and *clce* mutants (bars behind, lighter color) were grown in short-day conditions with 8 h light (120 µmol photons m^{-2} s^{-1})/16 h dark for 6 weeks. Total RNA was isolated after 16-h dark and 3 h exposure to low light (LL, 15 µmol photons m^{-2} s^{-1}), growth light (GL, 120 µmol photons m^{-2} s^{-1}) or high light (HL, 650 µmol photons m^{-2} s^{-1}), and changes in transcript abundance were determined by quantitative RT-PCR analysis. The expression of *CLCe, KEA3* and *VCCN1* genes was calculated relative to two reference genes and normalized to expression in samples collected after the 16-h of dark period. Data are the means ± S.E.M. (n = 4). Asterisks denote a statistically significant difference between each of the light treatments and the dark control according to Student's t-test (P< 0.05). **(B)** WT and *clce* plants were grown in short-day LL condition (15 µmol photons m^{-2} s^{-1}) for 8 months. Total RNA was isolated after 16-h dark and 3 h exposure to LL and changes in transcript abundance were determined by quantitative RT-PCR analysis. The relative expression of *CLCe, KEA3* and *VCCN1* genes was calculated as in **(A)**. Data are the means ± S.E.M. (n = 4).

by stromal metabolite levels, possibly by inorganic phosphate (Pi). Indeed, decreases in g_H^+ were reported in Pi deprivation and thylakoid Pi transporter PHT4;1 loss-of-function and were associated with high NPQ and low electron transport rates (Karlsson et al., 2015; Carstensen et al., 2018). However, we did not see any evidence of Pi limitation in our growth conditions. We postulate that H^+ are supplied to the ATP synthase by a H^+/Cl^- exchange activity of ClCe to explain its role in g_H^+ regulation.

Phylogenetic analysis of the ClC family indicated that the ClCe sequence is highly similar to bacterial ClCs, shown to function as H^+/Cl^- antiporters, and that its closest homologue is ClCf (Pfeil et al., 2014). Also, animal ClCs function as H^+/Cl^- exchangers in organellar membranes while they work as Cl^- channels at the plasma membrane (Jentsch, 2015). Since three selectivity filter residues important for H^+ (gating glutamate, proton glutamate) and Cl^- binding (Schrecker et al., 2020) are fully conserved in ClCe and ClCf, they are likely also working as exchangers (Scholl et al., 2021). ClCf is located on trans Golgi network, a compartment involved in protein transport to their destination. Here ClCf works together with the V-ATPase to maintain pH and ion homeostasis. By analogy, in chloroplasts a concerted action of ClCe and the ATP synthase may be required to maintain the optimal pH in low light. Like other ClCs, the amino acid sequence of ClCe consists of a transmembrane component for ion transport and a regulatory cystathionine beta-synthase (CBS)-pair domain which binds nucleotides (Dutzler et al., 2002). The ATP pool may vary according to the photosynthetic status of the chloroplast in different light conditions. We propose that the CBS domain is sensitive to a low ATP concentration in low light and activates ClCe to export Cl^- to stroma and import H^+ into the thylakoid lumen which in turn stimulates ATP synthesis.

A reduced ATP synthase activity in low light should impact various energy-dependent processes in the chloroplast. Indeed, *clce* displayed reduced starch degradation (Supplementary Figure 7), a process occurring in darkness and with high demand of ATP for the first phase taking place inside the chloroplast (Stitt and Zeeman, 2012). Since we observed no effect on carbon fixation (Supplementary Figure 5), we focus below our discussion on the LHCII phosphorylation that was most affected, and on its consequence for state transitions in low light conditions.

Role of ClCe in LHCII protein phosphorylation and state transitions

Among the studied thylakoid ion channels/transporters, a role in state transitions was proposed for ClCe (Herdean et al., 2016a). The envelope located KEA1 and KEA2 have been also studied, but no differences in either LHCII phosphorylation or state transitions could be found in the corresponding mutants (Koskela et al., 2018). Here we show a decreased level of LHCII phosphorylation in *clce* in low light (Figure 1). Among the factors that could be responsible for this effect, we exclude changes of the levels of protein substrates (LHCB1 and LHCB2) and of the involved STN7 kinase as they were unaltered in *clce* (Figure 3). The redox state of the PSII acceptor side, based on the qL parameter, was significantly more reduced in *clce* than in WT in low light, likely leading to an increase in non-regulated energy dissipation, Y(NO) (Table 1). This fluorescence phenotype resembles the reported increase in steady-state fluorescence levels (F/F_m) in mutants lacking STN7 (Grieco et al., 2012; Tikkanen et al., 2017), thus supporting the notion of affected state-transitions. The only conceivable factor for the scarcity of LHCII phosphorylation is the ATP availability which was lower in *clce* as based on the 40% reduced g_H^+ and v_H^+ (Figure 5). Availability of ATP as a driving force of state transitions in low light has not been emphasized previously, but in this study, we bring strong evidence for this type of regulation mediated by ClCe. A lower level of LHCII phosphorylation in *clce* was also observed in GL conditions (Figure 3). Since neither ATP synthase activity nor Y(NO) were significantly different, other factors could have prevented accumulation of phosphorylated LHCII in GL conditions.

For a long time, phosphorylation of LHCII was the main factor required for migration of LHCII during state transitions. Based on the decreased levels of LHCII phosphorylation, a slower migration would be expected in *clce*. However, Herdean et al. (2016a) reported a faster transition from state 1 to state 2 in this mutant as compared to WT, meaning a faster migration of LHCII from PSII to PSI. It should be noted that the rate of state transitions is also affected by the antenna composition of PSII (Kovacs et al., 2006) and PSI (Damkjaer et al., 2009). However, since KCl-pretreatment partially alleviated the faster state transition in *clce*, other factors like negative charges, could also influence the migration. Lack of the NUCLEAR SHUTTLE INTERACTING (NSI), enzyme for Lys acetylation of specific PSI, PSII, and LHCII subunits, slowed down state transitions despite similar levels of LHCII phosphorylation (Koskela et al., 2018). The authors proposed that a deficit of negative charges on the stromal side inhibited LHCII migration from PSII to PSI. Faster state transitions were reported in loss of function of the PsbW protein, known to harbor a stromal-exposed C-terminus rich in negative charges (Garcia-Cerdan et al., 2011). It can be reasoned that *clce* must have an excess of negative charges inside the lumen, leading to enhanced mobility and migration of LHCII in the membrane despite the decreased phosphorylation levels. Since KCl-pretreatment of leaves slowed down state transitions (even in WT) (Herdean et al., 2016a), this treatment likely balanced the distribution of negative charges on the two sides of the thylakoid membrane. We can conclude that while phosphorylation facilitates a more controlled LHCII migration, other factors increasing the negative charges of the LHC proteins also regulate state transitions.

Mutations in genes encoding ClCs lead to physiological disorders, including severe diseases in humans. The results of our phenotypic analyses reveal that ClCe regulates ATP availability for LHCII protein phosphorylation in state transitions. Since ClCe function is important for plant acclimation to low light, more in-depth studies are required for future applications towards crop improvement.

Data availability statement

The original contributions presented in the study are included in the article/Supplementary Material. Further inquiries can be directed to the corresponding author.

Author contributions

ED, PJG, AH, E-MA, and CS conceived the study and designed the experiments. ED carried out the ECS, Chl fluorescence and CO_2 fixation measurements, starch staining and qRT-PCR. SG contributed to the analysis and interpretation of the Chl fluorescence data. VP and PJG carried out the phosphorylation experiments and immunoblotting. ED, SG, E-MA, and CS wrote the manuscript. All authors contributed to the article and approved the submitted version.

Funding

This work was supported by the Swedish Research Council VR 2016-03836 and 2021-03790 (CS), and Jane and Aatos Erkko Foundation (E-MA).

Conflict of interest

The authors declare that the research was conducted in the absence of any commercial or financial relationships that could be construed as a potential conflict of interest.

Publisher's note

Supplementary material

The Supplementary Material for this article can be found online at: https://www.frontiersin.org/articles/10.3389/fpls.2022.1050355/full#supplementary-material

References

Carrillo, L. R., Froehlich, J. E., Cruz, J. A., Savage, L. J., and Kramer, D. M. (2016). Multi-level regulation of the chloroplast ATP synthase: the chloroplast NADPH thioredoxin reductase c (NTRC) is required for redox modulation specifically under low irradiance. *Plant J.* 87, 654–663. doi: 10.1111/tpj.13226

Carstensen, A., Herdean, A., Schmidt, S. B., Sharma, A., Spetea, C., Pribil, M., et al. (2018). The impacts of phosphorus deficiency on the photosynthetic electron transport chain. *Plant Physiol.* 177, 271–284. doi: 10.1104/pp.17.01624

Correa Galvis, V., Strand, D. D., Messer, M., Thiele, W., Bethmann, S., Hubner, D., et al. (2020). H(+) transport by K(+) EXCHANGE ANTIPORTER3 promotes photosynthesis and growth in chloroplast ATP synthase mutants. *Plant Physiol.* 182, 2126–2142. doi: 10.1104/pp.19.01561

Crepin, A., and Caffarri, S. (2015). The specific localizations of phosphorylated Lhcb1 and Lhcb2 isoforms reveal the role of Lhcb2 in the formation of the PSI-LHCII supercomplex in Arabidopsis during state transitions. *Biochim. Biophys. Acta* 1847, 1539–1548. doi: 10.1016/j.bbabio.2015.09.005

Crepin, A., and Caffarri, S. (2018). Functions and evolution of Lhcb isoforms composing LHCII, the major light harvesting complex of photosystem II of green eukaryotic organisms. *Curr. Protein Pept. Sci.* 19, 699–713. doi: 10.2174/1389203719666180222101534

Croce, R. (2020). Beyond 'seeing is believing': the antenna size of the photosystems *in vivo*. *New Phytol.* 228, 1214–1218. doi: 10.1111/nph.16758

Cruz, J. A., Avenson, T. J., Kanazawa, A., Takizawa, K., Edwards, G. E., and Kramer, D. M. (2005). Plasticity in light reactions of photosynthesis for energy production and photoprotection. *J. Exp. Bot.* 56, 395–406. doi: 10.1093/jxb/eri022

Cruz, J. A., Sacksteder, C. A., Kanazawa, A., and Kramer, D. M. (2001). Contribution of electric field (Delta psi) to steady-state transthylakoid proton motive force (pmf) *in vitro* and *in vivo*. control of pmf parsing into delta psi and delta pH by ionic strength. *Biochemistry* 40, 1226–1237. doi: 10.1021/bi0018741

Damkjaer, J. T., Kereiche, S., Johnson, M. P., Kovacs, L., Kiss, A. Z., Boekema, E. J., et al. (2009). The photosystem II light-harvesting protein Lhcb3 affects the macrostructure of photosystem II and the rate of state transitions in Arabidopsis. *Plant Cell* 21, 3245–3256. doi: 10.1105/tpc.108.064006

Dukic, E., Herdean, A., Cheregi, O., Sharma, A., Nziengui, H., Dmitruk, D., et al. (2019). K(+) and Cl(-) channels/transporters independently fine-tune photosynthesis in plants. *Sci. Rep.* 9, 8639. doi: 10.1038/s41598-019-44972-z

Dutzler, R., Campbell, E. B., Cadene, M., Chait, B. T., and MacKinnon, R. (2002). X-Ray structure of a ClC chloride channel at 3.0 A reveals the molecular basis of anion selectivity. *Nature* 415, 287–294. doi: 10.1038/415287a

Finazzi, G., Petroutsos, D., Tomizioli, M., Flori, S., Sautron, E., Villanova, V., et al. (2015). Ions channels/transporters and chloroplast regulation. *Cell Calcium* 58, 86–97. doi: 10.1016/j.ceca.2014.10.002

Franklin, K. A. (2008). Shade avoidance. *New Phytol.* 179, 930–944. doi: 10.1111/j.1469-8137.2008.02507.x

Garcia-Cerdan, J. G., Kovacs, L., Toth, T., Kereiche, S., Aseeva, E., Boekema, E. J., et al. (2011). The PsbW protein stabilizes the supramolecular organization of photosystem II in higher plants. *Plant J.* 65, 368–381. doi: 10.1111/j.1365-313X.2010.04429.x

Genty, B., Briantais, J.-M., and Baker, N. R. (1989). The relationship between the quantum yield of photosynthetic electron transport and quenching of chlorophyll fluorescence. *Biochim. Biophys. Acta* 990, 87–92. doi: 10.1016/S0304-4165(89)80016-9

Grieco, M., Suorsa, M., Jajoo, A., Tikkanen, M., and Aro, E. M. (2015). Light-harvesting II antenna trimers connect energetically the entire photosynthetic machinery - including both photosystems II and I. *Biochim. Biophys. Acta* 1847, 607–619. doi: 10.1016/j.bbabio.2015.03.004

Grieco, M., Tikkanen, M., Paakkarinen, V., Kangasjarvi, S., and Aro, E. M. (2012). Steady-state phosphorylation of light-harvesting complex II proteins preserves photosystem I under fluctuating white light. *Plant Physiol.* 160, 1896–1910. doi: 10.1104/pp.112.206466

Herdean, A., Nziengui, H., Zsiros, O., Solymosi, K., Garab, G., Lundin, B., et al. (2016a). The Arabidopsis thylakoid chloride channel AtCLCe functions in chloride homeostasis and regulation of photosynthetic electron transport. *Front. Plant Sci.* 7, 115. doi: 10.3389/fpls.2016.00115

Herdean, A., Teardo, E., Nilsson, A. K., Pfeil, B. E., Johansson, O. N., Unnep, R., et al. (2016b). A voltage-dependent chloride channel fine-tunes photosynthesis in plants. *Nat. Commun.* 7, 11654. doi: 10.1038/ncomms11654

Hohner, R., Galvis, V. C., Strand, D. D., Volkner, C., Kramer, M., Messer, M., et al. (2019). Photosynthesis in Arabidopsis is unaffected by the function of the vacuolar K(+) channel TPK3. *Plant Physiol.* 180, 1322–1335. doi: 10.1104/pp.19.00255

Jarvi, S., Suorsa, M., Paakkarinen, V., and Aro, E. M. (2011). Optimized native gel systems for separation of thylakoid protein complexes: novel super- and mega-complexes. *Biochem. J.* 439, 207–214. doi: 10.1042/BJ20102155

Jentsch, T. J. (2015). Discovery of CLC transport proteins: cloning, structure, function and pathophysiology. *J. Physiol.* 593, 4091–4109. doi: 10.1113/JP270043

Kanazawa, A., and Kramer, D. M. (2002). *In vivo* modulation of nonphotochemical exciton quenching (NPQ) by regulation of the chloroplast ATP synthase. *Proc. Natl. Acad. Sci. U.S.A.* 99, 12789–12794. doi: 10.1073/pnas.182427499

Karlsson, P. M., Herdean, A., Adolfsson, L., Beebo, A., Nziengui, H., Irigoyen, S., et al. (2015). The Arabidopsis thylakoid transporter PHT4;1 influences phosphate availability for ATP synthesis and plant growth. *Plant J.* 84, 99–110. doi: 10.1111/tpj.12962

Kohzuma, K., Froehlich, J. E., Davis, G. A., Temple, J. A., Minhas, D., Dhingra, A., et al. (2017). The role of light-dark regulation of the chloroplast ATP synthase. *Front. Plant Sci.* 8, 1248. doi: 10.3389/fpls.2017.01248

Koskela, M. M., Brunje, A., Ivanauskaite, A., Grabsztunowicz, M., Lassowskat, I., Neumann, U., et al. (2018). Chloroplast acetyltransferase NSI is required for state transitions in *Arabidopsis thaliana*. *Plant Cell* 30, 1695–1709. doi: 10.1105/tpc.18.00155

Kovacs, L., Damkjaer, J., Kereiche, S., Ilioaia, C., Ruban, A. V., Boekema, E. J., et al. (2006). Lack of the light-harvesting complex CP24 affects the structure and function of the grana membranes of higher plant chloroplasts. *Plant Cell* 18, 3106–3120. doi: 10.1105/tpc.106.045641

Kramer, D. M., Johnson, G., Kiirats, O., and Edwards, G. E. (2004). New fluorescence parameters for the determination of QA redox state and excitation energy fluxes. *Photosynth. Res.* 79, 209. doi: 10.1023/B:PRES.0000015391.99477.0d

Laemmli, U. K. (1970). Cleavage of structural proteins during the assembly of the head of bacteriophage T4. *Nature* 227, 680–685. doi: 10.1038/227680a0

Li, M., Svoboda, V., Davis, G., Kramer, D., Kunz, H. H., and Kirchhoff, H. (2021). Impact of ion fluxes across thylakoid membranes on photosynthetic electron transport and photoprotection. *Nat. Plants* 7, 979–988. doi: 10.1038/s41477-021-00947-5

Messant, M., Krieger-Liszkay, A., and Shimakawa, G. (2021). Dynamic changes in protein-membrane association for regulating photosynthetic electron transport. *Cells* 10, 1216. doi: 10.3390/cells10051216

Nikkanen, L., Toivola, J., and Rintamaki, E. (2016). Crosstalk between chloroplast thioredoxin systems in regulation of photosynthesis. *Plant Cell Environ.* 39, 1691–1705. doi: 10.1111/pce.12718

Oxborough, K., and Baker, N. R. (1997). Resolving chlorophyll a fluorescence images of photosynthetic efficiency into photochemical and non-photochemical components - calculation of qP and Fv'/Fm' without measuring f_0'. *Photosynth. Res.* 54, 135–142. doi: 10.1023/A:1005936823310

Pan, X., Ma, J., Su, X., Cao, P., Chang, W., Liu, Z., et al. (2018). Structure of the maize photosystem I supercomplex with light-harvesting complexes I and II. *Science* 360, 1109–1113. doi: 10.1126/science.aat1156

Pfeil, B. E., Schoefs, B., and Spetea, C. (2014). Function and evolution of channels and transporters in photosynthetic membranes. *Cell. Mol. Life Sci.* 71, 979–998. doi: 10.1007/s00018-013-1412-3

Porra, R. J., Thompson, W. A., and Kriedemann, P. E. (1989). Determination of accurate extinction coefficients and simultaneous-equations for assaying chlorophyll-a and chlorophyll-b extracted with four different solvents - verification of the concentration of chlorophyll standards by atomic-absorption spectroscopy. *Biochim. Biophys. Acta* 975, 384–394. doi: 10.1016/S0005-2728(89)80347-0

Rantala, M., Rantala, S., and Aro, E. M. (2020). Composition, phosphorylation and dynamic organization of photosynthetic protein complexes in plant thylakoid membrane. *Photochem. Photobiol. Sci.* 19, 604–619. doi: 10.1039/d0pp00025f

Rintamaki, E., Martinsuo, P., Pursiheimo, S., and Aro, E. M. (2000). Cooperative regulation of light-harvesting complex II phosphorylation *via* the plastoquinol and ferredoxin-thioredoxin system in chloroplasts. *Proc. Natl. Acad. Sci. U.S.A.* 97, 11644–11649. doi: 10.1073/pnas.180054297

Rintamaki, E., Salonen, M., Suoranta, U. M., Carlberg, I., Andersson, B., and Aro, E. M. (1997). Phosphorylation of light-harvesting complex II and photosystem II core proteins shows different irradiance-dependent regulation *in vivo*. application of phosphothreonine antibodies to analysis of thylakoid phosphoproteins. *J. Biol. Chem.* 272, 30476–30482. doi: 10.1074/jbc.272.48.30476

Scholl, S., Hillmer, S., Krebs, M., and Schumacher, K. (2021). ClCd and ClCf act redundantly at the trans-golgi network/early endosome and prevent acidification of the golgi stack. *J. Cell Sci.* 134, jcs258807. doi: 10.1242/jcs.258807

Schrecker, M., Korobenko, J., and Hite, R. K. (2020). Cryo-EM structure of the lysosomal chloride-proton exchanger CLC-7 in complex with OSTM1. *Elife* 9, e59555. doi: 10.7554/eLife.59555

Spetea, C., Herdean, A., Allorent, G., Carraretto, L., Finazzi, G., and Szabo, I. (2017). An update on the regulation of photosynthesis by thylakoid ion channels and transporters in Arabidopsis. *Physiol. Plant* 161, 16–27. doi: 10.1111/ppl.12568

Stitt, M., and Zeeman, S. C. (2012). Starch turnover: pathways, regulation and role in growth. *Curr. Opin. Plant Biol.* 15, 282–292. doi: 10.1016/j.pbi.2012.03.016

Szabo, I., and Spetea, C. (2017). Impact of the ion transportome of chloroplasts on the optimization of photosynthesis. *J. Exp. Bot.* 68, 3115–3128. doi: 10.1093/jxb/erx063

Tikkanen, M., and Aro, E. M. (2014). Integrative regulatory network of plant thylakoid energy transduction. *Trends Plant Sci.* 19, 10–17. doi: 10.1016/j.tplants.2013.09.003

Tikkanen, M., Rantala, S., Grieco, M., and Aro, E. M. (2017). Comparative analysis of mutant plants impaired in the main regulatory mechanisms of photosynthetic light reactions - from biophysical measurements to molecular mechanisms. *Plant Physiol. Biochem.* 112, 290–301. doi: 10.1016/j.plaphy.2017.01.014

Yokono, M., Takabayashi, A., Akimoto, S., and Tanaka, A. (2015). A megacomplex composed of both photosystem reaction centres in higher plants. *Nat. Commun.* 6, 6675. doi: 10.1038/ncomms7675

frontiers | Frontiers in Plant Science

TYPE Original Research
PUBLISHED 23 November 2022
DOI 10.3389/fpls.2022.1051340

OPEN ACCESS

EDITED BY
Pui Ying Lam,
Akita University, Japan

REVIEWED BY
Ali Taheri,
Tennessee State University, United States
Zhi Gang Meng,
Biotechnology Research institute of CAAS, China

*CORRESPONDENCE
Jean T. Greenberg
jgreenbe@uchicago.edu

SPECIALTY SECTION
This article was submitted to Plant Physiology, a section of the journal Frontiers in Plant Science

RECEIVED 22 September 2022
ACCEPTED 08 November 2022
PUBLISHED 23 November 2022

CITATION
Morgan JM, Jelenska J, Hensley D, Retterer ST, Morrell-Falvey JL, Standaert RF and Greenberg JT (2022) An efficient and broadly applicable method for transient transformation of plants using vertically aligned carbon nanofiber arrays.
Front. Plant Sci. 13:1051340.
doi: 10.3389/fpls.2022.1051340

An efficient and broadly applicable method for transient transformation of plants using vertically aligned carbon nanofiber arrays

Jessica M. Morgan[1], Joanna Jelenska[2], Dale Hensley[3], Scott T. Retterer[3,4], Jennifer L. Morrell-Falvey[4], Robert F. Standaert[5] and Jean T. Greenberg[2]*

[1]Biophysical Sciences, The University of Chicago, Chicago, IL, United States, [2]Department of Molecular Genetics and Cell Biology, The University of Chicago, Chicago, IL, United States, [3]Center for Nanophase Materials Science, Oak Ridge National Laboratory, Oak Ridge, TN, United States, [4]Biosciences Division, Oak Ridge National Laboratory, Oak Ridge, TN, United States, [5]Department of Chemistry, East Tennessee State University, Johnson City, TN, United States

Transient transformation in plants is a useful process for evaluating gene function. However, there is a scarcity of minimally perturbing methods for gene delivery that can be used on multiple organs, plant species, and non-excised tissues. We pioneered and demonstrated the use of vertically aligned carbon nanofiber (VACNF) arrays to efficiently perform transient transformation of different tissues with DNA constructs in multiple plant species. The VACNFs permeabilize plant tissue transiently to allow molecules into cells without causing a detectable stress response. We successfully delivered DNA into leaves, roots and fruit of five plant species (Arabidopsis, poplar, lettuce, *Nicotiana benthamiana*, and tomato) and confirmed accumulation of the encoded fluorescent proteins by confocal microscopy. Using this system, it is possible to transiently transform plant cells with both small and large plasmids. The method is successful for species recalcitrant to *Agrobacterium*-mediated transformation. VACNFs provide simple, reliable means of DNA delivery into a variety of plant organs and species.

KEYWORDS

transient plant transformation, nanomaterials, vertically aligned carbon nanofibers (VACNF), impalefection, fluorescence imaging

1 Introduction

The ability to introduce DNA into plants and achieve plant transformation has radically changed agriculture and provided a means to study fundamental processes in plants. Transformations can involve the integration of DNA into a plant genome (stable transformation) or the introduction of DNA into plant cells without the incorporation of transgenes into the genome (transient transformation) (Altpeter et al., 2016). Additionally, plastids, cellular organelles in plants with their own genomes, can be stably and transiently transformed (Maliga, 2004; Yu et al., 2020). Transient transformation is faster than stable transformation. It provides the opportunity to study the functions and regulation of genes either in single cells or within the context of plant organs (Birch, 1997; Sheen, 2001; Krenek et al., 2015). For example, reporters can be introduced to monitor transcriptional activation, the subcellular localization of proteins, and subcellular processes through the delivery of different molecular probes (Levy et al., 2018).

Three of the main methods employed for transient transformation in plants involve *Agrobacteria*, protoplast transfection, and particle bombardment. *Agrobacterium*-mediated transformation is limited to plant species, cultivars, and tissue types (roots, leaves, and seedlings) that are susceptible to this bacterium (Hwang et al., 2017). High cell densities of *Agrobacteria* are required to perform transient transformation (agroinfiltration), which can be harmful to plants (Karami, 2008; Li et al., 2009). For protoplast transfection, protoplasts are made *via* enzymatic breakdown of the cell wall after grinding up tissue. DNA is then delivered to the protoplasts *via* electroporation or polyethylene glycol using small vectors that are easy to manipulate. This process is advantageous because transient transformation can be achieved with a high frequency. Like *Agrobacterium*-mediated transformation, however, protoplast transfection is labor intensive, it requires optimization for each species (Baltes et al., 2017; Gou et al., 2020; Ren et al., 2020), and it does not allow studies of intact tissues. Finally, particle bombardment can be used to deliver DNA into a broader range of plants and tissues than agroinfiltration and protoplast transformation. The tissues to which particle bombardment can be applied include meristems, embryos, leaves, callus, stems, roots, pollen, styles, and petals (Lacroix and Citovsky, 2020). Particle bombardment, however, causes plant tissue damage when high bombardment pressures are used. Other limitations arise from the need to position plant material in the biolistic chamber or to align it with a gene gun, which limit the size of the specimen and the accessible sites (Haque et al., 2018; Mohan et al., 2019; Ozyigit and Yucebilgili Kurtoglu, 2020). Notably, all these methods affect plant physiology by inducing stress responses that may interfere with subsequent experiments using transiently transformed cells.

Nanomaterials are being developed for the delivery of biomolecules into plants because of their applicability to several different plant species and for their ability to increase transformation efficiency *in planta* (Kumar et al., 2020). The use of nanomaterials as vehicles for biomolecules has been widely studied in animal cells and tissues for drug delivery, but not in plants (McKnight et al., 2004; McKnight et al., 2005; Cunningham et al., 2018; Sanzari et al., 2019; Jain and Thareja, 2019; Jat et al., 2020). This may be due in part to the barriers presented by the cell wall and the fact that different plant species have varying physiologies, which need to be considered when addressing the interactions between the host environment and the nanomaterial (Pérez-de-Luque, 2017). To overcome the hurdles presented by plants, the size of the nanoparticles has been tuned, and surface modifications have been made to enable attachment of cargo to nanovehicles (Kumar et al., 2020). Some examples of these nanovehicles include: surface functionalized and pristine single walled carbon nanotubes (Liu et al., 2009; Demirer et al., 2019), mesoporous silica nanoparticles (MSNs) (Torney et al., 2007; Chang et al., 2013), gold nanoparticles and nanoparticles made of other materials coated with gold, polymeric nanoparticles (Zhang et al., 2019b), DNA nanostructures (Zhang et al., 2019), layered double hydroxide clay nanosheets (Mitter et al., 2017), magnetic nanoparticles (used for pollen magnetofection (Zhao et al., 2017)), silicon carbide whiskers (Arshad et al., 2013), and peptides as carriers for nucleic acids (Zheng et al., 2017; Jat et al., 2020). Of the nanovehicles used to deliver genes/DNA into plants, acicular shaped materials (carbon nanotubes) account for a large portion of the studies conducted. These materials have been delivered into plants through passive delivery, a needleless syringe, or with the aid of ultrasound, a magnetic field, or a gene gun (Jat et al., 2020).

A promising approach used for delivering biomolecules into cultured animal cells was the application of vertically aligned carbon nanofibers (VACNFs; McKnight et al., 2004; McKnight et al., 2005). Since these fibers are similar in scale to aphid stylets but with closed tips, they were assessed by Davern et al. (2016) for their potential to permit delivery of different sized molecules such as dyes, proteins, and dextrans to plant leaves. For this method, molecules dissolved in water were pipetted onto a leaf surface, and overlayed with the fiber array that was then gently tapped to promote penetration of the nanofibers and molecules into the leaf tissue. Importantly, the VACNFs enabled delivery of a variety of molecules into leaf tissue without causing a detectable stress response (Davern et al., 2016). Furthermore, fibers broke away from the backing and remained embedded in cells without causing loss of cell viability, providing markers for which cells potentially received molecules of interest.

Abbreviations: AALP, Arabidopsis aleurain-like protein; CNMS, Center for Nanophase Materials Sciences; VACNFs, Vertically aligned carbon nanofibers.

In this work, we have pioneered the use of VACNF arrays for the purpose of delivering DNA-encoded probes to plants to enable transient transformation (impalefection). We show the flexibility of the method by using it to transiently transform plant organs in several species with DNA encoding fluorescent proteins that can be detected by confocal microscopy. By examining the plant with a minimally invasive method, this approach will provide a more physiologically accurate picture of signaling pathways than most other studies that rely on detached tissues.

2 Materials and methods

2.1 Plants

Arabidopsis thaliana (Columbia-0 accession) plants 3-4 weeks post vernalization were used for leaf transformations and grown in long day conditions (16 h of light, 8 h of dark) in soil at 19-20°C, 35-75% relative humidity (RH), and 150-200 µmol m^{-2} s^{-1} light in a growth room. Seeds were vernalized in the dark at 4°C for 4 d prior to planting. *Populus trichocarpa* (Nisq-1 genotype) (poplar) plants were grown in soil in long day conditions at 30-60% RH, 150-200 µmol m^{-2} s^{-1} light intensity, 22°C in a greenhouse. Lettuce (*Lactuca sativa* cultivar Salinas) was grown in long day conditions at 19°C in a greenhouse. Second to fourth true leaves of young (20-30 day old) lettuce plants were used for transformation. For experiments with roots, lettuce seeds were germinated at 22°C (long day conditions) for 7-14 days in petri dishes with filter paper and 0.5 g/L MaxiGro (General Hydroponics). *Nicotiana benthamiana* was grown for 4-5 weeks in long day conditions at 24°C in a growth chamber. Tomato fruits, strawberries, apples, and peaches were purchased from a grocery store and were stored at room temperature prior to use. Roots used for VACNF delivery experiments came from Arabidopsis seedlings 5-6 d post planting grown on ½ MS plates supplemented with vitamins, grown under long day light conditions. Seeds for Arabidopsis seedlings were sterilized (70% ethanol for 5 min, 50% chlorine laundry bleach supplemented with 0.5% Tween-20 for 10 min, and washed 4x with dH_2O) and vernalized in the dark at 4°C for 4 d prior to planting.

2.2 Production of the vertically aligned carbon nanofibers

Carbon-based nanofibers with a lateral spacing (pitch) of 10, 20, or 35 µm and height ranging from 15-25 µm were made in the Center for Nanophase Material Science (CNMS) at Oak Ridge National Laboratory using nickel catalyst dots patterned across the top of a silicon wafer *via* electron beam lithography, metal evaporation, and conventional lift-off using the method described by (Melechko et al., 2005; Melechko et al., 2009). For the lithography step, the silicon wafers were coated with polymethyl methacrylate resist and exposed using a JEOL 9300FS electron beam lithography system and developed in a solution of 1:3 methyl-isobutyl ketone: isopropyl alcohol (Nano MIBK/IPA 1:3 Developer, MicroChem, Newton, MA). Electron beam lithography was necessary to define the catalyst dots with diameters between 200 nm and 500 nm. After developing the resist and cleaning with a 6-second exposure to oxygen plasma, electron beam evaporation was used to deposit a thin nickel film (100-125 nm) on the patterned resist. Sequential sonication in acetone and isopropyl alcohol was used to remove the underlying resist layer, leaving catalyst dots in the desired pattern behind. Nanofiber growth was then conducted using a direct current plasma-enhanced chemical vapor deposition chamber using an acetylene/ammonia mixture. Growth parameters were optimized to control the length and taper of the nanofibers (tapering less than 200 nm). After fabricating the VACNFs, their geometry was assessed using scanning electron microscopy (Zeiss Merlin FE-SEM) at a 30° tilt with an acceleration potential of 1 kV (Figure 1). To protect VACNF chips during transport and storage, the fibers were coated with a layer of photoresist (SPR955, spun at 1K for 45 s) (Davern et al., 2016). Photoresist was removed *via* increment washes of acetone (100%, 5 min), isopropyl alcohol (100%, 5 min), and water (5 min) prior to use.

2.3 DNA and dye delivery *via* VACNFs

2.3.1 Application to leaves, roots, and fruit "on-plant method"

Fiber delivery of DNA or dye to plant cells was conducted using a method modified from Davern et al. (2016). In brief, a 1 µL droplet containing fluorescein dye (1 mM), TAMRA dye (5 (6)-Carboxytetramethylrhodamine, 10 µM), or of 200 ng/µl of plasmid DNA purified from liquid bacterial cultures was applied to the surface of a leaf or fruit. For Arabidopsis and poplar leaves, abaxial surfaces of detached leaves were impaled. For lettuce and *N. benthamiana*, adaxial surfaces of leaves attached to plants were impaled. A VACNF chip (3x3 mm) was placed on top of the droplet (with the fibers oriented such that they came into contact with the droplet), and the fibers were tapped into the plant tissue with a pair of forceps, using a hard surface to support the other side of the plant organ. For control experiments, the VACNF chip was applied with its smooth back to the leaf or fruit. Fibers applied without DNA or dye were another control.

For dye delivery experiments, chips were left on the plants for 5 minutes and removed just before imaging. Chips were applied to roots of intact lettuce seedlings and roots were imaged 5 min – 1 h after dye delivery. After VACNF-mediated DNA delivery, Arabidopsis or Populus leaves were stored in a humid

10.3389/fpls.2022.1051340

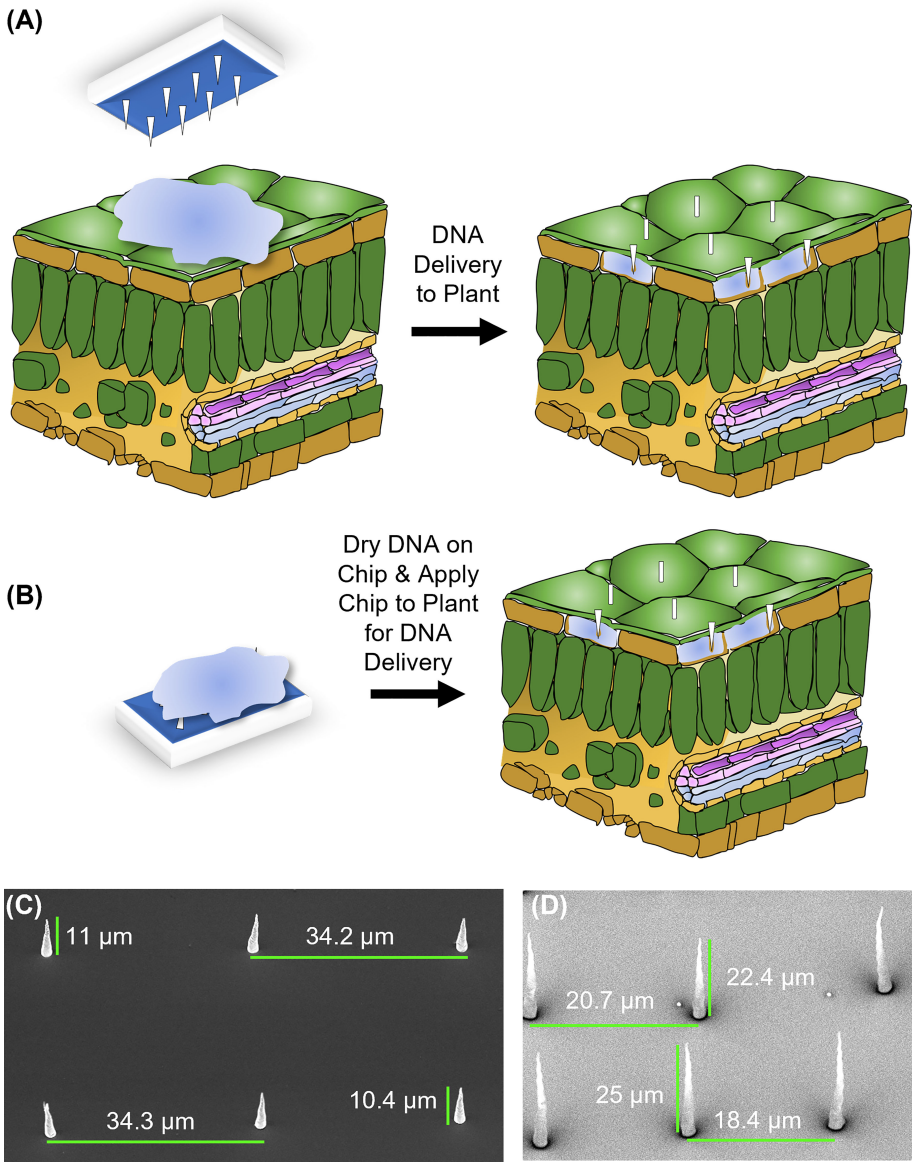

FIGURE 1
Design and application of carbon nanofibers. **(A)** On-plant of fiber delivery. A chip, placed on top of a leaf on which a 1 µL droplet of DNA solution is placed, is gently tapped to push the fibers into the leaf tissue. The chip is then removed, and nanofibers typically remain embedded in the tissue. **(B)** On-chip DNA method of fiber delivery. Fifteen minutes after a 1 µL drop of DNA is placed on a chip, it is placed on a plant organ surface and tapped with tweezers as in **(A)**. After tapping, the chip was removed, and nanofibers were left embedded in the tissue. For both methods, –fiber controls utilized the flat (fiberless) side of the chip. **(C)** Electron micrograph of VANCFs with ~35 µm pitch, 10-15 µm height, and imaged at a 30° angle. **(D)** Electron micrograph of VANCFs with ~20µm pitch, 20-30 µm height, and imaged at a 30° angle. Due to the fact that the fibers were imaged at 30° angle, the apparent heights appear to be smaller than the actual height by a factor of sin(30°)=1/2. Fibers were grown using 200-500 nm e-beam dot sizes and taper to a diameter less than 200 nm. Growth parameters: plasma current 1 amp, C2H2: NH3 = 0.55, 625°C, 10 torr.

chamber for 48 h in long-day conditions (16 h of light, 8 h of dark) prior to imaging. Tomato fruits were kept in long day conditions as well for 40 h after DNA delivery. Arabidopsis leaves transformed with AALP:GFP were stored in the dark for 48 h prior to imaging (Tamura et al., 2003) unless otherwise specified. Lettuce plants were maintained in long day condition for 4 d after impalefection (the period effective for transient transformation *via Agrobacteria* (Wroblewski et al., 2005) and *N. benthamiana* plants for 3 d. Just before imaging, the plant tissues that were in contact with the chips were excised and placed on glass slides. In the case of the tomato fruit, the epidermal layer was removed to expose the top layer of the

pericarp. Both the epidermal layer and the pericarp were examined for fibers and fluorescent protein accumulation.

2.3.2 Application to Arabidopsis leaves and roots "on-chip method"

When applying the chips to the Arabidopsis leaves using the "on-chip" method, 1 µL of 200 ng/µL DNA solution was drop-cast on to the fiber side of the chip and allowed to dry for 15 min prior to impaling tissue. When placing the droplet on the fibers, great effort was taken to ensure that the droplet was placed in the center of the chip and covering several fibers. Leaves were placed on a hard substrate and the fibers were applied on the abaxial side of the leaves using a pair of tweezers for the tapping. After VACNF-mediated delivery, plant leaves were stored in a humid chamber for 48 h in long-day conditions. For roots, the same method of drying DNA on VACNFs was applied. Roots were placed on agar plates and chips were applied to the organs while they were on top of the agar. Seedlings with roots transformed with biosensor FlincG (fluorescence indicator of cGMP) *via* VACNFs were kept on agar plates in long day light (16 h light, 8 h dark) conditions for 36 h prior to imaging.

2.4 *Agrobacterium*-mediated transformation

Lettuce (cultivar Salinas) and *N. benthamiana* leaves were infiltrated with *Agrobacterium tumefaciens* GV3101 carrying p35S-mCherry/pCambia (Kang et al., 2014) at OD_{600} = 0.6. Plants were grown in the same way as for VACNFs experiments and kept in their growth conditions for 4 d post infection for lettuce and 3 d post infection for *N. benthamiana* before imaging.

2.5 Plasmids

The binary ~11,000 bp plasmid pUbiquitin$_{10}$:YFP-Gateway from Michniewicz et al. (2015), the ~3000 bp protoplast vector pUC with p35S:Arabidopsis Aleurain Like Protein (AALP):GFP from Kang et al. (2014), and the ~3000 bp vector pUC with p35S: mCherry, were used for VACNF-mediated transformation. pCambia with identical p35S:mCherry cassette (~10,000 bp) was used for *Agrobacterium*-mediated transformation (Kang et al., 2014). The binary vector pART: delta-FlincG (N2105633 Nottingham Arabidopsis Stock Centre), 6857 bp, with the cGMP biosensor FlincG (Isner and Maathuis, 2011) was also used.

2.6 Treatment of seedlings with Pep1

40 µL of Pep1 peptide (20 nM, Biomatik) was added to a glass slide on top of the root prior to imaging to trigger cGMP production in seedlings transiently transformed with the FlincG sensor.

2.7 Microscopy

Images were captured with Zeiss LSM 800 or LSM 710 confocal microscope. GFP and fluorescein signals were collected with an emission range of 510 and 545 nm, excitation was 488 nm. YFP signal was collected with an emission range of 491-573 nm, excitation was 488 nm. mCherry was imaged with 561 nm excitation and 570-628 emission.

2.8 Integrated density measures for fluorescent proteins

Fluorescence values for AALP:GFP, mCherry, and YFP were measured as total fluorescence (integrated density) in 20 µm × 20 µm confocal image areas (Jelenska et al., 2017) and quantified using ImageJ/FIJI (Schindelin et al., 2012).

2.9 Statistical analysis

Statistical analysis (ANOVA and Tukey's test) was performed using PRISM 9 (GraphPad). Statistically different categories ($P<0.05$) are marked by different letters.

3 Results

3.1 Fiber design and application

Two approaches for introducing plasmid DNA into plant cells using VACNF chips were implemented: "on-plant" and "on-chip" methods (Figures 1A, B). For the on-plant method, a 1 µl droplet containing DNA was placed on the surface of a leaf. A VACNF chip was orientated such that the fibers came into contact with the droplet. Tweezers were then used to apply a force on the back side of the chip, driving the fibers into the tissue and delivering materials into the plant (Figure 1A). With the on-chip method, DNA was first applied to a chip, which was then used to impale the tissue (Figure 1B). In this work, we used 200 ng of plasmid DNA in 1 µL of water, after preliminary experiments using different concentrations and the on-plant method suggested this amount was optimal. Our conditions were similar to those used for successfully introducing DNA into mammalian cells using VACNF chips (McKnight et al., 2004; McKnight et al., 2005).

Previously, VACNFs were made to have the approximate diameter of aphid stylets (Davern et al., 2016) (Figure 1). These original nanofibers had a base diameter of 500 nm and tapered to 100 nm at the tip. Additionally, they had a lateral spacing (pitch) of 20 µm, to minimize the number of nanofibers penetrating individual epidermal cells in *Populus* leaves. We designed additional fiber arrays with longer (35 µm) or shorter (10 µm)

pitch, reasoning that those additional geometries may be useful for a broad array of plant cells of various sizes and shapes of plant cells (Figures 1C, D). In this study, fibers with 35 or 20 µm pitch were used for large Arabidopsis epidermal cells that have a jigsaw-like appearance and do not have a uniform shape; cells are 20 to 50 wide µm and can be as long as 100 µm. These fibers were also used for dye delivery in peaches, strawberries, and apples. Fibers with shorter pitch (10 µm and 20 µm) were used for tomato fruit, and leaves of poplar, lettuce, and *N. benthamiana*. All fibers were 10-25 µm in length and all designs were successful in transforming plants (Figures 1–6).

3.2 On-plant VACNF-mediated transformation of Arabidopsis leaves with a small plasmid

To test the applicability of VACNFs for transient transformation, we first employed a green fluorescent protein (GFP) fusion to the Arabidopsis aleurain-like protein (AALP) that transits through the endomembrane system and targets vacuoles (Sohn et al., 2003; Kim et al., 2005; Kang et al., 2014). We used a small (~3000 bp) pUC-based vector (used previously for protoplast transformation) and the VACNF on-plant method on excised leaves (Figure 1A). The accumulation of AALP:GFP was detected by confocal microscopy in Arabidopsis leaves 48 h after transformation (Figure 2A). We quantified success of delivery by comparing measurements of fluorescence that resulted from delivery of the vector (+DNA-AALP:GFP, +fibers) and the various controls (−DNA, +fibers; +DNA-AALP:GFP, −fibers (flat side of the chip); and −DNA, −fibers (no treatment)). GFP signal was present only in leaf areas in which plasmid was delivered *via* fibers (+DNA-AALP:GFP, +fibers) (Figures 2A–E) and was not observed in controls. Background signal in Figure 2 mainly comes from the stomatal guard cells, as indicated by asterisks, which were excluded from the analysis. When imaging the −DNA, +fibers control, fields of view were selected such that fibers (which are autofluorescent) were present (Figure 2B). These data show successful VACNFmediated transformation of Arabidopsis leaves, resulting in expression of a fluorescent reporter at levels easy to image by florescence microscopy.

3.3 On-plant and on-chip methods of VACNF-mediated transformation with a large plasmid

To further demonstrate the utility of the VACNF chips, we tested if a large plasmid encoding yellow fluorescent protein (YFP) could be used to transform leaves that were detached from plants. We used fibers with the on-plant method to transform Arabidopsis leaves with $pUBQ_{10}$:YFP carried on the ~11,000 bp Gateway plasmid, usually used for *Agrobacterium*-mediated transformation (Michniewicz et al., 2015) (Figure 3). The leaves to which the plasmid was delivered *via* fibers (+DNA-YFP, +fibers), had significantly greater signal in the YFP channel than the controls (−DNA, +fibers; +DNA-YFP, −fibers (flat side of the chip); −DNA, −fibers (no treatment)) (Figure 3I). Similar to a small plasmid, the use of a large binary vector resulted in easily detectable reporter fluorescence. Background signals observed in Figure 3 again mainly came from the guard cells, as indicated by the asterisks in the figure. In this experiment, we also compared the on-plant and on-chip methods of VACNF-mediated impalefection. There was no observable difference in the expression pattern of YFP in leaves transformed (Figures 3A, B). Additionally, there was no significant difference in measured fluorescence values for the on-chip and on-plant methods (Figure 3I). Therefore, we used the on-plant method in most subsequent experiments. Accounting for various factors, including where force was applied to the chip as well as the number of fibers that penetrated the leaf tissue, observable expression was detected in different areas within the 3mm×3mm area of leaf tissue under the chip. As the leaf surface is not completely flat, not all cells came into contact with the chip. These experiments show that detached leaves can be transformed with a large plasmid using VACNFs.

3.4 VACNF-mediated transformation of different plant species

To further substantiate the applicability of VACNF chips, the on-plant method was applied to excised poplar leaves to deliver DNA encoding AALP:GFP in the pUC vector. Arabidopsis leaves served as a positive control in this experiment to show that the quality of DNA was suitable for delivery and expression. GFP signals were observed in impaled regions 48 h post-delivery in Arabidopsis and poplar leaves (Figures 4). The fibers were also used to successfully deliver p35S:mCherry/pUC vector to lettuce (*Lactuca sativa* cv. Salinas) and *Nicotiana benthamiana* leaves attached to plants (Figures 5A, B). These results show that nanofibers can deliver DNA to different plants for the production of encoded proteins.

3.5 Comparison of VACNF and *Agrobacterium*-mediated transient transformation

Agrobacterium is commonly used for transformation of intact plants. Therefore, we compared expression of mCherry resulting from *Agrobacterium*-mediated transformation, using pCambia binary vector, to our VACNF-mediated delivery of p35S:mCherry/pUC in lettuce and *N. benthamiana* leaves attached to plants (Figure 5). mCherry fluorescence in lettuce leaf was much higher using VACNF-mediated impalefection than was found using agroinfiltration (Figures 5A, C, E). In

10.3389/fpls.2022.1051340

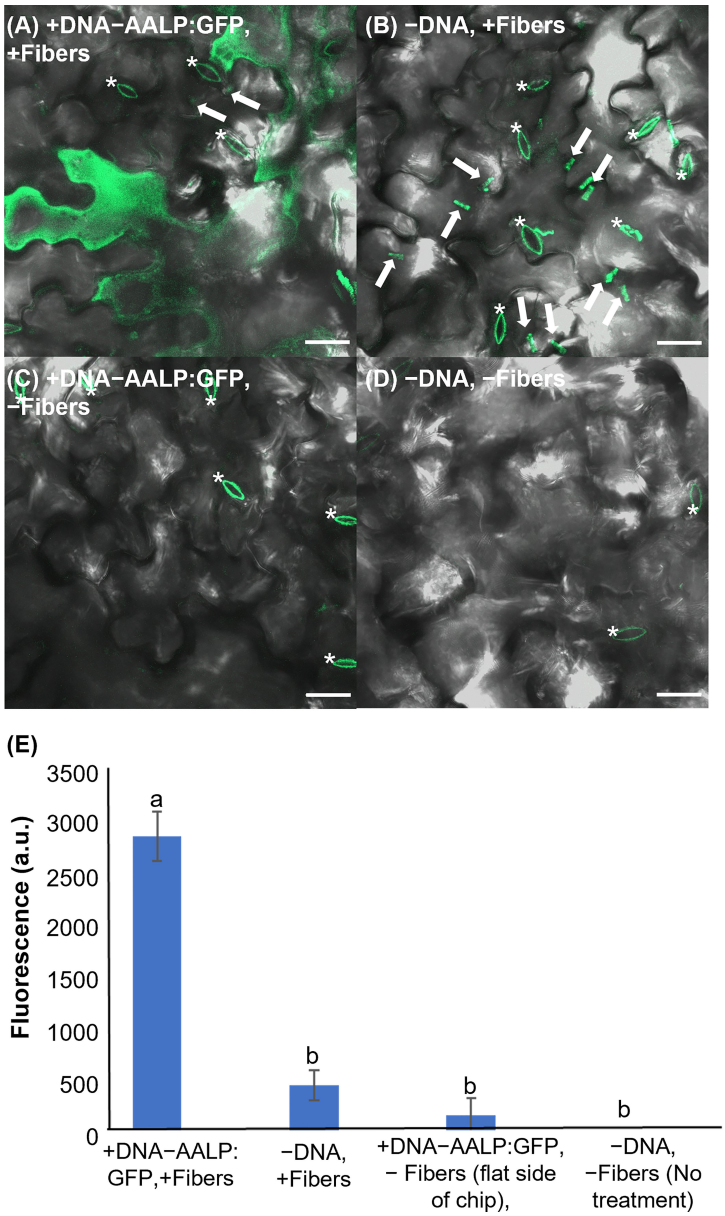

FIGURE 2
Fluorescent image analysis of Arabidopsis leaves transiently transformed with AALP:GFP 48 h after delivery *via* VACNF with a 35 µm pitch. **(A)** p35S: AALP:GFP/pUC plasmid delivery *via* VACNF using the on-plant method. GFP fluorescence is shown in green (+DNA-AALP:GFP, +fibers). **(B)** Fibers only (–DNA, +fibers). **(C)** AALP:GFP plasmid delivery without fibers (backside of chip with no fibers; +DNA-AALP:GFP, –fibers). **(D)** No treatment (–DNA, –fibers). **(E)** Graph of average integrated densities of GFP fluorescence (green channel) of defined 20×20 µm areas (n≥40 per condition, combined results from two experiments). Regions containing stomata (*) were excluded due to autofluorescence, and the average fluorescence signal intensity from the no-treatment condition was subtracted from each average. 2-way ANOVA (and Tukey test) was used for significance testing, and error bars represent the standard error of the mean. Different letters show significant differences between treatments ($P < 0.0001$). All images shown are maximum projections of 40 µm z-stacks. Scale bars are 20 µm and white arrows indicate fibers in the images.

contrast for *N. benthamiana*, which is highly amenable to transient transformation with *Agrobacteria*, mCherry fluorescence was higher after agroinfilitration than after imaplefection, as observed by microscopy (Figures 5B, D, F) and quantified (Figure 5G).

For the experiments described above with lettuce, it was necessary to optimize the timing of observations after VACNF-mediated transient transformation. In contrast to other plant species, we did not detect fluorescence in lettuce 2 d after transformation either *via* VACNFs or *Agrobacteria*. Wroblewski

10.3389/fpls.2022.1051340

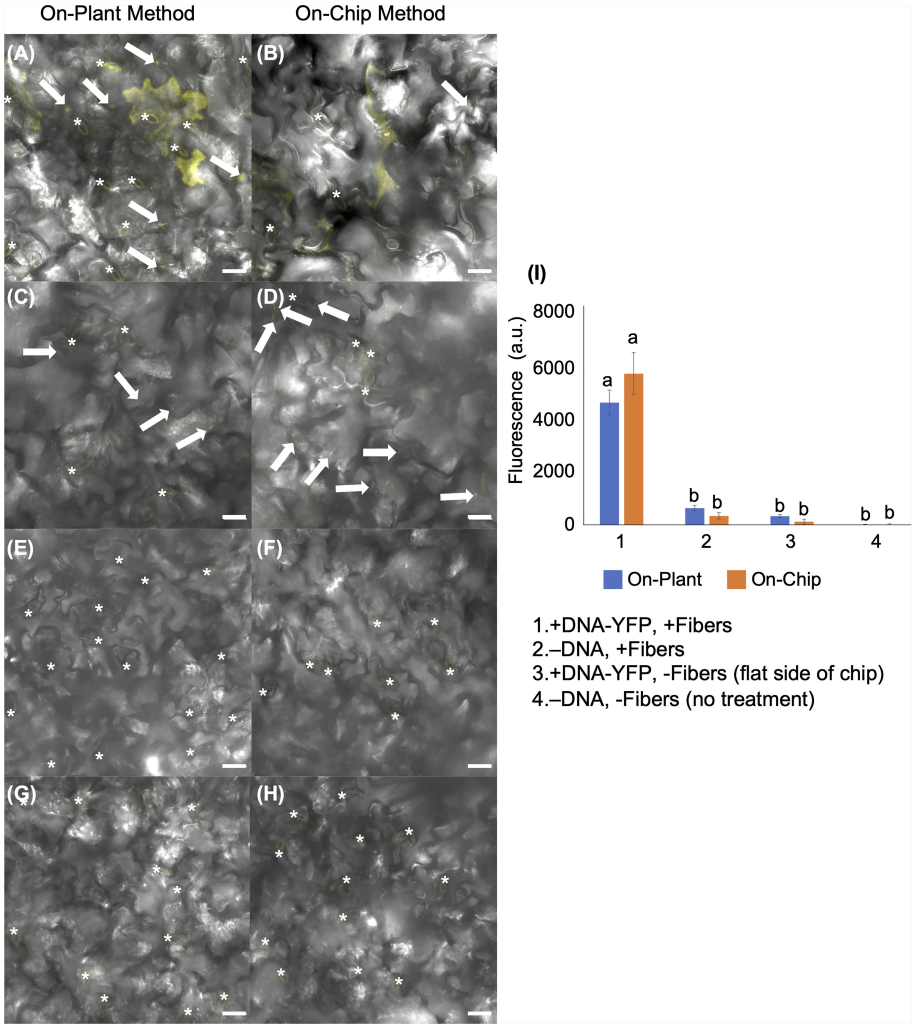

FIGURE 3
Fluorescent image analysis of Arabidopsis leaves transiently transformed with pUBQ$_{10}$:YFP 48 h after delivery *via* VACNF with a 35 µm pitch using the on-plant or on-chip methods. **(A)** and **(B)** DNA-YFP delivery *via* VACNF using the on-plant and on-chip methods, respectively (+DNA-YFP, +fibers). **(C)** and **(D)** Fibers only (–DNA, + fibers). **(E)** and **(F)** DNA-YFP delivery without fibers (flat chip: +DNA-YFP, –fibers). **(G)** and **(H)** No treatment (–DNA, –fibers). **(I)** Graph representing relative average fluorescence signal intensity of 25 20×20 µm areas from images of 5 biological replicates combined from 2–3 experiments using fluorescence from the YFP channel. Regions containing stomata (*) were excluded due to autofluorescence, and the average fluorescence intensity from the no-treatment condition was subtracted from each average. 2-way ANOVA (and Tukey test) was used for significance testing, and error bars represent the standard error of the mean. Different letters show significant differences between treatments ($P < 0.0001$). All images shown are maximum projections of 40 µm z-stacks. Scale bars are 20 µm, and white arrows indicate fibers in the images.

et al. (2005) previously noted that the highest transient expression occurred in lettuce 4-5 d after agroinfiltration. We detected mCherry signals 3-5 d after transformation of lettuce with both methods, with highest signal at 4 d. In *N. benthamiana* fluorescence was highest 3 d post transformation. Our results stress the importance of optimalization of VACNFs protocols for different plants, which may require different times for transgene expression after impalefection. The experiments with lettuce show that VACNFs can be a superior method for plant species and tissues recalcitrant to *Agrobacterium*-mediated transformation.

3.6 VACNFs may be useful for cargo delivery and transformation of different plant organs

Curved organs present a challenge for transient transformation using VACNFs, where having a relatively flat surface to tap the chip with nanofibers into the tissue is an advantage. Nevertheless, to establish broader applicability of the method, we tried various tissues, including hypocotyl, roots and fruit. While we did not get successful transformation of

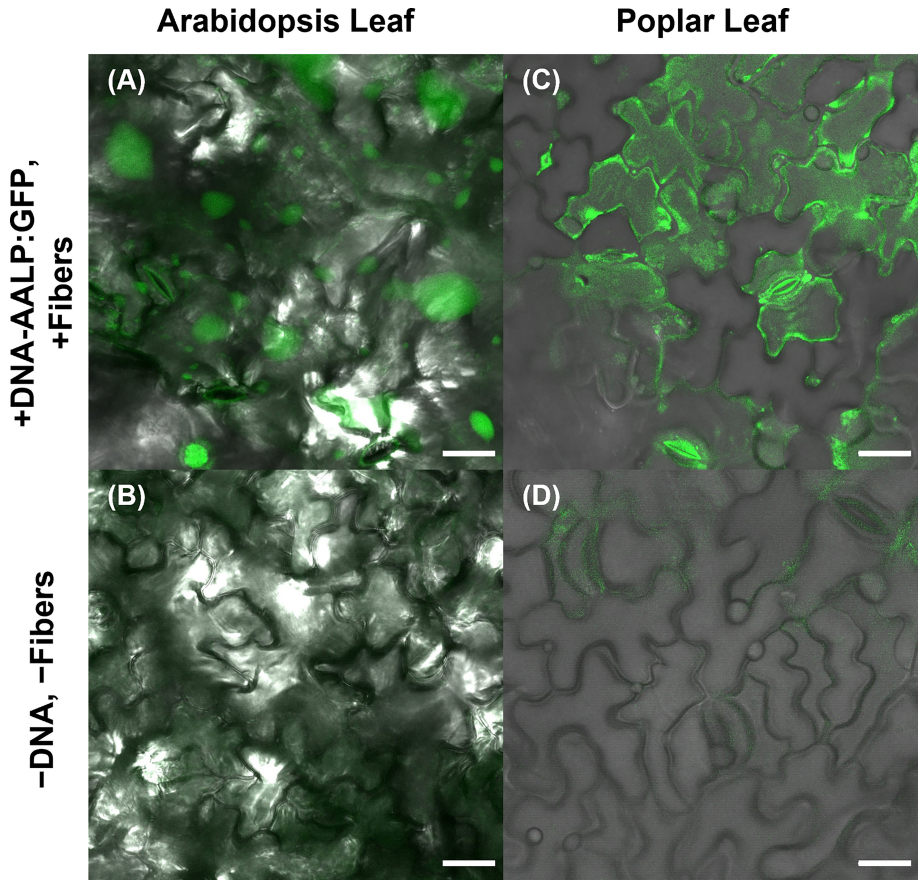

FIGURE 4
Use of VACNF to introduce DNA expression constructs into poplar leaves. Images were generated using confocal fluorescence microscopy. VACNFs delivered a small plasmid resulting in expression of a vacuolar marker, AALP:GFP (shown in green). **(A)** Arabidopsis leaf 48 h after delivery of p35S:AALP:GFP/pUC *via* fibers with 20 µm pitch (+DNA-AALP:GFP, + fibers), **(C)** Poplar leaf 48 h after delivery *via* fibers with 10-µm pitch (+DNA-AALP:GFP, +fibers). **(B, D)** Show untreated controls (–DNA, –fibers). All images are maximum projections of 40 µm z-stacks. Scale bar = 20 µm.

hypocotyls, we did have a few positive results with other curved organs. We found that it was useful as a first test to deliver a fluorescent dye (e.g., fluorescein or TAMRA) to the sample organ, as demonstrated by Davern et al. (2016). This permits a rapid assessment of whether the mechanics of the delivery method will work. In this way, we showed that VACNF arrays could successfully deliver dyes into fruit (store-bought strawberries, apples, and peaches) and lettuce roots (Figures 6A–H). In addition, we were able to transform tomato fruit with p35S:AALP:GFP/pUC using the on-plant method (Figure 6I). Specifically, after 40 h, GFP signals were observed in the tomato fruit pericarp when the chip contact area was excised from the fruit. We did not see significant GFP signals in the epidermal (skin) layer. For Arabidopsis roots, we used the on-chip method to deliver FlincG, a fluorescence-based reporter for cGMP. After delivery of the construct, we treated the roots with Pep1, a plant peptide that activates signaling, to induce cGMP, and monitored signal over time. We captured images of a transformed cell that showed increased fluorescence signal over time in response to Pep1 (Figure 6K), similar to what was previously reported (Ma et al., 2012). Controls for this experiment (+DNA-FlincG, +fibers, +water; and –DNA, +fibers, +Pep1) did not show an increase in green fluorescence over time (Figures 6L, M). Thus, delivery of the biosensor and application of an elicitor are necessary for increased fluorescence signal over time. This experiment indicates that a functional probe can be expressed in cells transformed using VACNF.

4 Discussion

In this work, two different VACNF chip impalefection protocols (on-plant and on-chip, Figure 1) were established for transient transformation of leaves, roots and fruit in a number of

10.3389/fpls.2022.1051340

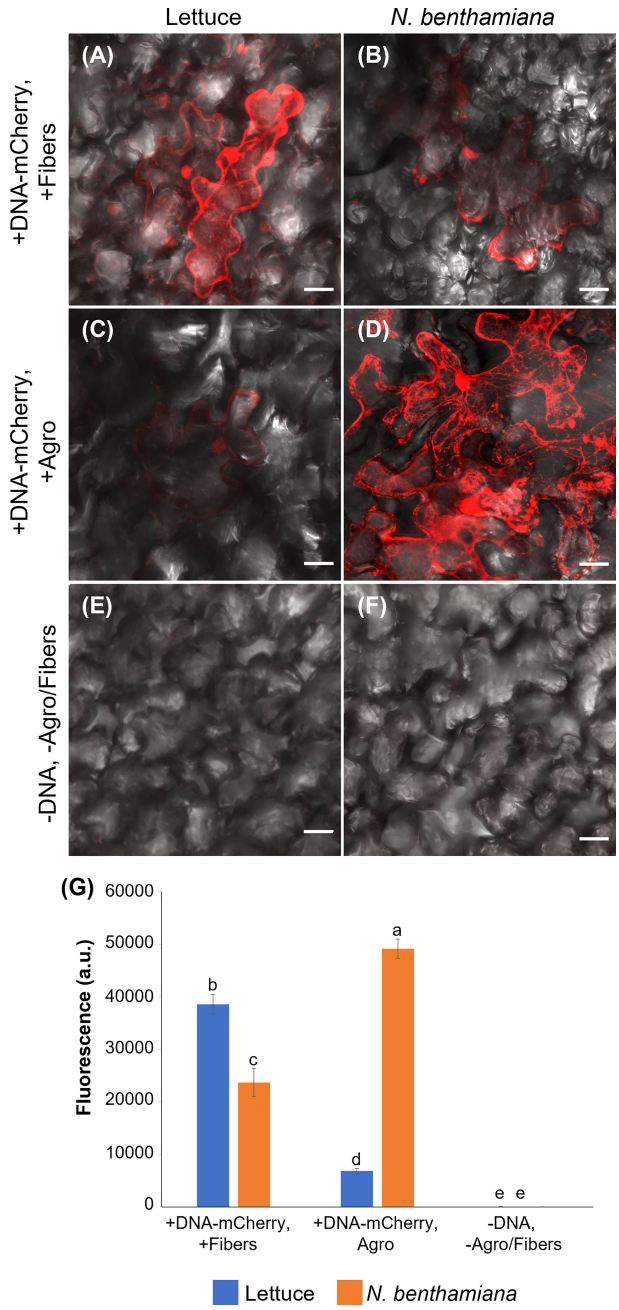

FIGURE 5
Comparison of VACNF- and *Agrobacterium*-mediated transient transformation. **(A)** p35S:mCherry/pUC expression 4 d after delivery *via* VACNFs with 10 µm pitch using the on-plant method in lettuce and **(B)** 3 d after delivery in *N. benthamiana*. **(C)** *Agrobacterium*-mediated delivery of p35S:mCherry/pCambia in lettuce, 4 d after agroinfiltration. **(D)** p35S:mCherry/pCambia 3 d after agroinfiltration in *N. benthamiana*. **(E)** and **(F)** show background signal for no treatment samples in lettuce and *N. benthamiana*, respectively. **(G)** Graph representing average fluorescence signal intensity of the mCherry fluorescence of 20×20 µm areas ($n \geq 40$, combined results from 2–3 experiments). Background signal (no treatment) was subtracted, 2-way ANOVA (and Tukey test) was used for significance testing, and error bars represent the standard error of the mean. Different letters show significant differences between treatments ($P < 0.0002$). All images are maximum projections of 20 µm z-stacks. Scale bars are 20 µm.

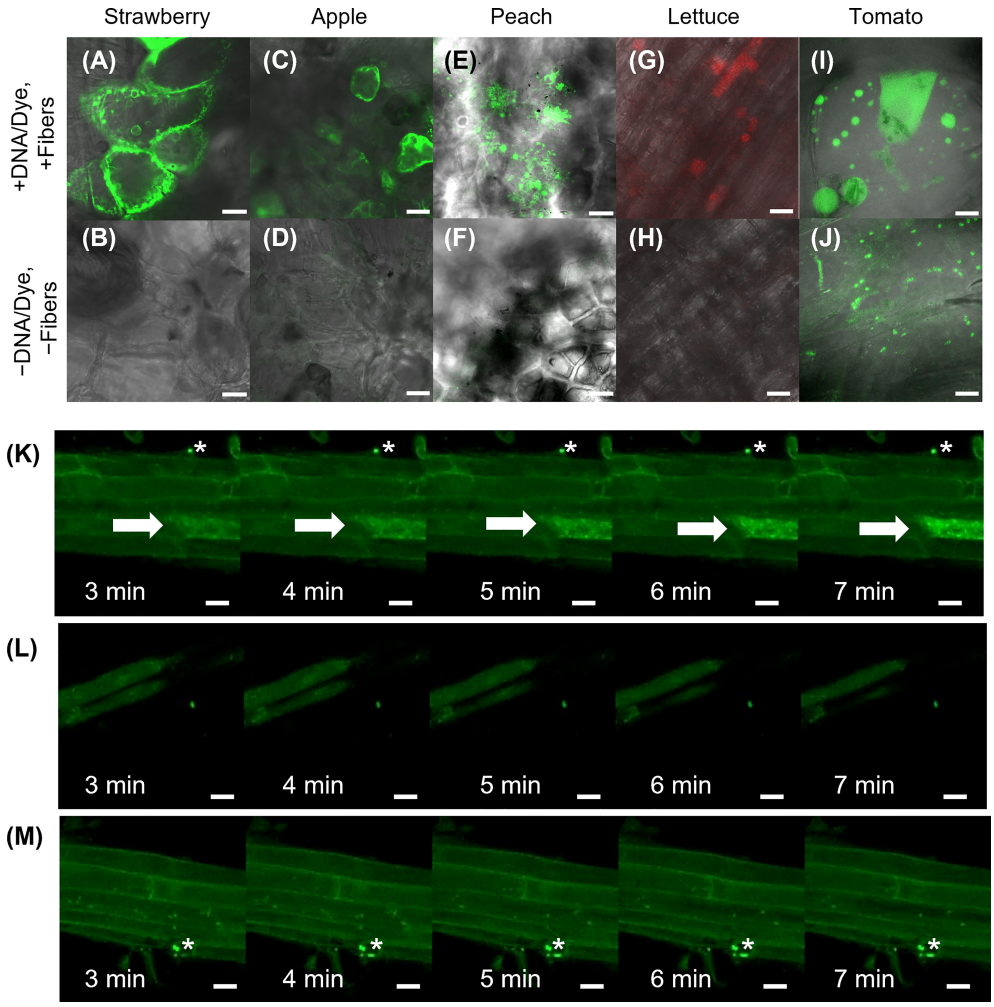

FIGURE 6
Application of VACNFs to curved organ surfaces. Images were generated using fluorescence confocal microscopy. Fluorescein dye was delivered to store-bought strawberry **(A)**, apple **(C)**, and peach **(E)** via fibers with 35 μm pitch with the on-plant method. **(G)** TAMRA dye was delivered to lettuce roots using the on-plant method with fibers with 10 μm pitch. **(I)** DNA (p35S:AALP:GFP/pUC) was delivered to store-bought tomato fruit and GFP fluorescence was imaged 40 h after delivery via on-plant method with fibers with 20 μm pitch. The area shown is approximately one large cell. Panels **(B, D, F, H,** and **J)** show no-treatment controls of plant tissue for panels **(A, C, E, G,** and **I)**, respectively. **(K–M)** DNA encoding FlincG was delivered to Arabidopsis roots via VACNFs with 35 μm pitch (on-chip method), and expression was assessed after 36 h. **(K)** 36 h after FlincG delivery, Arabidopsis roots were treated with Pep1 peptide (panels show different time points after exposure to elicitor Pep1 (20 nM)) (+DNA-FlincG, +fibers, +Pep1). The white arrow points to the transformed cell with signal increasing over time. **(L)** 36 h after FlincG delivery, Arabidopsis roots were treated with water (panels show different time points after exposure to water, which does not trigger production of cGMP) (+DNA-FlincG, +fibers, +water). **(M)** Arabidopsis roots with fibers without biosensor delivery treated with Pep1 (–DNA, +fibers, +Pep1). Scale bars are 20 μm. **(A–F)** are single images (0.5 μm thick) captured via confocal microscopy. **G, H** are maximum projections of 118 μm z-stacks and **I-M** are maximum projections of 40 μm z-stacks. * denote regions with fibers.

plant species (Figures 2–6). VACNF chips can be used on intact plants or on organs detached from plants. This raises the possibilities of a number of interesting applications, such as studying the impact of environmental perturbation on reporter gene activity. Both the on-plant and on-chip methods rely on the fibers to make small punctures in the cell wall and membrane through an impulse force resulting from the tapping of the tweezers on the back of the chip. Using the fibers in this manner is minimally invasive and was not found to be toxic or damaging to the plant (Davern et al., 2016). Importantly, these methods do not require fibers to be surface functionalized, unlike other existing methods (Demirer et al., 2019; Jat et al., 2020; Zhang et al., 2022b), and the fibers can be used to deliver different sized vectors. With the exception of hypocotyls, all plant organs that we tested could be transformed using VACNFs: leaves (Arabidopsis, poplar, lettuce, and *N. benthamiana*), roots (Arabidopsis) and fruit (tomato; Figures 2–6). Importantly, VACNF-mediated transformation may be successfully used in

a species, such as lettuce, for which Agrobacterium-mediated transient transformation is inefficient (Figure 5).

In this study, VACNFs were produced at Oak Ridge National Laboratory CNMS through their user program, using previously described protocols (Melechko et al., 2005; Melechko et al., 2009). These publications also provide an overview and workflow of the fabrication of nanofiber arrays. VANCFs can also be produced at university clean rooms with direct current plasma enhanced chemical vapor deposition machines (Liu et al., 2010; Salmeen et al., 2015). A workflow summarizing important design, quality-control and operational steps for impalefection is provided in Figure 7. Successful DNA delivery with the VACNFs in plants depends upon on the geometry of the fibers and the design of the chips. The fibers used herein were straight with a tapering diameter such that the tip was less than 200 nm and resembled an aphid stylet. It was found that sharp tips with smaller diameters were less damaging than blunt tips in Arabidopsis leaf epidermal cells (Forouzesh, 2012; Forouzesh et al., 2014). In their study, Forouzesh et al. (2013) used single tips (or a single fiber equivalent) for nanoindentation studies to quantify the failure stress of cell walls. If the fibers are bent, they are unable to make direct contact with the leaf tissue, hence unable to impale cells and achieve delivery. Straightness of fibers is one of the first things to check if VACNF-mediated transformation fails (Figure 7). Pitch is another consideration, although in our experience it did not impact delivery success. The chips used in our experiments were designed to limit the number of fibers penetrating each cell (limit 1-2 fibers) by varying the pitch. Another factor that did prove critical for protein expression after VACNF-mediated impalefection is the timing. Most fluorescent markers were detected after 2 d. However, in lettuce, expression took longer, 4 d (Figures 2–6). The fluorescent markers encoded by VACNF-delivered DNA were detected in expected localizations: endomembrane compartments and vacuoles for AALP:GFP (Sohn et al., 2003; Kim et al., 2005; Kang et al., 2014), cytosol and nuclei for free mCherry and YFP (e.g. Kang et al. (2014)).

Both large (binary vectors utilized for *Agrobacterium*-mediated transformation) and small vectors (previously used for protoplast transformations) can be successfully delivered and expressed in plants (Figures 2–6). Smaller plasmids are easier to manipulate and tend to have a higher transient transformation efficiency in protoplast transfections and particle bombardment than the larger vectors used for *Agrobacterium*-mediated transformations (Sainsbury et al., 2009). With fiber delivery, results using larger and smaller vectors were similar. Therefore, constructs designed for use with *Agrobacterium* can be successfully used with VACNFs.

Nanomaterials are increasingly being used for transient transformation. The most recent methods of nanoparticle-mediated transformation or delivery of nucleic acids to plants have relied upon using pressure infiltration to deliver nanoparticles into plants *via* a needleless syringe (Zhang et al., 2019; Demirer et al., 2019; Izuegbunam et al., 2021; Zhang et al., 2022). Together, these nanoparticle-mediated methods have

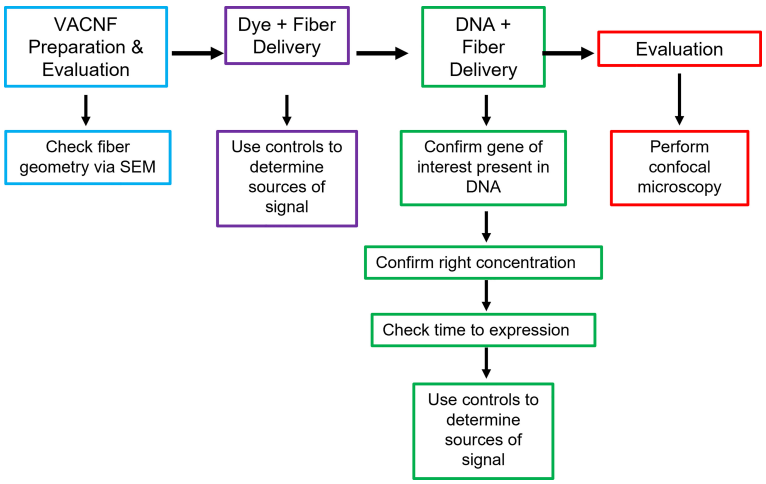

FIGURE 7
Workflow for VACNF mediated transient transformation of plants. When using the VACNFs for delivery of small molecules, there are a few problems that can arise. The first step in troubleshooting is to check the geometry of the fibers using scanning electron microscopy to ensure that the fibers are straight and have a sharp tip. After confirming the fiber geometry, the next step is to make sure that you are able to successfully deliver dye into your plant/organ of choice. For this purpose, place a 1 µL droplet on the plant surface and use the fibers to deliver the dye, checking for delivery with the microscope. With this step and all other steps moving forward, it is important to use appropriate controls (−dye,−fibers; −dye, +fibers; and +dye,−fibers), to be confident that you are getting signal from dye delivery. If both steps are successful, the next step would be to ensure that your gene of interest is present in your plasmid, you are using the right concentration of DNA, and you are waiting the right amount of time after delivery to check expression. The last step is to check expression using confocal microscopy.

enabled delivery of nucleic acids and other molecules into Arabidopsis, tobacco, onion, maize, wheat, rapeseed, mustard, carrot, cotton, tomato, spinach, arugula, watercress, cowpea, chamomile, barley, and moss (Kumar et al., 2020; Jat et al., 2020; Izuegbunam et al., 2021). Roots can take up nanoparticles through passive diffusion and plant leaves can easily be transformed with passive infiltration of nanoparticles entering through the stomata (Hubbard et al., 2020). To the knowledge of the authors, only one study previously used nanoparticles to transform other parts of a plants that were not leaves or roots. Specifically, in Izuegbunam et al. (2021), the authors used needleless syringes to deliver nanorods with anchored DNA to developing seed tissues in Arabidopsis, field mustard, barley, and wheat. This method, like the aforementioned nanomaterial-mediated delivery of DNA (Demirer et al., 2019; Jat et al., 2020; Zhang et al., 2022b), requires the conjugation of DNA to nanorods and subsequent release of DNA once inside cells.

In summary, we have demonstrated the utility of using vertically aligned carbon nanofibers to overcome the challenges of crossing plant cell walls and plasma membranes to deliver DNA into cells. There is no release of cargo necessary, since nanofibers facilitate delivery through mechanical means into the plant, probably by forming transient channels around the fibers through which material can enter cells (Davern et al., 2016). The level of transgene expression readily allowed detection of several fluorescent reporters. Previously, VACNFs were successfully used to deliver proteins to plants cells (Davern et al., 2016). In that study dextran and proteins were detected in plant cells as early as 5 minutes after introduction *via* VACNFs. Labeled peptides entered vascular tissues which allowed their distribution throughout the plant (Davern et al., 2016). In the present work, we have demonstrated the value of VACNF chips in delivering DNA into leaves, roots, and fruit, with the minimally invasive impalefection allowing subsequent expression of the intended gene products. Looking forward, VACNF chips could be utilized to deliver multiple types of biomolecules together (e.g., gene editing reagents) and for stable transformation *via* delivery to a meristem, plant cell culture, or plants undergoing early organogenesis.

Data availability statement

The original contributions presented in the study are included in the article/supplementary material. Further inquiries can be directed to the corresponding authors.

Author contributions

JM, JJ, JG, RS, and JM-F conceived the research and designed the experiments. JM, SR, and DH designed and fabricated the carbon nanofibers. JM and JJ performed the experiments and analyzed the data. JM and JJ wrote the manuscript with input from JG, RS, SR, DH, and JM-F. All authors contributed to the article and approved the submitted version.

Funding

This work has been funded by the Bioimaging Science Program, U.S. Department of Energy, Office of Science, Biological and Environmental Research, DE-SC001914 and the United States Department of Agriculture, 2021-67013-34835. JMM was supported by the United States Department of Agriculture: National Institute of Food and Agriculture: Agriculture and Food Research Initiative Predoctoral Fellowship 2021-67034-35167.

Acknowledgments

We thank Dr. Inhwan Hwang (Pohang University of Science and Technology) for CaMV p35S: AALP:GFP DNA and Dr. Jiyoung Lee (Korea Research Institute of Bioscience and Biotechnology) for p35S-mCherry constructs. We thank John Zdenek for assistance with plant growth and maintenance. We thank Mindy Clark from Oak Ridge National Laboratory and Dr. Gail Taylor from the University of California, Davis for *Populus trichocarpa* (Nisq-1 genotype). Nanofiber arrays were fabricated at the CNMS, which is a Department of Energy Office of Science User Facility (Proposal ID : CNMS2019-103). Support from CNMS is awarded through a peer-reviewed proposal system and is provided at no cost to successful applicants who intend to publish their results (http://www.cnms.ornl.gov/user/becoming_a_user.shtml). We thank the CNMS for assistance with the production of nanofiber arrays. We thank Dr. John Caughmen, Dr. Timothy McKnight, and Travis Bee for critical discussion about experimental design.

Conflict of interest

The authors declare that the research was conducted in the absence of any commercial or financial relationships that could be construed as a potential conflict of interest.

Publisher's note

References

Altpeter, F., Springer, N. M., Bartley, L. E., Blechl, A. E., Brutnell, T. P., Citovsky, V., et al. (2016). Advancing crop transformation in the era of genome editing. *Plant Cell* 28, 1510–1520. doi: 10.1105/tpc.16.00196

Arshad, M., Zafar, Y., and Asad, S. (2013). "Silicon carbide whisker-mediated transformation of cotton (Gossypium hirsutum l.)," in *Transgenic cotton*. Ed. B. Zhang (Totowa, NJ: Humana), 79–92. doi: 10.1007/978-1-62703-212-4_7

Baltes, N. J., Gil-Humanes, J., and Voytas, D. F. (2017). Genome engineering and agriculture: opportunities and challenges. *Prog. Mol. Bio. Transl. Sci.* 149, 1–26. doi: 10.1016/bs.pmbts.2017.03.011

Birch, R. G. (1997). Plant transformation: problems and strategies for practical application. *Annu. Rev. Plant Biol.* 48, 297–326. doi: 10.1146/annurev.arplant.48.1.297

Chang, F. P., Kuang, L. Y., Huang, C. A., Jane, W. N., Hung, Y., Yue-ie, C. H., et al. (2013). A simple plant gene delivery system using mesoporous silica nanoparticles as carriers. *J. Mater. Chem. B* 1, 5279–5287. doi: 10.1039/C3TB20529K

Cunningham, F. J., Goh, N. S., Demirer, G. S., Matos, J. L., and Landry, M. P. (2018). Nanoparticle-mediated delivery towards advancing plant genetic engineering. *Trends Biotechnol.* 36, 882–897. doi: 10.1016/j.tibtech.2018.03.009

Davern, S. M., McKnight, T. E., Standaert, R. F., Morrell-Falvey, J. L., Shpak, E. D., Kalluri, U. C., et al. (2016). Carbon nanofiber arrays: a novel tool for microdelivery of biomolecules to plants. *PLoS One* 11, e0153621. doi: 10.1371/journal.pone.0153621

Demirer, G. S., Zhang, H., Matos, J. L., Goh, N. S., Cunningham, F. J., Sung, Y., et al. (2019). High aspect ratio nanomaterials enable delivery of functional genetic material without DNA integration in mature plants. *Nat. Nanotechnol.* 14, 456–464. doi: 10.1038/s41565-019-0382-5

Forouzesh, E. (2012). *Nanoindentation-based methods for studying the mechanical behavior of living plant cells* (Lincoln, NE: University of Nebraska-Lincoln). Doctoral dissertation.

Forouzesh, E., Goel, A., Mackenzie, S. A., and Turner, J. A. (2013). *In vivo* extraction of arabidopsis cell turgor pressure using nanoindentation in conjunction with finite element modeling. *Plant J.* 73, 509–520. doi: 10.1111/tpj.12042

Forouzesh, E., Goel, A. K., and Turner, J. A. (2014). Quantifying plant cell-wall failure *in vivo* using nanoindentation. *MRS Commun.* 4, 107–111. doi: 10.1557/mrc.2014.22

Gou, Y. J., Li, Y. L., Bi, P. P., Wang, D. J., Ma, Y. Y., Hu, Y., et al. (2020). Optimization of the protoplast transient expression system for gene functional studies in strawberry (*Fragaria vesca*). *Plant Cell Tissue Organ Cult.* 141, 41–53. doi: 10.1007/s11240-020-01765-x

Haque, E., Taniguchi, H., Hassan, M., Bhowmik, P., Karim, M. R., Śmiech, M., et al. (2018). Application of CRISPR/Cas9 genome editing technology for the improvement of crops cultivated in tropical climates: recent progress, prospects, and challenges. *Front. Plant Sci.* 9. doi: 10.3389/fpls.2018.00617

Hubbard, J. D., Lui, A., and Landry, M. P. (2020). Multiscale and multidisciplinary approach to understanding nanoparticle transport in plants. *Curr. Opin. Chem. Eng.* 30, 135–143. doi: 10.1016/j.coche.2020.100659

Hwang, H. H., Yu, M., and Lai, E. M. (2017). *Agrobacterium*-mediated plant transformation: biology and applications. *Arabidopsis Book* 15, e0186. doi: 10.1199/tab.0186

Isner, J. C., and Maathuis, F. J. (2011). Measurement of cellular cGMP in plant cells and tissues using the endogenous fluorescent reporter FlincG. *Plant J.* 65, 329–334. doi: 10.1111/j.1365-313X.2010.04418.x

Izuegbunam, C. L., Wijewantha, N., Wone, B., Ariyarathne, M. A., Sereda, G., and Wone, B. W. (2021). A nano-biomimetic transformation system enables in planta expression of a reporter gene in mature plants and seeds. *Nanoscale Adv.* 3, 3240–3250. doi: 10.1039/D1NA00107H

Jain, A. K., and Thareja, S. (2019). *In vitro* and *in vivo* characterization of pharmaceutical nanocarriers used for drug delivery. *Artif. Cells Nanomed. Biotechnol.* 47, 524–539. doi: 10.1080/21691401.2018.1561457

Jat, S. K., Bhattacharya, J., and Sharma, M. K. (2020). Nanomaterial based gene delivery: a promising method for plant genome engineering. *J. Mater. Chem. B* 8, 4165–4175. doi: 10.1039/D0TB00217H

Jelenska, J., Davern, S. M., Standaert, R. F., Mirzadeh, S., and Greenberg, J. T. (2017). Flagellin peptide flg22 gains access to long-distance trafficking in arabidopsis *via* its receptor, FLS2. *J. Exp. Bot.* 68, 1769–1783. doi: 10.1093/jxb/erx060

Kang, Y., Jelenska, J., Cecchini, N. M., Li, Y., Lee, M. W., Kovar, D. R., et al. (2014). HopW1 from *Pseudomonas syringae* disrupts the actin cytoskeleton to promote virulence in arabidopsis. *PLoS Pathog.* 10, e1004232. doi: 10.1371/journal.ppat.1004232

Karami, O. (2008). Factors affecting *Agrobacterium*-mediated transformation of plants. *Transgenic Plant J.* 2, 127–137.

Kim, H., Park, M., Kim, S. J., and Hwang, I. (2005). Actin filaments play a critical role in vacuolar trafficking at the golgi complex in plant cells. *Plant Cell* 17, 888–902. doi: 10.1105/tpc.104.028829

Krenek, P., Samajova, O., Luptovciak, I., Doskocilova, A., Komis, G., and Samaj, J. (2015). Transient plant transformation mediated by *Agrobacterium* tumefaciens: Principles, methods and applications. *Biotechnol. Adv.* 33, 1024–1042. doi: 10.1016/j.biotechadv.2015.03.012

Kumar, S., Nehra, M., Dilbaghi, N., Marrazza, G., Tuteja, S. K., and Kim, K. H. (2020). Nanovehicles for plant modifications towards pest-and disease-resistance traits. *Trends Plant Sci.* 25, 198–212. doi: 10.1016/j.tplants.2019.10.007

Lacroix, B., and Citovsky, V. (2020). "Biolistic approach for transient gene expression studies in plants," in *Biolistic DNA delivery in plants*. Eds. S. Rugstgi and H. Luo (New York, NY: Humana), 125–139.

Levy, A., El-Mochtar, C., Wang, C., Goodin, M., and Orbovic, V. (2018). A new toolset for protein expression and subcellular localization studies in citrus and its application to citrus tristeza virus proteins. *Plant Methods* 14, 1–11. doi: 10.1186/s13007-017-0270-7

Li, J. F., Park, E., von Arnim, A. G., and Nebenführ, A. (2009). The FAST technique: a simplified *Agrobacterium*-based transformation method for transient gene expression analysis in seedlings of arabidopsis and other plant species. *Plant Methods* 5, 1–15. doi: 10.1186/1746-4811-5-6

Liu, Q., Chen, B., Wang, Q., Shi, X., Xiao, Z., Lin, J., et al. (2009). Carbon nanotubes as molecular transporters for walled plant cells. *Nano. Lett.* 9, 1007–1010. doi: 10.1021/nl803083u

Liu, J., Essner, J., and Li, J. (2010). Hybrid supercapacitor based on coaxially coated manganese oxide on vertically aligned carbon nanofiber arrays. *Chem. Mate.* 22, 5022–5030. doi: 10.1021/cm101591p

Maliga, P. (2004). Plastid transformation in higher plants. *Annu. Rev. Plant Biol.* 55, 289–313. doi: 10.1146/annurev.arplant.55.031903.141633

Ma, Y., Walker, R. K., Zhao, Y., and Berkowitz, G. A. (2012). Linking ligand perception by PEPR pattern recognition receptors to cytosolic Ca2+ elevation and downstream immune signaling in plants. *Proc. Natl. Acad. Sci. U. S. A.* 109, 19852–19857. doi: 10.1073/pnas.1205448109

McKnight, T. E., Melechko, A. V., Guillorn, M. A., Merkulov, V. I., Lowndes, D. H., and Simpson, M. L. (2005). "Synthetic nanoscale elements for delivery of materials into viable cells," in *NanoBiotechnology protocols*. Eds. S. Rosenthal and D. W. Wright (Nashville, TN: Humana Press), 191–208.

McKnight, T. E., Melechko, A. V., Hensley, D. K., Mann, D. G., Griffin, G. D., and Simpson, M. L. (2004). Tracking gene expression after DNA delivery using spatially indexed nanofiber arrays. *Nano. Lett.* 4, 1213–1219. doi: 10.1021/nl049504b

Melechko, A. V., Desikan, R., McKnight, T. E., Klein, K. L., and Rack, P. D. (2009). Synthesis of vertically aligned carbon nanofibres for interfacing with live systems. *J. Phys. D: Appl. Phys.* 42, 193001. doi: 10.1088/0022-3727/42/19/193001

Melechko, A. V., Merkulov, V. I., McKnight, T. E., Guillorn, M. A., Klein, K. L., Lowndes, D. H., et al. (2005). Vertically aligned carbon nanofibers and related structures: Controlled synthesis and directed assembly. *J. Appl. Phys.* 97, 3. doi: 10.1063/1.1857591

Michniewicz, M., Frick, E. M., and Strader, L. C. (2015). Gateway-compatible tissue-specific vectors for plant transformation. *BMC Res. Notes* 8, 1–8. doi: 10.1186/s13104-015-1010-6

Mitter, N., Worrall, E. A., Robinson, K. E., Li, P., Jain, R. G., Taochy, C., et al. (2017). Clay nanosheets for topical delivery of RNAi for sustained protection against plant viruses. *Nat. Plants* 3, 1–10. doi: 10.1038/nplants.2016.207

Mohan, C., Shibao, P. Y. T., and Silva, F. H. (2019). "Applications of genome Engineering/Editing tools in plants," in *Advances in plant transgenics: Methods and applications*. Eds. R. Sathiskkumar, S. R. Kumar, J. Hema and V. Baskar (Singapore: Springer), 143–165.

Ozyigit, I. I., and Yucebilgili Kurtoglu, K. (2020). Particle bombardment technology and its applications in plants. *Mol. Biol. Rep.* 47, 9831–9847. doi: 10.1007/s11033-020-06001-5

Pérez-de-Luque, A. (2017). Interaction of nanomaterials with plants: what do we need for real applications in agriculture? *Front. Environ. Sci.* 5. doi: 10.3389/fenvs.2017.00012

Ren, R., Gao, J., Lu, C., Wei, Y., Jin, J., Wong, S. M., et al. (2020). Highly efficient protoplast isolation and transient expression system for functional characterization of flowering related genes in cymbidium orchids. *Int. J. Mol. Sci.* 21, 2264. doi: 10.3390/ijms21072264

Sainsbury, F., Thuenemann, E. C., and Lomonossoff, G. P. (2009). pEAQ: versatile expression vectors for easy and quick transient expression of heterologous proteins in plants. *Plant Biotechnol. J.* 7, 682–693. doi: 10.1111/j.1467-7652.2009.00434.x

Salmeen, A. M., Shafiee, S., Krasia-Christoforou, T., Savva, I., Göransson, G., Desmaris, V, et al (2015). Low temperature and cost-effective growth of vertically aligned carbon nanofibers using spin-coated polymer-stabilized palladium nanocatalysts. *Sci. Technol. Adv. Mat.* 16, 015007. doi: 10.1088/1468-6996/16/1/015007

Sanzari, I., Leone, A., and Ambrosone, A. (2019). Nanotechnology in plant science: to make a long story short. *Front. Bioeng. Biotechnol.* 7. doi: 10.3389/fbioe.2019.00120

Schindelin, J., Arganda-Carreras, I., Frise, E., Kaynig, V., Longair, M., Pietzsch, T., et al. (2012). Fiji: an open-source platform for biological-image analysis. *Nat. Methods* 9, 676–682. doi: 10.1038/nmeth.2019

Sheen, J. (2001). Signal transduction in maize and arabidopsis mesophyll protoplasts. *Plant Physiol.* 127, 1466–1475. doi: 10.1104/pp.010820

Sohn, E. J., Kim, E. S., Zhao, M., Kim, S. J., Kim, H., Kim, Y. W., et al. (2003). Rha1, an arabidopsis Rab5 homolog, plays a critical role in the vacuolar trafficking of soluble cargo proteins. *Plant Cell* 15, 1057–1070. doi: 10.1105/tpc.009779

Tamura, K., Shimada, T., Ono, E., Tanaka, Y., Nagatani, A., Higashi, S. I., et al. (2003). Why green fluorescent fusion proteins have not been observed in the vacuoles of higher plants. *Plant J.* 35, 545–555. doi: 10.1046/j.1365-313X.2003.01822.x

Torney, F., Trewyn, B. G., Lin, V. S. Y., and Wang, K. (2007). Mesoporous silica nanoparticles deliver DNA and chemicals into plants. *Nat. Nanotechnol.* 2, 295–300. doi: 10.1038/nnano.2007.108

Wroblewski, T., Tomczak, A., and Michelmore, R. (2005). Optimization of *Agrobacterium*-mediated transient assays of gene expression in lettuce, tomato and arabidopsis. *Plant Biotechnol. J.* 3, 259–273. doi: 10.1111/j.1467-7652.2005.00123.x

Yu, Y., Yu, P. C., Chang, W. J., Yu, K., and Lin, C. S. (2020). Plastid transformation: how does it work? can it be applied to crops? what can it offer? *Int. J. Mol. Sci.* 21, 4854. doi: 10.3390/ijms21144854

Zhang, H., Demirer, G. S., Zhang, H., Ye, T., Goh, N. S., Aditham, A. J., et al. (2019). DNA Nanostructures coordinate gene silencing in mature plants. *Proc. Natl. Acad. Sci. U. S. A.* 116, 7543–7548. doi: 10.1073/pnas.1818290116

Zhang, H., Goh, N. S., Wang, J. W., Pinals, R. L., González-Grandío, E., Demirer, G. S., et al. (2022). Nanoparticle cellular internalization is not required for RNA delivery to mature plant leaves. *Nat. Nanotechnol.* 17, 197–205. doi: 10.1038/s41565-021-01018-8

Zhang, Z., Wan, T., Chen, Y., Chen, Y., Sun, H., Cao, T., et al. (2019b). Cationic polymer-mediated CRISPR/Cas9 plasmid delivery for genome editing. *Macromol. Rapid Commun.* 40, 1800068. doi: 10.1002/marc.201800068

Zhang, Q., Ying, Y., and Ping, J. (2022b). Recent advances in plant nanoscience. *Adv. Sci.* 9, 2103414. doi: 10.1002/advs.202103414

Zhao, X., Meng, Z., Wang, Y., Chen, W., Sun, C., Cui, B., et al. (2017). Pollen magnetofection for genetic modification with magnetic nanoparticles as gene carriers. *Nat. Plants* 3, 956–964. doi: 10.1002/advs.202103414

Zheng, N., Song, Z., Liu, Y., Yin, L., and Cheng, J. (2017). Gene delivery into isolated *Arabidopsis thaliana* protoplasts and intact leaves using cationic, α-helical polypeptide. *Front. Chem. Sci. Eng.* 11, 521–528. doi: 10.1007/s11705-017-1612-8

frontiers | Frontiers in Plant Science

TYPE Original Research
PUBLISHED 08 March 2023
DOI 10.3389/fpls.2023.1092013

OPEN ACCESS

EDITED BY
Lydia Pui Ying Lam,
Akita University, Japan

REVIEWED BY
Koji Miyamoto,
Teikyo University, Japan
Shifeng Zhu,
University of Kentucky, United States

*CORRESPONDENCE
Elena A. Dolgikh
dol2helen@yahoo.com

SPECIALTY SECTION
This article was submitted to Plant Physiology, a section of the journal Frontiers in Plant Science

RECEIVED 07 November 2022
ACCEPTED 17 February 2023
PUBLISHED 08 March 2023

CITATION
Kozyulina PY, Pavlova OA, Kantsurova (Rudaya) ES, Bovin AD, Shirobokova SA, Dolgikh AV, Dymo AM and Dolgikh EA (2023) Transcriptomic analysis of pea plant responses to chitooligosaccharides' treatment revealed stimulation of mitogen-activated protein kinase cascade.
Front. Plant Sci. 14:1092013.
doi: 10.3389/fpls.2023.1092013

Transcriptomic analysis of pea plant responses to chitooligosaccharides' treatment revealed stimulation of mitogen-activated protein kinase cascade

Polina Yu. Kozyulina, Olga A. Pavlova, Elizaveta S. Kantsurova (Rudaya), Andrey D. Bovin, Svetlana A. Shirobokova, Aleksandra V. Dolgikh, Alina M. Dymo and Elena A. Dolgikh*

Laboratory of Signal Regulation, All-Russia Research Institute for Agricultural Microbiology, St.-Petersburg, Russia

Since chitooligosaccharides (COs) are water-soluble, biodegradable and nontoxic compounds, their application may be considered as a promising plant-protecting agent. However, the molecular and cellular modes of action of COs are not yet understood. In this study, transcriptional changes in pea roots treated with COs were investigated *via* RNA sequencing. Pea roots treated with the deacetylated CO8-DA at low concentration (10^{-5} M) were harvested 24 h after treatment and their expression profiles were compared against medium-treated control plants. We observed 886 differentially expressed genes (fold change ≥ 1; p-value < 0.05) 24 h after treatment with CO8-DA. Gene Ontology term over-representation analysis allowed us to identify the molecular functions of the genes activated in response to CO8-DA treatment and their relation to biological processes. Our findings suggest that calcium signaling regulators and MAPK cascade play a key role in pea plant responses to treatment. Here we found two MAPKKKs, the PsMAPKKK5 and PsMAPKKK20, which might function redundantly in the CO8-DA-activated signaling pathway. In accordance with this suggestion, we showed that *PsMAPKKK* knockdown decreases resistance to pathogenic *Fusarium culmorum* fungi. Therefore, analysis showed that typical regulators of intracellular signal transduction pathways involved in triggering of plant responses *via* CERK1 receptors to chitin/COs in *Arabidopsis* and rice may also be recruited in legume pea plants.

KEYWORDS

RNAseq, chitooligosaccharides, signal transduction, MAP kinase signaling cascade, gene expression regulation, pea *Pisum sativum* L.

Introduction

The capacity of a plant to prevent pathogen attack can be defined by regulation of plant immunity. Plants have well-developed mechanisms regulating immunity and leading to activation of resistance to pathogens. These mechanisms are defined according to the pathogen molecules recognized by the plant. One of mechanism, known as microbe-associated molecular patterns (MAMPs)-triggered immunity (MTI), is based on the ability of plants to recognize MAMPs by cell surface transmembrane pattern recognition receptors (PRRs) (Zipfel, 2008; Dodds and Rathjen, 2010). Ligand perception by PRRs triggers intracellular signal transduction followed by plant defense responses activation and restriction of pathogen distribution. Despite the wide variety of MAMPs, plants demonstrate pretty similar responses to recognition of these diverse structures, based on activation of intracellular receptor-like cytoplasmic kinases and mitogen-activated protein kinases (MAPKs) triggering defense responses in the host. Among them, the MAPK cascade is highly conserved and involved in phosphorylation of various downstream protein targets, which leads to the activation of defense responses. In general, MAPK cascade consists of three protein kinases: a MAP kinase kinase kinase (MAPKKK), a MAP kinase kinase (MAPKK), and a MAP kinase (MAPK), which are involved in sequential activation by phosphorylation (Chen et al., 2021). In the model plant *Arabidopsis*, 21 MEKK1-type MAPKKKs, 10 MAPKKs and 20 MAPKs were identified (Ichimura et al., 2002).

To overcome the plant immune responses, pathogens produce a variety of effectors entering the host cells. The effectors are able to suppress plant immune response, targeting PRRs and downstream signaling regulators, allowing the pathogens to infect the plant (Ichimaru et al., 2022). In response plants have developed an effector-induced immune system referred to as effector-triggered immunity (ETI) (Dodds and Rathjen, 2010). The intracellular receptor proteins with nucleotide-binding and leucine rich domains (NBS-LRR or NLRs) were shown to be involved in the recognition of effectors and triggering plant resistance. In the absence of a specific NBS LRR to the effector, the plant became susceptible to microbial infection.

Derivatives of chitin and chitosan known as chitooligosaccharides (COs) are well-known MAMPs showing the ability to trigger resistance in plants by elicitation of defense responses. COs are defined as chitin or chitosan oligomers consisting of N-acetyl-D-glucosamine or D-glucosamine residues with a degree of polymerization less than 20 and molecular weight of up to 3900 Da (Jeon, 2001). Their application results in MTI-triggering resistance to a broad range of plant pathogens. These compounds act as plant-protecting agents and may be considered as safe and environmentally friendly agrochemicals. However, the influence of these compounds has been investigated mainly in model plants such as *Arabidopsis* and rice, while the mechanisms triggered by COs and operating in crop plants remain little studied.

Plants have a highly sensitive perception system for chitin, chitosan and COs as recent studies have shown (Kaku et al., 2006; Miya et al., 2007; Shimizu et al., 2010; Willmann et al., 2011; Liu et al., 2012; Cao et al., 2014; Shinya et al., 2014). These proteins belong to a specific class of PRRs receptors having Lysin motif (LysM) in extracellular domains. In *Arabidopsis* and rice, the Chitin Elicitor Receptor Kinase 1 (CERK1) receptors can recognize more than one elicitor molecules with the common elicitor motifs such as chitin/COs as well as peptidoglycan and its derivatives. These multifunctional receptors play a crucial role in plant resistance to pathogen attack (Miya et al., 2007; Liu et al., 2012; Wan et al., 2012). However, the precise mechanisms regulating signal transduction in CERK1-triggered immunity are still far from understanding. The pea (*Pisum sativum* L.) is one of the most important crops worldwide, however, the molecular and cellular modes of action of COs in this plant remain poorly characterized and require further study. Deacetylated oligomers such as heptamers and octamers (CO7-DA, CO8-DA) are the most effective elicitors inducing the accumulation of phytoalexins and synthesis of pathogenesis-related proteins in pea (Kendra and Hadwiger, 1984; Kendra et al., 1989; Hadwiger, 1994; Hadwiger, 2015). In accordance with this, we have shown recently a high affinity of CERK1-like receptor in legume plant pea *Pisum sativum* L., the PsLYK9, to CO7-DA and CO8-DA molecules (Leppyanen et al., 2021). Here we focused on transcriptomic analysis of CO8-DA-triggered immunity through PsLYK9 receptor in pea *Pisum sativum* L. and found a set of putative intracellular regulators, which may be involved in signal transduction and activation of plant responses to this elicitor.

Materials and methods

Plant material

Pea *Pisum sativum* L. cultivars Frisson and Finale were used for experiments. Pea seeds were sterilized with sulphuric acid for 5 min, washed 5 times with water, transferred on 1% water agar plates and germinated at room temperature in the dark. Four to five-day-old seedlings were used for treatment with elicitors or *Agrobacterium*-mediated transformation.

Plant treatment with chitooligosaccharides

Deacetylated COs with main degree of polymerization around eight (CO8-DA): Mn = 1089, Mw = 1514, Ip = 1.39, CDS = 93% in Cl-form (The Center of Bioengineering Russian Academy of Science, Moscow, Russia), were used for treatment. Four- to five-day-old seedlings of cv. Frisson were placed on the supporting foil surface in glass jars with 0.5x Jensen's medium (control) (van Brussel et al., 1982) or 0.5x Jensen's medium with CO8-DA (10^{-5} M) and incubated for 24 h. After treatment, the roots of pea seedlings were harvested for RNA extraction and gene expression analysis and immediately frozen at −80°C.

The substrate used for experiments with composite pea plants infected with pathogenic fungus *Fusarium culmorum* was 8–10 mm sterilized vermiculite. Two strains of phytopathogenic fungi *F. culmorum* (Wm. G. Sm.) Sacc. (weakly aggressive 891 and highly

aggressive 334 strains) were used to infect pea plants. To obtain inoculum, *F. culmorum* 891 or 334 strains were grown on Chapek's agar for 10–14 days and then washed from the plates with sterile water. Composite plants cv. Finale were placed into 250 ml plastic vessels with vermiculite saturated with Jensen's medium and containing 3 x 10^5 conidia of the pathogenic fungus *F. culmorum* 891 or 334 strains. Plants were grown in a growth chamber at 21°C in 16 h light/8 h dark cycles, at 60% humidity. The intensity of plant infection with phytopathogenic fungi was carried out according to the method proposed earlier (Leppyanen et al., 2017).

Plasmid constructs

Full-length encoding sequences for *PsMAPKKK5* (Psat5g044960), *PsMAPKKK20* (Psat4g086600) and *PsMAPKK1* (Psat1g131480), *PsMAPKK2* (Psat4g016480), *PsMAPKK3* (Psat1g054880), *PsMAPKK4* (Psat7g263320), *PsMAPKK5* (Psat1g050720), *PsMAPKK6* (Psat1g029480) were amplified by PCR from cDNAs prepared from roots of wild type pea plants cv. Finale using Phusion Flash High-Fidelity PCR Master Mix (Thermo Fisher Scientific, Waltham, MA, USA) and specific primers (Supplementary Table 1) and ligated into pENTRY/D-TOPO or pDONR221 vectors (Thermo Fisher Scientific, Waltham, MA, USA). For the *PsMAPKKK20* RNAi construct, the 328 bp DNA fragment corresponding to +162 to +489 region of *PsMAPKKK20* cDNA was amplified by PCR using specific primers (Supplementary Table 1), and transferred using the Gateway system with BP clonase to pDONR221 vector. At the next stage LR clonase reaction from pDONR221 into pK7GWIWG2 II Red Root vector was performed. The verified construct was transferred into the *Agrobacterium rhizogenes* ARqua 1.

For co-immunoprecipitation the full-length encoding sequences of *PsMAPKKK5, PsMAPKKK20* and *PsMAPKK1, PsMAPKK2, PsMAPKK3, PsMAPKK4, PsMAPKK5, PsMAPKK6* were cloned into pRSETa vectors with the sequences encoding 6xHIS or 3xFLAG using primers containing restriction sites. Electrocompetent *E. coli* C41 were transformed with constructs in pRSETa-6xHIS or pRSETa-3xFLAG vectors using Gene Pulser XCell electroporation system (Bio-Rad Laboratories, CA, USA) and grown on selective LB medium. A few fresh colonies were transferred into a big flask containing 200 ml LB with ampicillin 100 μg/ml and culture was grown up to OD600 = 0.6 at 37°C and then for 2 h at 28°C in presence of 0.5 mM IPTG with intensive shaking. The cell's pellets were used for protein extraction or stored at -80°C.

Co-immunoprecipitation assay

Co-immunoprecipitation was carried out using a μMACS kit (Miltenyi Biotec, Bergisch Gladbach, Germany) containing the MicroBeads with immobilized anti-HIS and anti-DYKDDDDK (also known as FLAG-tagged) antibodies. The pellet of *E. coli* cells was resuspended in lysis buffer (50 mM tris-HCl pH 8.0, 1% Triton X-100, 150 mM NaCl) containing 1× complete protease inhibitor cocktail (INHIB1, Merck, Darmstadt, Germany) and cell lysate was obtained *via* the sonication (3 × 20 s). These lysates containing HIS-tagged (PsMAPKKK5, PsMAPKKK20) or FLAG-tagged (PsMAPKK1, PsMAPKK2, PsMAPKK3, PsMAPKK4, PsMAPKK5, PsMAPKK6) proteins were co-incubated with MicroBeads for 1 – 1.5 h on ice and then were loaded onto a μMACS column placed in the magnetic stand of a μMACS separator. Then, the column with associated proteins was washed with a lysis buffer 3 - 4 times. After elution with a denaturing elution buffer (50 mM tris-HCl (pH 6.8), 50 mM DTT, 1% SDS, 1 mM EDTA, 0.005% bromophenol blue, 10% glycerol), the precipitated proteins were analyzed by sodium dodecyl sulfate polyacrylamide gel (SDS-PAGE). In our investigation, we used two approaches to study co-immunoprecipitation using a μMACS kit. In the first variant, we passed FLAG-tagged proteins and HIS-tagged proteins after co-incubation through magnetic MicroBeads with anti-HIS antibodies. In another variant, proteins were passed through the column with MicroBeads with immobilized anti-FLAG antibodies.

Agrobacterium-based plant transformation

The transformation of pea seedlings cv. Finale was performed as previously described (Leppyanen et al., 2019) with minor modifications. Seedlings at the stage of one internode were transformed with freshly grown *A. rhizogenes* strain ARqua 1 and placed on Jensen's medium (3 – 4 plants per box) in round plastic boxes with green filter (E1674, Duchefa, The Netherlands). When callus had been formed in 10 – 12 days, the plants were transferred to Emergence medium with 150 μg/ml and incubated for 3 – 4 days. Composite pea plants were transferred into pots with vermiculite saturated with Jensen's medium. Inoculation with rhizobial strain *Rhizobium leguminosarum* bv. *viciae* RIAM1026 was performed in 3 days after planting.

RNA isolation

To isolate the RNA from the frozen roots, the tissues were ground with mortar and pestle using liquid nitrogen. Extraction of RNA from the roots was done using the PuroZOL RNA isolation reagent (BioRad Laboratories, California, USA). DNA was eliminated using DNAse digestion (Thermo Fisher Scientific, USA). RNA quality and quantity were determined by Nanodrop (Implen GmbH, Munich, Germany).

RNA sequencing

The sequencing library was prepared following the guidelines for NEBNext mRNA magnetic isolation module purification kit (E7490) (https://www.neb-online.de/en/art/E7490) and NEBNext Ultra II directional RNA library prep kit for Illumina (E7760) (https://www.neb-online.de/en/art/E7770S) (New England Biolabs, USA). The quality of RNA was estimated using Bioanalyzer 2100 (Agilent Technologies, California, USA) prior to sequencing. The NEBNext Multiplex Oligos primer set for Illumina (Index Primers

Set 2) (E7500S) (New England Biolabs, USA) was used for preparation. At all stages, the material was cleaned using AMPure XP beads (Beckman Coulter, USA). The sequencing was conducted with an Illumina NovaSeq 6000 (Illumina, San Diego, CA, USA) with all 6 samples on one NovaSeq lane, resulting in 25-30 million 150-bp-reads per sample.

Data analysis

The analysis was started from raw sequencing data in fastq format. Two groups of libraries representing at least three independent biological repeats in both control and treated variants (3 - 4 plants for one replication), were sequenced on a NovaSeq 6000 (Illumina, San Diego, CA, USA) in paired-end 2 x 150 bp reads mode according to the manufacturer's protocol. The resulting reads were trimmed off Illumina adapters, additionally, read ends were trimmed by sequencing quality (phred33 score <20) using Trimmomatic (Bolger et al., 2014). To obtain read counts per gene fastq files were further processed with RSEM package (Li and Dewey, 2011) using *Pisum sativum* genome v1a (Kreplak et al., 2019) as a reference and bowtie2 aligner (Langmead and Salzberg, 2012). For visual exploration of the data and heatmap representation, the obtained read counts were normalized using variance stabilizing transformation function of DESeq2 R package (Love et al., 2014), which normalizes raw count data with respect to library size and transforms it into a matrix of counts with constant variance along the range of mean values. A visual inspection of the samples using principal component analysis (PCA) was followed by differential expression analysis on a raw count matrix of 6 individual biological replicas.

Differentially expressed genes

Data normalization and differential expression analysis were performed using R package "DESeq2" (Love et al., 2014). The data was divided per comparison into two groups: COs *vs.* Jensen's medium (control). Genes having adjusted p-value < 0.05 and absolute log2 fold change ≥ 1 were considered significantly differentially expressed.

Heatmaps of the top differentially expressed genes were created using "gplots" R package (Warnes et al., 2022). Gene ontology (Ashburner et al., 2000) gene set enrichment analysis was executed using the GSEABase R package (Morgan et al., 2022) with cutoff values: odds ratio > 2, and p-value < 0.05.

Heatmaps of the top differentially expressed genes were created using "gplots" R package (Warnes et al., 2022) with cutoff values: log2 fold change > 2, and p-value < 0.05, genes for heatmaps representing individual pathways for better readability were selected based on cutoff p-value < 0.1 from the results of differential expression analysis. Gene ontology (Ashburner et al., 2000) gene set enrichment analysis was executed using the GSEABase R package (Morgan et al., 2022) and GOstats R package (Falcon and Gentleman, 2007) with cutoff values: odds ratio > 2, and p-value < 0.05.

Real-time qPCR

After extracting the RNA as described above, first strand cDNAs were synthesized from 1 µg of total RNA using M-MLV Reverse Transcriptase (200 U/µL) (Thermo Fisher Scientific, USA) following the manufacturer's instructions. Highly specific primers were designed using Vector NTI with melting temperatures (Tm) between 54 and 58°C and amplicon lengths of 100-300 bp. As references, the housekeeping gene of the Ubiquitin (Ubiq) was used.

The qPCR cycler was a CFX96 Touch Real-Time PCR Detection System (Bio-Rad Laboratories, Hercules, CA, USA), with initial denaturation at 95°C for 3 min followed by 45 cycles of 95°C for 30 s, 54 - 58°C for 40 s and 72°C for 30 s. Melting curve analysis was performed from 54 to 95°C, where the temperature increased by 0.5°C every 5 s. The total volume was 10 µl per sample, containing 1 µl of cDNA and 5 µl of 2xiQ SYBR Green qPCR Supermix (Bio-Rad Laboratories, Hercules, CA, USA).

MAPK3/6 phosphorylation assay

Plant treatment was done with 10^{-5} M CO8-DA as elicitor for 15 min and 0.5x Jensen's medium as a control in glass jars. Total root protein was isolated in a buffer containing 100 mM MES-KON (pH 6.8), 10 mM $MgCl_2$, 1% sucrose, 0.1% Triton X-100, 1 mM DTT, 0.5 mM PMSF, 1× complete protease inhibitor cocktail (INHIB1, Merck, Darmstadt, Germany). Western-blots were done to visualize the phospho-MAPK3/6 and tubulin bands using anti–phospho-p44/42 MAPK and anti–α/β-tubulin antibodies (Cell Signaling, Danvers, MA, USA).

A phylogenetic tree construction

A phylogenetic tree was constructed using the Maximum Likelihood method with help of the IQ-TREE tool v.1.6.1 (Nguyen et al., 2015) and with automatically determined substitution model using ModelFinder (Kalyaanamoorthy et al., 2017), Tree was based on amino acid sequences that were aligned using the MAFFT tool v7.453 (Katoh and Standley, 2013) with default settings. The bootstrap values were obtained from 1000 bootstrap replicates using Ultrafast Bootstrap Approximation (Minh et al., 2013).

Results

Transcriptomic analysis of pea roots treated with deacetylated chitooligosaccharides (CO8-DA)

In the current work, we compared the transcriptomes of CO8-DA-treated pea *P. sativum* L. plants with plants incubated in medium without elicitors. In our experiments around 886 genes were found to be differentially expressed (Log2 fold change ≥ 1;

p-value < 0.05) 24 h after treatment of pea plants with deacetylated chitooligosaccharides CO8-DA (see Material and methods). Among these genes, 693 genes were up-regulated in CO8-DA-treated samples, while 193 genes were detected as down-regulated (Figure 1 and Supplementary Figure 1). Figure 1 shows the clustering of the differentially expressed genes based on their similar expression patterns. In all sample groups (CO8-DA versus control without treatment) the larger cluster represents the upregulated differentially expressed genes (Figure 1).

Gene Ontology term over-representation analysis was performed in order to check which molecular functions (Supplementary Figure 2) and biological processes (Supplementary Figure 3) are significantly activated in response to CO8-DA treatment. The highest rate of change was detected in chitinase and peroxidase activity, polysaccharide and phospholipid binding. We could also see the activation of protein kinases and calcium-dependent signaling and subsequent transcription factor activation (Supplementary Figure 2). Changes in biological processes were represented by over-representation of genes involved in cell death regulation and response to stress, such as wounding and external biotic stimulus, immune response and metabolic processes involved in defense mechanisms, such as and phenylpropanoid and flavonoid biosynthesis, chitin and cell wall polysaccharide metabolic processes, and hormone regulation mechanisms, such as response to salicylic acid (Supplementary Figure 3).

In accordance with the suggestion that in pea through CERK1-like receptor to COs, the LYK9, a complex of plant defense reactions was activated as one of the main reactions to treatment, we observed the up-regulation of genes encoding WRKY (Psat7g050880, Psat2g054280, Psat5g068680, Psat5g079680, Psat5g032760, Psat1g161840, Psat3g118040, Psat3g160600, Psat3g019520, Psat3g123560) and MYB (Psat1g209120, Psat7g159800) transcription factor family proteins, as well as C2H2 type zinc finger (Psat6g068960, Psat6g069040, Psat6g069000, Psat3g049400) transcription factor family protein (Figure 2 and Supplementary Table 2). In addition, the increased level of transcripts encoding LysM-receptor-like protein LYR4 (Psat2g024920) was revealed. This co-receptor was previously shown to be involved in the regulation of defense responses to CO8-DA through PsLYK9/PsLYR4 complex formation in pea plants (Leppyanen et al., 2021). Moreover, differentially expressed genes encoding phenylalanine ammonia-lyase 1 and 2 (PAL1 (Psat1g046920) and PAL2 (Psat3g023040)), isoflavone synthase (Psat7g117880), peroxidases (Psat6g159360, Psat2g068760, Psat6g099960) and chitinases (Psat5g291720, Psat5g020240, Psat1g084840, Psat6g194680) were also found in pea root transcriptome. They belong to typical pathogenesis related marker genes, which are activated during plant resistance stimulation. Up-regulation of genes encoding PAL1 and PAL2 and isoflavone synthase (IFS) is consistent with the suggestion that these enzymes are involved in the biosynthesis of phytoalexins and other secondary metabolites. To verify the results of RNA-seq analysis, the expression of several genes was also estimated by real-time qPCR (Supplementary Figure 4). The significant stimulation of genes encoding PAL1 (Psat1g046920), IFS (Psat7g117880), LysM-receptor-like protein LYR4 (Psat2g024920), WRKY (Psat7g050880, Psat2g054280, Psat3g019520) was confirmed by real-time qPCR (Supplementary Figure 4). High number of upregulated defense-related genes may indicate that CO8-DA induces a strong plant disease resistance in a short period after treatment.

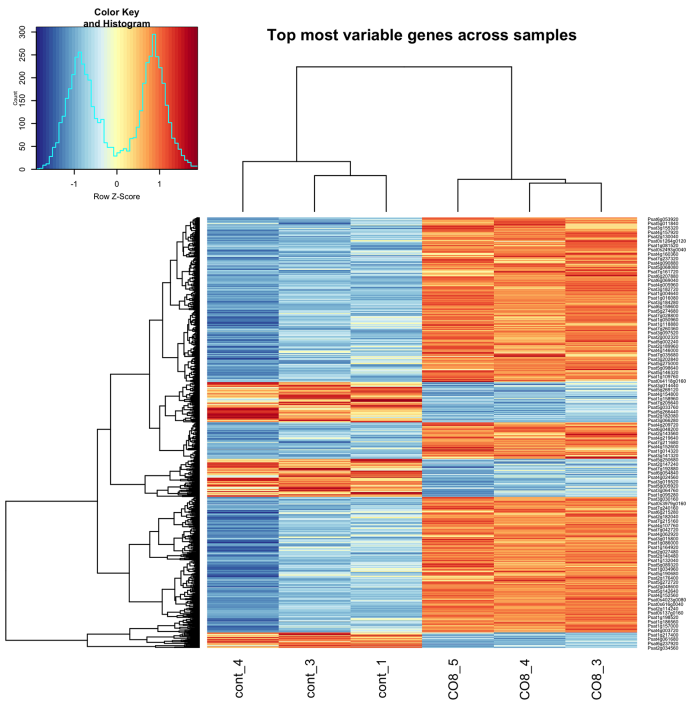

FIGURE 1
Differentially expressed genes (DEGs) in a cluster-wise heatmap of 6 biological replicas 24 h after CO8-DA treatment (Log2 fold change ≥ 1, p-value < 0.05).

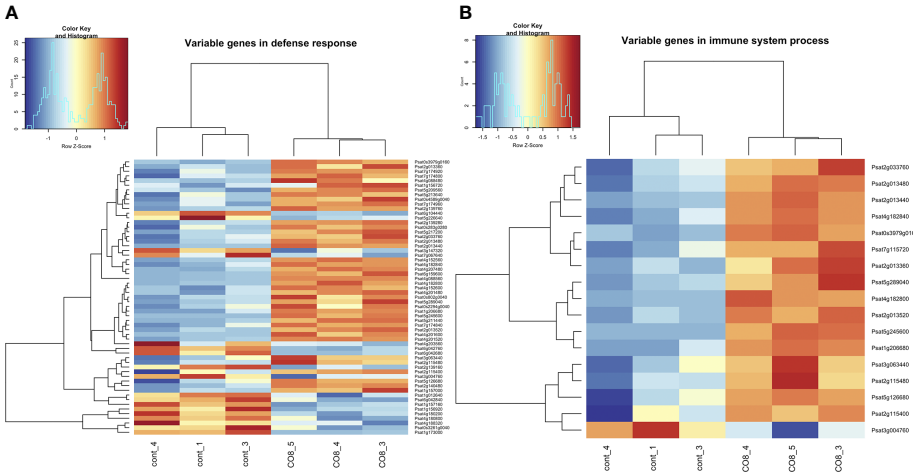

FIGURE 2
Heatmap of gene expression levels after CO8-DA treatment (3 biological replicas) in comparison to control (Jensen's medium) (3 biological replicas). The list of genes that changed expression levels and were annotated in Gene Ontology terms as a part of "defense response" **(A)** and "immune system process" **(B)** biological processes in pea roots 24 h after treatment.

Plant treatment with CO8-DA resulted in stimulation of processes related to a cell death response, as it is evidenced by the activation of genes encoding cysteine/histidine-rich C1 domain proteins (Psat3g183160, Psat3g182680) and a whole complex of NBS-LRR proteins or NLRs (Psat4g182840, Psat2g140480, Psat7g174920, Psat7g174880, Psat7g174840, Psat5g289040, Psat2g139760, Psat0s3979g0160) (Supplementary Table 2) (Dodds and Rathjen, 2010; Hwang et al., 2014). These findings suggest that stimulation of expression of these genes may be sufficient to trigger early defense responses, such as the hypersensitive response.

One of the most important aims during screening of differentially expressed genes may be searching for the genetic markers responsible for plant resistance to pathogens, since these genes can be the subject of direct genetic approaches to increase plant crop stability. Here we have found several genes encoding disease resistance proteins (Figure 2 and Supplementary Table 2). The gene Psat7g105600 encoding a probable homologue of LRR receptor-like serine/threonine-protein kinase At5g15730 is most likely a key candidate gene in triggering pea plant resistance. In *Arabidopsis* this gene is up-regulated and may be used as a marker of plant resistance to pathogen treatment (Kemmerling, 2011). The other gene Psat4g088560 encodes probable homologue of disease resistance protein At5g66900, which is important for regulation of *Arabidopsis* plant resistance to fungi (Saile et al., 2020).

Among the differentially expressed genes, a few genes (Psat1g029320, Psat2g044920) encoding Avr9/Cf-9 rapidly elicited proteins were also found (Figure 2 and Supplementary Table 2). These genes confer resistance to the fungal pathogen *Cladosporium fulvum* (Cf) through recognition of secreted avirulence (Avr) peptides. The gene Psat3g098040 encodes probable receptor-like serine/threonine-protein kinase At1g18390 involved in a positive regulation of abiotic stress response *via* abscisic acid signaling (Shin et al., 2015). The information of their homologous genes in *Arabidopsis* might provide deeper understanding of functions of these genes during resistance development.

Enhanced level of the Psat7g177240 and Psat7g177200 transcripts encoding lignin-forming anionic peroxidases was identified in treated pea roots (Supplementary Table 2). In plants Casparian strip membrane domain proteins were suggested to be crucial for the assembly and activity of lignin biosynthetic enzymes. The lignin polymer deposition determines tolerance to abiotic stresses *via* modulating nutrient uptake and pathogen distribution prevention (Yang et al., 2015). Therefore, it suggests that plant treatment with CO8-DA elicitor may stimulate a complex of genes involved in lignin deposition as response to biotic and abiotic stresses.

Hormonal regulation in plants as a response to CO8-DA treatment

Here, among differentially expressed genes we have identified the enrichment of genes belonging to the "response to salicylic acid" and "programmed cell death" pathways (Figure 3 and Supplementary Table 2). Our transcriptomic analysis revealed that a number of genes related to jasmonic acid (JA) and salicylic acid (SA) signaling events and required for plant defense response development showed different expression levels between control and CO8-DA- treated pea roots. Among them, DCD (development and cell death) domain protein B2 (Psat7g024720), nematode resistance HSPRO2-like protein (Psat2g033760), patatin-like phospholipase (Psat5g043960), calmodulin-binding-like protein (Psat1g036680), heavy metal-induced protein 6B (Psat4g016000), probable serine/threonine-protein kinase Cx32 (Psat2g149240), serine/threonine-protein kinase RIPK-like (Psat1g133080), tubby-like C 2 protein (Psat7g228880) were observed. The Psat0s802g0040 encodes NIM1-interacting 1-like (NIMIN1) protein, which *via* physical interaction with Nonexpresser of PR genes (NPR1) regulates the signal transduction pathway leading to systemic acquired resistance (Weigel et al., 2005). Homologous proteins may function as positive

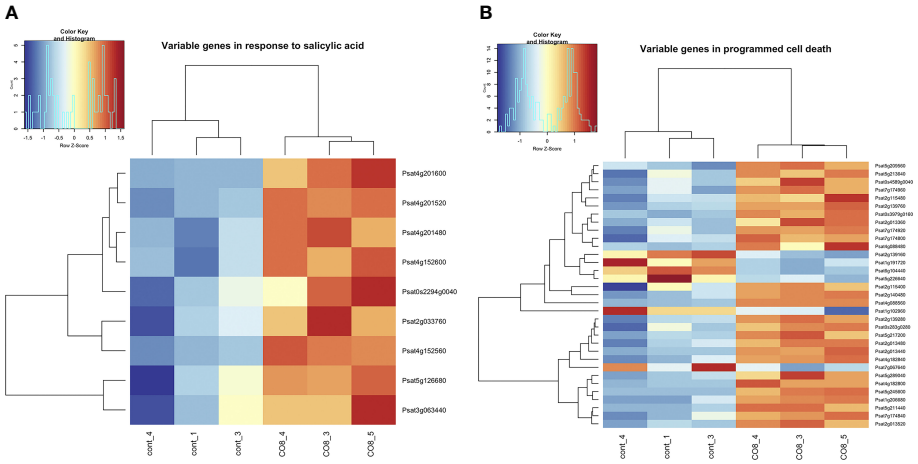

FIGURE 3
Heatmap of gene expression levels after CO8-DA treatment (3 biological replicas) in comparison to control (Jensen's medium) (3 biological replicas). The list of genes that changed expression levels and were annotated in Gene Ontology terms as a part of "response to salicylic acid" **(A)** and "programmed cell death" **(B)** biological processes in pea roots 24 h after treatment.

regulators of plant cell death and SA-dependent defense responses in plants (Hwang et al., 2014).

We also identified the enhanced expression of genes encoding several transcription factors which had been reported to SA and JA mediated signaling pathways such as NAC-like transcription factor (Psat5g058640), MYB transcription factor (Psat4g080720), AP2/ERF domain transcription factor (Psat7g124720), AP2 domain class transcription factor (Psat5g063960) and others.

Ethylene-mediated signaling pathway is activated by CO8-DA. Among of ethylene-induced genes, the Psat3g176000 and Psat5g140800 encoding putative calcium-binding protein CML19 and calcium-binding protein CML38-like as well as Psat3g176000 and Psat2g042000 encoding putative calcium-binding protein CML19 and calcium-binding protein CML24 were found.

Furthermore, the expression of genes presumed to be involved in the auxin transport and response was also changed in roots treated with CO8-DA. The analysis showed enhanced level of Psat5g267280 and Psat0s1162g0080 transcripts encoding calcium-binding PINOID-binding protein 1 (PBP1-like) involved in auxin transport and SAUR-like auxin-responsive family proteins (Psat0s2933g0120) involved in response to auxin stimulus.

These results demonstrate that CO8-DA may essentially affect the hormonal status of pea plants.

Intracellular regulators of signal transduction pathways

Among differentially expressed genes we have identified the enrichment of genes belonging to the "calcium ion binding", "signaling receptor activity" pathways (Figure 4 and Supplementary Table 2). A few up-regulated genes encoding E3 ubiquitin-protein ligases such as plant U-box (PUB) ubiquitin ligases PUB14-like (Psat6g113600), PUB22-like (Psat5g260880) and PUB23-like (Psat3g028280, Psat6g119200, Psat6g119080) proteins were found in our experiments (Figure 4 and Supplementary Figure 4). Recent studies have revealed that PUB proteins are involved in the negative and positive regulation of defense responses against pathogens (González-Lamothe et al., 2006; Trujillo et al., 2008; Yamaguchi et al., 2017). Since in *Arabidopsis* E3 ubiquitin-protein ligases AtPUB12 and AtPUB13 are involved in the negative regulation of the AtCERK1/AtLYK5 chitin receptor complex through its turnover (Liao et al., 2017; Yamaguchi et al., 2017), the activation of these proteins in pea may also contribute to the transient desensitization of chitin-induced responses. However, this assumption needs to be verified in further experiments.

Active oxygen species (AOS) generated in response to stimuli and during development can function as signaling molecules in plants, leading to specific downstream responses. The gene Psat4g205560 encoding serine/threonine-kinase OXI1-like protein was shown to be induced after CO8-DA treatment (Figure 4 and Supplementary Table 2). Expression of an *Arabidopsis thaliana OXI1* gene encoding a serine/threonine kinase is induced in response to a wide range of elicitors and other H_2O_2-generating stimuli (Rentel et al., 2004). OXI1 is required for full activation of the mitogen-activated protein kinases MPK3 and MPK6 after treatment. Moreover, the activation Psat3g011120 encoding putative respiratory burst oxidase-like protein A (RbohA) in CO8-9 treated roots may be related to H_2O_2 generation.

Receptor-like cytoplasmic kinases (RLCKs), which lack extracellular ligand-binding domains, comprise a major class of signaling proteins that regulate plant cellular activities. Among of them, the OsRLCK185 and OsRLCK176 function downstream of CERK1 in the microbial peptidoglycan and fungal chitin signaling pathways that mediate innate immunity (Ao et al., 2014; Wang et al., 2017; Yamaguchi et al., 2017). The homologous RLCK AtPBL27 in *Arabidopsis* participates in the activation of defense genes during response to chitin, peptidoglycan and their derivatives. The expression levels of Psat1g187600, Psat1g187560 transcripts encoding OsRLCK185/AtPBL27-like protein and Psat3g139680 encoding OsRLCK176-like protein were quite high in the CO8-

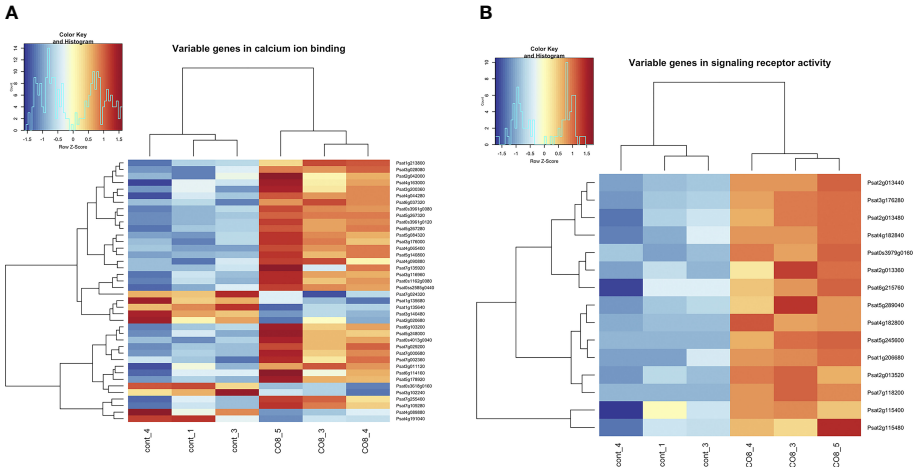

FIGURE 4
Heatmap of gene expression levels after CO8-DA treatment (3 biological replicas) in comparison to control (Jensen's medium) (3 biological replicas). The list of genes that changed expression levels and were annotated in Gene Ontology terms as a part of "calcium ion binding" **(A)** and "signaling receptor activity" **(B)** biological processes in pea roots 24 h after treatment.

DA-treated and control roots in our experiments, although they did not fall into the group of differentially expressed genes (Supplementary Table 3). Since these protein kinases may be related to endogenous intracellular signaling downstream of CERK1-like receptor, the LYK9, the role of pea AtPBL27/OsRLCK185-like and OsRLCK176-like protein kinases will be verified in our subsequent experiments.

An essential up-regulation of Psat3g028080 transcript encoding calcium-dependent protein kinase may be related to calcium signaling after CO8-DA perception. In addition, stimulation of the Psat7g118200 encoding glutamate receptor-like channel may be related to calcium influx into the cell as previous studies showed (Kwaaitaal et al., 2011). It demonstrates that CO8-DA elicitor might induce elevation in the concentration of free cytosolic calcium (Figure 4 and Supplementary Table 2). Indeed, among differentially expressed genes a lot of calcium-binding proteins were found. As examples, the Psat5g257040, Psat3g061280, Psat2g004960 encoding calcium-transporting ATPase and Psat3g049400 encoding IQ1 calcium, calmodulin-binding protein were found to be differentially regulated. Moreover, the Psat0s3961g0080, Psat0s3961g0120, Psat5g084320, Psat0ss2585g0440, Psat4g090880, Psat3g200360 encoding EF hand calcium-binding family proteins were also up-regulated after treatment.

Another type of intracellular regulators appearing as mitogen-activated protein kinase kinase kinases (MAPKKKs) such as Psat5g044960 encoding PsMAPKKK5 and Psat4g086600 encoding PsMAPKKK20 were revealed to be stimulated (Figure 4 and Supplementary Table 2). These proteins showed a high level of homology with genes encoding MAPKKKs in *Arabidopsis*, rice, tobacco and model legume *Medicago truncatula* (Figure 5). Therefore, analysis showed that typical regulators of intracellular signal transduction pathways involved in triggering of plant responses *via* CERK1 receptors in *Arabidopsis* and rice may also be recruited in legume pea plants. Activation of several MAPKKKs indicates that these regulators might function redundantly in chitin/COs signaling. It is important to note, that pea PsMAPKKK5 protein showed the highest homology level with *Arabidopsis* AtMAPKKK5 and rice OsMAPKKK18, OsMAPKKK11 involved in chitin and COs perception (Figure 5) (Rao et al., 2010; Yamada et al., 2016; Kawasaki et al., 2017; Wang et al., 2017; Yamada et al., 2017). Another PsMAPKKK20 protein belongs to previously unstudied type of MAPKKKs. The AtMAPKKK5 and OsMAPKKK18, OsMAPKKK11 from *Arabidopsis* and rice were shown to be up-regulated in response to chitin/COs treatment and involved in subsequent phosphorylation of downstream MAPKK and MAPK signal regulators (Yamada et al., 2016; Kawasaki et al., 2017; Yamada et al., 2017). Since we also observed the up-regulation of *PsMAPKKK5* and *PsMAPKKK20*, this was in line with previous results.

Searching the components of chitin/COs-triggered MAP kinase cascade activation

To address whether PsMAPKKK5 and PsMAPKKK20 are involved in CO8-DA-induced defense activation, the searching of downstream targets such as MAP kinase kinases (MAPKKs) (Figure 6) was performed. To demonstrate direct interaction between MAPKKKs with their substrates, the MAPKKs, we expressed the full-length PsMAPKKK5 and PsMAPKKK20 in *Escherichia coli* as recombinant proteins fused to the N-terminus of 6xHIS (Figures 7A, B), and loaded them onto the columns with immobilized anti-6xHIS antibodies for co-immunoprecipitation (Co-IP). In the pea genome six genes encoding MAPKK were identified (Figure 6). All these six pea MAPKK such as PsMAPKK1, PsMAPKK2, PsMAPKK3, PsMAPKK4, PsMAPKK5 and PsMAPKK6 were expressed fused with 3xFLAG and used for Co-IP onto the columns with immobilized anti-6xHIS antibodies (Figures 7A, B and Supplementary Figure 5). Additionally, the Co-IP on the columns with immobilized anti-FLAG antibodies was also carried out for PsMAPKK1, PsMAPKK2, PsMAPKK3,

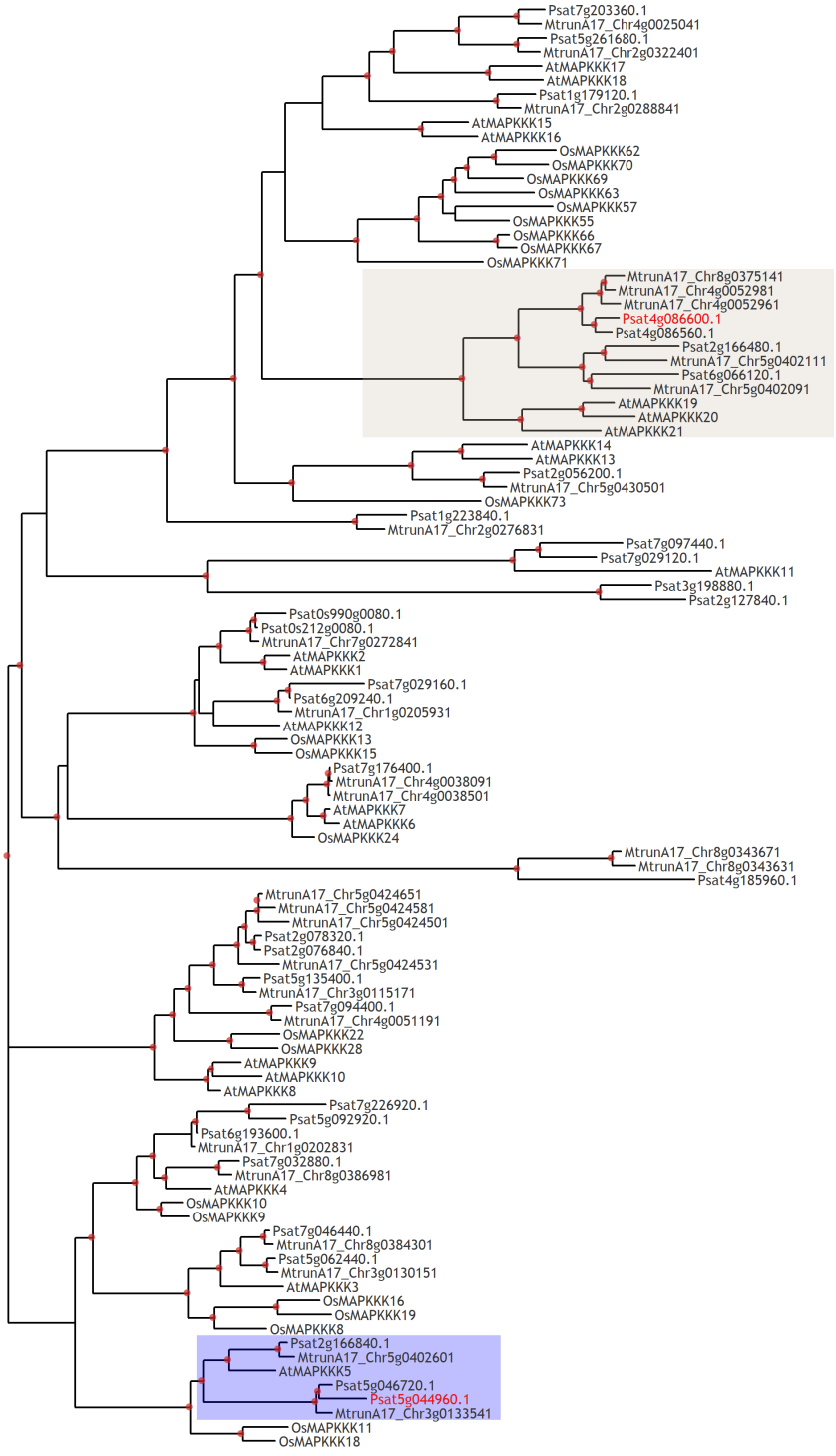

FIGURE 5
Phylogenetic tree constructed by the Maximum Likelihood method based on amino acid sequences of MAPKKKs from *Arabidopsis thaliana*, rice *Oryza sativa* and legumes: *Medicago truncatula*, *Pisum sativum*. Red dots indicate branch support more than 80 based on 1000 bootstrap replicates. Red labels show genome identifiers of PsMAPKKK5 (Psat5g044960) and PsMAPKKK20 (Psat4g086600).

PsMAPKK4, PsMAPKK5, PsMAPKK6 fused with 3xFLAG and PsMAPKKK5 fused with 6xHIS (Figure 7D). The Co-IP assays showed that both PsMAPKKK5 and PsMAPKKK20 were able to directly and strongly interact with PsMAPKK6 and showed only weak interaction with other PsMAPKKs (Figures 7A, B, D). The control experiments were also performed to test the non-specific binding of proteins with both type of beads (Supplementary Figure 6). Although we failed to detect it for almost all proteins, some non-specific binding was found for PsMAPKK6 on beads with immobilized anti-HIS antibodies (Supplementary Figure 6). To confirm the real interaction between two PsMAPKKKs and PsMAPKK6, the HIS-tagged PsMAPKK6 was also obtained in *E.*

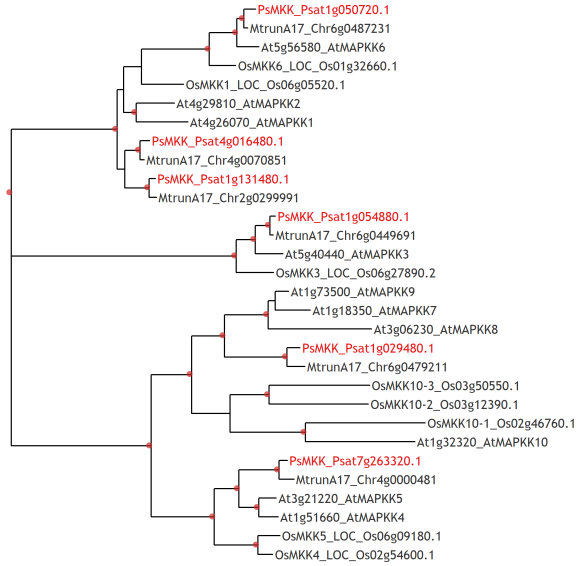

FIGURE 6
Phylogenetic tree constructed by the Maximum Likelihood method based on amino acid sequences of MAPKKs from *Arabidopsis thaliana*, rice *Oryza sativa* and legumes: *Medicago truncatula*, *Pisum sativum*. Red labels show genome identifiers of PsMAPKK6 (Psat1g029480), PsMAPKK2 (Psat4g016480), and PsMAPKK1 (Psat1g131480).

coli and tested with FLAG-tagged PsMAPKKK20 (Figure 7C). After Co-IP using anti-HIS beads, both proteins were found in eluted fraction. These results confirmed the interaction between tested proteins (Figure 7C). Therefore, our experiments showed the potential targets of two MAPKKKs during signal transduction in response to CO8-DA perception by pea plants.

It was previously shown that the CERK1-like receptors in model legume plants *M. truncatula* (MtLYK9) and *Lotus japonicus*

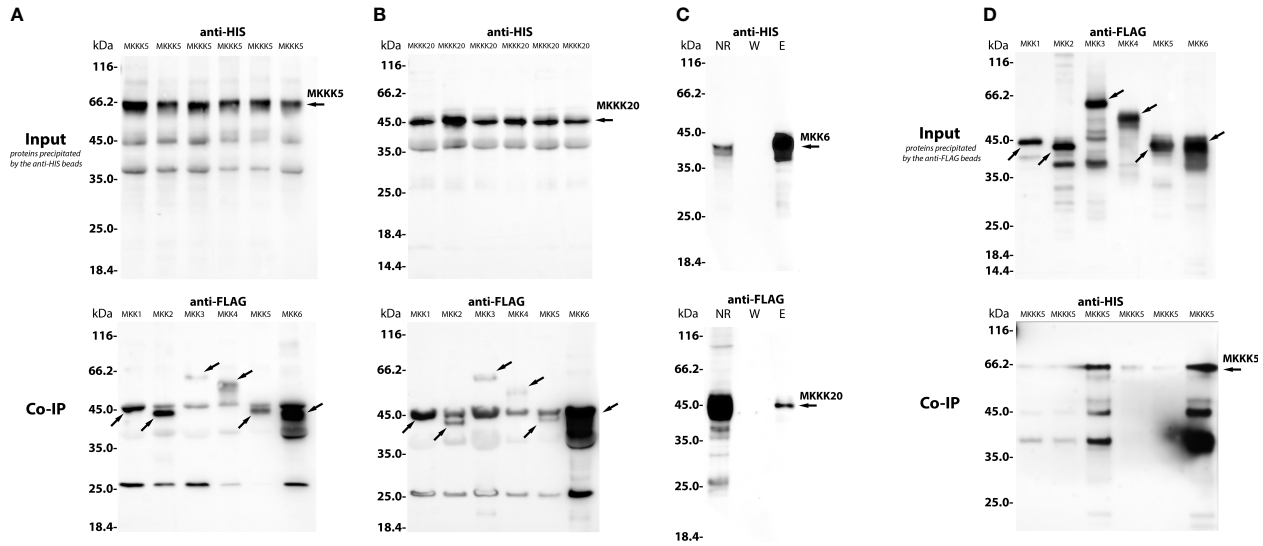

FIGURE 7
The co-immunoprecipitation of PsMAPKKK5, PsMAPKKK20 and PsMAPKK1, PsMAPKK2, PsMAPKK3, PsMAPKK4, PsMAPKK5, PsMAPKK6 from *P. sativum* cv. Finale. A heterologous protein expression was carried out in *Escherichia coli* C41, allowing high levels of expression of all proteins of interest fused to 6xHIS or 3xFLAG tag **(A–D)**. The lysates containing HIS-tagged and FLAG-tagged proteins were co-incubated with beads for 1 – 1.5 h on ice and then were loaded onto a μMACS column placed in the magnetic stand. After washing 3 - 4 times, the elution was done with a denaturing elution buffer followed by Western-blot analysis. In panels **(A, B)**, the HIS-tagged proteins (PsMAPKKK5, PsMAPKKK20) and FLAG-tagged proteins (PsMAPKK1, PsMAPKK2, PsMAPKK3, PsMAPKK4, PsMAPKK5, PsMAPKK6) were precipitated by anti-HIS magnetic beads **(A, B)**. In panel **(C)**, the PsMAPKK6 HIS-tagged protein and PsMAPKKK20 FLAG-tagged protein were also precipitated by anti-HIS beads **(C)**. In panel **(D)**, the FLAG-tagged proteins (PsMAPKK1, PsMAPKK2, PsMAPKK3, PsMAPKK4, PsMAPKK5, PsMAPKK6) and PsMAPKKK5 HIS-tagged protein were precipitated by anti-FLAG beads **(D)**. (NR – non retained fraction, W – washing, El – elution). The molecular weight of MKKK5 is about 65 kDa, while the weight of MKKK20 is about 45 kDa **(A, B)**. The molecular weight of MKK1 is about 45 kDa, MKK2 – 43 kDa, MKK3 – 65 kDa, MKK4 – 55 kDa, MKK5 – 43 kDa and MKK6 – 43 kDa **(C, D)**. The assays revealed the strong interaction between PsMAPKKK5 and PsMAPKK6 **(A)** as well as PsMAPKKK20 and PsMAPKK6 **(B–D)**, while both PsMAPKKK5 and PsMAPKKK20 showed only weak interactions with other PsMAPKKs.

(LjCERK6) are able to activate MAPK3/MAPK6 after COs perception (Bozsoki et al., 2017; Gibelin-Viala et al., 2019). Indeed, using specific anti-phospho-p44/42 MAPK antibodies the phosphorylation of PsMAPK3/PsMAPK6 in pea in response to CO8-DA treatment was also revealed in our experiments (Figure 8).

Analysis of involvement of MAPKKK in plant resistance to pathogens

To further verify the role of MAPKKKs in pea plant response to CO8-DA found in transcriptome assay, the RNAi based experiments were performed. We focused on gene encoding PsMAPKKK20, because it belongs to another type of MAPKKKs not previously studied in plants. To better understand the role of this signal component in plants, the suppression of *PsMAPKKK20* was done using RNA interference and showed to be around 50 – 60% in comparison to control plants transformed with *GUS* gene under 35S promoter (GUS-overexpression, GUS-OE) (Figures 9A, B). Infection of these composite plants with phytopathogenic fungi *Fusarium culmorum* 891 and 334 strains differing in aggressiveness showed increased susceptibility of *PsMAPKKK20*-RNAi pea plants to pathogens, especially to highly aggressive 334 fungal strain (Figure 9C). Therefore, the silencing of *PsMAPKKK20* by RNAi enhances susceptibility to infection. It suggests that stimulated CO8-DA elicitor treatment *PsMAPKKK20* can be involved in the regulation of pea plant resistance to pathogens.

Discussion

Since our experiments were aimed at clarifying the molecular and cellular modes of action of COs in crop legume *P. sativum* L., we investigated the transcriptional changes in control and treated pea roots *via* RNA sequencing. Here we describe the pathways and mechanisms triggered by CO8-DA and operating in crop legume plant *P. sativum* L.

Taken together, our results point to a rapid and significant activation of pea genes involved in regulation of host defense responses, induced by CO8-DA, in accordance with previous findings for chitin-related compounds in *Arabidopsis*, rice, potato, tea (Chen et al., 2020; Lemke et al., 2020; Siriwong et al., 2021; Ichimaru et al., 2022; Ou et al., 2022). We have shown that a set of genes encoding specific enzymes involved in the biosynthesis of phytoalexins and other secondary metabolites was up-regulated in response to CO8-DA, that was in line with previous findings in other plants (Vasyukova et al., 2001; Khan et al., 2003; Zhang et al., 2020). The pea plant treatment with CO8-DA stimulated the synthesis of such components as lignins, reinforcing the cell wall. Similar effect of COs was previously shown in rice and tea (Siriwong et al., 2021; Ou et al., 2022).

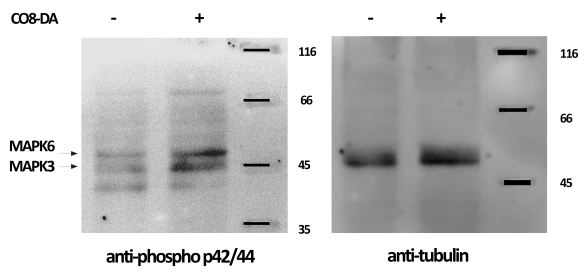

FIGURE 8
CO8-DA-induced MAPK3/6 phosphorylation in *Pisum sativum* cv. Finale. Plant treatment was done with 10^{-5} M CO8-DA (+) as elicitor for 15 min and 0.5x Jensen's medium (-) as a control in glass jars. Western-blots were done to visualize the phospho-MAPK3/6 and tubulin bands using anti–phospho-p44/42 MAPK and anti–α/β-tubulin antibodies.

At the same time, one of the most important aims during screening of differentially expressed genes may be searching for the specific genes responsible for plant resistance activation to pathogens. Since these genes may be the subject of direct genetic manipulations to increase plant crop stability. Indeed, some genes encoding disease resistance proteins such as Psat7g105600, Psat4g088560, Psat7g083880 were identified in our experiments as probable orthologs of genes previously found and well-studied in *Arabidopsis* (At5g15730, At5g66900, At1g18390). The information about homologous genes in *Arabidopsis* indicates their involvement in a positive regulation of resistance to biotic and abiotic stress responses. Therefore, these genes are potential targets for increasing legume plant resistance to pathogens.

Based on our transcriptomic analysis there is some evidence that CO8-DA elicitor may stimulate expression of genes encoding NBS-LRRs or NLRs, thereby increasing plant immune response. In susceptible plants, pathogens inject effectors into the host cell to prevent the immune response. In contrast, recognition of effectors by NLRs leads to ETI activation resulting in the "hypersensitive response" followed by death of the host cell and restriction of pathogen growth (Heath, 2000; Jones and Dangl, 2006). Recent studies showed that heterologous expression of the *NBS-LRR* genes may significantly enhance pathogen resistance in recipient plants (Li et al., 2018). It demonstrates that application of CO elicitors for stimulation of these genes may be considered as a promising tool for manipulation with plant resistance.

The results demonstrate that CO8-DA treatment may affect the hormonal status of pea plants. We have shown that ethylene mediated signaling pathway is up-regulated by CO8-DA. Moreover, a number of genes related to jasmonic acid (JA) and salicylic acid (SA) signaling events were found to be differentially regulated. Analysis of literature data suggests that these pathways are required for plant defense response development as it was shown previously for other plants (Jwa et al., 2002; Miller et al., 2017).

Calcium signaling plays a key role in plant responses to environmental stimuli. In *Arabidopsis*, stimulation of PRRs by MAMPs (flg22, elf18, chitin/COs) results in a rapid transient influx of extracellular Ca^{2+} into the cytosol, followed by the activation of receptor-like cytoplasmic kinases and mitogen-activated protein kinases (Ranf et al., 2011; Bigeard et al., 2015). Indeed, our results suggest the existence of a signaling pathway from CERK1-like receptor, the LYK9, to intracellular activation of calcium signaling and an MAPK cascade in response to treatment in

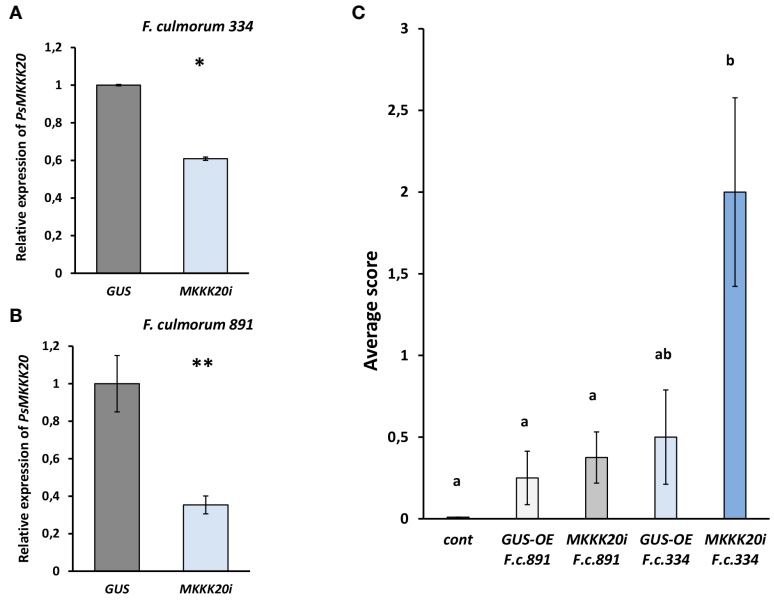

FIGURE 9
The effect of *PsMAPKKK20* gene suppression on resistance to the pathogenic fungus *Fusarium culmorum* highly aggressive 334 **(A)** and weakly aggressive 891 strains **(B)** in *Pisum sativum* cv. Finale plants. Composite plants with the *PsMAPKKK20* gene suppression in transgenic roots (*PsMAPKKK20-RNAi*) were compared with control plants with β-glucuronidase gene overexpression (*GUS-OE*). Analysis was performed two weeks after infection with *F. culmorum*. Approximately 50 - 60% suppression of the *PsMAPKKK20* gene in the transgenic roots of pea was revealed **(A, B)**. One-way ANOVA test was used to compare gene expression levels. The resistance to infection in transgenic roots of *PsMAPKKK20*-RNAi plants was significantly reduced in comparison to *GUS-OE* control **(C)**. Two biological replicates were analyzed for *P. sativum*, each containing 10 – 15 plants per variant. Totally about 40 and 30 transgenic fluorescent roots of *PsMAPKKK20*-RNAi and *GUS-OE* plants, correspondingly, were included in the analysis. Kruskal-Wallis test (R-studio) was used to compare infection scores in *PsMAPKKK20*-RNAi and *GUS-OE* variants. Values are means ± SEM. *, values with various letters are significantly different at $P < 0.05$; **, significant difference at $P < 0.01$.

pea *Pisum sativum* L. Perception of CO8-DA by pea plant induced the expression of genes related to regulation of calcium signaling in the cells. Among them, the gene encoding glutamate receptor-like channel and calcium-dependent protein kinase were found in our experiments. Here we found two MAPKKKs, the PsMAPKKK5 and PsMAPKKK20, which might function redundantly in the chitin/COs signaling pathway. At the next step, the PsMAPKK6 plays the most important role in the signal transduction pathway that is followed by PsMAPK3/PsMAPK6 activation. In accordance with this suggestion, we showed that *PsMAPKKK20*-RNAi knockdown may decrease chitin-induced defense marker activation and resistance to pathogenic *Fusarium* fungus.

These results were consistent with those in *Arabidopsis* and rice, where CERK1 elicitation was able to activate signal transduction, including calcium-regulated channels, receptor-like cytoplasmic kinases and mitogen-activated protein kinases, which might regulate the plant resistance. Previously, receptor-like cytoplasmic kinase AtPBL27 was reported to connect CERK1-mediated chitin/COs perception to MAPK cascade activation (AtMAPKKK5) in *Arabidopsis* (Shinya et al., 2014; Yamada et al., 2017). In rice, OsRLCK185 and OsRLCK176 might function redundantly and activate OsMAPKKK18 and OsMAPKKK11, rice orthologs of AtMAPKKK5, in the OsCERK1-induced chitin and peptidoglycan signaling pathways (Ao et al., 2014; Wang et al., 2017; Yamada et al., 2017; Yamaguchi et al., 2017). Therefore, our findings suggest that in pea the calcium signaling regulators and MAPK cascade activated by CO8-DA induce immune responses by phosphorylating a complex of downstream targets.

Data availability statement

The data presented in the study are deposited in the NCBI repository, accession number GEO Submission (GSE218057).

Author contributions

PK: Investigation, writing original draft preparation, methodology, and data analysis. OP: Investigation, heterologous protein synthesis, co-immunoprecipitation, library preparation. EK: Investigation, plant transformation, and library preparation. AB: Investigation, heterologous protein synthesis, and co-immunoprecipitation. AVD: Genome-based searching, analysis and graphic output of phylogenetic trees. SS: Methodology and cloning. AMD: Methodology and cloning. ED: Conceptualization, writing and editing, and supervision. All authors contributed to the article and approved the submitted version.

Funding

This work was supported financially by the Russian Science Foundation RSF 21-16-00106.

Acknowledgments

The research was performed using equipment of the Core Centrum "Genomic Technologies, Proteomics and Cell Biology" in ARRIAM.

Conflict of interest

The authors declare that the research was conducted in the absence of any commercial or financial relationships that could be construed as a potential conflict of interest.

Publisher's note

Supplementary material

The Supplementary Material for this article can be found online at: https://www.frontiersin.org/articles/10.3389/fpls.2023.1092013/full#supplementary-material

References

Ao, Y., Li, Z., Feng, D., Xiong, F., Liu, J., Li, J.-F., et al. (2014). OsCERK1 and OsRLCK176 play important roles in peptidoglycan and chitin signaling in rice innate immunity. *Plant J.* 80, 1072–1084. doi: 10.1111/tpj.12710

Ashburner, M., Ball, C. A., Blake, J. A., Botstein, D., Butler, H., Cherry, J. M., et al. (2000). Gene ontology: Tool for the unification of biology. *Nat. Genet.* 25, 25–29. doi: 10.1038/75556

Bigeard, J., Colcombet, J., and Hirt, H. (2015). Signaling mechanisms in pattern-triggered immunity (PTI). *Mol. Plant* 8, 521–539. doi: 10.1016/j.molp.2014.12.022

Bolger, A. M., Lohse, M., and Usadel, B. (2014). Trimmomatic: A flexible trimmer for illumina sequence data. *Bioinformatics* 30, 2114–2120. doi: 10.1093/bioinformatics/btu170

Bozsoki, Z., Cheng, J., Feng, F., Gysel, K., Vinther, M., Andersen, K. R., et al. (2017). Receptor-mediated chitin perception in legume roots is functionally separable from nod factor perception. *Proc. Natl. Acad. Sci.* 114, E8118–E8127. doi: 10.1073/pnas.1706795114

Cao, Y., Liang, Y., Tanaka, K., Nguyen, C. T., Jedrzejczak, R. P., Joachimiak, A., et al. (2014). The kinase LYK5 is a major chitin receptor in arabidopsis and forms a chitin-induced complex with related kinase CERK1. *Elife* 3, 1–19. doi: 10.7554/eLife.03766

Chen, J., Wang, L., and Yuan, M. (2021). Update on the roles of rice MAPK cascades. *Int. J. Mol. Sci.* 22, 1679. doi: 10.3390/ijms22041679

Chen, L., Xia, W., Song, J., Wu, M., Xu, Z., Hu, X., et al. (2020). Enhanced thermotolerance of arabidopsis by chitooligosaccharides-induced CERK1n-ERc fusion gene. *Plant Signal. Behav.* 15, 1816322. doi: 10.1080/15592324.2020.1816322

Dodds, P. N., and Rathjen, J. P. (2010). Plant immunity: Towards an integrated view of plant–pathogen interactions. *Nat. Rev. Genet.* 11, 539–548. doi: 10.1038/nrg2812

Falcon, S., and Gentleman, R. (2007). Using GOstats to test gene lists for GO term association. *Bioinformatics* 23, 257–258. doi: 10.1093/bioinformatics/btl567

Gibelin-Viala, C., Amblard, E., Puech-Pages, V., Bonhomme, M., Garcia, M., Bascaules-Bedin, A., et al. (2019). The medicago truncatula LysM receptor-like kinase LYK9 plays a dual role in immunity and the arbuscular mycorrhizal symbiosis. *New Phytol.* 223, 1516–1529. doi: 10.1111/nph.15891

Gonzaílez-Lamothe, R., Tsitsigiannis, D. I., Ludwig, A. A., Panicot, M., Shirasu, K., and Jones, J. D. G. (2006). The U-box protein CMPG1 is required for efficient activation of defense mechanisms triggered by multiple resistance genes in tobacco and tomato. *Plant Cell* 18, 1067–1083. doi: 10.1105/tpc.106.040998

Hadwiger, L. A. (1994). Chitosan polymer sizes effective in inducing phytoalexin accumulation and fungal suppression are verified with synthesized oligomers. *Mol. Plant-Microbe Interact.* 7, 531. doi: 10.1094/MPMI-7-0531

Hadwiger, L. A. (2015). Anatomy of a nonhost disease resistance response of pea to fusarium solani: PR gene elicitation *via* DNase, chitosan and chromatin alterations. *Front. Plant Sci.* 6. doi: 10.3389/fpls.2015.00373

Heath, M. C. (2000). Hypersensitive response-related death. *Plant Mol. Biol.* 44, 321–334. doi: 10.1023/A:1026592509060

Hwang, I. S., Choi, D. S., Kim, N. H., Kim, D. S., and Hwang, B. K. (2014). The pepper cysteine/histidine-rich DC1 domain protein binds both RNA and DNA and is required for plant cell death and defense response. *New Phytol.* 201, 518–530. doi: 10.1111/nph.12521

Ichimaru, K., Yamaguchi, K., Harada, K., Nishio, Y., Hori, M., Ishikawa, K., et al. (2022). Cooperative regulation of PBI1 and MAPKs controls WRKY45 transcription factor in rice immunity. *Nat. Commun.* 13, 1–16. doi: 10.1038/s41467-022-30131-y

Ichimura, K., Shinozaki, K., Tena, G., Sheen, J., Henry, Y., Champion, A., et al. (2002). Mitogen-activated protein kinase cascades in plants: A new nomenclature. *Trends Plant Sci.* 7, 301–308. doi: 10.1016/S1360-1385(02)02302-6

Jeon, Y.-J. (2001). Antimicrobial effect of chitooligosaccharides produced by bioreactor. *Carbohydr. Polym.* 44, 71–76. doi: 10.1016/S0144-8617(00)00200-9

Jones, J. D. G., and Dangl, J. L. (2006). The plant immune system. *Nature* 444, 323–329. doi: 10.1038/nature05286

Jwa, N. S., Agrawal, G. K., Rakwal, R., Kim, J. A., and Agrawal, V. P. (2002). Differential regulation of an early and late responsive rice endosperm kinase mRNA in seedling leaves. *Plant Physiol. Biochem.* 40, 1025–1031. doi: 10.1016/S0981-9428(02)01467-5

Kaku, H., Nishizawa, Y., Ishii-Minami, N., Akimoto-Tomiyama, C., Dohmae, N., Takio, K., et al. (2006). Plant cells recognize chitin fragments for defense signaling through a plasma membrane receptor. *Proc. Natl. Acad. Sci.* 103, 11086–11091. doi: 10.1073/pnas.0508882103

Kalyaanamoorthy, S., Minh, B. Q., Wong, T. K. F., von Haeseler, A., and Jermiin, L. S. (2017). ModelFinder: Fast model selection for accurate phylogenetic estimates. *Nat. Methods* 14, 587–589. doi: 10.1038/nmeth.4285

Katoh, K., and Standley, D. M. (2013). MAFFT multiple sequence alignment software version 7: Improvements in performance and usability. *Mol. Biol. Evol.* 30, 772–780. doi: 10.1093/molbev/mst010

Kawasaki, T., Yamada, K., Yoshimura, S., and Yamaguchi, K. (2017). Chitin receptor-mediated activation of MAP kinases and ROS production in rice and arabidopsis. *Plant Signal. Behav.* 12, 4–8. doi: 10.1080/15592324.2017.1361076

Kemmerling, B. (2011). A genome-wide survey for arabidopsis leucine-rich repeat receptor kinases implicated in plant immunity. *Front. Plant Sci.* 2. doi: 10.3389/fpls.2011.00088

Kendra, D. F., Christian, D., and Hadwiger, L. A. (1989). Chitosan oligomers from fusarium solani/pea interactions, chitinase/β-glucanase digestion of sporelings and from fungal wall chitin actively inhibit fungal growth and enhance disease resistance. *Physiol. Mol. Plant Pathol.* 35, 215–230. doi: 10.1016/0885-5765(89)90052-0

Kendra, D. F., and Hadwiger, L. A. (1984). Characterization of the smallest chitosan oligomer that is maximally antifungal toFusarium solani and elicits pisatin formation inPisum sativum. *Exp. Mycol.* 8, 276–281. doi: 10.1016/0147-5975(84)90013-6

Khan, W., Prithiviraj, B., and Smith, D. L. (2003). Chitosan and chitin oligomers increase phenylalanine ammonia-lyase and tyrosine ammonia-lyase activities in soybean leaves. *J. Plant Physiol.* 160, 859–863. doi: 10.1078/0176-1617-00905

Kreplak, J., Madoui, M.-A., Cápal, P., Novák, P., Labadie, K., Aubert, G., et al. (2019). A reference genome for pea provides insight into legume genome evolution. *Nat. Genet.* 51, 1411–1422. doi: 10.1038/s41588-019-0480-1

Kwaaitaal, M., Huisman, R., Maintz, J., Reinstädler, A., and Panstruga, R. (2011). Ionotropic glutamate receptor (iGluR)-like channels mediate MAMP-induced calcium influx in arabidopsis thaliana. *Biochem. J.* 440, 355–373. doi: 10.1042/BJ20111112

Langmead, B., and Salzberg, S. L. (2012). Fast gapped-read alignment with bowtie 2. *Nat. Methods* 9, 357–359. doi: 10.1038/nmeth.1923

Lemke, P., Moerschbacher, B. M., and Singh, R. (2020). Transcriptome analysis of solanum tuberosum genotype RH89-039-16 in response to chitosan. *Front. Plant Sci.* 11. doi: 10.3389/fpls.2020.01193

Leppyanen, I. V., Kirienko, A. N., and Dolgikh, E. A. (2019). Agrobacterium rhizogenes —mediated transformation of pisum sativum l. roots as a tool for studying the mycorrhizal and root nodule symbioses. *PeerJ* 7, e6552. doi: 10.7717/peerj.6552

Leppyanen, I. V., Pavlova, O. A., Vashurina, M. A., Bovin, A. D., Dolgikh, A. V., Shtark, O. Y., et al. (2021). LysM receptor-like kinase LYK9 of pisum sativum l. may regulate plant responses to chitooligosaccharides differing in structure. *Int. J. Mol. Sci.* 22, 711. doi: 10.3390/ijms22020711

Leppyanen, I. V., Shakhnazarova, V. Y., Shtark, O. Y., Vishnevskaya, N. A., Tikhonovich, I. A., and Dolgikh, E. A. (2017). Receptor-like kinase LYK9 in pisum sativum l. is the CERK1-like receptor that controls both plant immunity and AM symbiosis development. *Int. J. Mol. Sci.* 19, 8. doi: 10.3390/ijms19010008

Li, B., and Dewey, C. N. (2011). RSEM: Accurate transcript quantification from RNA-seq data with or without a reference genome. *BMC Bioinf.* 12, 323. doi: 10.1186/1471-2105-12-323

Li, N.-Y., Zhou, L., Zhang, D.-D., Klosterman, S. J., Li, T.-G., Gui, Y.-J., et al. (2018). Heterologous expression of the cotton NBS-LRR gene GbaNA1 enhances verticillium wilt resistance in arabidopsis. *Front. Plant Sci.* 9. doi: 10.3389/fpls.2018.00119

Liao, D., Cao, Y., Sun, X., Espinoza, C., Nguyen, C. T., Liang, Y., et al. (2017). Arabidopsis E3 ubiquitin ligase PLANT U-BOX13 (PUB 13) regulates chitin receptor LYSIN MOTIF RECEPTOR KINASE5 (LYK 5) protein abundance. *New Phytol.* 214, 1646–1656. doi: 10.1111/nph.14472

Liu, T., Liu, Z., Song, C., Hu, Y., Han, Z., She, J., et al. (2012). Chitin-induced dimerization activates a plant immune receptor. *Sci. (80).* 336, 1160–1164. doi: 10.1126/science.1218867

Love, M. I., Huber, W., and Anders, S. (2014). Moderated estimation of fold change and dispersion for RNA-seq data with DESeq2. *Genome Biol.* 15, 550. doi: 10.1186/s13059-014-0550-8

Miller, R. N. G., Alves, G. S. C., and Van Sluys, M. A. (2017). Plant immunity: Unravelling the complexity of plant responses to biotic stresses. *Ann. Bot.* 119, 681–687. doi: 10.1093/aob/mcw284

Minh, B. Q., Nguyen, M. A. T., and von Haeseler, A. (2013). Ultrafast approximation for phylogenetic bootstrap. *Mol. Biol. Evol.* 30, 1188–1195. doi: 10.1093/molbev/mst024

Miya, A., Albert, P., Shinya, T., Desaki, Y., Ichimura, K., Shirasu, K., et al. (2007). CERK1, a LysM receptor kinase, is essential for chitin elicitor signaling in arabidopsis. *Proc. Natl. Acad. Sci.* 104, 19613–19618. doi: 10.1073/pnas.0705147104

Morgan, A. M., Falcon, S., and Gentleman, R. (2022) *Gene set enrichment data structures and methods. version 1.59.0*. Available at: https://git.bioconductor.org/packages/GSEABase.

Nguyen, L.-T., Schmidt, H. A., von Haeseler, A., and Minh, B. Q. (2015). IQ-TREE: A fast and effective stochastic algorithm for estimating maximum-likelihood phylogenies. *Mol. Biol. Evol.* 32, 268–274. doi: 10.1093/molbev/msu300

Ou, L., Zhang, Q., Ji, D., Li, Y., Zhou, X., and Jin, L. (2022). Physiological, transcriptomic investigation on the tea plant growth and yield motivation by chitosan oligosaccharides. *Horticulturae* 8, 68. doi: 10.3390/horticulturae8010068

Ranf, S., Eschen-Lippold, L., Pecher, P., Lee, J., and Scheel, D. (2011). Interplay between calcium signalling and early signalling elements during defence responses to microbe- or damage-associated molecular patterns. *Plant J.* 68, 100–113. doi: 10.1111/j.1365-313X.2011.04671.x

Rao, K. P., Richa, T., Kumar, K., Raghuram, B., and Sinha, A. K. (2010). In silico analysis reveals 75 members of mitogen-activated protein kinase kinase kinase gene family in rice. *DNA Res.* 17, 139–153. doi: 10.1093/dnares/dsq011

Rentel, M. C., Lecourieux, D., Ouaked, F., Usher, S. L., Petersen, L., Okamoto, H., et al. (2004). OXI1 kinase is necessary for oxidative burst-mediated signalling in arabidopsis. *Nature* 427, 858–861. doi: 10.1038/nature02353

Saile, S. C., Jacob, P., Castel, B., Jubic, L. M., Salas-Gonzáles, I., Bäcker, M., et al. (2020). Two unequally redundant "helper" immune receptor families mediate arabidopsis thaliana intracellular "sensor" immune receptor functions. *PloS Biol.* 18, e3000783. doi: 10.1371/journal.pbio.3000783

Shimizu, T., Nakano, T., Takamizawa, D., Desaki, Y., Ishii-Minami, N., Nishizawa, Y., et al. (2010). Two LysM receptor molecules, CEBiP and OsCERK1, cooperatively regulate chitin elicitor signaling in rice. *Plant J.* 64, 204–214. doi: 10.1111/j.1365-313X.2010.04324.x

Shin, K. H., Yang, S. H., Lee, J. Y., Lim, C. W., Lee, S. C., Brown, J. W. S., et al. (2015). Alternative splicing of mini-exons in the arabidopsis leaf rust receptor-like kinase LRK10 genes affects subcellular localisation. *Plant Cell Rep.* 34, 495–505. doi: 10.1007/s00299-014-1729-x

Shinya, T., Yamaguchi, K., Desaki, Y., Yamada, K., Narisawa, T., Kobayashi, Y., et al. (2014). Selective regulation of the chitin-induced defense response by the arabidopsis receptor-like cytoplasmic kinase PBL27. *Plant J.* 79, 56–66. doi: 10.1111/tpj.12535

Siriwong, S., Thepbandit, W., Hoang, N. H., Papathoti, N. K., Teeranitayatarn, K., Saardngen, T., et al. (2021). Identification of a chitooligosaccharide mechanism against bacterial leaf blight on rice by *In vitro* and in silico studies. *Int. J. Mol. Sci.* 22(15), 7990. doi: 10.3390/ijms22157990

Trujillo, M., Ichimura, K., Casais, C., and Shirasu, K. (2008). Negative regulation of PAMP-triggered immunity by an E3 ubiquitin ligase triplet in arabidopsis. *Curr. Biol.* 18, 1396–1401. doi: 10.1016/j.cub.2008.07.085

van Brussel, A. A., Tak, T., Wetselaar, A., Pees, E., and Wijffelman, C. (1982). Small leguminosae as test plants for nodulation of rhizobium leguminosarum and other rhizobia and agrobacteria harbouring a leguminosarum sym-plasmid. *Plant Sci. Lett.* 27, 317–325. doi: 10.1016/0304-4211(82)90134-1

Vasyukova, N. I., Zinov'eva, S. V., Il'inskaya, L. I., Perekhod, E. A., Chalenko, G. I., Gerasimova, N. G., et al. (2001). Modulation of plant resistance to diseases by water-soluble chitosan. *Appl. Biochem. Microbiol.* 37, 103–109. doi: 10.1023/A:1002865029994

Wan, J., Tanaka, K., Zhang, X.-C., Son, G. H., Brechenmacher, L., Nguyen, T. H. N., et al. (2012). LYK4, a lysin motif receptor-like kinase, is important for chitin signaling and plant innate immunity in arabidopsis. *Plant Physiol.* 160, 396–406. doi: 10.1104/pp.112.201699

Wang, C., Wang, G., Zhang, C., Zhu, P., Dai, H., Yu, N., et al. (2017). OsCERK1-mediated chitin perception and immune signaling requires receptor-like cytoplasmic kinase 185 to activate an MAPK cascade in rice. *Mol. Plant* 10, 619–633. doi: 10.1016/j.molp.2017.01.006

Warnes, G., Bolker, B., Bonebakker, L., Gentleman, R., Huber, W., Liaw, A., et al. (2022) *Various r programming tools for plotting data. version 3.1.3*. Available at: https://github.com/talgalili/gplots.

Weigel, R. R., Pfitzner, U. M., and Gatz, C. (2005). Interaction of NIMIN1 with NPR1 modulates PR gene expression in arabidopsis. *Plant Cell* 17, 1279–1291. doi: 10.1105/tpc.104.027441

Willmann, R., Lajunen, H. M., Erbs, G., Newman, M.-A., Kolb, D., Tsuda, K., et al. (2011). Arabidopsis lysin-motif proteins LYM1 LYM3 CERK1 mediate bacterial peptidoglycan sensing and immunity to bacterial infection. *Proc. Natl. Acad. Sci.* 108, 19824–19829. doi: 10.1073/pnas.1112862108

Yamada, K., Yamaguchi, K., Shirakawa, T., Nakagami, H., Mine, A., Ishikawa, K., et al. (2016). The arabidopsis CERK 1-associated kinase PBL 27 connects chitin perception to MAPK activation. *EMBO J.* 35, 2468–2483. doi: 10.15252/embj.201694248

Yamada, K., Yamaguchi, K., Yoshimura, S., Terauchi, A., and Kawasaki, T. (2017). Conservation of chitin-induced MAPK signaling pathways in rice and arabidopsis. *Plant Cell Physiol.* 58, 993–1002. doi: 10.1093/pcp/pcx042

Yamaguchi, K., Mezaki, H., Fujiwara, M., Hara, Y., and Kawasaki, T. (2017). Arabidopsis ubiquitin ligase PUB12 interacts with and negatively regulates chitin elicitor receptor kinase 1 (CERK1). *PloS One* 12, e0188886. doi: 10.1371/journal.pone.0188886

Yang, J., Ding, C., Xu, B., Chen, C., Narsai, R., Whelan, J., et al. (2015). A casparian strip domain-like gene, CASPL, negatively alters growth and cold tolerance. *Sci. Rep.* 5, 14299. doi: 10.1038/srep14299

Zhang, X., Hu, C., Sun, X., Zang, X., Zhang, X., Fang, T., et al. (2020). Comparative transcriptome analysis reveals chitooligosaccharides-induced stress tolerance of gracilariopsis lemaneiformis under high temperature stress. *Aquaculture* 519, 734876. doi: 10.1016/j.aquaculture.2019.734876

Zipfel, C. (2008). Pattern-recognition receptors in plant innate immunity. *Curr. Opin. Immunol.* 20, 10–16. doi: 10.1016/j.coi.2007.11.003

frontiers | Frontiers in Plant Science

TYPE Original Research
PUBLISHED 11 April 2023
DOI 10.3389/fpls.2023.1099474

OPEN ACCESS

EDITED BY
Alessandra Boccaccini,
Università di Tor Vergata, Italy

REVIEWED BY
Candela Cuesta Moliner,
University of Oviedo, Spain
Ismayil S. Zulfugarov,
Azerbaijan National Academy of Sciences, Azerbaijan

*CORRESPONDENCE
Kollipara Padmasree
kpssl@uohyd.ac.in

SPECIALTY SECTION
This article was submitted to Plant Physiology, a section of the journal Frontiers in Plant Science

RECEIVED 15 November 2022
ACCEPTED 13 March 2023
PUBLISHED 11 April 2023

CITATION
Mahati K and Padmasree K (2023) Brassinolide promotes interaction between chloroplasts and mitochondria during the optimization of photosynthesis by the mitochondrial electron transport chain in mesophyll cell protoplasts of *Arabidopsis thaliana*. *Front. Plant Sci.* 14:1099474. doi: 10.3389/fpls.2023.1099474

Brassinolide promotes interaction between chloroplasts and mitochondria during the optimization of photosynthesis by the mitochondrial electron transport chain in mesophyll cell protoplasts of *Arabidopsis thaliana*

Kandarpa Mahati and Kollipara Padmasree*

Department of Biotechnology and Bioinformatics, School of Life Sciences, University of Hyderabad, Gachibowli, Hyderabad, India

The current experimental data unveils the role of brassinolide (BL), a phytohormone of class brassinosteroids (BRs), in augmenting the cross-talk between the mitochondrial electron transport chain (mETC) and chloroplasts to strengthen the efficiency of the Calvin-Benson cycle (CBC) for higher assimilation of carbon dioxide in the mesophyll cell protoplasts (MCP) of *Arabidopsis thaliana*. The outcome of total respiration (TR) and photosynthetic carbon assimilation (PCA) was monitored as O_2 uptake under dark and $NaHCO_3$-dependent O_2 evolution under light, respectively, after pre-incubation of MCP at a broad spectrum of BL concentration from 0.05 pM to 5 pM at 25 °C and optimum light intensity of 1000 µmol m^{-2} s^{-1}. The addition of optimal concentration (0.5 pM) of BL to MCP stimulated the (i) TR, (ii) PCA, and (iii) *para*-benzoquinone-dependent O_2 evolution (PSII activity). Further, in response to BL, the enzyme activity or transcript levels of redox-regulated CBC enzymes and glucose-6-phosphate raised considerably. Also, the addition of BL to MCP remarkably accelerated the capacity of the cytochrome oxidase (COX) and alternative oxidase (AOX) pathways concurrently with an increase in total cellular pyruvate and reactive oxygen species (ROS) levels. Besides, malate valve components (Malate, *Chl-MDH*, *M-MDH*) increased in response to BL. At the same time, the cellular redox ratios of pyridine nucleotides (NADPH and NADH) were kept low in the presence of BL. However, BL could not keep up the CBC activity of photosynthesis along with its associated light-activated enzymes/transcripts when mETC through COX or AOX pathway is restricted by antimycin A (AA) or salicylhydroxamic acid (SHAM), respectively. In contrast, adding BL to MCP under restricted mETC showed aggravation in total cellular ROS, pyruvate, malate, and redox ratio of pyridine nucleotides with a concomitant increase in transcripts associated with malate valve and antioxidant systems. These results

suggest that BL enhances the PCA by coordinating in cross-talk of chloroplasts and mitochondria to regulate the cellular redox ratio or ROS through the involvement of COX and AOX pathways along with the malate valve and antioxidant systems.

KEYWORDS

brassinolide, chloroplastic photosynthesis, mitochondrial respiration, cytochrome oxidase and antimycin A, alternative oxidase and salicylhydroxamic acid, malate valve, reactive oxygen species and antioxidant system

Introduction

In plant mitochondrial electron transport chain (mETC), the movement of electrons bifurcate at ubiquinone to follow either the cyanide-sensitive cytochrome oxidase (COX) pathway or cyanide-resistant alternative oxidase (AOX) pathway respectively to reduce the molecular oxygen (O_2) into the water (Moore and Siedow, 1991; Vanlerberghe and McIntosh, 1997; Millar et al., 2011). Electron transport through the COX pathway generates proton gradient and ATP synthesis. In contrast, electron transport through the AOX pathway is not coupled to ATP synthesis, and energy is dissipated as heat (Day and Wiskich, 1995; Siedow and Umbach, 2000; Millenaar and Lambers, 2003; Schertl and Braun, 2014).

In a photosynthesizing cell, the COX and AOX pathways of mETC play an essential role in benefiting photosynthetic carbon assimilation (Raghavendra and Padmasree, 2003; Scheibe, 2004; Noguchi and Yoshida, 2008; Vanlerberghe et al., 2020). The involvement of mETC in the optimization of photosynthesis has been demonstrated using the approach of chemical inhibitors or reverse genetics under various environmental stress conditions such as limiting CO_2 (Padmasree and Raghavendra, 1999a; Padmasree and Raghavendra, 1999b; Padmasree and Raghavendra, 1999c; Padmasree and Raghavendra, 2001a), high light (Saradadevi and Raghavendra, 1992; Dinakar et al., 2010a; Vishwakarma et al., 2014; Garmash et al., 2021a), drought (Dahal and Vanlerberghe, 2017; Challabathula et al., 2022), osmotic (Saradadevi and Raghavendra, 1994; Dinakar et al., 2016); temperature (Saradadevi and Raghavendra, 1994; Searle et al., 2011; Dinakar et al., 2016), salt (Analin et al., 2020), normoxia and hypoxia (Jayawardhane et al., 2020). The mETC is known to benefit photosynthesis by the following suggested mechanisms: (i) indirect removal of surplus amount of chloroplastic reducing equivalent by malate-OAA and triose-P-PGA shuttle (Krömer and Scheibe, 1996; Padmasree and Raghavendra, 1999c; Scheibe et al., 2005; Yoshida et al., 2007; Dinakar et al., 2010a; Zhang et al., 2017; Garmash, 2021b) (ii) dampening excess ROS through nonenzymatic and enzymatic ROS scavengers (Dinakar et al., 2010b; Vishwakarma et al., 2015; Dinakar et al., 2016; Cheng et al., 2020; Garmash et al., 2020; Challabathula et al., 2022; Manbir et al., 2022) (iii) expedite photosynthetic induction and light activation of major chloroplastic enzymes (Padmasree and Raghavendra, 1999b, Padmasree and Raghavendra, 2001a; Batnini et al., 2020) and (iv) bestow ATP to the cytosol for the synthesis of sucrose (Padmasree and Raghavendra, 1999c; Igamberdiev et al., 2006).

Several recent studies revealed the involvement of brassinosteroids (BRs) in various physiological processes such as photosynthesis (Jiang et al., 2012a; Jiang et al., 2012b), stress tolerance (Lima and Lobato, 2017; Dos Santos Ribeiro et al., 2019; Fu et al., 2019) and activation of mitochondrial AOX pathway to alleviate photoinhibition (Deng et al., 2015; Wei et al., 2015; Arfan et al., 2019). Apart, BRs, which are known to be ubiquitously distributed in the plant kingdom (Clouse and Sasse, 1998; Bishop and Koncz, 2002; Krishna, 2003; Bajguz and Hayat, 2009; Bhanu, 2019; Peres et al., 2019; Hussain et al., 2020; Raza et al., 2022), play imperative roles in a multitude of physiological function, including the stimulation of a broad spectrum of cellular responses such as cell lengthening (Clouse and Sasse, 1998; Lanza et al., 2012; Liu et al., 2018; Ruan et al., 2018), pollen tube growth (Ye et al., 2010), blossom phase (Domagalska et al., 2010), seed establishment (Jiang et al., 2013a) induction of ethylene biosynthesis (Wei et al., 2015), regulation of expression of the photosynthetic genes (Cheng et al., 2014). BRs are also known to activate adaptive mechanisms in response to diverse environmental stresses, i.e., high temperature (Zhang et al., 2013), water deficit (Lima and Lobato, 2017; Dos Santos Ribeiro et al., 2019; Wang et al., 2022), cold (Fu et al., 2019; Heidari et al., 2021; Fu et al., 2022; Wang et al., 2022), salt (Rattan et al., 2020), drought (Naservafaei et al., 2021), and chromium (Basit et al., 2022). Thus, BRs are suggested as promising plant growth regulators for improving the yield of essential crops (Khripach et al., 2000; Divi and Krishna, 2009; Nolan et al., 2020). Further, the cellular redox environment is reconfigured in the presence of BRs to enhance photosynthetic efficiency (Jiang et al., 2012b). However, so far, no clear information is available on intracellular adjustments of redox and ROS through modulating mETC during the optimization of photosynthesis in response to BRs.

The present study was performed using *A. thaliana* mesophyll cell protoplasts as an experimental prototype to ascertain the significance of BRs along with mETC in mediating the beneficial interactions between chloroplasts and mitochondria during the optimization of photosynthesis by monitoring changes in various biochemical components associated with malate valve and antioxidant systems.

Materials and methods

Plant material and growth conditions

The seeds of *Arabidopsis thaliana* L. Heynh ecotype of Columbia (Col-0) were sown on artificial soil (SOILRITE-MIX, Keltech Energies Limited, Bengaluru, India) supplemented with half-strength Murashige and Skoog (MS) medium (Murashige and Skoog, 1962) and kept in the dark for 3 to 4 d at 2 to 4°C for stratification as described in Vishwakarma et al. (2014). Later, the pots were transferred to a growth chamber set at 8h photoperiod and grown under a light intensity of 50-60 µmol m^{-2} s^{-1} at 22°C (Vishwakarma et al., 2015). After 30 days, young plants, which are at the 4 to 6th leaf stage, were transferred to individual pots. The fully grown leaves were collected from 12 to early 14 weeks old plants as it was easy to peel the lower epidermis for isolation of mesophyll cell protoplasts (MCP) and preparation of leaf discs because of the expanded lamina. The leaf discs were made from the leaf blade excluding the midrib using a sharp paper puncher under the water.

Separation of mesophyll cell protoplasts

MCP was separated from *A. thaliana* leaves with minor modifications to the protocol described by Riazunnisa et al. (2007). Leaf strips of 1cm^2 in size, without lower epidermis (abaxial) and midrib, were placed in a Petri plate with a peeled surface touching the pre-plasmolysis medium (0.60 M sorbitol, 1mM $CaCl_2$, 5mM MES-KOH pH 6.0). After 30 min, the pre-plasmolysis medium was removed. The digestion medium containing 0.65 M sorbitol, 1mM $CaCl_2$, 5mM MES-KOH (pH 5.5), 0.25 mM Na_2EDTA, 5mM sodium ascorbate, 0.2% BSA, 1% Cellulase Onozuka R-10 and 0.4% Macerozyme R-10 (Yakult Honsha Co. Ltd, Nishinomiya, Japan) was added to the leaf strips present in Petri plate and kept at 30°C for 45 min, under the illumination of 50-100 µmol $m^{-2}s^{-1}$ to digest the cell wall. After digestion, the digestion medium was discarded, and immediately washing medium (0.65 M sorbitol, 1 mM $CaCl_2$, 5 mM MES-KOH pH 6.0) was supplied. MCP was released in the washing medium by gently tapping and swirling the Petri plate. The released MCP was filtered through a nylon membrane (60 µm) to remove the debris. The intact pure MCP was collected using a swing-out head centrifuge. The MCP is delicate and therefore centrifuged at a low speed of 1000 rpm for 5min at 4°C. The centrifugation step was repeated twice/thrice to remove the broken MCP. The pellet was subsequently suspended in a suspension medium (0.65 M sorbitol, 1 mM $CaCl_2$, 10 mM HEPES-KOH pH 7.0) and centrifuged to remove the traces of the washing medium. A small aliquot of suspension medium was added to the final pellet, and the MCP suspension was kept on ice to perform all the experiments described below. Neutral red and Evans blue were used to analyze the quality and viability of MCP under the microscope. More than 90% intact protoplasts were used. The Arnon (1949) method for the estimation of chlorophyll (Chl) was used to estimate the amount of Chl.

Treatment with brassinolide in the presence (or) absence of mitochondrial inhibitor

Initially, MCP have been exposed independently to a wide range of brassinolide (BL) (0.5 pM to 5 pM) concentrations in a pre-incubation chamber (perplex) containing reaction medium (0.65 M sorbitol, 1mM $CaCl_2$, 1mM $MgCl_2$, 10mM HEPES-KOH pH 7.5) for 10 min in light at 25°C. In later experiments, MCP is pre-incubated with an optimized concentration of BL (0.5 pM) in the presence and absence of AA (100 nM) or SHAM (0.5 mM), respectively under similar conditions described above. During pre-incubation, an illumination of 1000 µmol m^{-2} s^{-1} was provided using LED lamps as this light intensity resulted in maximal photosynthetic rates in MCP of *A. thaliana* (Strodtkötter et al., 2009). Subsequently, the MCP is used either for monitoring photosynthesis, respiration, the capacity of COX or AOX pathway, ROS, enzyme assay (or) stored in liquid nitrogen to quantify total cellular redox ratios of pyridine nucleotide(s), pyruvate, malate, and glucose-6-phosphate (Glc-6-P).

For transcript analysis, leaf discs that were treated with 0.1µM BL in the presence and absence of 20 µM AA or 1mM SHAM were used (Strodtkötter et al., 2009; Deng et al., 2015). All the treatments were given in light (50 µmol $m^{-2}s^{-1}$) for 6 hours under DDW containing 0.01% Tween-20 (Vishwakarma et al., 2015) and transferred to liquid N_2.

Monitoring photosynthesis and respiration in MCP

An aliquot (10 µg Chl) of MCP after treatment with BL in the presence or absence of mitochondrial inhibitors was transferred to an Oxygraph cuvette comprising of Clark-type oxygen electrode system (Model DW2, Hansatech Ltd., King's Lynn, UK) to monitor respiration and photosynthesis at 25°C. The total respiration (TR) was determined as O_2 uptake under dark conditions (for 5 min). Besides, photosynthesis was measured as (i) a $NaHCO_3$ (1mM) dependent O_2 evolution which represents photosynthetic carbon assimilation (PCA) or Calvin-Benson cycle (CBC) activity, and (ii) *para*-Benzoquinone (1mM) dependent O_2 evolution which represents PSII activity, under the optimal light intensity of 1000 µmol $m^{-2}s^{-1}$ for 10 min (Padmasree and Raghavendra, 2001b; Strodtkötter et al., 2009). $NaHCO_3$ or *para*-Benzoquinone is added to the reaction medium soon after switching on a light.

Evaluation of the different components of TR in MCP

The various components of TR, i.e., the capacity of the COX pathway, AOX pathway, and residual respiration (RR), were assessed in MCP, as explained by Dinakar et al. (2010a). Thus, the capacity of the AOX pathway was examined as the O_2 uptake sensitive to 10 mM SHAM in the presence of 1 mM KCN. On the

other hand, the capacity of the COX pathway was analyzed as O_2 uptake sensitive to 1mM KCN in the co-existence of 10mM SHAM and 1μM CCCP (Carbonyl cyanide-3-chlorophenylhydrazone). CCCP was used to ensure that adenylate control does not limit respiration (McDonald et al., 2002).

Assessment of reduced and oxidized forms of pyridine nucleotide in MCP

MCP corresponding to 25 μg Chl was subjected to various treatments and quickly stored in cryogenic nitrogen. Later, samples were liquefied and spun at a centrifugal force of 3000 g for 2 min. Further, 0.2 N HCl and 0.2 M NaOH were treated with pelleted MCP to analyze $NAD(P)^+$ and NAD(P)H, respectively. The homogenized extract was centrifuged at 10,000 *g* for 10 min at 4° C (Dinakar et al., 2016). The supernatant was heated at 100 °C for 1 min, followed by cooling on ice. The pH of the supernatant was modified for the quantification of $NAD(P)^+$ (pH 5 to 6) and NAD (P)H (pH 7 to 8). Further, NAD(H) levels were assessed by ethanol consumption with the help of alcohol dehydrogenase, which in turn coupled with phenazine methosulfate-dependent reduction of dichlorophenolindophenol. In contrast, the NADP(H) amounts were quantified by utilization of glucose-6-phosphate (Glc-6-P) by Glc-6-P dehydrogenase, which in turn linked with phenazine methosulfate-dependent reduction of dichlorophenolindophenol. Declined absorbance at 600 nm was examined for 3 min. The amount of pyridine nucleotides was determined by respective standards of $NAD(P)^+$ and NAD(P)H (Queval and Noctor, 2007).

Evaluation of reactive oxygen species in MCP

MCP was loaded with 5μM fluorescent dye 2,7-dichlorofluorescein diacetate (H_2DCFDA) to monitor the intracellular production of ROS as described in Dinakar et al. (2010b). After incubation, MCP was treated with or without BL in the presence or absence of AA or SHAM for 10 min in a preincubation chamber under a photon flux density of 1000 μmol m^{-2} s^{-1} at 25 °C. Subsequently, the treated MCP was used to quantify DCF fluorescence using a spectrofluorometer (FP-8500, Jasco, Japan) run at excitation and emission wavelengths of 488 and 525 nm, respectively. Further, fluorescence generated due to ROS formation in MCP was observed under a Laser scanning confocal microscope (LSM 710, Carl Zeiss, Oberkochen, Germany) with excitation and an emission filter of 488 nm and 525 nm, respectively.

Quantification of pyruvate, malate, and Glc-6-P in MCP

The MCP equal to 100 μg Chl contained in 600 μl reaction medium subjected to various treatments was treated with $HClO_4$ (final concentration of 3%) and instantly frozen in liquid nitrogen as described in Padmasree and Raghavendra (1999a, 1999b). Later, the thawed samples were neutralized with KOH and immediately spun at 7000 g. Subsequently, the supernatant was chosen to assess the total cellular level of pyruvate, malate, and Glc-6-P using a UV-Visible spectrophotometer (Shimadzu-1700 PharmaSpec UV-Vis). The pyruvate levels were measured using an enzymatic assay coupled with the utilization of NADH. In contrast, Glc-6-P levels were measured by an enzymatic assay associated with the formation of NADPH. In contrast, the malate is quantified as an enzymatic assay linked with the generation of NADH.

Enzyme assays in MCP

MCP equivalent to 1 to 5 μg Chl in the reaction medium was subjected to various treatments and immediately used for enzyme assays. The maximal and actual enzymatic activities of the following light-activated chloroplastic enzymes of CBC: NADP-glyceraldehyde-3-phosphate dehydrogenase [NADP-GAPDH (EC 1.2.1.13)], fructose-1,6-bisphosphatase [FBPase (EC 3.1.3.11)] and phosphoribulokinase [PRK (EC 2.7.1.19)] was quantified spectrophotometrically (Shimadzu-1700 PharmaSpec UV-Vis). Protoplasts were added to the sample and reference cuvette during the assays. In contrast, the substrate(s) were added to only the sample cuvette according to the protocol described in Padamsree and Raghavendra (2001a). Triton X-100 [0.02% (v/v)] was included in the assay medium to solubilize the protoplasts. The activity of FBPase was assayed by monitoring the NADP reduction (increase in A340), while the activity of NADP-GAPDH was assayed by monitoring the NADPH oxidation (decrease in A340). However, the PRK activity is quantified by NADH oxidation (decline in A340). The maximal enzymatic activity of these three enzymes was determined after adding 50 mM DTT to the reaction medium containing protoplast in light.

Total RNA isolation and cDNA synthesis from leaf discs

Total RNA was extracted from 100 mg of leaf tissue from different treatments using TRI Reagent (Sigma Aldrich, USA) according to the manufacturer's instructions. The total RNA and its quality in each sample were analyzed using a Nano-Drop ND-2000c spectrophotometer (Thermo-Fisher Scientific). One μg of total RNA with an A_{260}/A_{280} ratio between 1.9 to 2.0 and an A_{260}/A_{230} ratio between 2.0 to 2.2 was used for first-strand cDNA synthesis using Prime Script ^{TM} 1st strand cDNA Synthesis kit (Takara Bio Inc., Shiga, Japan) according to the instructions given by the manufacturer.

Real-time PCR

The PCR sample comprised 2 μl of diluted cDNA, 5 μl of TB Green Premix Ex Taq^{TM} II Master Mix (Takara Bio Inc., Shiga, Japan), 0.8 μl of ROX dye and 1μl (0.1pM) of specific primers in a final volume of 10 μl. Real-time PCR was carried out after preincubation at 95°C for 10 min followed by 40 cycles comprised of denaturation at 95°C for 15 s and annealing/

extension at 60°C each for 1 min using Step One plus real-time PCR machine (Applied Biosystems, USA) as described by Vishwakarma et al. (2014). Cycle threshold (C_T) values were deduced from the log phase of PCR amplification. The results were evaluated using the comparative C_T method (Livak and Schmittgen, 2001). This procedure produced a C_T value (ΔC_T = GOIC_T-*UBQ5*C_T) by comparing the expression of a gene of interest (GOI) to that of *UBQ5* (a reference gene). Equation $2^{-\Delta\Delta C_T}$ were then used to quantify the transcript abundance.

Real-time PCR primers

Real-time PCR primers for the genes ubiquitin (*UBQ5*) as a reference, chloroplastic-malate dehydrogenase (*Chl-MDH*), mitochondrial malate dehydrogenase (*M-MDH*), peroxisomal/chloroplastic catalase (*CAT1*), cytosolic superoxide dismutase (*CSD1*), thylakoid ascorbate peroxidase (*tAPX*), stromal ascorbate peroxidase (*sAPX*) were same as described in Vishwakarma et al. (2014). In contrast, the primer for the following genes: glutathione reductase (*GR*), monodehydroascorbate reductase (*MDHAR*), dehydroascorbate reductase (*DHAR*), glyceraldehyde-3-phosphate dehydrogenase (*GAPDH*), fructose-1,6- bisphosphatase (*FBPase*) and phosphoribulokinase (*PRK*) was designed using Primer-Blast, NCBI, NIH, Bethesda, Maryland, USA. Before primer blasts, the 5'UTR sequence of the respective gene was retrieved from transcriptomic sequence using Phytozome, the plant comparative genomic portal of the Department of Energy Joint Genome Institute, University of California and Gene Structure and Display Server (GSDS), Centre for Bioinformatics, Peking University. The sequence of forward and reverse primers for all the genes examined in the present study is shown in the Supplementary Table 1.

Statistical analysis

The experimental data depicted in the present study is an average of the observations from three studies carried out on different days. One-way ANOVA was used to compare the variation among treatments. The Tukey's test of multiple comparison analysis was performed using the Sigma Plot 14.0 program (San Jose, CA, USA).

Results

TR and PCA of MCP pre-incubated under a series of BL concentration

The effect of BL regimes on TR as O_2 uptake and PCA as bicarbonate-dependent O_2 evolution is determined using MCP as the experimental system (Figures 1A, B). Among the series of BL concentrations (0.05 to 5.0 pM) used in the present study, the maximum rates of O_2 uptake (24.5 ± 0.5 µmol mg^{-1}Chl h^{-1}) and O_2 evolution (158.5 ± 1.43 µmol mg^{-1}Chl h^{-1}) was observed at 0.5 pM BL as compared to the rates of O_2 uptake (17.5 ± 0.8 µmol mg^{-1}Chl h^{-1}) and O_2 evolution (125 ± 2.5 µmol mg^{-1}Chl h^{-1}) without BL under optimal conditions of light and temperature (Figures 1A, B).

Effect of BL on the different components of TR in MCP

The effect of optimal concentration of BL (0.5 pM) on the capacity of the COX pathway, AOX pathway, and residual respiration (RR) was evaluated with reference to TR in MCP after pre-incubation under light (Figure 2A). BL enhanced the O_2 uptake of the COX pathway by 36%, the AOX pathway by 81%, and residual respiration by 13% when compared with their O_2 uptake rates in the absence of BL (Figure 2A). However, the ratio of AOX pathway capacity to TR is significantly enhanced upon treatment with BL from 0.38 ± 0.01 (without BL) to 0.45 ± 0.016. In contrast, the addition of BL decreased the ratio of COX pathway capacity to TR from 0.34 ± 0.02 (without BL) to 0.32 ± 0.02 and the ratio of RR to TR from 0.27± 0.021 (without BL) to 0.21± 0.011 (Figure 2B).

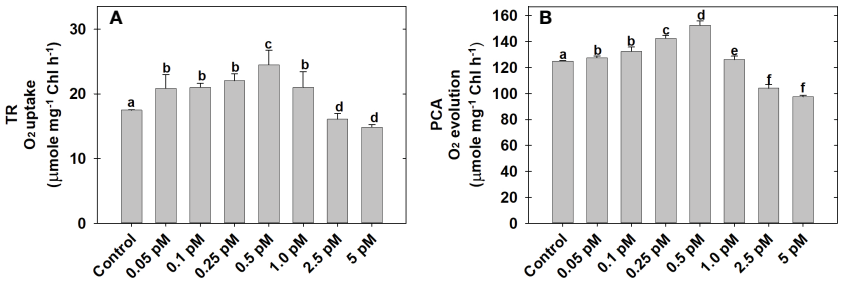

FIGURE 1
Effect of different concentrations of BL on TR **(A)** and PCA **(B)** in MCP of *A. thaliana*. The MCP in the reaction medium was pre-incubated with a series of BL concentrations (0.05 to 5 pM) for 10 min under a light intensity of 1000 µmol m^{-2} s^{-1} at 25°C. After treatment, the TR was recorded as O_2 uptake for 5 minutes in the dark and PCA was traced as $NaHCO_3$-dependent (1.0 mM) O_2 evolution for 10 min in light (1000 µmol m^{-2} s^{-1}) using a Clark-type oxygen electrode. More detailed information on the procedure is mentioned in the "materials and methods" section. A statistically significant difference is represented by different lowercase alphabetical letters ($P < 0.05$) and values represent the average (± SE) of three experiments.

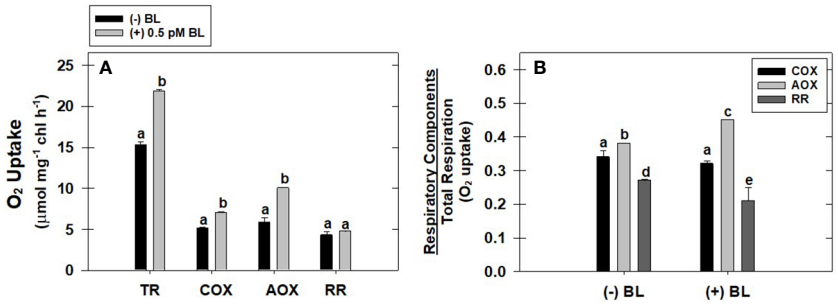

FIGURE 2
Effect of BL on the different components of TR: capacity of COX pathway, AOX pathway, and RR **(A)**. The ratio of O_2 uptake by each of these components to total respiration in MCP of *A. thaliana* **(B)**. The MCP in the reaction medium was pre-incubated for 10 min in the presence of 0.5 pM BL at a light intensity of 1000 µmol m^{-2} s^{-1} at 25°C. After treatment, MCP was shifted to an oxygraph cuvette to monitor various components of respiration. Further, the section "materials and methods" mentions more detailed information on the procedure. A statistically significant difference is represented by different lowercase alphabetical letters ($P \leq 0.05$) and values represent the average (± SE) of three experiments.

Effect of BL on TR, PCA, and PSII in the presence of mitochondrial inhibitors

The TR of MCP was enhanced by 30% after pre-incubation with 0.5 pM BL in light when compared with TR in the absence of BL in light. But, when the COX or AOX pathway of mETC is partially disrupted either with AA (or) SHAM, BL could not enhance the TR to the extent observed in the absence of mitochondrial inhibitors. Thus, adding BL in the presence of AA or SHAM could enhance the TR by ~15% of their control rates, i.e., observed in the presence of AA and SHAM alone (Figure 3A).

The PCA rate of MCP was significantly enhanced by 27% upon adding BL in light. However, adding BL to MCP after disrupting mETC with either AA or SHAM could not stimulate the PCA. The decrease in rates of PCA was further aggravated by ~40% when BL was added to MCP containing AA or SHAM when compared with rates of PCA that were decreased in the presence of AA (37%) or SHAM (42%) alone (Figure 3B).

Similar to PCA, the PSII activity of MCP was significantly enhanced by 33% upon treatment with BL in light. But, BL could not stimulate the PSII activity to this extent when mETC is disrupted with either AA or SHAM. However, BL enhanced the PSII rates in the presence of AA or SHAM by ~14% as compared to the PSII rates that were decreased with the addition of AA or SHAM alone (Figure 3C).

Effect of BL on the activity of CBC enzymes in the presence of mitochondrial inhibitors

The actual activity (≤65%) and the maximal activity (≤91%) of redox-sensitive CBC enzymes NADP-GAPDH, PRK, and FBPase were increased significantly in MCP upon the addition of BL in light (Figures 4A–F). But, both of these activities could not be promoted in MCP by BL when the mETC is disrupted by either AA or SHAM, as observed in samples without mitochondrial inhibitors. Thus, the addition of BL to MCP containing AA (≤43%) or SHAM (≤55%) further aggravated the decreased pattern in the enzymatic activities (maximal and actual) of all the enzymes that were observed with the addition of AA or SHAM alone (Figures 4A–F).

Effect of BL on Glc-6-P, pyruvate, and malate in the presence of mitochondrial inhibitors

Adding BL to MCP has remarkably increased the total cellular levels of Glc-6-P by ~15% in light. Similar to PCA observed above, the addition of BL decreased the cellular Glc-6-P levels when mETC was disrupted by either AA or SHAM. In fact, the decrease in Glc-6-P levels was further aggravated when BL was added to MCP containing AA (20%) or SHAM (40%) when compared with the Glc-6-P levels of MCP that were decreased with the addition of AA (<10%) or SHAM (26%) alone (Figure 5A).

Similar to Glc-6-P, the total cellular levels of malate were increased remarkably by ~15% with the addition of BL to MCP in light. The addition of BL to MCP containing either AA or SHAM further enhanced the cellular malate levels. But, the rise in malate levels was marginal (<4%) when BL was added to MCP containing AA or SHAM when compared with the increase in malate levels of MCP that were treated with AA (19%) or SHAM alone (34%) (Figure 5B).

The total cellular levels of pyruvate increased marginally by <5% when BL was added to MCP in light. Also, adding BL to MCP containing AA or SHAM further raised the pyruvate levels. But the rise in pyruvate levels was marginal (<5%) when BL was added to MCP having either AA or SHAM when compared with the pyruvate levels of MCP treated with AA (11%) or SHAM (20%) alone (Figure 5C).

Effect of BL on redox ratio of pyridine nucleotides in the presence of mitochondrial inhibitors

Adding BL to MCP significantly decreased the cellular redox ratio of (i) NADPH to $NADP^+$ and NADPH and (ii) NADH to NAD^+ and NADH by 31% and 21%, respectively, in light. But, this

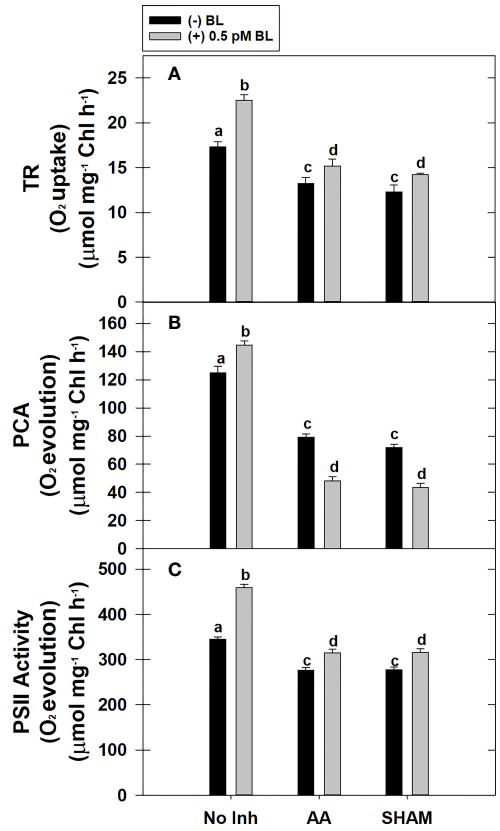

FIGURE 3
Effect of BL on TR **(A)**, PCA **(B)** and PS II activity **(C)** under the disruption of COX pathway or AOX pathway in MCP of *A. thaliana*. The MCP in the reaction medium was pre-incubated with or without 0.5 pM BL in the presence or absence of 100nM AA (COX pathway Inhibitor) or 0.5 mM SHAM (AOX pathway inhibitor) for 10 min at a light intensity of 1000 µmol m^{-2} s^{-1} at 25°C. After treatment, MCP was shifted to an oxygraph cuvette to monitor respiration in the dark and photosynthesis under the light. Further, the section "materials and methods" mentions more detailed information on the procedure. No Inhibitor (No Inh) depicts a sample without mETC inhibitors. A statistically significant difference is represented by different lowercase alphabetical letters ($P \leq 0.05$) and values represent the average (± SE) of three experiments.

effect of BL on redox ratios related to NADPH or NADH was reversed when it was added to MCP containing either AA or SHAM. However, the rise in redox ratio related to NADPH upon adding BL to MCP having either AA or SHAM did not vary with those samples of MCP containing AA (32%) or SHAM (26%) alone. In contrast, the rise in redox ratio related to NADH was further aggravated upon the addition of BL to MCP containing either AA (17%) or SHAM (18%) than that of MCP (without BL) where redox ratio of NADH was enhanced by 8% in the presence of AA and 35% in the presence of SHAM, respectively (Figures 6A, B).

Effect of BL on cellular ROS in the presence of mitochondrial inhibitors

Adding BL to MCP significantly raised the total cellular ROS levels by 21% in light. This increase in ROS was further enhanced when mETC was disrupted with mitochondrial inhibitors. But, the rise in ROS was marginal (<7%) upon the addition of BL to MCP containing either AA or SHAM when compared with their respective control samples where MCP had AA (63%) or SHAM (69%) alone (Figure 7A).

The cellular ROS of MCP upon treatment with BL in the presence and absence of mitochondrial inhibitors was further confirmed by confocal microscopic studies using H_2DCF-DA (Figure 7B). The ROS in the chloroplastic region was shown by a pseudo-orange/yellow color formed due to the superimposition of chlorophyll autofluorescence and DCF fluorescence, and the ROS in the extra-chloroplastic region is visible as DCF fluorescence. In the control (MCP without BL or mitochondrial inhibitors), a marginal level of DCF fluorescence was observed. At the same time, adding BL enhanced fluorescence in both chloroplastic and extra-chloroplastic regions (Figure 7A, a, b). This increase in both chloroplastic and extra-chloroplastic fluorescence was further aggravated when BL was added to MCP containing mitochondrial inhibitors when compared with fluorescence in MCP with AA or SHAM alone (Figure 7B, c–f).

Effect of BL on the transcript levels of important genes associated with CBC enzymes, malate valve, and antioxidant system in the presence of mitochondrial inhibitors

The relative changes in the transcript levels of genes related to redox-sensitive CBC enzymes, malate valve, and antioxidant system were examined in leaf discs under the light in the presence of BL under the restriction of either COX or AOX pathway (Figures 8A–C).

Adding BL to leaf discs has significantly increased the expression of CBC enzymes *NADP-GAPDH*, *FBPase*, and *PRK* by ≤3.5-fold in light (Figure 8A). But, when BL was added to the leaf discs in the presence of AA or SHAM, the expression of these genes was enhanced but not to the extent observed in leaf discs without mitochondrial inhibitors. Thus, the expression of CBC enzymes increased from 0.5 (without BL) to ≤0.97 (with BL) in leaf discs when mETC is inhibited in the presence of AA. In contrast, with the addition of BL to leaf discs containing SHAM, the expression of CBC enzymes either remained the same or decreased as compared to leaf discs treated with SHAM (<0.4) alone (Figure 8A).

The expression of genes related to malate valve (*Chl-MDH* and *M-MDH*) was enhanced significantly by ≤26% when BL was added to leaf discs in light. The expression of these genes was further promoted when BL was added to leaf discs treated with either AA (≤67%) or SHAM (≤72%) as compared to their expression in leaf discs treated with AA (≤45%) or SHAM (≤57%) alone (Figure 8B).

The expression of genes related to ROS scavenging anti-oxidant system (*CSD1*, *CAT1*, *tAPX*, *sAPX*, *MDHAR*, *DHAR*, and *GR*) was significantly increased by ≤ 2.8-fold in the presence of BL. The addition of BL to MCP containing AA (≤6.9 fold) or SHAM (≤11.2 fold) further enhanced the expression of these genes when compared with the expression of genes in MCP with AA (≤3.5 fold) or SHAM (≤5.9 fold) alone (Figures 8C).

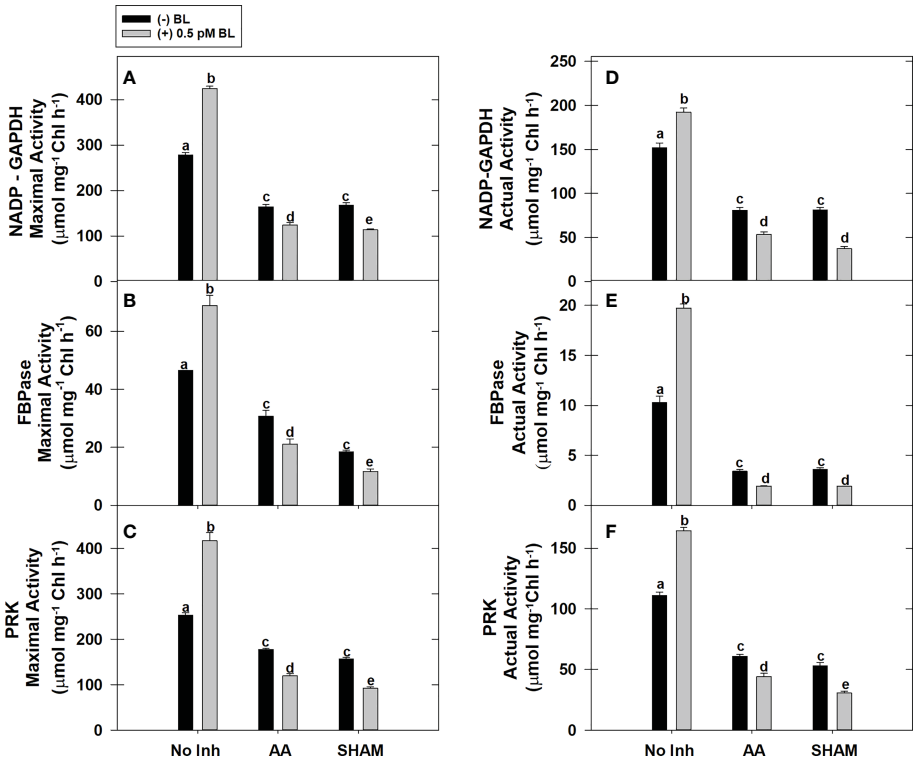

FIGURE 4
Effect of BL on maximal activity **(A–C)** and actual enzymatic activity **(D–F)** of NADP-GAPDH, Stromal FBPase, and PRK under the disruption of COX pathway or AOX pathway in MCP of *A. thaliana*. The MCP in the reaction medium was pre-incubated with or without 0.5 pM BL in the presence or absence of 100nM AA (COX pathway Inhibitor) or 0.5 mM SHAM (AOX pathway inhibitor) for 10 min at a light intensity of 1000 µmol m^{-2} s^{-1} at 25°C. After treatment, MCP was immediately used to monitor maximal and actual activity. Further, the section "materials and methods" mentions more detailed information on the procedure. No Inhibitor (No Inh) depicts a sample without mETC inhibitors. A statistically significant difference is represented by different lowercase alphabetical letters ($P \leq 0.05$) and values represent the average (± SE) of three experiments.

Discussion

In higher plants, both photosynthesis and respiration form an integral component of plant growth as the former metabolic process is involved in the net gain of biomass while the later metabolic process helps in the release of energy and turnover of carbon skeletons derived from amino- and fatty acids in rapidly growing tissues (Raghavendra et al., 1992). Apart, the respiratory rate is known to increase after long hours of illumination in leaves as well as after short periods (5 to 10 min) of illumination in MCP, called 'light-enhanced dark respiration' (Azcón-Bieto and Osmond, 1983; Vani et al., 1990; Reddy et al., 1991). Besides such long term and short term beneficial effects of photosynthesis in promoting mitochondrial respiration, the crucial roles of mETC in optimizing photosynthesis under normal light as well as under various environmental conditions is well established using the system of MCP due to the following benefits over the usage of leaf discs or whole plants: (i) absence of cellulose cell wall and intercellular spaces facilitate the rapid exchange of gases (O_2 and CO_2); (ii) minimize the artifact associated with stomatal patchiness during gas exchange; (iii) allow the metabolic process especially the respiration and photosynthesis (PSI, PSII and PCA) to get monitored quickly at low dosage of the exogenous chemical such as metabolic inhibitor, activator or a phytohormone and (iv) ease in imaging ROS and sub-cellular localization of target molecule (Padmasree and Raghavendra, 1999a; Padmasree and Raghavendra, 1999b; Padmasree and Raghavendra, 1999c; Padmasree and Raghavendra, 2001b; Strodtkötter et al., 2009; Dinakar et al., 2010a; Dinakar et al., 2010b; Selinski et al., 2014; Nie et al., 2015; Yan et al., 2015; Dinakar et al., 2016; Sunil et al., 2020).

In the present study, the MCP was treated with a light intensity of 1000 µmol m^{-2} s^{-1} during both pre-incubation and monitoring of photosynthesis (Calvin-Benson cycle and PSII) as it was found to be optimal intensity for achieving maximal photosynthetic rates (data not shown). Also, the studies of Strodtkötter et al. (2009) monitored the photosynthesis rates of MCP from *A. thaliana* at 1000 µmol m^{-2} s^{-1}. Besides, the MCP isolated from *Pisum sativum* showed steady photosynthetic rates for up to 30 min. Similarly, the MCP from *A. thaliana* also showed stable photosynthetic rates up to 30 to 40 min (data not shown). Therefore, we assume that MCP was active during the entire duration (25 min) of the assay conducted in the present study which includes the time required for pre-incubation under light (10 min) and, monitoring of respiration (5 min) and photosynthesis (10 min). Further, it is easy to perform transcript analysis using leaf discs as compared to MCP due to either one or more of the following reasons: (i) oxygraph chamber or pre-incubation chamber cannot be

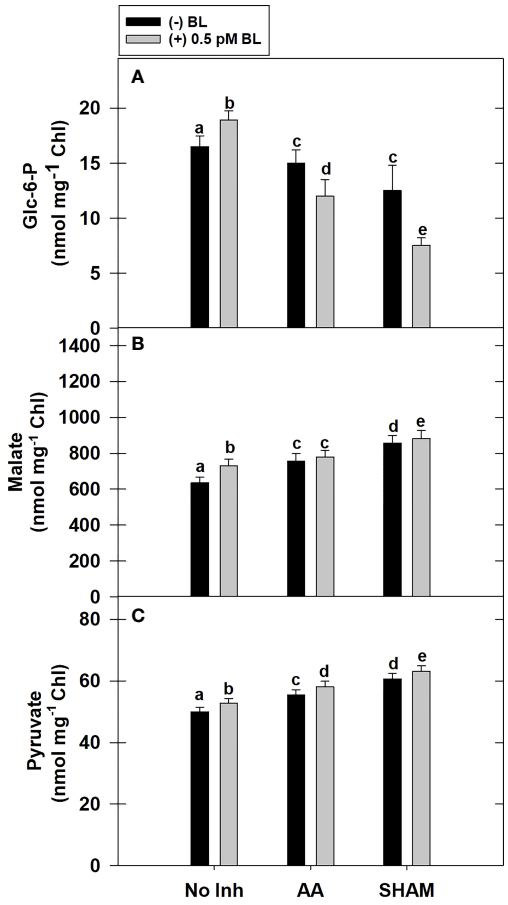

FIGURE 5
Effect of BL on the total cellular level of Glc-6-P **(A)**, Malate **(B)** and Pyruvate **(C)** under the disruption of COX or AOX pathway in MCP of *A. thaliana*. The MCP in the reaction medium was pre-incubated with or without 0.5 pM BL in the presence or absence of 100nM AA (COX pathway Inhibitor) or 0.5 mM SHAM (AOX pathway inhibitor) for 10 min at a light intensity of 1000 µmol m^{-2} s^{-1} at 25°C. After treatment, MCP was immediately quenched by $HClO_4$ and stored in liquid N_2 for analysis. Further, the section "materials and methods" mentions more detailed information on the procedure. No Inhibitor (No Inh) depicts a sample without mETC inhibitors. A statistically significant difference is represented by different lowercase alphabetical letters. ($P \leq 0.05$) and values represent the average (± SE) of three experiments.

autoclaved as it is mostly made from acrylic material; (ii) consume a large volume of nuclease-free and sterile water to prepare various media used during preparation of MCP and (iii) require leaf tissue in abundance to prepare MCP. Furthermore, despite treating MCP and leaf discs with different light intensities, the transcript levels, as well as maximal/actual activities of CBC enzymes, exhibited a more or less similar trend upon treatment with BL in the presence of mitochondrial inhibitors. Therefore, transcript data obtained from the leaf discs perhaps could be clubbed with the other parameters analyzed in MCP to decipher the role of mETC in BL-promoted photosynthesis.

Several recent studies showed that BRs influence the interaction between chloroplasts and mitochondria to protect the photosynthetic electron transport chain from photo-inhibition by up-regulating the AOX pathway during salt and drought stress (Wei et al., 2015; Hu et al., 2019). Though the influence of BRs in promoting PCA is known, it is not clear if BR has any role along with mETC in optimizing PCA under normal growth conditions. Thus, the present study revealed the significance of BL in optimizing PCA along with mETC by treating MCP with specific metabolic inhibitors AA (inhibitor of COX pathway) and SHAM (inhibitor of AOX pathway) in light.

BL promoted both photosynthesis and respiration in MCP

BRs are a set of polyhydroxy steroidal phytohormones. Plant tissues contained BRs in trace quantities i.e., 0.01-100 ng g^{-1} of fresh weight, which is far less than any other phytohormone or metabolite present in it (Clouse, 2004; Xin et al., 2013a; Tarkowská et al., 2016). Further, its level varied according to plant organ type, tissue age, and species (Clouse, 2004). Moreover, the content of BL was not detected even in 1 gm rosette tissue of *A. thaliana* using high-end techniques such as UPLC-MRM3-MS and UPLC-MRM-MS (Xin et al., 2013b). Among the seventy identified BRs, Brassinolide (BL), 24-epibrassinolide (EBL), and 28-homobrassinolide (HBL) are the important biologically active forms and their external application is used in various experimental studies (Peres et al., 2019; Tanveer et al., 2019; Raza et al., 2022). However, all other forms of BRs are either biosynthetic precursors or metabolic products of BL (Clouse, 2004). Therefore, in the present study, BL is used to treat the MCP. In general, phytohormones are effective at a very minimal concentration in reprogramming various physiological processes in plants (Siddiqui et al., 2018). Exogenous application of BRs showed a dose-dependent effect on the growth of plants, where they promoted growth at lower concentrations and retarded growth at higher concentrations (Chaiwanon and Wang, 2015; Nolan et al., 2020). The studies of Jiang et al. (2012b) noted that a moderate concentration of BRs increased the efficiency of PCA. Similarly, in the current study, BL enhanced both TR and PCA in MCP when its concentration was increased from 0.05 to 0.5 pM but decreased when its concentration was increased further from 1.0 to 5.0 pM under optimal conditions of light (1000 µmoles m^{-2} s^{-1}) and temperature (25°C) (Figures 1A, B). Therefore, 0.5 pM of BL was considered the optimal concentration where both TR and PCA were found to be at maximal rates. This concentration of BL is chosen to treat MCP in all the rest of the experiments performed in the present study.

Mitochondria are known to perform a vital role as a sensor for external stimuli (such as BRs) and can trigger elaborative cellular responses for acclimatization (Berkowitz et al., 2016). In previous reports, plants treated with BRs significantly increased the TR under both control (Deng et al., 2015; Derevyanchuk et al., 2015; Zhu et al., 2016; Arfan et al., 2019) and stress conditions such as salt stress (Derevyanchuk et al., 2017) and cold stress (Arfan et al., 2019). The studies of Derevyanchuk et al. (2015) suggested that enhancement in TR might play a role in reorienting the metabolic fluctuations which occurred in response to BRs. Also, the changes in respiratory rate are directly associated with the changes in

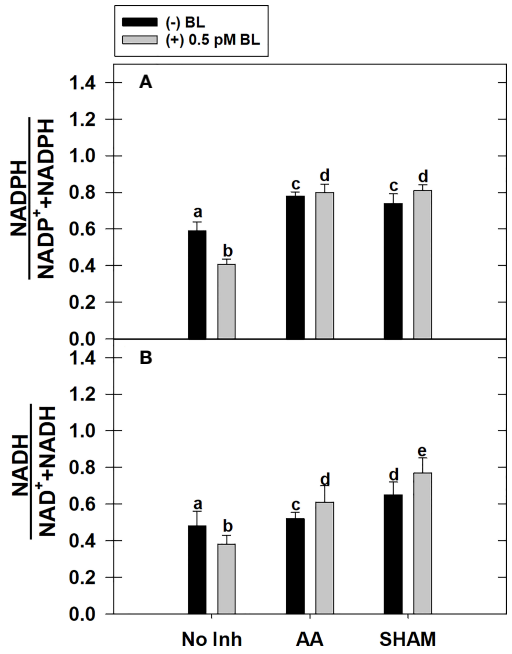

FIGURE 6
Effect of BL on the total cellular level of redox ratio related to NADP (H) **(A)** and NAD(H) **(B)** under the disruption of COX pathway or AOX pathway in MCP of *A. thaliana*. The MCP in the reaction medium was pre-incubated with or without 0.5 pM BL in the presence or absence of 100nM AA (COX pathway Inhibitor) or 0.5 mM SHAM (AOX pathway inhibitor) for 10 min at a light intensity of 1000 µmol m^{-2} s^{-1} at 25°C. After treatment, MCP was immediately stored in liquid N_2 for analysis. Further, the section "materials and methods" mentions more detailed information on the procedure. No Inhibitor (No Inh) depicts a sample without mETC inhibitors. A statistically significant difference is represented by different lowercase alphabetical letters ($P \leq 0.05$) and values represent the average (± SE) of three experiments.

respiratory pathway capacity (Noguchi et al., 2001; Dinakar et al., 2010b). This flexibility in mETC makes plants adapt to various environmental conditions such as high light (Dinakar et al., 2010a), salt (Derevyanchuk et al., 2015), cold (Arfan et al., 2019) and drought (Hu et al., 2019). Thus, the addition of BL not only increased the TR in MCP but also significantly enhanced the capacity of the COX and AOX pathways (Figures 2A, 3A). However, the AOX pathway capacity and the ratio of AOX pathway capacity to TR were significantly increased when compared with the COX pathway capacity and its ratio to TR (Figure 2B). This result is in corroboration with previous findings (Deng et al., 2015; Derevyanchuk et al., 2015; Zhu et al., 2016; Arfan et al., 2019; Derevyanchuk et al., 2019; Hu et al., 2019).

Similar to TR, an increase in rates of PCA and PSII is observed in MCP upon treatment with BL (Figures 3B, C). Further, this increase in PCA rates corroborated well with the rise in both maximal and actual activities and transcripts associated with CBC enzymes (NADP-GAPDH, FBPase, and PRK) examined in the present study (Figures 3B, 4, 8A). Many previous reports revealed that BRs stimulates the enzymatic activity/transcripts of redox-sensitive CBC enzyme through ROS such as H_2O_2 (Jiang et al., 2012b; Li et al., 2022). Further, the studies of Jiang et al. (2012b) demonstrated that BRs enhanced the activity of redox-sensitive CBC enzyme to promote CO_2 assimilation by a modest rise in ROS levels and maintenance of cellular redox related to glutathione. Similarly to this study, BL caused a marginal rise in ROS levels, increased activity and transcripts of CBC enzymes, and reduced redox ratios of pyridine nucleotides (Figures 4, 6, 7, 8A).

Besides, several studies showed an increase in PSII activity in response to BRs under both control (Lima and Lobato, 2017) and stress conditions such as salt (Zhu et al., 2016), cold (Arfan et al., 2019) and drought (Hu et al., 2019). This increase in PSII activity in the presence of BRs is attributed to the rise in the efficiency of light utilization and the dissipation of excitation energy at PS II antennae (Hu et al., 2013). The studies of Li et al. (2015) suggested that treatment with BRs increased the proportion of open PSII centers and thereby, the efficiency in capturing the light energy for the photochemical reactions.

BL sustained the interdependence of photosynthesis and respiration in MCP

Any restriction in the transport of electrons through COX or AOX pathways caused over-reduction of mETC, leading to a decrease in various components associated with the process of respiration as well as photosynthesis (Padmasree and Raghavendra, 1999a; Padmasree and Raghavendra, 1999b; Padmasree and Raghavendra, 1999c; Padmasree and Raghavendra, 2001a; Dinakar et al., 2010b; Vishwakarma et al., 2015; Analin et al., 2020; Challabhathula et al., 2022). Similar to earlier reports, the restriction of COX and AOX pathways of mETC in MCP resulted in a decrease in TR, PSII activity, PCA, and activity/transcripts of CBC enzymes (Figures 3, 4, 8A).

Further, treatment of MCP with BL in the presence of AA or SHAM recovered the TR and PSII activity marginally but not to the extent observed in the absence of inhibitors (Figures 3A, C). This could be possible because only one pathway is inhibited while the other pathway of mETC is operative. Thus, under restricted electron transport through mitochondria, BL might try to maintain the flux of electrons either through COX or AOX to support the electron flow at the photochemical reaction centers of chloroplasts. The previous studies suggested that BRs might play a role in balancing the electron transfer from chloroplast to mitochondria through the AOX pathway to reduce the over-accumulation of ROS (Deng et al., 2015; Wei et al., 2015; Hu et al., 2019). Also, the studies of Jiang et al. (2013b) suggested that the positive effect of EBR on the recovery of PSII may be related to its impact on the activity of physiological metabolism, which provides ATP for the repair of D1 protein.

Further, adding BL to MCP in the presence of AA or SHAM also showed a significant decrease in the responses of PCA and activities/transcripts associated with redox-regulated CBC enzymes (Figures 3B, 4, 8A). However, this decline in PCA was more pronounced when BL treatment was superimposed with SHAM than AA. This result suggests that an over-reduced environment caused by inhibition in either COX or AOX pathways might severely affect the redox-regulated CBC enzymes at the biochemical and molecular levels, resulting in decreased

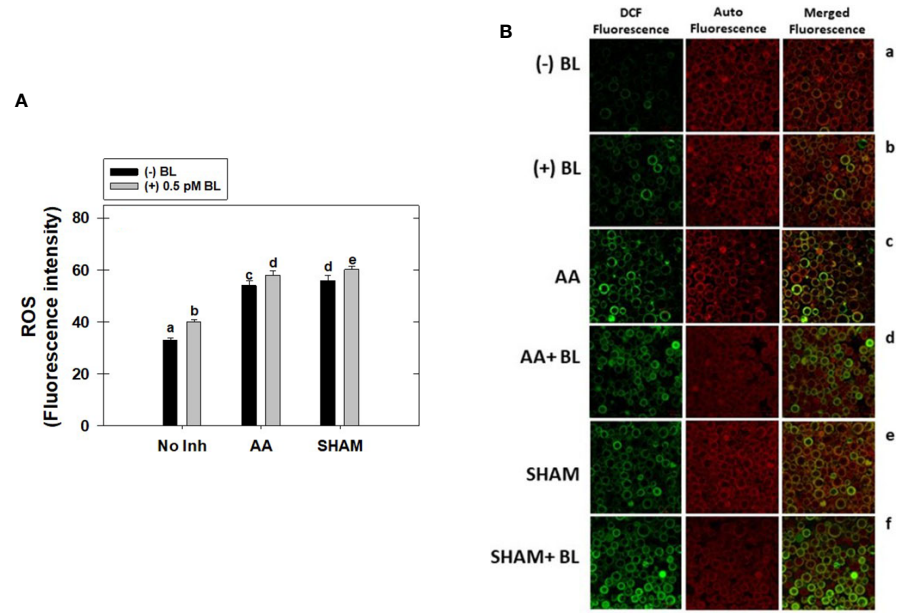

FIGURE 7
Effect of BL on total cellular ROS **(A)** and Confocal Microscopic images of ROS **(B)** under the disruption of COX pathway or AOX pathway in MCP of *A. thaliana*. The MCP in the reaction medium was pre-incubated with or without 0.5 pM BL in the presence or absence of 100nM AA (COX pathway Inhibitor) or 0.5 mM SHAM (AOX pathway inhibitor) for 10 min at a light intensity of 1000 µmol m^{-2} s^{-1} at 25°C. Further, the section "materials and methods" mentions more detailed information on the procedure. No Inhibitor (No Inh) depicts a sample without mETC inhibitors. A statistically significant difference is represented by different lowercase alphabetical letters ($P \leq 0.05$) and values represent the average (± SE) of three experiments.

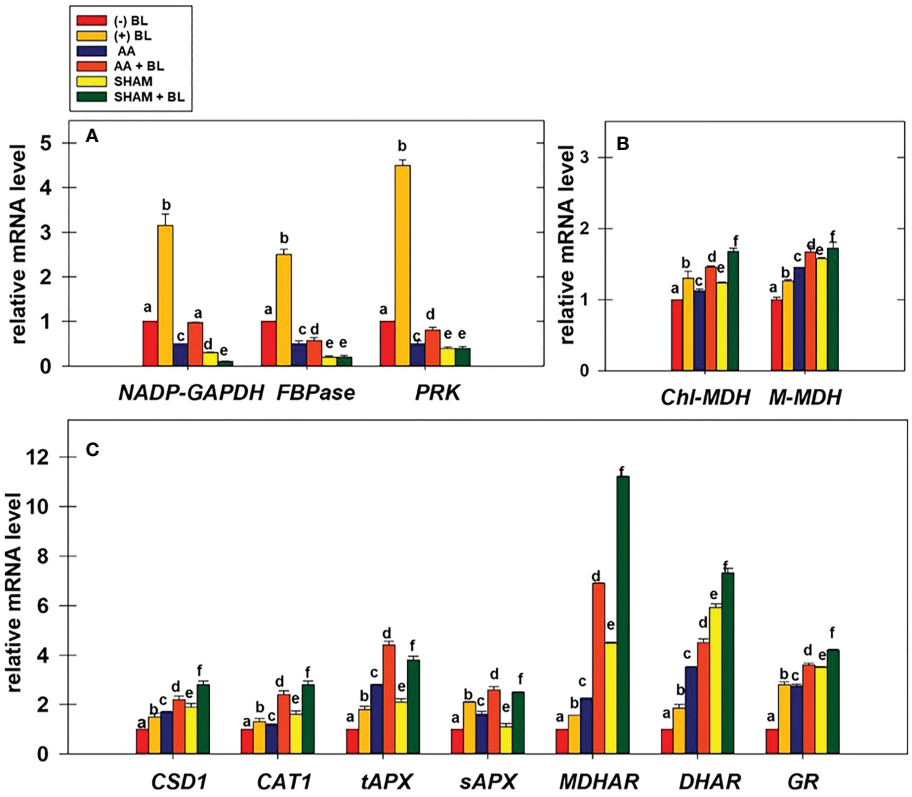

FIGURE 8
Effect of BL on gene expression profiles of enzymes related to CBC: *NADP-GAPDH*, *FBPase*, and *PRK* **(A)**; malate valve: *Chl-MDH*, *M-MDH* **(B)**; antioxidant system: *CSD1*, *CAT1*, *tAPX*, *sAPX*, *MDHAR*, *DHAR*, and *GR* **(C)** under the disruption of COX pathway or AOX pathway. Total mRNA was isolated after treatment of leaf discs with or without BL (0.1 µM) in the presence or absence of AA (20 µM) or SHAM (0.5 mM) for 6 hours at a light intensity of 50 µmol m^{-2} s^{-1} at 25 °C. The amount of transcript was quantified by $\Delta\Delta C_T$ using *UBQ5* as a positive control. Further, the section "materials and methods" mentions more detailed information on the procedure. No Inhibitor (No Inh) depicts a sample without mETC inhibitors. A statistically significant difference is represented by different lowercase alphabetical letters ($P \leq 0.05$) and values represent the average (± SE) of three experiments.

expression and activity of CBC enzymes. Furthermore, adding BL in such an over-reduced condition might not relieve the injury to redox-regulated CBC enzymes, which play an essential role in PCA.

BL keeps up malate valve and maintains a low cellular redox state in coordination with mETC to promote photosynthesis in MCP

During active photosynthesis, the photochemical reactions produce reducing equivalents at substantially exponential rates than the demand of CBC. Under this circumstance, the malate valve permits the exchange of malate for OAA across the chloroplast membrane to export extra reducing equivalents from chloroplasts to mitochondria *via* the cytosol through dicarboxylate transporters present in both chloroplasts and mitochondrial membranes (Scheibe, 2004; Selinski and Scheibe, 2019). An NADP-specific malate dehydrogenase (Chl-MDH) present in chloroplasts significantly transfers excess reducing equivalents from NADPH to OAA and generates malate to be transported to cytosol or mitochondria. Besides, in mitochondria, malate formed during the TCA cycle and imported through the malate valve is transformed into OAA by NAD-specific malate dehydrogenase (Dinakar et al., 2010a). The studies of Dinakar et al. (2016) observed a pronounced increase in malate levels under hyper-osmotic stress conditions in the presence of SHAM, depicting the role of malate in chloroplast and mitochondrial interactions. Besides, numerous reports showed that BRs maintain cellular redox homeostasis *via* increment in the ratios of reduced glutathione (GSH) to oxidized glutathione (GSSG) (Jiang et al., 2012b; Ramakrishna and Rao, 2013; Xia et al., 2018; Li et al., 2022).

In the present study, the addition of BL to MCP showed a decrease in the redox ratios related to both NADPH and NADH along with an increase in malate and transcripts associated with malate valve, i.e., *Chl-MDH* and *M-MDH* (Figures 5B, 6, 8B). These results suggest that BL participates in the crosstalk between chloroplast and mitochondria by modulating the malate valve to maintain cellular redox homeostasis and enhance photosynthesis. Also, the studies of Hu et al. (2019) showed an increment in the activity of both NADP-MDH and NAD-MDH upon treatment of leaves with EBL under drought. Further, an aggravation in a decrease of PCA along with an enhancement in the redox ratio of NADPH and NADH during treatment of MCP with BL in the presence of AA or SHAM confirm the significance of BRs along with mETC in keeping up the activity of malate valve and maintaining the cellular redox state at low levels to optimize chloroplastic photosynthesis (Figures 3B, 5B, 6, 8B). Also, the present study reveals that BL could not overcome the negative effect of excess reducing equivalents on PCA, which is generated during disrupted mETC. However, the component of malate valve was active and maintained in response to BL. Thus, it might be trying to reverse or cope with the tremendous loss that occurred by metabolic fluctuation under restricted mETC.

BL prevented excess ROS generation by activating AOX through malate valve and enhancing the capacity of mETC and antioxidant system

AOX regulates the cellular redox and ROS generation to optimize photosynthesis by modulating the malate valve (Padmasree and Raghavendra, 1999c; Yoshida et al., 2007; Dinakar et al., 2010a; Vishwakarma et al., 2015; Dinakar et al., 2016; Cheng et al., 2020; Garmash et al., 2020; Manbir et al., 2022; Challabathula et al., 2022). Further, malate formed in mitochondria gets utilized by the malic enzyme to form pyruvate (an activator of AOX). The studies of Day et al. (1995) demonstrated using isolated mitochondria that intra-mitochondrial pyruvate production and subsequent AOX activation are associated with malic enzyme activity. The studies of Sankar et al. (2022) demonstrated through molecular docking that Cys177 residue present in the binding pocket for pyruvate plays a role in regulating the activity of AtAOX1a post-translationally. Further, the studies of Dinakar et al. (2010a, 2016) illustrated that the pyruvate accumulated in response to stress (high light, osmotic, and temperature) enhanced the AOX pathway capacity. Also, adding BL to MCP resulted in an enhancement in pyruvate and malate, which might contribute to the enhancement of the AOX pathway capacity observed in the present study (Figures 2, 5B, C). Thus, malate might be converted to pyruvate by NAD-ME, which activates the AOX pathway for oxidation of excess reducing equivalents and maintenance of ROS at an optimal level. Further, an aggravation in cellular ROS and redox ratios of NAD(P)H when BL was added to MCP in light under restricted electron transport through the AOX pathway confirms that BL prevents excess ROS generation by activating the AOX pathway through the malate valve during active photosynthesis (Figures 2A, 5B, C, 6, 7, 8B).

BR-induced ROS is also known to enhance the expression of the antioxidant system (Xia et al., 2009; Lima and Lobato, 2017). In the present study, BL increased the ROS marginally along with transcripts of the antioxidant system (Figures 7, 8C). The studies of Fu et al. (2019) demonstrated that BRs improved cold tolerance in *Elymus nutans* by enhancing the activities of CAT, APX, GR, DHAR, and MDAR but not SOD. Also, under restricted COX or AOX pathway, over-accumulation of ROS was shown in *P. sativum* and *Arabidopsis*, which activated the antioxidant system (Dinakar et al., 2010b; Vishwakarma et al., 2015). The present study has shown that adding BL to MCP under disrupted mETC aggravated the cellular ROS and transcripts associated with the antioxidant system in parallel to the reduction in PCA and CBC enzyme activity/transcripts (Figures 3B, 4, 7, 8A, C). Further, the minimal increase in the redox ratio of NADPH as compared to NADH under disrupted conditions of mETC suggests that NADPH might have been utilized in the ascorbate-glutathione cycle to minimize the H_2O_2 levels (Figures 6, 7, 8C). These results suggest that BL might play a role in preventing excess ROS generation by stimulating antioxidant activity along with mETC to optimize photosynthesis.

Conclusion

The present study demonstrates the interaction between chloroplasts and mitochondria in response to BL for balancing carbon and redox energy. This BL-triggered interaction facilitates the reconfiguration of biochemical factors (ROS, pyruvate, malate, and redox ratios of pyridine nucleotides [NAD(P)H], resulting in the enhancement of TR, PCA, and PSII activity with a concomitant rise in activity/transcripts of redox-regulated CBC enzymes and the capacity of COX and AOX pathways. The results highlight the studies using COX or AOX pathway inhibitors to confirm the interactive role of BL with mETC in a coordinated manner for optimizing photosynthesis that is evident by a decrease in the PCA and CBC enzymes activity/transcripts, which in turn is caused due to imbalance in the ratios of reduced to oxidized pyridine nucleotides [NAD(P)H] leading to accumulation of ROS. Thus, BL prevents (i) over-reduction of the cellular environment by activating the AOX pathway through malate valve and (ii) excessive ROS generation by enhancing the capacity of COX and AOX pathways along with antioxidant systems in a photosynthesizing cell.

Data availability statement

The original contributions presented in the study are included in the article. Further inquiries can be directed to the corresponding author.

Author contributions

KP conceived the project. KM performed the experiments. KP and KM interpreted the data. KM wrote the manuscript. KP edited the manuscript. Both authors contributed to the article and approved the submitted version.

Funding

KM acknowledges DST/INSPIRE Fellowship/[IF160219] for JRF/SRF and contingency grants, Department of Science and Technology, Government of India, India.

Acknowledgments

We gratefully acknowledge Prof. Renate Scheibe (University of Osnabruck, Germany) for her generous gift of *Arabidopsis thaliana* (Columbia) seeds to our laboratory. We profusely thank Prof. A. S. Raghavendra [IOE-Chair Professor, University of Hyderabad (UoH)] and Prof. Saradadevi Tetali [Department of Plant Sciences, University of Hyderabad (UoH)] for extending critical suggestions on experimental protocols/results and their lab facilities during the execution of the project. We also thank Dr. Leena Bhashyam (Genomic Facility, School of Life Sciences, UoH) for helping with RT-PCR and its data analysis. We also thank Mrs. Nalini Manthapuram (Confocal Microscopy facility, Center for Nanotechnology, UoH) for assisting in Confocal studies. Department(s)/School facilities of UoH were supported by grants received from DST-FIST-I, UGC-SAP-DRS, UPE-Phase I/II, UGC-SAP-CAS, DBT-CREBB, DBT-BUILDER and UoH-IoE-RC4-21-022, all from New Delhi, India.

Conflict of interest

The authors declare that the research was conducted in the absence of any commercial or financial relationships that could be construed as a potential conflict of interest.

Publisher's note

Supplementary material

The Supplementary Material for this article can be found online at: https://www.frontiersin.org/articles/10.3389/fpls.2023.1099474/full#supplementary-material

SUPPLEMENTARY TABLE 1
List of Primer used in Real Time-PCR studies:

References

Analin, B., Mohanan, A., Bakka, K., and Challabathula, D. (2020). Cytochrome oxidase and alternative oxidase pathways of mitochondrial electron transport chain are important for the photosynthetic performance of pea plants under salinity stress conditions. *Plant Physiol. Biochem.* 154, 248–259. doi: 10.1016/j.plaphy.2020.05.022

Arfan, M., Zhang, D.-W., Zou, L.-J., Luo, S.-S., Tan, W.-R., Zhu, T., et al. (2019). Hydrogen peroxide and nitric oxide crosstalk mediates brassinosteroids induced cold stress tolerance in *Medicago truncatula*. *Int. J. Mol. Sci.* 20, 1. doi: 10.3390/ijms20010144

Arnon, D. I. (1949). Copper enzymes in isolated chloroplasts. Polyphenoloxidase in *Beta vulgaris*. *Plant Physiol.* 24, 1–15. doi: 10.1104/pp.24.1.1

Azcón-Bieto, J., and Osmond, C. B. (1983). Relationship between photosynthesis and respiration: The effect of carbohydrate status on the rate of CO_2 production by respiration in darkened and illuminated wheat leaves. *Plant Physiol.* 71, 574–581. doi: 10.1104/pp.71.3.574

Bajguz, A., and Hayat, S. (2009). Effects of brassinosteroids on the plant responses to environmental stresses. *Plant Physiol. Biochem.* 47, 1–8. doi: 10.1016/j.plaphy.2008.10.002

Basit, F., Bhat, J. A., Dong, Z., Mou, Q., Zhu, X., Wang, Y., et al. (2022). Chromium toxicity induced oxidative damage in two rice cultivars and its mitigation through external supplementation of brassinosteroids and spermine. *Chemosphere* 302, 134423. doi: 10.1016/j.chemosphere.2022.134423

Batnini, M., Fernández Del-Saz, N., Fullana-Pericàs, M., Palma, F., Haddoudi, I., Mrabet, M., et al. (2020). The alternative oxidase pathway is involved in optimizing photosynthesis in *Medicago truncatula* infected by *Fusarium oxysporum* and *Rhizoctonia solani*. *Physiol. Plant* 169, 600–611. doi: 10.1111/ppl.13080

Berkowitz, O., De Clercq, I., Van Breusegem, F., and Whelan, J. (2016). Interaction between hormonal and mitochondrial signaling during growth, development and in plant defence responses. *Plant Cell Environ.* 39, 1127–1139. doi: 10.1111/pce.12712

Bhanu, A. N. (2019). Brassinosteroids: Relevance in biological activities of plants and agriculture. *J. Plant Sci. Res.* 35, 1–15. doi: 10.32381/JSPR.2019.35.01.1

Bishop, G. J., and Koncz, C. (2002). Brassinosteroids and plant steroid hormone signaling. *Plant Cell.* 14, 97–110. doi: 10.1105/tpc.001461

Chaiwanon, J., and Wang, Z.-Y. (2015). Spatiotemporal brassinosteroid signaling and antagonism with auxin pattern stem cell dynamics in arabidopsis roots. *Curr. Biol.* 25, 1031–1042. doi: 10.1016/j.cub.2015.02.046

Challabathula, D., Analin, B., Mohanan, A., and Bakka, K. (2022). Differential modulation of photosynthesis, ROS and antioxidant enzyme activities in stress-sensitive and -tolerant rice cultivars during salinity and drought upon restriction of COX and AOX pathways of mitochondrial oxidative electron transport. *J. Plant Physiol.* 268. doi: 10.1016/j.jplph.2021.153583

Cheng, D., Gao, H., and Zhang, L. (2020). Upregulation of mitochondrial alternative oxidase pathway protects photosynthetic apparatus against photodamage under chilling stress in rumex K-1 leaves. *Photosynthetica* 58, 1116–1121. doi: 10.32615/ps.2020.060

Cheng, F., Zhou, Y. H., Xia, X. J., Shi, K., Zhou, J., and Yu, J. Q. (2014). Chloroplastic thioredoxin-f and thioredoxin-m1/4 play important roles in brassinosteroids-induced changes in CO_2 assimilation and cellular redox homeostasis in tomato. *J. Exp. Bot.* 65, 4335–4347. doi: 10.1093/jxb/eru207

Clouse, S. D. (2004). "Brassinosteroids," in *Encyclopedia of biological chemistry* (New York: Elsevier).

Clouse, S. D., and Sasse, J. M. (1998). Brassinosteroids: Essential regulators of plant growth and development. *Annu. Rev. Plant Physiol. Plant Mol. Biol.* 49, 427–451. doi: 10.1146/annurev.arplant.49.1.427

Dahal, K., and Vanlerberghe, G. C. (2017). Alternative oxidase respiration maintains both mitochondrial and chloroplast function during drought. *New Phytol.* 213, 560–571. doi: 10.1111/nph.14169

Day, D. A., Whelan, J., Millar, H., Siedow, J. N., and Wiskich, J. T. (1995). Regulation of the alternative oxidase in plants and fungi. aust. *J. Plant Physiol.* 22, 497–509. doi: 10.1071/PP995049

Day, D. A., and Wiskich, J. T. (1995). Regulation of alternative oxidase activity in higher plants. *J. Bioenerg. Biomembr.* 27, 379–385. doi: 10.1007/BF02110000

Deng, X.-G., Zhu, T., Zhang, D.-W., and Lin, H.-H. (2015). The alternative respiratory pathway is involved in brassinosteroid-induced environmental stress tolerance in *Nicotiana benthamiana*. *J. Exp. Bot.* 66, 6219–6232. doi: 10.1093/jxb/erv328

Derevyanchuk, M., Kretynin, S., Iakovenko, O., Litvinovskaya, R., Zhabinskii, V., Martinec, J., et al. (2017). Effect of 24-epibrassinolide on *Brassica napus* alternative respiratory pathway, guard cells movements and phospholipid signaling under salt stress. *Steroids* 117, 16–24. doi: 10.1016/j.steroids.2016.11.006

Derevyanchuk, M., Kretynin, S., Kolesnikov, Y., Litvinovskaya, R., Martinec, J., Khripach, V., and Kravets, V. (2019). Seed germination, respiratory processes and phosphatidic acid accumulation in Arabidopsis diacylglycerol kinase knockouts - The effect of brassinosteroid, brassinazole and salinity. *Steroids*, 147, 28–36. doi: 10.1016/j.steroids.2019.04.002

Derevyanchuk, M., Litvinovskaya, R., Khripach, V., Martinec, J., and Kravets, V. (2015). Effect of 24-epibrassinolide on *Arabidopsis thaliana* alternative respiratory pathway under salt stress. *Acta Physiol. Plant* 37, 1–10. doi: 10.1007/s11738-015-1967-8

Dinakar, C., Raghavendra, A. S., and Padmasree, K. (2010a). Importance of AOX pathway in optimizing photosynthesis under high light stress: Role of pyruvate and malate in activating AOX. *Physiol. Plant* 139, 13–26. doi: 10.1111/j.1399-3054.2010.01346.x

Dinakar, C., Abhaypratap, V., Yearla, S. R., Raghavendra, A. S., and Padmasree, K. (2010b). Importance of ROS and antioxidant system during the beneficial interactions of mitochondrial metabolism with photosynthetic carbon assimilation. *Planta* 231, 461–474. doi: 10.1007/s00425-009-1067-3

Dinakar, C., Vishwakarma, A., Raghavendra, A. S., and Padmasree, K. (2016). Alternative oxidase pathway optimizes photosynthesis during osmotic and temperature stress by regulating cellular ROS, malate valve and antioxidative systems. *Front. Plant Sci.* 7. doi: 10.3389/fpls.2016.00068

Divi, U. K., and Krishna, P. (2009). Brassinosteroid: A biotechnological target for enhancing crop yield and stress tolerance. *New Biotechnol.* 26, 131–136. doi: 10.1016/j.nbt.2009.07.006

Domagalska, M. A., Sarnowska, E., Nagy, F., and Davis, S. J. (2010). Genetic analyses of interactions among gibberellin, abscisic acid, and brassinosteroids in the control of flowering time in *Arabidopsis thaliana*. *PloS One* 5. doi: 10.1371/journal.pone.0014012

Dos Santos Ribeiro, D. G., da Silva, B. R. S., and da Silva Lobato, A. K. (2019). Brassinosteroids induce tolerance to water deficit in soybean seedlings: Contributions linked to root anatomy and antioxidant enzymes. *Acta Physiol. Plant* 41, 82. doi: 10.1007/s11738-019-2873-2

Fu, J., Sun, P., Luo, Y., Zhou, H., Gao, J., Zhao, D., et al. (2019). Brassinosteroids enhance cold tolerance in elymus nutans via mediating redox homeostasis and proline biosynthesis. *Environ. Exp. Bot.* 167, 103831. doi: 10.1016/j.envexpbot.2019.103831

Fu, J., Zhang, S., Jiang, H., Zhang, X., Gao, H., Yang, P., et al. (2022). Melatonin-induced cold and drought tolerance is regulated by brassinosteroids and hydrogen peroxide signaling in perennial ryegrass. *Environ. Exp. Bot.* 196, 104815. doi: 10.1016/j.envexpbot.2022.104815

Garmash, E. V., Velegzhaninov, I. O., Ermolina, K. V., Rybak, A. V., and Malyshev, R. V. (2020). Altered levels of AOX1a expression result in changes in metabolic pathways in *Arabidopsis thaliana* plants acclimated to low dose rates of ultraviolet b radiation. *Plant Sci.* 291, 110332. doi: 10.1016/j.plantsci.2019.110332

Garmash, E. V., Belykh, E. S., and Velegzhaninov, I. O. (2021a). The gene expression profiles of mitochondrial respiratory components in arabidopsis plants with differing amounts of ALTERNATIVE OXIDASE1a under high-intensity light. *Plant Signal. Behav.* 16, 1864962. doi: 10.1080/15592324.2020.1864962

Garmash, E. V. (2021b). Role of mitochondrial alternative oxidase in the regulation of cellular homeostasis during development of photosynthetic function in greening leaves. *Plant Biol.* 23, 221–228. doi: 10.1111/plb.13217

Heidari, P., Entazari, M., Ebrahimi, A., Ahmadizadeh, M., Vannozzi, A., Palumbo, F., et al. (2021). Exogenous EBR ameliorates endogenous hormone contents in tomato species under low-temperature stress. *Hortic* 7, 84. doi: 10.3390/horticulturae7040084

Hu, W. H., Yan, X. H., He, Y., and Xi, R. (2019). 24-epibrassinolide alleviate drought-induced photoinhibition in *Capsicum annuum via* up-regulation of AOX pathway. *Sci. Hortic.* 243, 484–489. doi: 10.1016/j.scienta.2018.09.016

Hu, W. H., Yan, X. H., Xiao, Y. A., Zeng, J. J., Qi, H. J., and Ogweno, J. O. (2013). 24-epibrassinosteroid alleviate drought-induced inhibition of photosynthesis in C*apsicum annuum*. *Sci. Hortic.* 150, 232–237. doi: 10.1016/j.scienta.2012.11.012

Hussain, M. A., Fahad, S., Sharif, R., Jan, M. F., Mujtaba, M., Ali, Q., et al. (2020). Multifunctional role of brassinosteroid and its analogues in plants. *Plant Growth Regul.* 92, 141–156. doi: 10.1007/s10725-020-00647-8

Igamberdiev, A. U., Shen, T., and Gardeström, P. (2006). Function of mitochondria during the transition of barley protoplasts from low light to high light. *Planta* 224, 196–204. doi: 10.1007/s00425-005-0198-4

Jayawardhane, J., Cochrane, D. W., Vyas, P., Bykova, N. V., Vanlerberghe, G. C., and Igamberdiev, A. U. (2020). Roles for plant mitochondrial alternative oxidase under normoxia, hypoxia, and reoxygenation conditions. *Front. Plant Sci.* 11. doi: 10.3389/fpls.2020.00566

Jiang, Y. P., Cheng, F., Zhou, Y. H., Xia, X. J., Mao, W. H., Shi, K., et al. (2012a). Hydrogen peroxide functions as a secondary messenger for brassinosteroids-induced CO_2 assimilation and carbohydrate metabolism in *Cucumis sativus*. *J. Zhejiang Univ Sci. B* 13, 811–823. doi: 10.1631/jzus.B1200130

Jiang, Y. P., Cheng, F., Zhou, Y. H., Xia, X. J., Mao, W. H., Shi, K., et al. (2012b). Cellular glutathione redox homeostasis plays an important role in the brassinosteroid-induced increase in CO_2 assimilation in *Cucumis sativus*. *New Phytol.* 194, 932–943. doi: 10.1111/j.1469-8137.2012.04111.x

Jiang, W. B., Huang, H. Y., Hu, Y. W., Zhu, S. W., Wang, Z. Y., and Lin, W. H. (2013a). Brassinosteroid regulates seed size and shape in arabidopsis. *Plant Physiol.* 162, 1965–1977. doi: 10.1104/pp.113.217703

Jiang, Y. P., Huang, L. F., Cheng, F., Zhou, Y. H., Xia, X. J., Mao, W. H., et al. (2013b). Brassinosteroids accelerate recovery of photosynthetic apparatus from cold stress by balancing the electron partitioning, carboxylation and redox homeostasis in cucumber. *Physiol. Plant* 148, 133–145. doi: 10.1111/j.1399-3054.2012.01696.x

Khripach, V., Zhabinskii, V., and De Groot, A. (2000). Twenty years of brassinosteroids: steroidal plant hormones warrant better crops for the XXI century. *Ann. Bot.* 86, 441–447. doi: 10.1006/anbo.2000.1227

Krishna, P. (2003). Brassinosteroid-mediated stress responses. *J. Plant Growth Regul.* 22, 289–297. doi: 10.1007/s00344-003-0058-z

Krömer, S., and Scheibe, R. (1996). Function of the chloroplastic malate valve for respiration during photosynthesis. *Biochem. Soc Trans.* 24, 761–766. doi: 10.1042/bst0240761

Lanza, M., Garcia-Ponce, B., Castrillo, G., Catarecha, P., Sauer, M., Rodriguez-Serrano, M., et al. (2012). Role of actin cytoskeleton in brassinosteroid signaling and in its integration with the auxin response in plants. *Dev. Cell.* 22, 1275–1285. doi: 10.1016/j.devcel.2012.04.008

Li, J., Sohail, H., Nawaz, M. A., Liu, C., and Yang, P. (2022). Physiological and proteomic analyses reveals that brassinosteroids application improves the chilling stress tolerance of pepper seedlings. *Plant Growth Regul.* 96, 315–329. doi: 10.1007/s10725-021-00778-6

Li, J., Yang, P., Gan, Y., Yu, J., and Xie, J. (2015). Brassinosteroid alleviates chilling-induced oxidative stress in pepper by enhancing antioxidation systems and maintenance of photosystem II. *Acta Physiol. Plant* 37. doi: 10.1007/s11738-015-1966-9

Lima, J., and Lobato, A. (2017). Brassinosteroids improve photosystem II efficiency, gas exchange, antioxidant enzymes and growth of cowpea plants exposed to water deficit. *Physiol. Mol. Biol. Plants.* 23, 59–72. doi: 10.1007/s12298-016-0410-y

Liu, X., Yang, Q., Wang, Y., Wang, L., Fu, Y., and Wang, X. (2018). Brassinosteroids regulate pavement cell growth by mediating BIN2- induced microtubule stabilization. *J. Exp. Bot.* 69, 1037–1049. doi: 10.1093/jxb/erx467

Livak, K. J., and Schmittgen, T. D. (2001). Analysis of relative gene expression data using real-time quantitative PCR and the 2-ΔΔCT method. *Methods* 25, 402–408. doi: 10.1006/meth.2001.1262

Manbir,, Singh, P., Kumari, A., and Gupta, K. J. (2022). Alternative oxidase plays a role in minimizing ROS and RNS produced under salinity stress in *Arabidopsis thaliana*. *Physiol. Plant* 174, e13649. doi: 10.1111/ppl.13649

McDonald, A. E., Sieger, S. M., and Vanlerberghe, G. C. (2002). Methods and approaches to study plant mitochondrial alternative oxidase. *Physiol. Plant* 116, 135–143. doi: 10.1034/j.1399-3054.2002.1160201.x

Millar, A. H., Whelan, J., Soole, K. L., and Day, D. A. (2011). Organization and regulation of mitochondrial respiration in plants. *Annu. Rev. Plant Biol.* 62, 79–104. doi: 10.1146/annurev-arplant-042110-103857

Millenaar, F., and Lambers, H. (2003). The alternative oxidase: *in vivo* regulation and function. *Plant Biol.* 5, 2–15. doi: 10.1055/s-2003-37974

Moore, A. L., and Siedow, J. N. (1991). The regulation and nature of the cyanide-resistant alternative oxidase of plant mitochondria. *Biochim. Biophys. Acta Bioenerg.* 1059, 121–140. doi: 10.1016/S0005-2728(05)80197-5

Murashige, T., and Skoog, F. (1962). A revised medium for rapid growth and bio assays with tobacco tissue cultures. *Physiol. Plant* 15, 473–497. doi: 10.1111/j.1399-3054.1962.tb08052.x

Naservafaei, S., Sohrabi, Y., Moradi, P., Sweeney, E. M., and Mastinu, A. (2021). Biological response of *Lallemantia iberica* to brassinolide treatment under different watering conditions. *Plants* 10, 496. doi: 10.3390/plants10030496

Nie, S., Yue, H., Zhou, J., and Xing, D. (2015). Mitochondrial-derived reactive oxygen species play a vital role in the salicylic acid signaling pathway in *Arabidopsis thaliana*. *PloS One* 10, e0119853. doi: 10.1371/journal.pone.0119853

Noguchi, K., Nakajima, N., and Terashima, I. (2001). Acclimation of leaf respiratory properties in *Alocasia odora* following reciprocal transfers of plants between high- and low-light environments. *Plant Cell Environ.* 24, 831–839. doi: 10.1046/j.1365-3040.2001.00728.x

Noguchi, K., and Yoshida, K. (2008). Interaction between photosynthesis and respiration in illuminated leaves. *Mitochondrion* 8, 87–99. doi: 10.1016/j.mito.2007.09.003

Nolan, T. M., Vukašinović, N., Liu, D., Russinova, E., and Yin, Y. (2020). Brassinosteroids: Multidimensional regulators of plant growth, development, and stress responses. *Plant Cell* 32, 295–318. doi: 10.1105/tpc.19.00335

Padmasree, K., and Raghavendra, A. S. (1999a). Importance of oxidative electron transport over oxidative phosphorylation in optimizing photosynthesis in mesophyll protoplasts of pea (*Pisum sativum* L). *Physiol. Plant* 105, 546–553. doi: 10.1034/j.1399-3054.1999.105321.x

Padmasree, K., and Raghavendra, A. S. (1999b). Prolongation of photosynthetic induction as a consequence of interference with mitochondrial oxidative metabolism in mesophyll protoplasts of pea (*Pisum sativum* L.). *Plant Sci.* 142, 29–36. doi: 10.1016/S0168-9452(98)00252-0

Padmasree, K., and Raghavendra, A. S. (1999c). Response of photosynthetic carbon assimilation in mesophyll protoplasts to restriction on mitochondrial oxidative metabolism: Metabolites related to the redox status and sucrose biosynthesis. *Photosynth. Res.* 62, 231–239. doi: 10.1023/A:1006382518725

Padmasree, K., and Raghavendra, A. S. (2001a). Consequence of restricted mitochondrial oxidative metabolism on photosynthetic carbon assimilation in mesophyll protoplasts: Decrease in light activation for four chloroplastic enzymes. *Physiol. Plant* 112, 582–588. doi: 10.1034/j.1399-3054.2001.1120417.x

Padmasree, K., and Raghavendra, A. S. (2001b). Restriction of mitochondrial oxidative metabolism leads to suppression of photosynthetic carbon assimilation but not of photochemical electron transport in pea mesophyll protoplasts. *Curr.Sci* 81, 680–684.

Peres, A. L. G., Soares, J. S., Tavares, R. G., Righetto, G., Zullo, M. A., Mandava, N. B., et al. (2019). Brassinosteroids, the sixth class of phytohormones: A molecular view from the discovery to hormonal interactions in plant development and stress adaptation. *Int. J. Mol. Sci.* 20, 331. doi: 10.3390/ijms20020331

Queval, G., and Noctor, G. (2007). A plate reader method for the measurement of NAD, NADP, glutathione, and ascorbate in tissue extracts: Application to redox profiling during arabidopsis rosette development. *Anal. Biochem.* 363, 58–69. doi: 10.1016/j.ab.2007.01.005

Raghavendra, A. S., and Padmasree, K. (2003). Beneficial interactions of mitochondrial metabolism with photosynthetic carbon assimilation. *Trends Plant Sci.* 8, 546–553. doi: 10.1016/j.tplants.2003.09.015

Raghavendra, A. S., Saradadev, K., and Padmasree, K. (1992). Short-term interactions between photosynthesis and mitochondrial respiration in leaves and protoplasts. *Transaction Malaysian Soc. Plant Physiol.* 3, 12–18.

Ramakrishna, B., and Rao, S. S. R. (2013). Preliminary studies on the involvement of glutathione metabolism and redox status against zinc toxicity in radish seedlings by 28-homobrassinolide. *Environ. Exp. Bot.* 96, 52–58. doi: 10.1016/j.envexpbot.2013.08.003

Rattan, A., Kapoor, D., Kapoor, N., Bhardwaj, R., and Sharma, A. (2020). Brassinosteroids regulate functional components of antioxidative defense system in salt stressed maize seedlings. *J. Plant Growth Regul.* 39, 1465–1475. doi: 10.1007/s00344-020-10097

Raza, A., Salehi, H., Rahman, M. A., Zahid, Z., Madadkar Haghjou, M., Najafi-Kakavand, S., et al. (2022). Plant hormones and neurotransmitter interactions mediate antioxidant defenses under induced oxidative stress in plants. *Front. Plant Sci.* 13. doi: 10.3389/fpls.2022.961872

Reddy, M. M., Vani, T., and Raghavendra, A. S. (1991). Light-enhanced dark respiration in mesophyll protoplasts from leaves of pea. *Plant Physiol.* 96, 1368–1371. doi: 10.1104/pp.96.4.1368

Riazunnisa, K., Padmavathi, L., Scheibe, R., and Raghavendra, A. S. (2007). Preparation of Arabidopsis mesophyll protoplasts with high rates of photosynthesis. *Physiol. Plant* 129, 679–686. doi: 10.1111/j.1399-3054.2007.00867.x

Ruan, Y., Halat, L. S., Khan, D., Jancowski, S., Ambrose, C., Belmonte, M. F., et al. (2018). The microtubule associated protein CLASP sustains cell proliferation through a brassinosteroid signaling negative feedback loop. *Curr. Biol.* 28, 2718–2729. doi: 10.1016/j.cub.2018.06.048

Sankar, T. V., Saharay, M., Santhosh, D., Vishwakarma, A., and Padmasree, K. (2022). Structural and biophysical characterization of purified recombinant *Arabidopsis thaliana's* alternative oxidase 1A (rAtAOX1A): Interaction with inhibitor (s) and activator. *Front. Plant Sci.* 13. doi: 10.3389/fpls.2022.871208

Saradadevi, K., and Raghavendra, A. S. (1992). Dark respiration protects photosynthesis against photoinhibition in mesophyll protoplasts of pea (*Pisum sativum*). *Plant Physiol.* 99, 1232–1237. doi: 10.1104/pp.99.3.1232

Saradadevi, K., and Raghavendra, A. S. (1994). Inhibition of photosynthesis by osmotic stress in pea (*Pisum sativum*) mesophyll protoplasts is intensified by chilling or photoinhibitory light; intriguing responses of respiration. *Plant Cell Environ.* 17, 739–746. doi: 10.1111/j.1365-3040.1994.tb00166.x

Scheibe, R. (2004). Malate valves to balance cellular energy balance. *Physiol. Plant* 120, 21–26. doi: 10.1111/j.0031-9317.2004.0222.x

Scheibe, R., Backhausen, J. E., Emmerlich, V., and Holtgrefe, S. (2005). Strategies to maintain redox homeostasis during photosynthesis under changing conditions. *J. Exp. Bot.* 56, 1481–1489. doi: 10.1093/jxb/eri181

Schertl, P., and Braun, H. P. (2014). Respiratory electron transport pathways in plant mitochondria. *Front. Plant Sci.* 5. doi: 10.3389/fpls.2014.00163

Searle, S. Y., Thomas, S., Griffin, K. L., Horton, T., Kornfeld, A., Yakir, D., et al. (2011). Leaf respiration and alternative oxidase in field-grown alpine grasses respond to natural changes in temperature and light. *New Phytol.* 189, 1027–1039. doi: 10.1111/j.1469-8137.2010.03557.x

Selinski, J., König, N., Wellmeyer, B., Hanke, G. T., Linke, V., Neuhaus, H. E., et al. (2014). The plastid-localized NAD-dependent malate dehydrogenase is crucial for energy homeostasis in developing *Arabidopsis thaliana* seeds. *Mol. Plant* 7 (1), 170–186. doi: 10.1093/mp/sst151

Selinski, J., and Scheibe, R. (2019). Malate valves: Old shuttles with new perspectives. *Plant Biol.* 21, 21–30. doi: 10.1111/plb.12869

Siddiqui, H., Hayat, S., and Bajguz, A. (2018). Regulation of photosynthesis by brassinosteroids in plants. *Acta Physiol. Plant* 40 (3), 1–15. doi: 10.1007/s11738-018-2639-2

Siedow, J. N., and Umbach, A. L. (2000). The mitochondrial cyanide– Resistant oxidase: structural conservation amid regulatory diversity. *Biochim. Biophys. Acta Bioenerg.* 1459, 432–449. doi: 10.1016/S0005-2728(00)00181-X

Strodtkötter, I., Padmasree, K., Dinakar, C., Speth, B., Niazi, P. S., Wojtera, J., et al. (2009). Induction of the AOX1D isoform of alternative oxidase in *A. thaliana* T-DNA insertion lines lacking isoform AOX1A is insufficient to optimize photosynthesis when treated with antimycin A. *Mol. Plant* 2, 284–297. doi: 10.1093/mp/ssn089

Sunil, B., Rajsheel, P., Aswani, V., Bapatla, R. B., Talla, S. K., and Raghavendra, A. S. (2020). Photosynthesis is sensitive to nitric oxide and respiration sensitive to hydrogen peroxide: Studies with pea mesophyll protoplasts. *J. Plant Physiol.* 246, 153133. doi: 10.1016/j.jplph.2020.153133

Tanveer, M., Shahzad, B., Sharma, A., and Khan, E. A. (2019). 24-epibrassinolide application in plants: An implication for improving drought stress tolerance in plants. *Plant Physiol. Biochem.* 135, 295–303. doi: 10.1016/j.plaphy.2018.12.013

Tarkowská, D., Novák, O., Oklestkova, J., and Strnad, M. (2016). The determination of 22 natural brassinosteroids in a minute sample of plant tissue by UHPLC–ESI–MS/MS. *Anal. Bioanal. Chem.* 408, 6799–6812. doi: 10.1007/s00216-016-9807-2

Vani, T., Reddy, M. M., and Raghavendra, A. S. (1990). Beneficial interaction between photosynthesis and respiration in mesophyll protoplasts of pea during short light-dark cycles. *Physiol. Plant* 80, 467–471. doi: 10.1111/j.1399-3054.1990.tb00069.x

Vanlerberghe, G. C., Dahal, K., Alber, N. A., and Chadee, A. (2020). Photosynthesis, respiration and growth: A carbon and energy balancing act for alternative oxidase. *Mitochondrion* 52, 197–211. doi: 10.1016/j.mito.2020.04.001

Vanlerberghe, G. C., and McIntosh, L. (1997). Alternative oxidase: From gene to function. *Annu. Rev. Plant Biol.* 48, 703–734. doi: 10.1146/annurev.arplant.48.1.703

Vishwakarma, A., Bashyam, L., Senthilkumaran, B., Scheibe, R., and Padmasree, K. (2014). Physiological role of AOX1a in photosynthesis and maintenance of cellular redox homeostasis under high light in *Arabidopsis thaliana*. *Plant Physiol. Biochem.* 81, 44–53. doi: 10.1016/j.plaphy.2014.01.019

Vishwakarma, A., Tetali, S. D., Selinski, J., Scheibe, R., and Padmasree, K. (2015). Importance of the alternative oxidase (AOX) pathway in regulating cellular redox and ROS homeostasis to optimize photosynthesis during restriction of the cytochrome oxidase pathway in *Arabidopsis thaliana*. *Ann. Bot.* 116, 555–569. doi: 10.1093/aob/mcv122

Wang, T., Zhang, D., Chen, L., Wang, J., and Zhang, W.-H. (2022). Genomewide analysis of the glutathione s-transferase family in wild *Medicago ruthenica* and drought-tolerant breeding application of *MruGSTU39* gene in cultivated alfalfa. *Theor. Appl. Genet.* 135, 853–864. doi: 10.1007/s00122-021-04002-x

Wei, L. J., Deng, X. G., Zhu, T., Zheng, T., Li, P. X., Wu, J. Q., et al. (2015). Ethylene is involved in brassinosteroids induced alternative respiratory pathway in cucumber (*Cucumis sativus* L.) seedlings response to abiotic stress. *Front. Plant Sci.* 6. doi: 10.3389/fpls.2015.00982

Xia, X.-J., Fang, P.-P., Guo, X., Qian, X.-J., Zhou, J., Shi, K., et al. (2018). Brassinosteroid-mediated apoplastic H_2O_2-glutaredoxin 12/14 cascade regulates

antioxidant capacity in response to chilling in tomato. *Plant Cell Environ.* 41, 1052–1064. doi: 10.1111/pce.13052

Xia, X.-J., Wang, Y.-J., Zhou, Y.-H., Tao, Y., Mao, W.-H., Shi, K., et al. (2009). Reactive oxygen species are involved in brassinosteroid-induced stress tolerance in cucumber. *Plant Physiol.* 150, 801–814. doi: 10.1104/pp.109.138230

Xin, P., Yan, J., Fan, J., Chu, J., and Yan, C. (2013a). A dual role of boronate affinity in high-sensitivity detection of vicinal diol brassinosteroids from sub-gram plant tissues *via* UPLC-MS/MS. *R. Soc. Chem.* 138, 1342–1345. doi: 10.1039/c3an36533f

Xin, P., Yan, J., Fan, J., Chu, J., and Yan, C. (2013b). An improved simplified high-sensitivity quantification method for determining brassinosteroids in different tissues of rice and *Arabidopsis*. *Plant Physiol.* 162, 2056–2066. doi: 10.1104/pp.113.221952

Yan, J., Guan, L., Sun, Y., Zhu, Y., Liu, L., Lu, R., et al. (2015). Calcium and ZmCCaMK are involved in brassinosteroid-induced antioxidant defense in maize leaves. *Plant Cell Physiol.* 56 (5), 883–896. doi: 10.1093/pcp/pcv014

Ye, Q., Zhu, W., Li, L., Zhang, S., Yin, Y., Ma, H., et al. (2010). Brassinosteroids control male fertility by regulating the expression of key genes involved in Arabidopsis anther and pollen development. *Proc. Natl. Acad. Sci. U.S.A.* 107, 6100–6105. doi: 10.1073/pnas.0912333107

Yoshida, K., Terashima, I., and Noguchi, K. (2007). Up-regulation of mitochondrial alternative oxidase concomitant with chloroplast over-reduction by excess light. *Plant Cell Physiol.* 48, 606–614. doi: 10.1093/pcp/pcm033

Zhang, Z.-S., Liu, M.-J., Scheibe, R., Selinski, J., Zhang, L.-T., Yang, C., et al. (2017). Contribution of the alternative respiratory pathway to PSII photoprotection in C3 and C4 plants. *Mol. Plant* 10, 131–142. doi: 10.1016/j.molp.2016.10.004

Zhang, Y. P., Zhu, X. H., Ding, H. D., Yang, S. J., and Chen, Y. Y. (2013). Foliar application of 24-epibrassinolide alleviates high-temperature induced inhibition of photosynthesis in seedlings of two melon cultivars. *Photosynthetica* 51, 341–349. doi: 10.1007/s11099-013-0031-4

Zhu, T., Deng, X.-G., Tan, W.-R., Zhou, X., Luo, S.-S., Han, X.-Y., et al. (2016). Nitric oxide is involved in brassinosteroid-induced alternative respiratory pathway in *Nicotiana benthamiana* seedlings' response to salt stress. *Physiol. Plant* 156, 150–163. doi: 10.1111/ppl.12392

Glossary

AOX	Alternative oxidase
AA	Antimycin A
APX	Ascorbate peroxidase
BL	Brassinolide
BRs	Brassinosteroids
CAT	Catalase
CBC	Calvin-Benson cycle
CCCP	Carbonyl cyanide-3-chlorophenylhydrazone
Chl	Chlorophyll
COX	Cytochrome oxidase
DHAR	Dehydroascorbate reductase
EBR	Epibrassinolide
FBPase	Fructose-1,6-bisphosphatase
Glc-6-P	Glucose-6-Phosphate
GSH	Reduced glutathione
GSSG	Oxidized glutathione
GR	Glutathione reductase
H_2DCFDA	2,7-dichlorofluorescein diacetate
KCN	Potassium cyanide
MDHAR	Monodehydroascorbate reductase
mETC	Mitochondrial electron transport chain
MCP	Mesophyll cell protoplasts
NAD	Oxidized nicotinamide adenine dinucleotide
NADH	Reduced nicotinamide adenine dinucleotide
NADP	Oxidized nicotinamide adenine dinucleotide phosphate
NADPH	Reduced nicotinamide adenine dinucleotide phosphate
NADP-GAPDH	NADP-dependent Glyceraldehyde-3-phosphate dehydrogenase
NADP-MDH (Chl-MDH)	(Chloroplastic-MDH), NADP-dependent Malate dehydrogenases
NAD-MDH (M-MDH)	(Mitochondrial-MDH), NAD-dependent Malate dehydrogenases
NAD-ME	NAD-dependent Malic Enzyme
OAA	Oxaloacetic acid
PCA	Photosynthetic carbon assimilation
PRK	Phosphoribulokinase
tAPX	Thylakoid ascorbate peroxidase
TCA	Tricarboxylic acid cycle
TR	Total respiration
RR	Residual respiration
ROS	Reactive oxygen species
sAPX	Stromal ascorbate peroxidase
SOD	Superoxide dismutase
SHAM	Salicylhydroxamic acid

Frontiers in Plant Science

Cultivates the science of plant biology and its applications

The most cited plant science journal, which advances our understanding of plant biology for sustainable food security, functional ecosystems and human health.

Discover the latest Research Topics

See more →

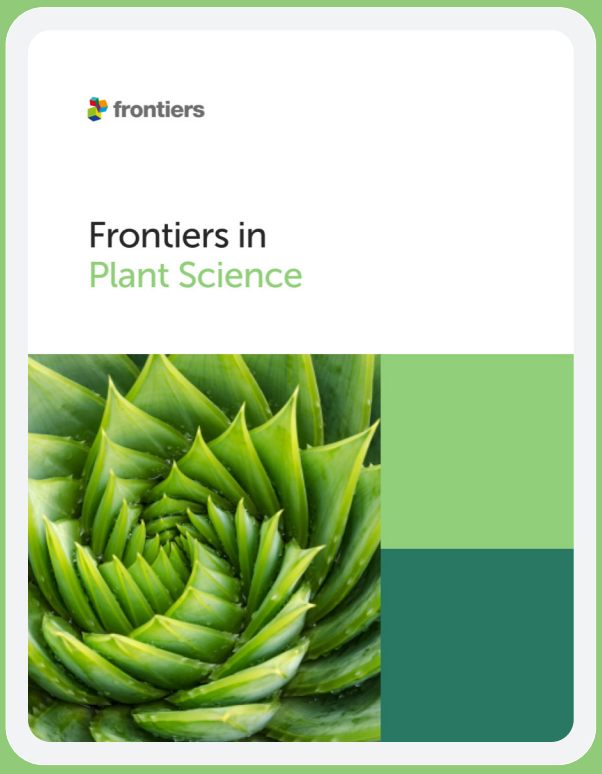

Frontiers

Avenue du Tribunal-Fédéral 34
1005 Lausanne, Switzerland
frontiersin.org

Contact us

+41 (0)21 510 17 00
frontiersin.org/about/contact